LOS ALAMOS SCIENTIFIC LABORATORY
of the
University of California

LOS ALAMOS • NEW MEXICO

Quarterly Status Report on the

Advanced Plutonium Fuels Program

April 1 to June 30, 1969

and Third Annual Report, FY 1969

UNITED STATES
ATOMIC ENERGY COMMISSION
CONTRACT W-7405-ENG. 36

This LA. . .MS report presents the status of the LASL Advanced Plutonium Fuels Program. Previous Quarterly Status Reports in this series, all unclassified, are:

LA-3607-MS	LA-3760-MS*	LA-4073-MS
LA-3650-MS	LA-3820-MS	LA-4114-MS
LA-3686-MS	LA-3880-MS	LA-4193-MS
LA-3708-MS*	LA-3933-MS	
LA-3745-MS	LA-3993-MS	

This report, like other special-purpose documents in the LA. . .MS series, has not been reviewed or verified for accuracy in the interest of prompt distribution.

*Advanced Reactor Technology (ART) Series.

Distributed: October 15, 1969

LA-4284-MS
SPECIAL DISTRIBUTION

LOS ALAMOS SCIENTIFIC LABORATORY
of the
University of California
LOS ALAMOS • NEW MEXICO

Quarterly Status Report on the

Advanced Plutonium Fuels Program

April 1 to June 30, 1969

and Third Annual Report, FY 1969

FOREWORD

This is the third annual report on the Advanced Plutonium Fuels Program conducted at the Los Alamos Scientific Laboratory. Results of the current (twelfth) quarter's work has been in most cases incorporated into the summary of the year's work, and is therefore specifically identified.

Most of the investigations discussed are of the continuing type. Results and conclusions described may therefore be changed or augmented as the work continues. Published reference to results cited in the report should not be made without obtaining explicit permission to do so from the persons in charge of the work.

TABLE OF CONTENTS

TABLE OF CONTENTS
(continued)

PROJECT 401

EXAMINATION OF FAST REACTOR FUELS

Person in Charge: R. D. Baker
Principal Investigators: J. W. Schulte
J. A. Leary
C. F. Metz

I. INTRODUCTION

This project is directed toward the examination and comparison of the effects of neutron irradiation on LMFBR Program fuel materials. Irradiated materials are examined as requested by the Fuels and Materials Branch of DRD & T.

Another phase of this project is the development of an analytical chemistry program designed to assure the high-quality well-characterized fuel required by the LMFBR/FFTF Program. An analytical program has been developed which has the following objectives:

1. To evaluate the present capabilities of potential fuel producers for making the analytical measurements on FFTF fuel that are necessary to assure the uniformly high quality fuel required by the LMFBR/FFTF Program.
2. To provide technical guidance to fuel producers, as may be required, to assure these capabilities are established at the level required by FFTF reactor fuel specifications.
3. To establish and conduct a monitoring program that will assure continuing technical competence of fuel producers for the analysis of FFTF fuel at the level required by fuel specifications.

II. HOT CELL EQUIPMENT DEVELOPMENT

Inert Atmosphere Systems

(C. E. Frantz, M. D. Keehn, R. F. Velkinburg)

The first recirculating inert gas (Ar) system for the disassembly cell was extensively tested. Initial results indicated that under normal operating conditions it was possible to obtain atmosphere purities of < 25 ppm $O_2 + H_2O$. With continued testing of the Ar system and with the disassembly box in normal operation, massive in-leakage of air occurred which apparently poisoned the absorbent chemicals used to remove the impurities. This leakage was traced to holes in the manipulator boots and in some penetrations which had not been adequately sealed. The leaks have been corrected, and at the suggestion of the manufacturer replacement charges of absorbent have been ordered. A simple mixing system has been installed and successfully operated to provide a 5% H_2, 95% Ar gas mixture for regeneration of the O_2 and H_2O absorption beds.

A second Ar purification unit was procured to provide an inert atmosphere for the two metallography cells and the containment box which houses the remote metallograph. This purification unit, which was delivered in November, 1968, was subjected to different tests as part of the acceptance procedure. The few minor deficiencies noted were corrected by using materials and instructions furnished by the manufacturer. Detailed drawings for installing this system have been completed, and it is anticipated that the unit will be available about September 1, 1969 for the examination of the irradiated mixed carbide fuels.

Of the eight cells currently equipped with containment boxes for handling irradiated U-Pu fuels, only the

disassembly cell, the two metallography cells and the metallograph "blister" are being provided with inert atmosphere capability. However, the other two containment boxes recently installed for DTA and heat content measurements, as well as those planned for the future, will be provided with the necessary fittings to convert to a recirculating Ar purification system.

Considerations have been given to future systems which would provide more economical and reliable performance. The use of sealed Model L manipulators should reduce the probability of massive air leaks and thereby permit the use of a smaller purification unit.

Shipping Casks
(C. D. Montgomery, J. W. Schulte)

The design of the cask for shipping irradiated fuel elements was approved by the AEC and Department of Transportation and has been designated as DOT Permit No. 5885. This cask has 6-1/2 in. of depleted U for shielding and a cavity with dimensions of 6 in. i.d. and 45 in. high. Calculations indicate that the cask can be used for shipping, in an upright position, as many as 19 EBR-II type capsules each containing 159 g fissile material which has been irradiated to 100,000 MWD/T and cooled for 30 days. The fabrication is nearly completed, and the finished assembly is expected in August, 1969.

Two casks with DOT Approval (Special Permit No. DOT 5645), were obtained from LASL's Rover Program. These casks, which are rectangular, have 10 in. of Pb shielding and a cavity size of 62 in. long x 16 in. x 16 in. They must be loaded and shipped in a horizontal position. One cask has already been used for shipping five PNL-X series capsules, a mixed carbide LASL Capsule, and two EBR-II Driver Fuel Elements from the EBR-II to LASL. The mixed carbide capsule, mentioned above, was nondestructively tested at LASL and then returned to the EBR-II in the same cask.

Radiography Equipment and Methods
(M. E. Lazarus)

A portable shield system has been designed for use during betatron radiography. The shield improves the x-ray image by reducing the fog caused by exposure of the film to the gamma radiation from the irradiated pin. The shield system consists of three parts: a lead plate with an aperture, placed close to the pin; a second lead plate with an aperture, placed close to the film; and a lead shutter which is placed over the aperture on the second lead plate.

The lead shutter is closed while the pin is being moved into position for x-raying and then is remotely opened for obtaining the picture. The two shield plates provide collimated shielding so that only gamma radiation from the section of the pin being photographed reaches the film. The shields have been tested without the shutter and have provided a definite improvement in the photographs. The effect of the shutter will be tested in the near future.

III. IN-CELL EQUIPMENT

A. Wing 9 Facility
(G. R. Brewer, D. B. Court, E. L. Ekberg, C. E. Frantz, F. J. Fitzgibbon, M. E. Lazarus, J. M. Ledbetter, C. D. Montgomery, T. Romanik, A. E. Tafoya, R. F. Velkinburg)

1. Installation of New Metallography Boxes

It was agreed in a meeting held with DRDT personnel at Washington in April, 1969, that the old metallography boxes should be removed. The two boxes had been used for a period of 7 years in disassembly of fuel pins and in the preparation of metallographic specimens. In that period, approximately 40 kg of irradiated Pu from the LAMPRE reactor had been handled. Recently mixed oxide fuel, having burnups as high as 100,000 MWD/T, was processed in these cells. After remote decontamination and removal of some of the equipment by bagging techniques, the boxes were taken from the cells by conventional techniques. One box had a radiation reading of 1 r/hr beta-gamma at contact, whereas the second unit had a level of 100 mr/hr at contact. A photograph of the polishing-grinding box is shown in Figure 401-1. Note the 100 mr/hr reading on the "Caution" sign. The Homalite CR-39 plastic window had discolored only slightly during this period, and it still appeared to be structurally sound.

The new units with improved equipment would be put into service as soon as possible. The installation of the boxes and equipment was started in May, and it is

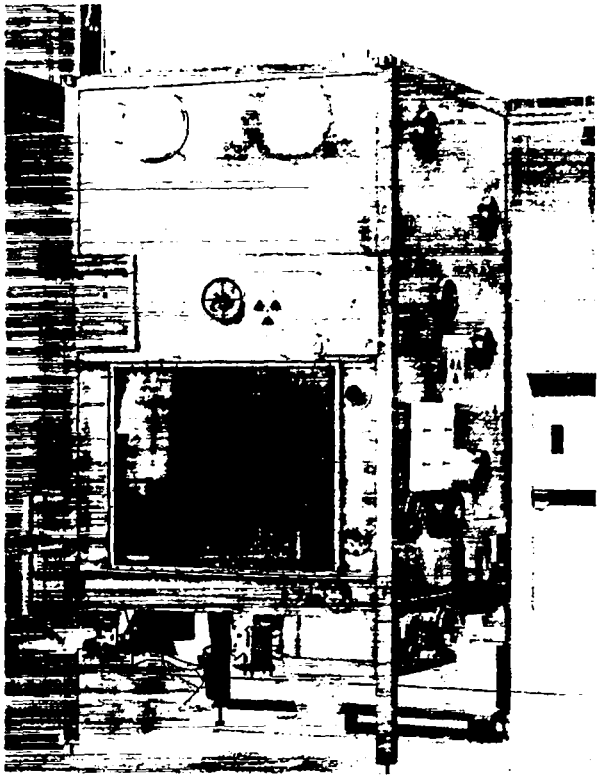

Fig. 401-1. Alpha Containment Box - removed from hot cell after 7 years' use in preparing Pu specimens.

anticipated that this work will be completed about August 1.

Metallography and associated examinations will first be started on mixed oxide fuel from the five PNL-X series pins and then on PNL-1-16 and PNL-1-18. At the conclusion of this work, the system for providing Ar atmosphere to the metallography boxes should be available. It will be used, if needed, during the examination of mixed carbide fuels from UNC and other sponsors.

Some of the major improvements being incorporated into the new boxes are listed as follows:

a. Transfer Systems

To facilitate transfer of materials between metallography cells, special transfer tunnels were designed in a manner compatible with maintaining inert atmospheres. A 10-in. diam tunnel is used to connect the two metallography cells. A conveyor is installed in the tunnel, and one end of the tunnel is sealed with a commercial 10-in. vacuum valve. Between the polishing cell and the metallography blister, the transfer tunnel also serves as an air lock. Each end of the 8-in. diam tunnel is sealed with a commercial 8-in. vacuum valve, and a conveyor is located in the tunnel. The air lock is required since the cell will often have an inert Ar atmosphere while the blister may have an air atmosphere at times. The air lock can be evacuated and backfilled with Ar, thereby making possible transfers in and out of the cell without contaminating the atmosphere.

A new transfer system has been designed to enable rapid one-way transfer of "cold" materials from the operating area into the polishing cell and to provide rapid removal of low level β-γ contaminated containers and materials from the grinding cell. Drawing details are now being prepared to incorporate these two systems into the new metallography boxes.

b. Waste Removal

A waste compactor has been designed and is now being constructed to consolidate waste products from operations in the two metallographic cells. The compaction of wastes should decrease the frequency of transfer operations from the boxes.

c. Other Equipment

Unipol grinder-polishers and Syntron vibratory polishers have been modified for efficient remote operation.

A photography capability, similar to those used in other LASL facilities, was installed for obtaining macrophotographs of polished specimens.

Improvements to the metallograph are being made under the direction of a Service Engineer.

A bag-out system is being provided in the metallograph blister for the removal of replicas, alpha autoradiographs, beta-gamma autoradiographs, and other low-level samples.

2. Dimensioning Equipment

The mechanical profilometer developed for taking diameters of irradiated fuel capsules and pins was used successfully during this fiscal year. A series of standards, having diameters approximating those of the irradiated pins, was provided for frequent checking of the

profilometer. The standards had diameter measurements which were traceable to the National Bureau of Standards. A statistical study of a standard was made to check the reproducibility of the profilometer. The results obtained indicate that the standard deviation of < 0.0001 in. in the range of 0.298 - 0.305 in.

The apparatus for obtaining dimensions of 1/4 in. x 1/4 in. pellets was successfully used on several hundred mixed carbide pellets. According to the users the instrument provided good diametral traces. However, the length perpendicularity, concave, and convex measurements were not easily obtained. An improved model has been fabricated and tested in a glovebox operation. The improvements which are adaptable to hot cell operation will be incorporated into a remotized unit when final drawings of the successful model have been prepared.

3. Fission Gas Sampling and Void Volume Determination

Two fission gas sampling systems have been constructed and used successfully for void volume and quantitative fission gas measurements. The apparatus in the disassembly cell is used only for sampling from fuel pins since it obtains a sample by puncturing the pins with a needle and can penetrate only up to 0.020 in. wall. This system can measure void volumes to better than ± 0.2 cc.

The other system is designed to obtain gas samples by drilling a 1/16-in. diam hole in fuel pin capsules. It will accommodate any capsule which is less than 1-1/8 in. o.d. This system can measure void volumes to better than ± 0.5 cc.

4. Carbon Evaporator

A remotely-operated carbon evaporator was installed and successfully used for coating irradiated EBR-II Driver Fuel specimens for the microprobe. Samples of UO_2 (simulating mixed oxide fuel) were also coated satisfactorily. The evaporator was installed in the containment box of the cell where the remotely-operated DTA equipment is also located.

5. Shielded Electron Microprobe

(D. B. Court, W. V. Cummings, E. A. Hakkila, C. D. Montgomery)

Installation of a MAC (Materials Analysis Corporation) shielded electron microprobe was completed (see Fig. 401-2) except for a few minor components on back-order or returned to the vendor for warranty replacement or repair. Check-out tests indicated that specifications had been met, and the instrument was operational.

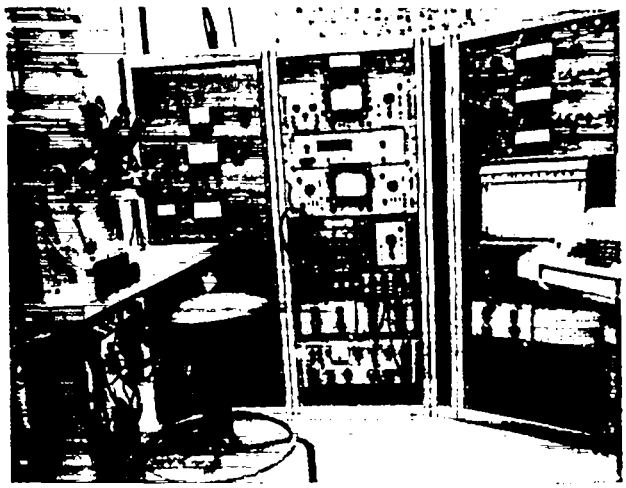

Figure 401-2. Shielded electron microprobe.

A ^{60}Co source having an activity of 100 r/hr was placed in the probe to test the integrity of the shielding and to determine the effects of sample radioactivity on the precision of the x-ray measurements. Surface readings were no greater than 5 mr/hr, and x-ray detection was not adversely affected. Minimum diameter of the electron probe beam was less than 1 μ.

A transfer cart to transport the 800-lb microprobe cask from the sample preparation hot cell to the microprobe laboratory was designed, fabricated, and tested. Figure 401-3 shows the transfer cart in position to receive the sample cask from the microprobe. A vacuum evaporator for depositing thin, electrically

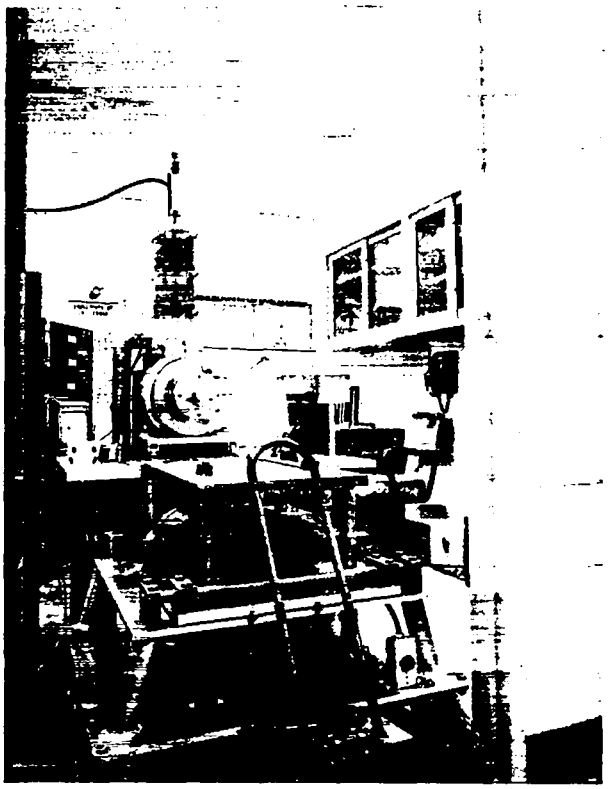

Figure 401-3. Transfer cart in position to receive sample cask.

conducting and protective layers of either carbon or various metals on the sample surface was extensively modified and placed in-cell. Remote operations for coating, loading, and transferring were tested and found to be satisfactory.

At the present time, a sample of EBR-II Driver fuel is being examined.

6. Other Support Equipment

a. A satisfactory procedure has been developed to clean and move a contaminated, polished metallographic specimen from the polishing cell to a cell in which the carbon coating is done, and then to the microprobe shield. The technique employs a combination of ultrasonic cleaning, fax film cover on the polished surface, and a coating with Flo-master ink.[1] The loose alpha contamination is first reduced to a 500-1000 c/m "swipe" level in the corridor. The side and bottom surface of the mount is then coated with the ink film. A second coat is applied after a 30-min drying period. Using this procedure on several trial samples, no loose contamination was found on the coated surfaces. The polished surfaces, protected by the fax film, had a contamination level of < 1000 c/m as determined by measuring the swipes.

b. Various prototype containers were developed to arrive at an acceptable design for sealing sections of fuel pins into containers for storage or shipment. A system has been designed and fabricated which utilizes an electromechanical vertical ram for crimping the end of the container and a soft solder seal applied by a built-in soldering iron. A small modification is in process on this soldering iron after which the apparatus will handle pins up to 16 in. long and 5/16 in. diam and provide a positive containment.

c. The cart for transporting the specimen cask between the hot cells and the microprobe was completed and placed in service. It is shown in Fig. 401-3.

d. An Aminco mercury porosimeter was procured for remotizing and installing at a later date in the same cell which contains the Heat Content apparatus.

e. All major equipment, with the exception of a furnace, is now on hand for the thermal diffusivity measuring system. Further work on diffusivity has, however, been suspended until higher priority tasks are completed.

B. DP West Facility

A feasibility study for examining fast reactor fuel elements at a rate of 150 per year indicated that the eight hot cells at Wing 9 were space-limited. Consequently, it was decided to utilize the four hot cells at DP West as beta-gamma cells (no Pu-bearing materials will be exposed) for the nondestructive tests. The Wing 9 cells will be used for the specialized tests to be carried out in containment boxes.

Designs are presently in progress to modify the building at DP West to accept the large shielded casks and to provide the cells with equipment for the nondestructive tests. All designs are being made in an attempt

(1) The Use of Solvent-Soluble Films in Decontamination, J. W. Schulte, F. J. Fitzgibbon, D. S. Shaffer, Proceedings of the Eighth Conference on Hot Laboratories and Equipment, pp. 332-337 (1960).

to accommodate the 61-in. long unencapsulated fuel pins. It is anticipated that the installation will be completed by July 1, 1970.

Among the capabilities planned for this facility are those listed below. Radiography with the betatron will continue to be done at GT Site.

1. Measurements at Time of Unloading

When the fuel elements are unloaded from the cask, the following measurements are immediately taken:

a. Length and weight
b. Temperature along the length
c. Swipes for alpha and beta-gamma contamination
d. Radiation in r/hr at 1 meter
e. Center of balance

2. Profilometry

A new profilometer for measuring capsules and pins is now being designed based on a Physitech electro-optical sensor. The electro-optical sensor works similar to a shadowgraph and it allows the sensor equipment to remain outside of the cell. The equipment for this system can be divided as follows:

a. The Light Source - to provide uniform light for the shadow image.

b. Pin Transport System - to accurately hold and transfer the pin across the periscope field of view, and to accurately identify the portion of the pin being viewed.

c. Periscope System - to transfer the shadow image from the pin to a ground glass screen in the operating area outside the cell.

d. Ground Glass Screen - to present the pin image to the electro-optical sensor.

e. Electro-Optical Sensor - to translate the optical image into an electrical signal which can be recorded.

f. Data Storage System - to record, store and analyze the data.

Items a, b, c, d, and f will be constructed at LASL. Item e has been ordered from Physitech Corporation and will arrive complete. All systems should be available for operations before July, 1970. It is intended that this profilometer would be adequate for taking measurements on both capsules and pins.

3. Gamma Scanning

A shield assembly utilizing approximately 6 in. thickness of special low radioactivity lead for housing an anti-coincidence counter is in fabrication and has an expected delivery of August 1, 1969.

The Ge-Li crystal has been received from Princeton Gamma Tech. along with a partial shipment of electronic components for the detector. Additional data processing and storage items are on order. Holes have been drilled through the concrete shielding of the gamma scan cell, and additional provisions are being made to accommodate the mechanical equipment.

4. Viewing and Photography

The exterior surfaces of capsules and pins will be inspected and photographed with equipment that had previously been used in the Wing 9 facility.

5. Sampling of Cover Gas in Capsule

Apparatus similar to that in use at the Wing 9 Facility for determining pressure and void volume will be installed. Analysis of the gas sample will be done at another location.

6. Removal of Capsule Clad and Na

The technique used in this operation will depend on the nature and history of the fuel element as well as the requirements of the sponsor.

Differential Thermal Analysis
(D. B. Court, G. R. Brewer)

During the past year, the DTA capability was completed. All operational testing has been completed. Complete calibration of the system remains to be done. Calibrating will be accomplished by observing the thermal arrests of approximately seven standards whose melting points cover the temperature range of 1700°C to 2850°C. The equipment installed is nearly identical to that described in a previous report.[2] Only such changes were made as were required to permit operation in a hot cell.

A secondary unit, for use in DTA work at low temperatures, has been added to the high temperature

(2) Differential Thermal Analysis Apparatus for Observation of Refractory Plutonium Compounds, J. G. Reavis, J. F. Buchen, J. A. Leary, LA Report 4103 (1969).

system. This unit consists of a resistance type laboratory furnace, a nickel furnace tube, sample and reference crucibles, and thermocouples for temperature measurement. Thermocouple outputs are displayed on a two-pen strip chart recorder.

Heat Content Measurement
(D. B. Court, C. E. Frantz, J. R. Trujillo)

The alpha box for heat content measurements is installed and equipped. The heat content measurement will be done by a drop calorimeter. Tests have been made on the calorimeter furnace up to 2200°C, and no limitations on the furnace were observed at this temperature. The furnace should be capable of reaching 2500°C. The calorimeter has been calibrated, and the accuracy of the calibration is about 0.07% standard deviation. Standards, viz. alumina and tungsten, are being prepared to check the calorimeter.

A new type dropping device was designed and fabricated for the calorimeter. The device appears to be adequate for remote hot cell work, but additional tests will be run to provide added assurance.

Since the calorimeter uses specimens sealed in tungsten capsules, a welding fixture was built and installed. Except for the welding probe holder, which is being redesigned, the welder is operating properly.

IV. HOT CELL APPLICATIONS OF METHODS OF ANALYSIS

Identification of Metallic Fission Product Inclusions in Irradiated $(U,Pu)O_2$
(J. W. Dahlby and O. R. Simi)

A 0.1515-g sample of $(U,Pu)O_2$, having undergone approximately 12% burnup, was partially dissolved by repeated treatments with hot HNO_2-HF during a 60-h period followed by heating with 6N HCl. The small quantity of insoluble residue was washed with water, dried, and analyzed semiquantitatively by a spectrographic method. As expected, the residue contained significant concentrations of Mo, Tc, Ru, Rh, and Pd. In addition, Ti, U, Ba, Mg, Al, Ca, Cr, Fe, Cu, B, Si, Mn, Co, Ni, Sr, and Sn were found at concentrations greater than 0.1%.

Measurement of U and Pu
(J. W. Dahlby and G. R. Waterbury)

The controlled-potential coulometric equipment for titrating U and Pu was modified and tested in-cell to show proper functioning with manipulator operation. The modifications for in-cell use consisted of redesign of the titrating cells to use magnetic stirring and simplify hot cell operations by eliminating stirring motors and other apparatus above the titrating cup. The same cup was satisfactory for titrations of either Pu or U by interchanging working electrodes. In-cell titrations of volumetric aliquots of U and Pu solutions lacked the required precision, but repeated analyses of weighed aliquots containing known amounts of U or Pu showed that the precision (1 σ) for a single determination was 0.07 relative percent in titrating Pu and 0.08 relative percent in measuring U. In these measurements, the titration current was integrated while U(VI) was coulometrically reduced at a Hg electrode to U(IV) following a preliminary reduction of more-easily reduced impurities. Titration of Pu involved a quantitative reduction to Pu(III) at a Pt working electrode followed by an oxidation to Pu(IV) while the current was integrated.

The determination of Pu or U was unbiased if the equipment was calibrated using a chemical standard, but a small positive bias existed in the U measurement if electrical calibration was used. Improvement in electrode design and purification of the Ar cover gas in the titration cup reduced the bias to an almost insignificant level of 0.04 relative percent. Further investigation of conditions to eliminate the bias was started.

A $(U,Pu)O_2$ pellet, having undergone 1% burnup, was dissolved, and weighed aliquots taken of the solution. Measurements are now being made of the U and Pu in these aliquots to show the effects on the method, if any, of the highly radioactive fission products.

Microsampling of Fuel Pellets
(G. C. Swanson and G. R. Waterbury)

An ultrasonic "impact grinder" was modified to take microcores of fuel in an inert atmosphere to provide small and pinpointed samples for chemical, mass spectrometric, and x-ray diffraction analyses. Modifications included changing the tip of the tool cone, and replacing the flowing aqueous slurry system for the grinding compound with a small static reservoir of slurry containing 800 grit BC in Dow Corning 200 Fluid. Following

these modifications, the hypodermic needle tip vibrated at 25,000 cycles/sec and an amplitude of 0.0004 in. The sample was held in the slurry in contact with the tip of the needle.

Microcores were taken by full penetration of sintered UC pellets 0.06-in. thick and UO_2 pellets 0.25 in. thick using needles having bores ranging between 0.047 in. and 0.013 in. The smallest microcores were difficult to locate in the slurry, but the sampling method was generally satisfactory.

Work remains to be done in adapting the microsampler for remote operation and to provide an adequate in-cell indexing system.

Measurement of Pd and Rh in U Fissium Alloys
(E. A. Hakkila, H. L. Barker, and R. G. Hurley)

An x-ray fluorescence spectrometric method was developed for determining Rh and Pd in alloys with U. Samples weighing 200 mg were dissolved in HCl, and Y and Ir were added to serve as an internal standard and as a carrier, respectively. The Rh, Pd, Y, and Ir were precipitated hydrolytically by adding $NaBrO_3$ and $NaHCO_3$, the precipitates were filtered through glass fiber filter discs, and the intensities of the Kα x-rays for Rh, Pd, and Y and the Lα_1 x-ray for U were measured from the dried discs. Concentrations were obtained by comparing the Rh/Y and Pd/Y intensity ratios to ratios measured for samples having known compositions. The relative standard deviations for measuring between 100 and 1000 μg of Rh or Pd (0.05 to 0.5%) ranged between 6 and 1%. The method tolerated 0.25% of Nb, 0.5% of Zr or La, 1.5% of Fe or Cs, or 2.5% of Mo, Ru, or W in the samples analyzed. Several non-irradiated U-Pd-Rh alloys were analyzed successfully using this method.

Determination of Burnup
(E. A. Hakkila and R. G. Hurley)

Considerations of recent proposals to determine burnup by measuring the concentrations of fission product Zr, rare earths, or stable ^{148}Nd indicated promise for the nonradioactive isotope as a burnup monitor. A specific determination was required, and an x-ray fluorescence measurement seemed appropriate.

For testing the proposed method, a solution was prepared that contained U, Ru, Rh, Mo, Zr, Nb, and Nd at relative concentrations that would be found in a U fuel having undergone 10% burnup. The Nd, along with Y and Tb added as a carrier and an internal standard, respectively, was separated from U and fluoride-soluble elements by fluoride precipitation. Further purification of the rare earths was effected by adsorbing them from HCl-butanol solution onto cation exchange filter paper. Measurement of the intensities of the Lβ_1 x-ray for Nd and the Lα_1 x-ray for Tb on the paper permitted calculation of intensity ratios which were compared to ratios measured from discs containing known quantities of Nd and Tb. Repeated measurements under optimum conditions of 1 to 50 μg of Nd in aliquots containing 200 mg of U showed that the precision (1 σ) was 0.7 relative percent in measuring 20 to 50 μg of Nd, 5% in measuring 5 μg, and 16% at the 1 μg of Nd level. The method tolerated 50 μg of Ce, 100 μg of La, 500 μg of Er, or 2 mg of stainless steel. A Fortran IV computer program was used to calculate Nd concentrations. It was anticipated that the method would apply to measurement of burnup in irradiated fuels such as the mixed oxide, and further, that it would be adaptable to hot cell operation.

V. EXAMINATION OF UNIRRADIATED FUELS

Examination of PNWL Oxides
(J. A. Leary, M. W. Shupe, E. A. Hakkila, R. T. Phelps, G. R. Waterbury)

Four unirradiated $(U_{0.75}Pu_{0.25})O_2$ pellets have been examined by metallographic, chemical, and x-ray diffraction analysis. The summary report was distributed to PNL and F & M/DRDT on March 6, 1969.

One pellet of $(U,Pu)O_2$ AUA-20 is presently being examined by metallography and electron microprobe analysis.

Examination of UNC Carbides and Oxides
(J. A. Leary, M. W. Shupe, E. A. Hakkila, R. T. Phelps, G. R. Waterbury)

Five (U,Pu)C pellets from UNC batches H and K were evaluated. Examinations performed were immersion densities vs geometric densities, metallographic and microprobe analysis. Emission spectrographic analysis for trace elements and chemical analysis for uranium, plutonium, oxygen, nitrogen and carbon were made on lot K. A macrophotograph of UNC pellets compared with

LASL-CMB-11 carbide pellets was prepared. Results were reported to UNC and F & M/DRDT in document CMB-11-9490 on April 1, 1969.

Samples of $(U,Pu)O_2$ were received from UNC to be examined by alpha autoradiography techniques, metallography, electron microprobe, microhardness, x-ray diffraction, emission spectrochemistry and chemical analysis. These examinations are presently being conducted.

Examination of WAPD Carbides
(J. A. Leary, M. W. Shupe, E. A. Hakkila, R. T. Phelps, G. R. Waterbury)

Eight Westinghouse (U,Pu)C pellets and two $Cr_{23}C_6$ pellets were characterized by metallographic examination and microhardness determination on all phases. Six of the pellets were examined by electron microprobe analysis. In addition, x-ray diffraction, chemical analysis for tungsten and emission spectrochemical analysis were completed on lots No. 511, 514 and 518.

A pellet of modified UC prepared by Atomics International was characterized by metallographic, microhardness, and electron microprobe examinations. The results were compared to a LASL single phase UC specimen.

Document CMB-11-9492 describing the results was transmitted to WARD and F & M/DRDT on April 11.

Examination of EBR-II Driver Fuel Pins
(J. A. Leary, M. W. Shupe, M. Tokar, A. W. Nutt, J. G. Reavis, E. A. Hakkila, R. T. Phelps, G. R. Waterbury)

Characterization of unirradiated EBR-II driver fuel pins has been made. Examinations performed were metallography, electron microprobe analysis, emission spectrographic analysis, differential thermal analysis, thermal expansion, immersion density, and hot hardness.

Results have been reported to DRDT and ANL in weekly reports.

Thermal Conductivity
(K. W. R. Johnson and J. F. Kerrisk)

A 3M, Model TC-200 comparative type thermal conductivity apparatus was installed in an inert atmosphere glovebox. Calibrations were made on 1/2-in. x 1/2-in. right cylindrical specimens of Alloy A-286 and hot pressed UC. These materials were selected because of the potential use of Alloy A-286 for "meter bars" and because of the similarity in the reactivity of UC and future specimens.

Thermal conductivity measurements were made on a series of uranium-plutonium carbide specimens of varying densities. Chemical analysis indicated that each specimen was essentially $U_{0.8}Pu_{0.2}C$ with total nitrogen and oxygen impurities ≤ 1000 ppm. Metallographic examination showed that the specimens were single phase except for two instances where the presence of trace quantities of platelets indicated a second phase.

Shown in Table 401-I are the results of all thermal conductivity measurements on $U_{0.8}Pu_{0.2}C$. The average deviation of the values calculated from the upper and lower meter bar values was 4.13%. The thermal conductivities increased linearly with temperature and also increased with increasing densities.

Table 401-I

Thermal Conductivity of $U_{0.8}Pu_{0.2}C$

Temperature °C	Thermal Conductivity (cal/sec cm °C)	Specimen Density % Theor.
109	0.0244	86.8
228	0.0264	"
556	0.0310	"
823	0.0346	"
1016	0.0369*	"
117	0.0283	89.7
306	0.0290	"
554	0.0327	"
808	0.0383	"
1001	0.0414*	"
120	0.0272	90.5
210	0.0296	"
532	0.0325*	"
93	0.0312	93.0
222	0.0342	"
404	0.0384	"
44	0.0293	"
121	0.0302	"
226	0.0328	"

*Corrected for slight surface oxidation.

Initial measurements on the 93.0 and 93.4% theoretical density samples were terminated prematurely because of excessive oxidation of the specimen at moderate temperatures. After further equipment modification the rate of oxidation was substantially reduced. Some oxidation still occurred at higher temperatures; however, chemical and metallographic evidence showed that the reaction was confined to the peripheral surface of the specimen. Calculated thermal conductivity values at high

temperatures were accordingly corrected to reflect the reduced cross sectional area. Further modifications of the apparatus are anticipated.

A statistical model frequently used to describe the thermal conductivity of a porous material is the simplified Loeb[1] equation:

$$K_p = K_{100}(1-P) \qquad (1)$$

Where, K_p = thermal conductivity of porous material
K_{100} = thermal conductivity of 100% dense material
P = pore fraction

Calculated values for the thermal conductivity of fully dense material varied widely at any given temperature indicating that the model was not applicable to this system. A more general model results in the modified Maxwell[2]-Eucken[3] equation:

$$K_p = K_{100}\left(\frac{1-P}{1+\beta P}\right), \qquad (2)$$

where β is a constant which is characteristic of the pore shape and distribution. Using Eq. (2) to represent the density dependence, and assuming a linear temperature dependence, independent of density, the thermal conductivity of the porous material can be written as

$$K_p = (a + bT)\left(\frac{1-P}{1+\beta P}\right), \qquad (3)$$

where T is the temperature in ^{o}C, and a and b are constants representing the temperature variation of the thermal conductivity. The data in Table 401-I were fitted to Eq. (3) by a least squares method, resulting in

$$a = 0.0394$$
$$b = 0.0000253$$
$$\beta = 4.01$$

Thermal conductivity values predicted by Eq. (3) have a maximum deviation of 7% from the measured values.

(1)A. L. Loeb, "Thermal Conductivity: VIII. A Theory of Thermal Conductivity of Porous Materials," J. Am. Cer. Soc., 37, 2, Pt. II, 96 (1954).

(2)J. C. Maxwell, "A Treatise on Electricity and Magnetism," Vol. I, 3rd Ed., Oxford Univ. Press (1891) reprinted by Dover, N. Y. (1954).

(3)A. Eucken, "The Heat Conductivities of Ceramic Refractory. Calculations of Heat Conductivity from the Constituents," Forsh. Gebiete Ingenieurw B3, Forschungsheft No. 353, 16 (1932).

Further thermal conductivity measurements on single phase, high density material will be made and a study of the effects of stoichiometry is planned.

Equipment has been ordered for thermal diffusivity and electrical resistivity measurements.

Compressive Creep
(M. Tokar)

The compressive creep behavior of the uranium-plutonium ceramic fuels is being investigated so as to obtain information which may be of use in predicting the behavior of these materials under reactor operating conditions. The apparatus used in obtaining the creep measurements is a modification of a design now in use elsewhere[4] for hot-pressing UC-graphite composites. With this apparatus, solid cylindrical specimens about 1/2 in. diam x 1/2 in. long are subjected to compressive loads (8000 psi max) in vacuo. During the creep test the specimen is contained within a graphite die, which is induction-heated. The compressive force is applied by a hydraulic pump.

The amount of deformation of the specimen is determined from measurements of its dimensions before and after the test. These measurements are currently being made with a micrometer at room temperature. Because of the obvious limitations of this method of measurement, an optical extensometer has been obtained which will allow measurements to be made continuously in situ.

Before committing the creep-testing apparatus to use with plutonium-containing materials, hot-pressed uranium monocarbide and dicarbide specimens were used. Data on UC (but not UC_2) are available in the literature[5-7] and can be readily compared to results obtained here, thus

(4)K. V. Davidson, R. E. Riley, and J. M. Taub, "Carbide-Graphite Composites," Report LA-3569-MS, Los Alamos Scientific Laboratory (1966).

(5)J. J. Norreys, "The Compressive Creep of Uranium Monocarbide," Carbides in Nuclear Energy, Vol. 1, Harwell (1963).

(6)D. E. Stellrecht, M. S. Farkas, and D. P. Moak, "Compressive Creep of Uranium Carbide," J. Amer. Cer. Soc., 51 (8), 455-8 (1968).

(7)M. H. Fossler, F. J. Huegel, and M. A. DeCrescente, "Compressive Creep of UC and UN," Report PWAC 482 (Oct., 1964).

providing a check on the accuracy and reliability of the test apparatus. A graphical comparison of data on UC at 1300°C is shown in Fig. 401-4. The creep rates determined here at 1300°C, 4000 and 6000 psi are in reasonably good agreement with Norreys[5] and Stellrecht et al.[6] The differences in creep rate shown in the figure appear to be due to differences in specimen microstructure rather than to differences in testing procedure.

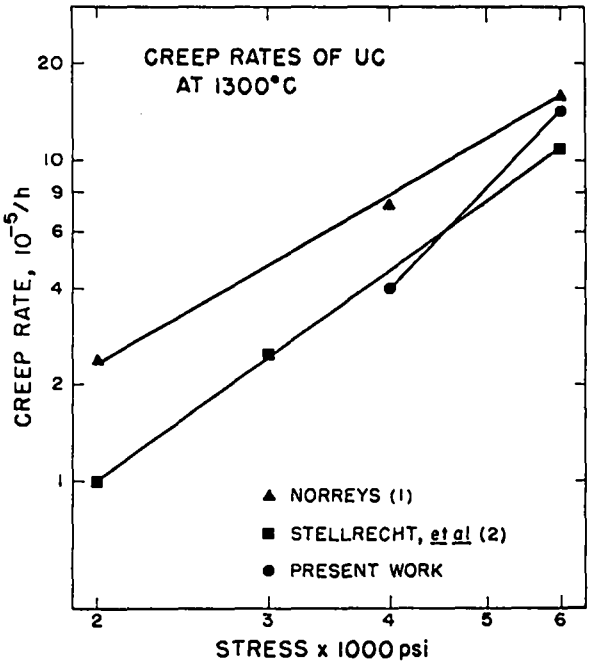

Figure 401-4

Specimens of $U_{0.8}Pu_{0.2}C_{0.96}$ of about 95% theoretical density are now being tested at temperatures from 1200-1500°C and stresses of 2000-6000 psi. These specimens are single-phase, containing no dicarbide or sesquicarbide, but future work will include an investigation of the effects of carbon content on creep rate.

Creep is highly structure-sensitive and microstructural variables of interest here include grain size, porosity, and amount, shape, and distribution of secondary phases. Ceramographic examinations and density measurements of the $U_{0.8}Pu_{0.2}C_{0.96}$ creep specimens have revealed that the porosity is relatively unchanged by the creep test; i.e., the amount, distribution and shape of the pores remain constant. Likewise, grain size measurements have shown that the grain size (about 20 μm) does not change appreciably. Ceramographic examinations have revealed, however, that specimens which were initially single phase and which were tested under low vacuum (~ 15 μ of Hg) contained second-phase platelets following tests. These specimens yielded classic-appearing creep curves with a small initial region of decreasing creep rate (primary creep) followed by a constant creep rate region (secondary creep). Since the changes in slope of these creep curves coincided with the formation of second-phase platelets, doubt was cast on the validity of the tests, and a diffusion pump was installed to provide a high vacuum. Specimens have now been tested at 1 x 10^{-6} Torr, 1400°C, at pressures from 2000-4000 psi. These specimens had creep rates on the order of 10^{-2}/h vs 10^{-5}/h for the low-vacuum test specimens. Ceramographic examinations and chemical analyses are now being conducted on these specimens to determine the reasons for these differences in creep behavior.

Hot Hardness
(M. Tokar)

A microindentation hardness tester has been installed for use at elevated temperatures. The furnace is resistance-heated with a molybdenum wire heating element wound around an aluminum silicate muffle. The specimen, heating element, indentor (200 g load) and stainless steel radiation shields are all enclosed in a water-cooled stainless steel bell jar in which vacuums of ~ 1 x 10^{-6} Torr are maintained during the heating and cooling cycle. The maximum temperature is presently limited to about 1000°C, mainly due to the temperature limitations of the muffle, radiation shields, and indentor materials (sapphire or diamond). Modifications are being made in the apparatus which will raise the upper limit of test temperature to at least 1500°C. A B_4C indentor is being fabricated, and tantalum radiation shields will be used in place of the stainless steel.

Before contaminating the apparatus with plutonium, it was used to test the hot hardness of materials such as

347 stainless steel and Armco ingot iron. Armco iron is a particularly interesting material to test because of the bcc to fcc transition at 910°C. The diamond pyramid hardness vs temperature from 500-1005°C is shown in Fig. 401-5. These results are in good agreement with those of Hallerman and Gray,[1] particularly with regard to changes in slope near the transformation temperature.

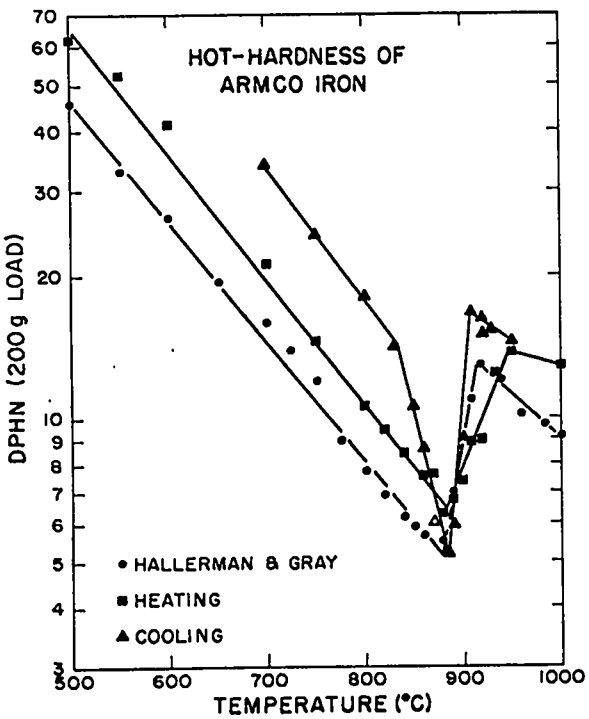

Figure 401-5

The hot hardness tester has also been calibrated at room temperature on several standard hardness blocks and the results cross-checked against a Leitz hardness tester. The Leitz hardness tester and the hot hardness tester results agreed within ± 5%.

The hot hardness apparatus has now been committed to use with plutonium-containing materials. Materials which have been tested include U-15% Pu-6.8% Zr alloy and U-5% Fs. Future work will include the testing of the mixed U-Pu carbides, with particular emphasis on the effects of plutonium and carbon content on hardness at elevated temperatures.

(1)George Hallerman and R. J. Gray, "Equipment for Hardness Testing at Elevated Temperature," Report ORNL-3448, July 31, 1963.

VI. LMFBR/FFTF MIXED OXIDE ANALYTICAL STUDIES

FFTF Analytical Chemistry Program

A program was designed and executed that had as its main objective to uncover the problems that might exist in adequately characterizing FFTF mixed oxide fuel. This was accomplished by having the interested potential fuel suppliers make as many measurements as the experience and laboratory equipment of each would permit. Pellets of mixed oxide fuel were supplied by PNL. The measurements program was designed around the tentative specifications developed by PNL. This program which was called Phase I is described in a separate report, forwarded under cover letter dated May 9, 1968. The results of the program are described in a separate report, CMB-1-861, dated November 1, 1968.

A statistical analysis of the data obtained in Phase I indicated clearly the needs for common standards for methods calibration, standardization of certain methods, updating of equipment in some cases and the development of better methods in some instances.

In order to plug these loopholes, Phase II was developed and essentially completed by June 30, 1969. A summary of Phase II will appear as a separate report as soon as feasible. It is expected that these data will be valuable in developing a statistically designed program of sampling and analysis for fuel suppliers.

Discussions were held with PNL representatives concerning supply problems and an analytical program for the starting materials UO_2 and PuO_2. These are reported in a separate Trip Report dated July 15, 1969.

In addition to the above activities, the following work has been done as a part of the development of analytical methods necessary to the program.

Development of Methods

Determination of F in Sintered $(U,Pu)O_2$
(T. K. Marshall and G. R. Waterbury)

The fluoride ion specific electrode was shown to be applicable to measurement of F at trace concentrations in U_3O_8, used as a stand-in for sintered $(U,Pu)O_2$, by

making repeated determinations of 1 to 10 μg quantities added as NaF to 1-g portions of the sintered oxide. In these analyses, the pyrohydrolytic separation of F^-, that had been proved to be satisfactory in previous work, was coupled with the specific ion electrode measurement of the F^- in the distillate.

First attempts to use the electrode were unsuccessful because the internal electrolyte had dried up, and very erratic readings were obtained. It was found that the electrode could be rejuvenated by disassembly, cleaning, and recharging with a solution 0.1M in NaF and KCl. The electrode was then calibrated using six HF solutions containing known concentrations of F^- between 0.010 and 0.206 μg/ml. The calibration curve was not linear, making the use of several concentrations mandatory.

The pyrohydrolysis was carried out in an all-nickel apparatus by passing steam, generated from slightly alkaline H_2O containing $KMnO_4$, over the sample until approximately 50 ml of condensate were collected. The F^- was measured with the electrode, and then titrated with $Th(NO_3)_4$ for comparison. The results obtained by the two measurement methods were approximately equal, and the less-sensitive titrations were discontinued. The average recovery of 1.9 to 9.3 μg of added fluoride was 97% and the precision (1 σ) was 4%, showing satisfactory operation of the method.

The effects on the F^- recovery caused by use of a SiO_2 boat and/or furnace tube in the pyrohydrolysis were investigated. Known quantities of F^-, as NaF, between 0.9 and 9.3 μg were added to 1-g samples of U_3O_8 to prepare test samples. Between thirteen and eighteen test samples were analyzed under each of the following conditions: (1) Ni furnace tube - SiO_2 boat, (2) SiO_2 furnace tube - Ni boat, and (3) SiO_2 furnace tube - SiO_2 boat. Average recoveries of F^- were: (1) 94%, (2) 90%, and (3) 85%, under the respective conditions, as compared to 97% recovery using an all Ni system. Determinations of F^- added to $(U,Pu)O_2$ are under way.

O/M Ratios in Sintered $(U,Pu)O_2$

(J. W. Dahlby, T. K. Marshall, G. C. Swanson, G. R. Waterbury)

One of the thermogravimetric methods[1] proposed for determining the O/M ratio of mixed oxide fuel recommends that the sample be heated to 750°C in air to form a slightly hyperstoichiometric mixed oxide, then reduced to the stoichiometric oxide by heating at 700°C in a reducing atmosphere of He - 6% H_2. The final result is based on the assumption that under these reducing conditions the final oxide is actually stoichiometric. A test of this assumption was made by starting with very high purity metals (> 99.99% pure) and carrying each through the recommended procedure. It was observed that a final heating at 700°C was not an adequate temperature to produce a stoichiometric oxide in either case. The temperature at which stoichiometry was obtained was 1000°C. (The O/M ratios at 700°C were 2.019 for the dioxide and 2.010 for the Pu dioxide.) A similar situation was found with a mixture of U and Pu dioxides in the ratio of 3 to 1.

Another thermogravimetric method[2] is based on the thermodynamic calculations that indicate the mixed oxide should be stoichiometric at a temperature of 800°C in an atmosphere having an oxygen potential equivalent to 4 mm partial pressure of H_2O. This method recommends the sample be heated to 800°C in an atmosphere of Ar-8% H_2-4 mm partial pressure H_2O. Each high purity metal, when heated under these conditions produced a hyperstoichiometric oxide, as did a mixture of oxides in the ratio of 3 U oxide to one Pu oxide. (U gave an O/M ratio of 2.019; Pu gave an oxide of 2.016, and the mixture gave an O/M ratio of 2.017.) When the mixed oxide (3 U oxide to one Pu oxide) was heated in Ar-8% H_2-4 mm partial pressure H_2O at 1000°C, the average O/M ratio was reduced to 2.008. When heated to 1000°C in dry He-6% H_2, O/M ratios of 2.001 ± 0.001 were observed.

It was concluded from the above data that neither method would produce an unbiased result unless modified as indicated above.

A third method,[3] developed by LASL, involves measurement of total oxygen as well as the U and Pu.

---

(1) Lyon, W. L., GEAP-4271 (1963).

(2) Chikalla, T. D., "Quarterly Progress Report, Oct.-Dec., 1966," F. W. Albaugh et al, pp. 4.1, BNWL-CC-957 (1967).

(3) MacDougall, C. S., Smith, M. E., and Waterbury, G. R., Analy. Chem. 41, 372 (1969).

The O/M atom ratio is calculated from these measurements.

Unfortunately each of the above methods is subject to bias from impurities. A correction can be made if the extent and nature of these are known.

These studies are being continued using sintered pellets as the starting material.

Gas Evolution from Sintered $(U,Pu)O_2$
(D. E. Vance and M. E. Smith)

One of the specifications under consideration for FFTF fuel is total gas evolution, including water vapor. An apparatus was constructed for measuring separately the quantities of H_2O evolved at 800°C from one pellet, and of other gases evolved as another sample was heated to 1600°C. The H_2O was swept by Ar through a moisture monitor, and the total quantity of H_2O was obtained by electronically integrating the monitor signal. Then the system was evacuated prior to the measurement of other volatiles, and the gases evolved at 1600°C were collected with a Toeppler pump. The volume and pressure of the collected gases were measured, and provision was made for sampling the gas for mass spectrometric analysis. Testing of the apparatus was started.

The furnace is capable of temperatures as high as 2200°C, and a new furnace capable of heating samples to 2500°C is being considered.

Measurement of N_2 in $(U,Pu)O_2$
(G. C. Swanson and J. W. Dahlby)

A LECO Nitrox-6 analyzer was calibrated for measuring N_2 in $(U,Pu)O_2$. The advantage of this instrument is that dissolution of the sample is not required without the tedious sample dissolution required in the Kjeldahl method. A linear calibration curve was obtained from which relative standard deviations, ranging from 30% to 12 μg of nitrogen to 2% for 160 μg were calculated. The analyzer was modified to place the sample loader, furnace tube, and induction coil in a gloved box for analysis of Pu materials. Testing will resume when installation is completed.

Determination of C in Sintered $(U,Pu)O_2$ Pellets
(C. S. MacDougall and M. E. Smith)

Preliminary tests of a combustion manometric method for measuring C showed that grinding of sintered $(U,Pu)O_2$ pellets was required to ensure quantitative oxidation of the C at 1000°C in a stream of O_2. Grinding of the oxide in a stainless steel mixer-mill capsule was satisfactory only in a C-free inert-atmosphere enclosure. Concentrations of 2 to 3 ppm of CO_2 in the enclosure atmosphere were found to exist if this impurity was not removed completely by molecular sieve. Reconditioning of the molecular sieve in the gas purification system at a temperature not lower than 300°C while purging with dry He was recommended. The CO_2 content of the inert-atmosphere was held by the reconditioned molecular sieve at a level so low that a ground sample could be left exposed for at least 2 weeks without apparent increase in C content. With this sample preparation, the method performed satisfactorily in measuring C in the sintered oxides.

Determination of U and Pu in Sintered $(U,Pu)O_2$
(G. B. Nelson, W. W. Wilson, G. R. Waterbury)

Testing of previously reported controlled-potential coulometric and potentiometric titration methods was continued by repeatedly analyzing sintered $(U,Pu)O_2$ pellets for U and Pu without prior separation of these elements. The potentiometric method titrates Pu(VI) to Pu(IV) with standardized Fe(II) without interference from U. The U concentration is calculated by subtracting the Pu concentration from the total Pu and U measured by titrating Pu(III) and U(IV), obtained by reduction in a Pb reductor, with Ce(IV) to U(VI) and Pu(IV). The coulometric method measures the quantity of electricity to oxidize Pu(III) to Pu(IV), following electrolytic reduction of all Pu to the (III) oxidation state, or the quantity of electricity to reduce U(VI) to U(IV), following a pre-reduction of easily reduced impurities.

The results of ten to twelve measurements of each element by each method showed that the relative standard deviations of the coulometric titrations were 0.13 and 0.14%, respectively, in measuring U and Pu. The precisions (1 σ) for the potentiometric titrations were 0.06 and 0.08 relative percent in measuring U and Pu. The average U concentration by coulometry of 66.25% was slightly higher than the 66.13% obtained by potentiometric titration. The average Pu concentrations by the two

methods were 22.06 and 22.05%.

The effect of small amounts of Am on the controlled-potential coulometric titration of Pu was determined by titrating aliquots containing 7 mg of Pu and between 170 and 6800 ppm of Am. Five to eight titrations were made at each of five Am concentrations. The average recoveries of Pu ranged from 99.91 to 100.06% and the precision (1 σ) was in the range between 0.04 and 0.10 relative percent, showing that at least 0.68% of Am was tolerated by the method.

Determination of O_2 in $(U,Pu)O_2$: Gas Chromatographic Method

(D. E. Vance, M. E. Smith, C. S. MacDougall)

Investigation of an inert-gas-fusion method utilizing a gas chromatographic finish was completed with a comparison of results obtained by this method and by a previously described gravimetric method. In either method, 1 g of the oxide is mixed with 0.2 g C and pressed into a pellet which is heated to 2000°C in a C crucible to evolve the O_2 as CO and CO_2. In the gravimetric method the gases are weighed as CO_2. For the gas chromatographic measurement, the CO and CO_2 are mixed with Ne internal standard, and the chromatographic peaks are integrated electronically to provide a measure of the O_2.

Results for ten determinations by each method on one lot of powdered $(U,Pu)O_2$ were 11.88% O_2 with a relative standard deviation of 0.8% by the chromatographic measurement, and 11.80% with a relative standard deviation of 0.2% for the gravimetric method. Because of the substantially better precision by the gravimetric method, investigation of the chromatographic method was discontinued.

VII. REQUESTS FROM DRDT

A. Examination of Irradiated Material

(R. J. Bard, D. M. Holm (K-1), K. A. Johnson, E. D. Loughran (GMX-2), J. W. Schulte, J. F. Torbert (GMX-1), J. R. Trujillo, G. R. Waterbury)

1. Examination of Irradiated Peach Bottom Reactor Fuel Element

Investigations were made of several sections of sleeve and of portions of 8 fuel compacts from a failed fuel element. Examinations included macrophotography, measurements of physical properties, chemical and spectrographic analyses, and metallography. Meaningful correlations of chemical analyses for U and Th were made with data for bead loadings in the compacts, and techniques were developed to obtain chemical evidence, as well as metallographic, for the extent of bead coating damage. Based upon results of the investigation, a mode of failure of the element was postulated. A final report describing the investigation was sent to GGA and DRDT (CMB-1494, November 7, 1968).

2. Examination of EBR-II Driver Fuel Elements Containing ANL Fuel

The extensive investigations of 6 irradiated and 5 unirradiated EBR-II Driver Fuel Rods, received in January, 1968, were completed. Many of the examinations were finished and reported in LA-3993-MS, the Second Annual Report, FY 1968. The results of subsequent work are given below:

a. Isotopic Analysis

The isotopic compositions of the U in sections taken from the top, middle, and bottom of each of 4 irradiated and 3 unirradiated fuel pins were measured on a mass spectrometer. The compositions (Table 401-II) of the unirradiated pins were within the concentration ranges listed in Product Specifications for the EBR-II Driver

Table 401-II

Mass Spectrometric Analyses of U Isotopic Compositions

Sample	U Isotopic Concentration, % 235	234 + 236 + 238	234 + 236
0121 H-05 (Unirrad.)			
Middle	52.20	47.80	< 1.0
Bottom	52.15	47.86	< 1.0
0121 H-27 (Unirrad.)			
Middle	52.28	47.71	< 1.0
Bottom	52.14	47.86	< 1.0
4087-53 (Irrad.)			
Top	51.26	48.43	< 1.0
Middle	51.02	48.66	< 1.0
Bottom	51.15	48.43	< 1.0
4088-100 (Irrad.)			
Top	51.37	48.08	1.0
Middle	51.18	48.41	1.0
Bottom	51.25	48.44	1.0
SL 42-17 (Irrad.)			
Top	51.83	47.03	< 1.0
Middle	51.26	48.62	< 1.0
Bottom	51.43	48.30	< 1.0
Specified Concentrations[a]	52.18 ± 0.50	47.82 ± 0.50	< 1.0

[a]Product specifications for unirradiated EBR-II Driver Fuel Elements, FCF-1.

Fuel Elements, FCF-1. As expected, burnup of the ^{235}U in the unirradiated fuel pins reduced the concentration of this isotope and increased the relative concentrations of other isotopes.

b. Electron Microprobe Examinations

A top and a bottom section of fuel pin 0121-H-05 were examined to identify inclusions and to determine distributions of the fissium elements. Niobium was not detected in either sample showing that Nb was not segregated to the extent that concentrations higher than the 0.05% detection limit existed in isolated areas. The other fissium elements (Mo, Ru, Rh, Pd, and Zr) were found throughout the matrix and also in two types of inclusions. The more common inclusion contained only U and Zr. The less common inclusion generally occurred in grain boundaries and contained Ru, Pd, Rh, Mo, Si, and U.

3. Examinations of EBR-II Driver Fuel Elements Containing AGC Fuel

DRDT was provided with a Weekly Report of the results from these examinations, consequently only brief mention will be made of the types of examinations conducted on the 5 fuel elements (2 irradiated and 3 unirradiated) which were received from ANL.

a. Nondestructive Tests on Fuel Elements

Examinations carried out on the fuel elements are listed in Table 401-III.

Table 401-III

Nondestructive Examination of EBR-II Fuel Elements

Description of Test	Fuel Element Identification				
	3481-119[a]	1136-115[a]	2249-100[a]	2421-119[b]	1682-115[b]
Photography	--	—	—	x	x
Weight	x	—	x	x	x
Diameter, Length	x	x	x	x	x
Center of Balance	x	x	x	x	x
Contamination Swipe	x	x	x	x	x
Temperature readings	—	--	--	x	x
Radiation readings	—	—	—	x	x
Eddy Current	x	—	x	x	x
Radiography	x	x	x	x	x
Gamma Scanning	—	—	—	x	x

[a] Unirradiated fuel element

[b] Irradiated fuel element

b. Chemical Analyses of Fuel Elements 1136 (Unirrad.) and 1682 (Irrad.)

Fuel: Concentrations of U, Mo, Ru, Rh, and Pd in the unirradiated fuel pin and of U, Mo, Ru, and Pd in the irradiated fuel pin were determined by spectrophotometric methods. Determinations were made on solutions prepared by dissolving 0.1- to 1.0-g samples taken from the top, middle, and bottom of each pin. Emission spectrographic determination of impurities were made on samples taken from the top and bottom halves of each fuel pin. Electron microprobe examinations of metallographically polished sections from each pin were started simultaneously, using one shielded and one unshielded instrument.

c. Analyses Performed on Fuel

The types of analyses performed on the fuel are shown in Table 401-IV below.

Table 401-IV

Fuel from Element No.

Type of Analysis	3481-119	1136-115	1682-115
Metallography	--	x	x
Hot Hardness	—	x	—
DTA	--	x	x
Dilatometry	—	x	—

d. Gas Analyses

Samples of gas from fuel elements 1136 (unirrad.) and 1682 (irrad.) were analyzed mass spectrometrically, and isotopically on No. 1682.

4. Examinations of Al Fuel and Flux Monitoring Wires

Four flux monitoring wires and 120 UC pellets doped with W from EXP-NRX-9-101 Irradiation Experiment were received for specific examinations. Contamination swipes and radiation level readings were obtained on four wires, and gamma scans were completed on three wires. Seven 0.25-in. sections from one Al-Co wire were analyzed radiochemically to measure the absolute specific activity of each section. Gamma scanning and radiochemical analyses are in progress on the remaining wires.

Two of the pellets were examined metallographically, and replicas were prepared for evaluation by AI. Four of the pellets were packaged and shipped to Idaho Nuclear Corporation for burnup analyses.

5. Examination of Irradiated Pins and Capsules from BNWL

Twelve assemblies (11 capsules and 2 pins) were received from BNWL during FY 1969. Since detailed reports were provided to BNWL and DRDT at frequent

intervals, only those examinations and operations which were performed on the fuel elements and components are listed in Table 401-V. In the table, "C" indicates that the capsule was examined, whereas "P" indicates pin. In some cases the examination was performed on both capsules and pins.

a. Physical Measurements

Table 401-V
Examination of Pins and Capsules from BNWL

Operation or Measurement	Identification of Capsules and Pins											
	PNL-1					BNW-1		PNL-X				
	15	16	17	18	19	9	11	1	3	4	6	7
Balance point	-	-	-	-	-	-	-	C	C	C	C	C
Temperature	P	C	P	C	P	C	C	C	C	C	C	C
Radiation	P	C	P	C	P	C	C	C	C	C	C	C
Photography	P	CP	P	CP	P	CP	CP	CP	CP	CP	CP	CP
Radiography	P	C	P	C	P	C	C	C	C	C	C	C
Profilometry	P	P	P	P	P	P	P	P	P	P	P	P
Diameter by micrometer	-	-	-	-	-	-	-	C	C	C	C	C
Clad removal	-	C	-	C	-	C	C	C	C	C	C	C
Gas sample (and analysis)	P	CP	P	CP	P	CP	CP	CP	CP	CP	CP	CP
Metallography	P	-	P	-	P	P	P	-	-	-	-	-
Replication	P	-	P	-	P	P	P	-	-	-	-	-
α autoradiography	P	-	P	-	P	P	P	-	-	-	-	-
β-γ autoradiography	P	-	P	-	P	P	P	-	-	-	-	-

In addition to all results being furnished to BNWL, original data or suitable copies were provided wherever feasible.

b. Chemical Analyses

The kerosene used to wash the retained traces of NaK from capsule BNW-1-9 was analyzed qualitatively for metallic constituents by an x-ray fluorescence method in an attempt to determine the cause of the red-brown color of the wash liquid.

A sample of Na from an irradiated capsule (PNL-X-1) and a black reticulate coating on the stainless steel cladding above the Na were analyzed semi-quantitatively by spectrographic methods to determine the impurity content of the Na and to identify the black coating. As a basis for comparison, Na from an unirradiated capsule also was analyzed.

6. Examination of Irradiated Pins and Capsules for UNC

The examinations performed on three mixed carbide pins from UNC are listed in Table 401-VI.

7. Examination of Irradiated Capsules from Westinghouse (WARD)

Three Westinghouse capsules each containing 3 mixed carbide pins were received on February 19. The following operations have been carried out on the capsules:

Table 401-VI
Examination of Pins and Capsules from UNC

Operation or Measurement	Identification of Capsules and Pins		
	UNC-87	UNC-89	UNC-90
Temperature	C[a]	C	C
Radiation	C	C	C
Photography	CP[b]	CP	CP
Radiography	C	C	C
Gamma scanning	C	C	C
Clad removal	C	C	C
Profilometry	P	P	P
Gas analysis	C	C	C

[a] Measurement taken on capsule

[b] Measurement taken on pin

radiation and temperature measurements; visual inspection and photography; and radiography. When gamma scanning is completed, the NaK and capsule clad will be removed to retrieve the individual pins for further measurements.

8. Examination of Irradiated Mixed Carbide Capsule for LASL

An irradiated mixed carbide capsule identified as LASL 42-B was received from the EBR-II on February 7, 1969. The following nondestructive tests were performed: (a) Radiography; (b) Gamma Scanning; (c) Diameter Measurements by Micrometer; (d) Temperature Along the Length; (e) Radiation Measurements.

Approval was received for re-inserting the capsule in EBR-II, and it was returned to Idaho.

9. Shielding Integrity Test of the Paducah Cask

The hot cell facility was used for testing the the attenuation of the radiation from 90,000 Ci of ^{60}Co which was placed in the cavity of the Demonstration Cask fabricated at Paducah. The cask had been previously subjected to the hypothetical accident conditions listed in Chapter 0529 of the AEC Manual. The results, on the basis of radiation measurements, indicated the cask had no significant voids.

The attenuation provided by the walls of the hot

cell facility were adequate for handling of the 90,000 Ci of ^{60}Co. A previous integrity test of the walls indicated that ~ 50,000 Ci of fission products could be safely handled.

VIII. PUBLICATIONS

"Radiographic Inspection of Irradiated Fuel Elements Using the 22-MeV Betatron," Proceedings of the 16th Conference on Remote Systems Technology, Amer. Nucl. Soc., pp. 22-27, 1969.

"Health Physics at the Los Alamos 'Wing 9' Hot Cell Facility," LA-4074.

"Gravimetric Determination of O_2 in Pu and U Oxide Fuel Materials; Inert Gas Fusion," C. S. MacDougall, M. E. Smith, G. R. Waterbury, Twelfth Conference on Analytical Chemistry in Nuclear Technology, October 8-10, 1968, Gatlinburg, Tenn.

"An Evaluation of Two Methods for Determining U and Pu in Ceramic Reactor-Fuel Materials," G. B. Nelson, K. S. Bergstresser, G. R. Waterbury and C. F. Metz, Twelfth Conference on Analytical Chemistry in Nuclear Technology, October 8-10, 1968, Gatlinburg, Tenn.

"Characterizing Compositions of Irradiated Fuel at Operating Temperatures-Future Needs," G. R. Waterbury and C. F. Metz, Proceedings of the 16th Conference on Remote Systems Technology, March 11-13, 1969, 301-306, Amer. Nucl. Soc., Hinsdale, Ill.

PROJECT 462

SODIUM TECHNOLOGY

Person in Charge: D. B. Hall
Principal Investigator: J. C. Biery

I. INTRODUCTION

For the successful operation of high temperature sodium systems contemplated for use in fast, central station reactor concepts, impurities in the sodium must be monitored and controlled. Nonradioactive impurities such as oxygen must be maintained at low concentration levels to limit corrosion processes. Radioactive impurities introduced into sodium from failed fuel elements should be removed to facilitate "contact maintenance" and to minimize safety and detection problems. To control the levels of these impurities, a knowledge of their behavior and interactions in sodium must be developed. Acquisition of this information has been subdivided in the LMFBR Program Plan into a number of task areas. The sodium technology program at LASL has projects which contribute to six of these areas. The broad tasks and current LASL projects within those areas are summarized below:

Task Area 1: Materials Compatibility

- A. Correlation of sodium and helium leaks.
- B. Study of carbon transport in thermal convection loops.

Task Area 2: Sodium Purification

- A. Study of sodium oxide kinetics in cold traps.
- B. Study of soluble getters for removal of impurities from sodium.
- C. Study of gas diffusion through metals into sodium.

Task Area 3: Fission Products in Sodium Systems

- A. Study of fission product distribution in loop experiments.
- B. Study of fission product gettering in capsule experiments.

Task Area 4: On-Line Monitoring Methods

- A. Plugging meter studies.

Task Area 5: Sampling and Analysis

- A. Vacuum distillation studies.
- B. Study of gamma ray activation analysis for Carbon and Oxygen.
- C. Absorption spectrometry development for metal impurity analysis.
- D. Total carbon analysis development.
- E. Development of remotely operated distillation samplers for EBR-II.

Task Area 7: Cover Gas and Maintenance Atmospheres

- A. Development of a high temperature quadrupole mass spectrometer for cover gas analysis.

Details of the work in these programs are presented below.

II. MATERIALS COMPATIBILITY

A. Correlation of Sodium and Helium Leaks
(J. P. Brainard, D. C. Kirkpatrick)

1. General

The correlation of sodium leak development with measured helium leak rates observed during acceptance testing provides information on the degree of component integrity which must be attained for safe, long-term sodium plant operation. No firm criteria now exist that establish acceptable levels of leak-tightness for various situations.

This study uses fabricated stainless steel leaks and leaks that occur naturally in stainless steel bar stock. The length of the leaks tested is 1/4 in. Selected samples having a range of helium leak rates are incorporated into small sodium systems (Fig. 462-1) which are held at predetermined temperatures. Thirty-six cm^3 of sodium and a helium cover gas at

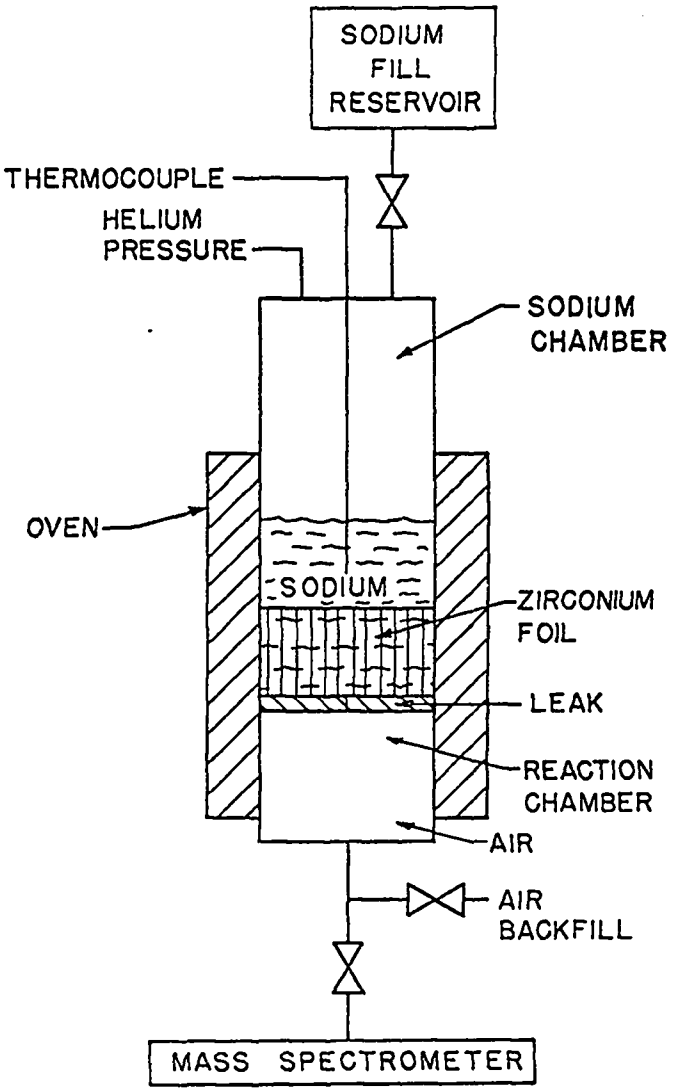

Fig. 462-1. Schematic of the Test Cell.

5 psig are placed above the leak in the sodium chamber. The reaction chamber under the leak is filled with air (atmospheric pressure). The air is analyzed periodically in a mass spectrometer and the chamber is then refilled with air. The absence or reduction of the oxygen peak in the air sample indicates a sodium leak into the reaction chamber. From these observations it may be possible to establish, for mass spectrometer acceptance tests on sodium system components, the maximum tolerable helium rate which is consistent with adequate long-term containment of sodium by that component.

An interesting side effect from this work has been observation of the elusiveness of what are considered to be large leaks (10^{-5} to 10^{-6} atm cm^3/sec). Normal contaminants such as grease, water and some solvents can completely mask leaks of this size and invalidate a leak test, unless proper pretreatment of the component is performed. In some cases this treatment involves firing of the component in a hydrogen atmosphere. If meaningful helium leak tests are to be performed on LMFBR components, procedures must be developed for treating and handling of the part prior to leak test.

2. Results in FY 1969

Eight leaks have been tested: four at 400°C and four at 650°C. Data on these test specimens are given in Table 462-I. The experimental apparatus is shown in Fig. 462-2.

Three of the 400°C cells have not leaked sodium after 420 days of operation. Recent observations after 370 days of exposure show a slight leak in Cell 4 of approximately 2×10^{-4} cm^3/day. The reaction chambers of these cells were preoxidized for three days prior to sodium insertion to prevent stainless steel oxidation from interfering with measurement of possible sodium oxidation.

Within 93 days of operation, all the 650°C cells with the exception of the control cell (No. 6) leaked sodium. These cells were preoxidized for one day. Cell 7, with an initial helium leak rate of 10^{-1} atm cm^3/sec, leaked and filled the reaction chamber with sodium during the first day in test. The sodium leak rate was at least 25 cm^3/day and was very likely greater because the measurement was made after a day of operation, i.e., the reaction chamber could have been filled in much less than a day.

Cell 5, with an initial helium leak rate of 6.8×10^{-6} atm cm^3/sec, began to leak sodium after 18 days of operation. A sodium leak rate of approximately 1 cm^3/day was calculated by assuming a uniform leak rate over the time of leakage and by radiographically determining the amount of sodium that had flowed out of the cell.

Cell 8, which was plugged by metal oxides, began leaking sodium after 93 days. The leak was estimated to be about 2×10^{-2} cm^3/day. The leakage followed an accidental power outage to the ovens. Thus, thermal cycling may play a role in sodium leakage. This leak is being allowed to continue in order to observe sodium leak development.

Each cell contains approximately 11 g of zirconium foil in the sodium chamber. The ability of

Table 462-I

Test Specimen Data

Cell No.	Type of Leak Stainless Steel Type: 304	Initial He Leak Rate (Room Temp.)	Test Temp.	History of Sample Prior to Sodium Exposure
1	Fabricated from tube	1.1×10^{-4} atm cm^3/sec	400°C	Leak rate doubled during initial heat treatment. Vacuum fired.
2	Fabricated from tube	None	400°C	Sealed shut during fabrication. Vacuum fired.
3	Flaw in bar stock	1.7×10^{-4} atm cm^3/sec	400°C	Vacuum fired. This leak sealed during preoxidation of the cell.
4	Flaw in bar stock	None	400°C	Known to have flaw, but did not open with vacuum firing.
5	Flaw in bar stock	6.8×10^{-6} atm cm^3/sec	650°C	Opened by hydrogen firing, closed by heating in air, then reopened by hydrogen firing.
6	Solid bar stock	None (Control Specimen)	650°C	Hydrogen fired.
7	Flaw in bar stock	1.2×10^{-1} atm cm^3/sec	650°C	Opened to 1×10^{-4} atm cm^3/sec by vacuum firing, was then hydrogen fired, heated in air, and hydrogen fired.
8	Flaw in bar stock	None (Metal oxide plugged)	650°C	Opened to 3.5×10^{-6} by hydrogen firing, closed by heating in air, remained closed after hydrogen firing.

the foil to remove oxygen from the sodium serves two purposes: first, to keep the sodium clean, and second, to measure the oxygen intake into the system through the leak. Each cell's zirconium is accurately weighed before and after an experiment to determine its oxygen intake during the experiment.

The zirconium has been weighed before and after operation of Cells 5, 6, and 7. There appears to be no correlation between the initial helium leak rate and the observed weight increase. Because the sodium used in the experiment was pre-exposed to zirconium at 600°C, and initially contained little oxygen, it is believed the increase in weight is due to the sodium leaching oxygen from the stainless steel and the subsequent zirconium reaction with this oxygen. Apparently, the large source of oxygen from the stainless steel overshadows that of the leaks. It was calculated that about 5×10^{-5} g O_2/cm^2 of stainless steel was transferred from the stainless steel to the zirconium.

A simple mathematical model was developed in an attempt to explain the mechanics of sodium leakage. This model assumes that a sodium oxide plug in the leak channel prevents leakage of liquid sodium. The plug behavior has been mathematically studied using the assumption that sodium and oxygen diffuse through the plug and sodium oxide dissolves into the sodium. Proof of its validity awaits much more data.

3. Summary and Conclusion

Large helium leaks of 10^{-4} atm cm^3/sec, and presumably smaller ones as well, do not appear to be a problem in sodium systems at the low temperature of 400°C. However, helium leaks as small as 10^{-6} atm cm^3/sec do appear to lead to subsequent sodium leakage at the temperature of 650°C.

The importance of opening a masked leak before helium mass spectrometer testing was shown when an oxide-masked leak path (Cell 8) leaked sodium. After oxidation in air, no initial leakage of helium could be detected in the specimen. However, sodium did leak through the flaw after 93 days of exposure at 650°C.

Much more information on sodium leakage is needed before any firm criteria can be developed for defining an acceptable leak as detected and measured by means of a helium mass spectrometer. However, no further studies can be initiated because of scheduled reduction in funding for this project. No further

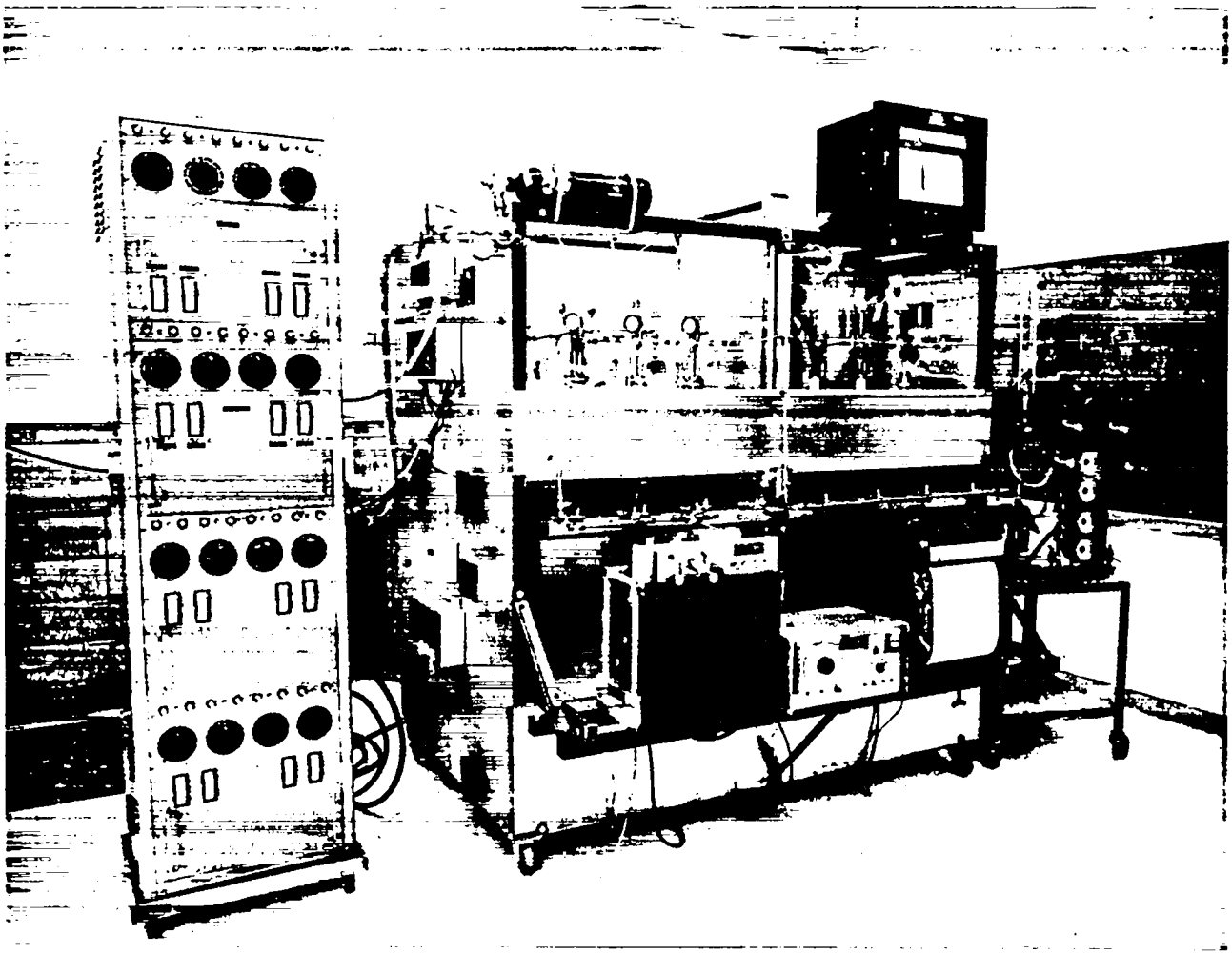

Fig. 462-2. Experimental Apparatus for the Study of Sodium Leakage.

reporting of results is planned. Cells 1 through 4, and 8 will be allowed to continue operation through FY 1970, or until they leak. Monthly gas analysis of their reaction chambers will be made. A detailed report of the work to date was written in LA-4129-MS.

B. Study of Carbon Transport in Thermal Convection Loops
(J. C. Biery, C. R. Cushing)

1. General

Studies have indicated that the use of carbon beds may be useful in the gettering of ^{137}Cs in sodium systems. Carbon, however, is slightly soluble in sodium and can carburize austenitic stainless steels and refractory metals. Therefore, the purpose of this study is to determine the conditions, if any, under which carbon mass transfer rates are sufficiently low to allow the use of carbon beds in a sodium system.

The carbon transfer rates from carbon rods are being studied in thermal convection loops. The Type 304 stainless steel loop itself is serving as the carbon sink.

2. Results in FY 1969

The fabrication of the thermal harp and its installation on an existing sodium loop was completed. Initially, sodium from the loop was passed through the harp to condition the internal surfaces to the oxygen concentration in the sodium. The cold trap temperature in the main loop was 150°C. The conditioning period continued 208 h. During 67 h of that time 250°C sodium from the supply loop was intermittently pumped through at 1 gpm. For 141 h the pumped flow was discontinued, and thermal convection at 500°C was allowed. The periods of forced and natural convection flow were alternated, with the minimum period in either mode of operation being 24 h.

On March 6, 1969, when the conditioning had been completed, a graphite rod 1/4 in. in diam and 2-9/16-in. long was submersed in the sodium at the top of the hot leg of the loop. As of July 1, 1969, the rod had been exposed to the thermally convecting sodium for 2784 h. The temperature around the loop varies from a low of 460°C in the cool leg to a high of 515°C in the hot leg. The flow velocity as measured by a flowmeter is 2-3 cm/sec.

Present plans call for continuation of the test for approximately 8000 h. At termination of the run the loop will be sacrificed and examined for carburization effects. Also, the graphite rod will be cleaned by heating under vacuum, weighed, and then burned and analyzed for sodium content. No additional experiments are planned.

III. STUDY OF PURIFICATION METHODS FOR NONRADIOACTIVE IMPURITIES

A. Study of Na_2O Kinetics in Cold Traps

(C. C. McPheeters, J. C. Biery, W. W. Schertz, R. Martinez)

1. General

In sodium coolant systems for future LMFBR's it will be necessary to use cold traps for removal and control of oxygen and other contaminants. These cold traps should be designed to handle adequately the impurity loads and to maintain the impurity concentration level below some specified upper limit. For economic reasons, cold traps must be the smallest and simplest designs which can meet the above requirements.

Knowledge of the mechanisms of impurity deposition in cold traps is necessary to permit the optimum design for a given sodium coolant system. The rate of mass transfer of impurity species to cold trap surfaces must be measured and the effect of various flow patterns, surface conditions, and temperature on the mass transfer rates must be determined. The effect of the above variables on the mass transfer coefficient for removal of oxygen from sodium systems can then be predicted. Knowledge of the mechanisms involved, and of the mass transfer coefficients, will allow calculation of the rate of oxygen removal and the location of deposited oxides in the cold trap for any given system size and cold trap geometry. Proposed cold trap designs could be evaluated in terms of total oxide capacity and expected system cleanup rates.

Cold trap tests are being conducted with a 60-gal sodium system which has analytical capabilities including a vacuum distillation sampler, a plugging indicator, and two UNC oxygen meters. The cold trap tests consist of measurement of the rates of change of oxygen concentration in the system. Various conditions of temperature and flow rates in the trap are tested to determine the effect of these variables on the oxygen removal rates. When the rate of change of oxygen concentration, the cold trap temperatures, and the deposition surface area is known, an overall mass transfer coefficient can be calculated.

The mass transfer coefficient is defined by Eq. 1.

$$\frac{dm}{dt} = (ka)\, A\, (C - C_e) \qquad (1)$$

where $\frac{dm}{dt}$ = the rate of oxygen mass deposition from solution onto a solid surface, g/h.

(ka) = the overall mass transfer coefficient with the term (a) accounting for roughness of the surface which gives more area per unit sub-surface-area, g/cm^2-h-ppm.

A = the bare surface area, cm^2.

C = oxygen concentration in the supersaturated solution, ppm.

C_e = equilibrium oxygen concentration at the temperature of the surface, ppm.

2. Results in FY 1969

Three cold traps have been operated during FY 1969. Experiments with Cold Trap No. 1 were completed during the first quarter. The cold trap test loop was then modified to accomodate a "removable-core" cold trap; it has a NaK-cooled insert which can be removed for examination and analysis of the precipitate. Experiments with the first insert (designated Cold Trap No. 2) were completed during the third quarter. The second NaK-cooled insert (Cold Trap No. 3) was installed during the fourth quarter.

a. Cold Trap No. 1 - (Unpacked-Annular Trap)

A total of 35 runs were made with Cold Trap No. 1. An isometric cutaway drawing of the unpacked annular type cold trap was shown in an earlier quarterly report.[1] Tests were conducted over a range of temperatures (115-250°C) and flow rates (0.1-1.5 gpm) in both precipitation and dissolution runs. No definite correlation between temperature and the mass transfer coefficient could be found; the scatter in

the data appears to mask any temperature effect. The effect of sodium velocity (or Reynold's number) on the mass transfer coefficient is shown in Fig. 462-3. The relationship is approximately linear, with unit slope, on a log-log plot between Reynold's numbers of 200 and 1200; however, the coefficients increase sharply above 1200. A slope of 1/2 is expected if true laminar flow conditions exist. The steep slope is probably due to radial cross-flow in the cold trap caused by poor entrance conditions.

The large effect of Reynold's number on the mass transfer coefficient indicates that the oxide deposition process is liquid phase diffusion limited. Good agreement between the results from precipitation and dissolution runs indicates that the same mechanism is occurring in both processes. The mechanism for dissolution involves transfer of material from crystals attached to solid surfaces into the sodium stream; therefore, the mechanism for precipitation must involve transfer of material from the sodium stream to the cold trap solid surface where heterogeneous nucleation and growth of oxide crystals occurs. A complete summary of the results from experiments with Cold Trap No. 1 was presented at the International Conference on Sodium Technology and Large Fast Reactor Design at Argonne National Laboratory, November 7-9, 1968.

b. Cold Trap No. 2

The second cold trap includes a NaK-cooled insert which can be removed for examination and identification of species. Inlet sodium flows downward in an annular space surrounding the insert. Beyond the end of the insert, the sodium passes through a regenerative heat exchanger and back into the main system.

During the initial loop operations after installation of Cold Trap No. 2, an impurity which was saturated at 220°C with the cold trap temperature at 300°C (the system temperature) was detected with the oscillating plugging indicator. This impurity did not have the kinetic behavior typical of oxygen. The kinetics of an oxygen impurity with a saturation temperature of 220°C are such that it precipitates and dissolves very rapidly; however, this impurity precipitated and dissolved slowly.

Five cold trap runs were made to determine the mass transfer coefficients for the impurity. The results of the three precipitation and two dissolution runs are shown in Table 462-II. For this calculation, the oxygen solubility curve of Rutkauskas[2] was utilized. These coefficients are 1.5 to 2 times longer than the coefficients calculated for oxygen in Cold Trap No. 1 and presented in Fig. 462-3. This difference lends credence to the suspicion that the impurity was not oxygen, and other solubility curves will be tried in the calculation. (For instance, the hydrogen solubility curve of Addision is now being tried in the calculation.)

Table 462-II

Results of Runs with Cold Trap No. 2

Run No.	Run Type	Reynold's No.	Minimum Cold Trap Temp	Mass Transfer Coefficient (lb/ft^2-h-ppm)
2.01	Precipitation	300	141°C	13.6×10^{-6}
2.02	Dissolution	300	196°C	20.0×10^{-6}
2.03	Precipitation	300	141°C	18.5×10^{-6}
2.04	Dissolution	300	233°C	17.1×10^{-6}
2.05	Precipitation	300	152°C	16.3×10^{-6}

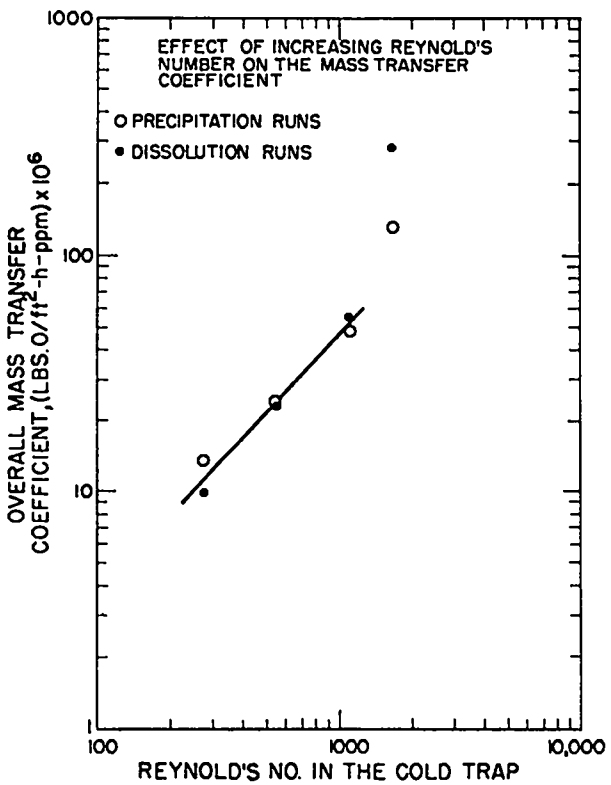

Fig. 462-3. The Effect of Reynold's Number on the Mass Transfer Coefficient.

After completion of the runs with Cold Trap No. 2, the sodium was dumped from the cold trap into a dump tank. The cold trap was evacuated and the insert was heated to 250°C for 4 h to distill residual sodium from the impurity deposits. The insert was then removed into an inert chamber where it was observed and photographed. Figure 462-4 shows an overall view of the entire insert which was covered with a thin layer of very small crystals. The length of the insert from the bottom to the flange is 24 in., and its appearance before test was that of electropolished stainless steel. The lower 4 in. was covered with a thin layer of sodium over a crystalline sub-layer. The middle 14 in. was covered with a thin layer of small crystals, and the upper 6 in. was nearly free of any deposit. Figure 462-5 shows the lower portion of the insert. The bright spots are crystalline areas in which the

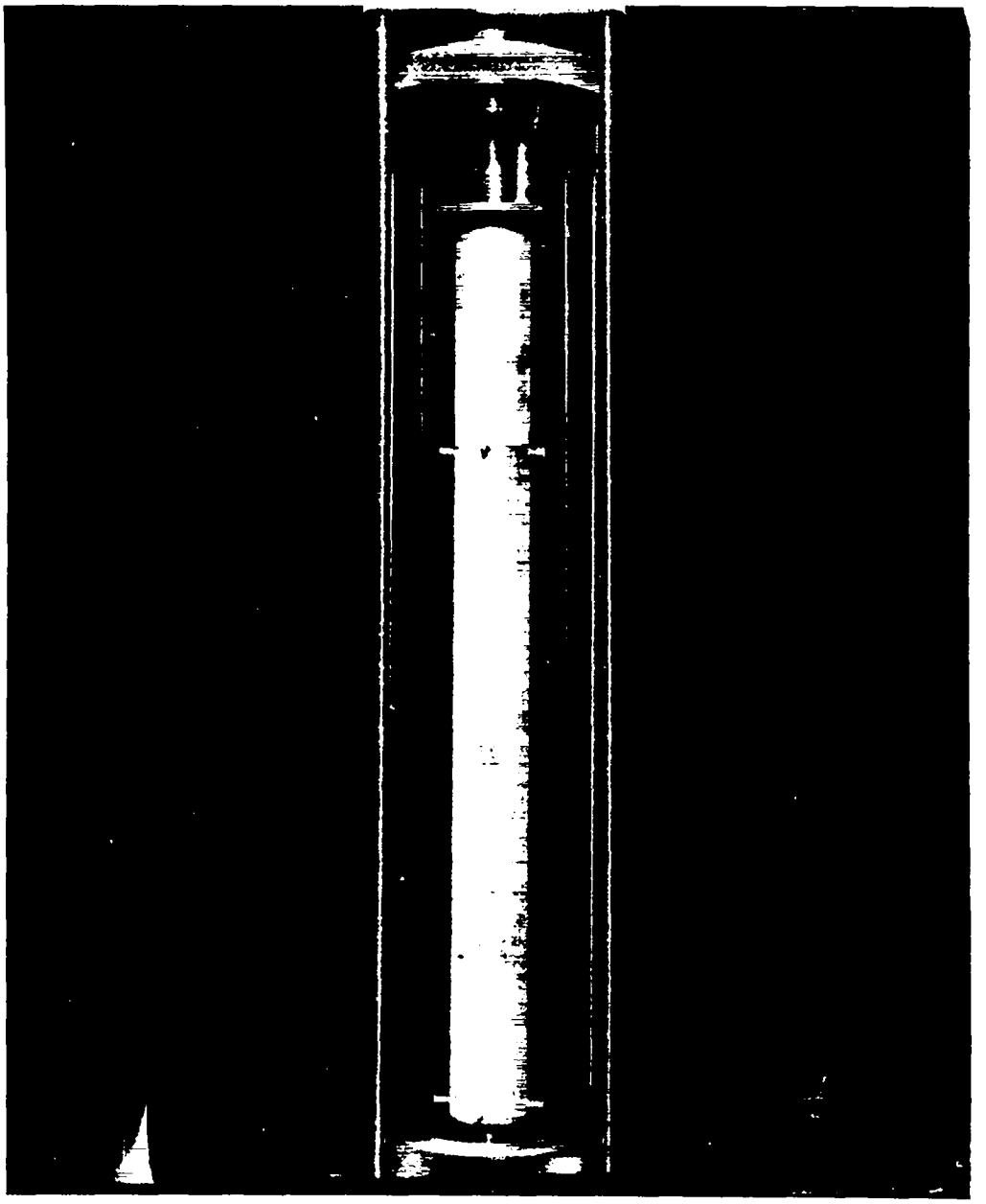

Fig. 462-4. Overall View of Cold Trap No. 2 Insert in an Inert Chamber after Test.

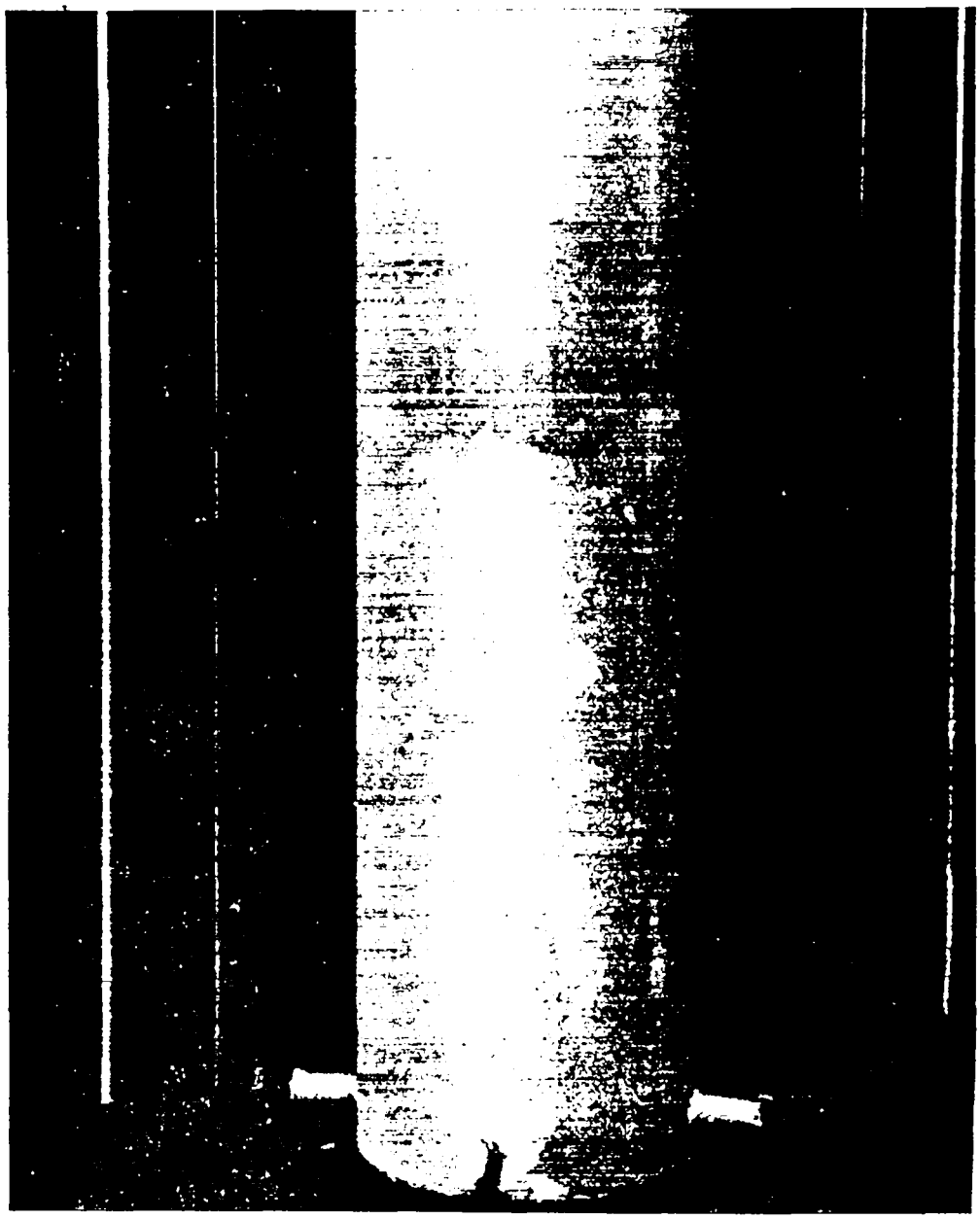

Fig. 462-5. View of Lower 6 in. of Cold Trap No. 2 Insert Showing Crystalline Nature of the Impurity Deposit.

crystals have the same orientation so that they reflect light in a common direction.

The insert was transferred to a dry box where the deposit was scraped off and loaded into capillary tubes for x-ray analysis. The results of the analysis are not yet available.

c. Cold Trap No. 3

Mass transfer data from cold traps packed with wire mesh are necessary for the purpose of designing packed cold traps for near-term impurity removal systems. Cold Trap No. 3 is identical to Cold Trap No. 2 with the exception that wire mesh packing was placed around the central cylinder. The packed assembly which is shown in Fig. 462-6 was inserted into the cold trap body. The packed cold trap is currently in service; however, no cold trap runs have been made.

d. Oxygen Addition System

The presence of impurities other than oxygen in the test loop has made it necessary to devise a

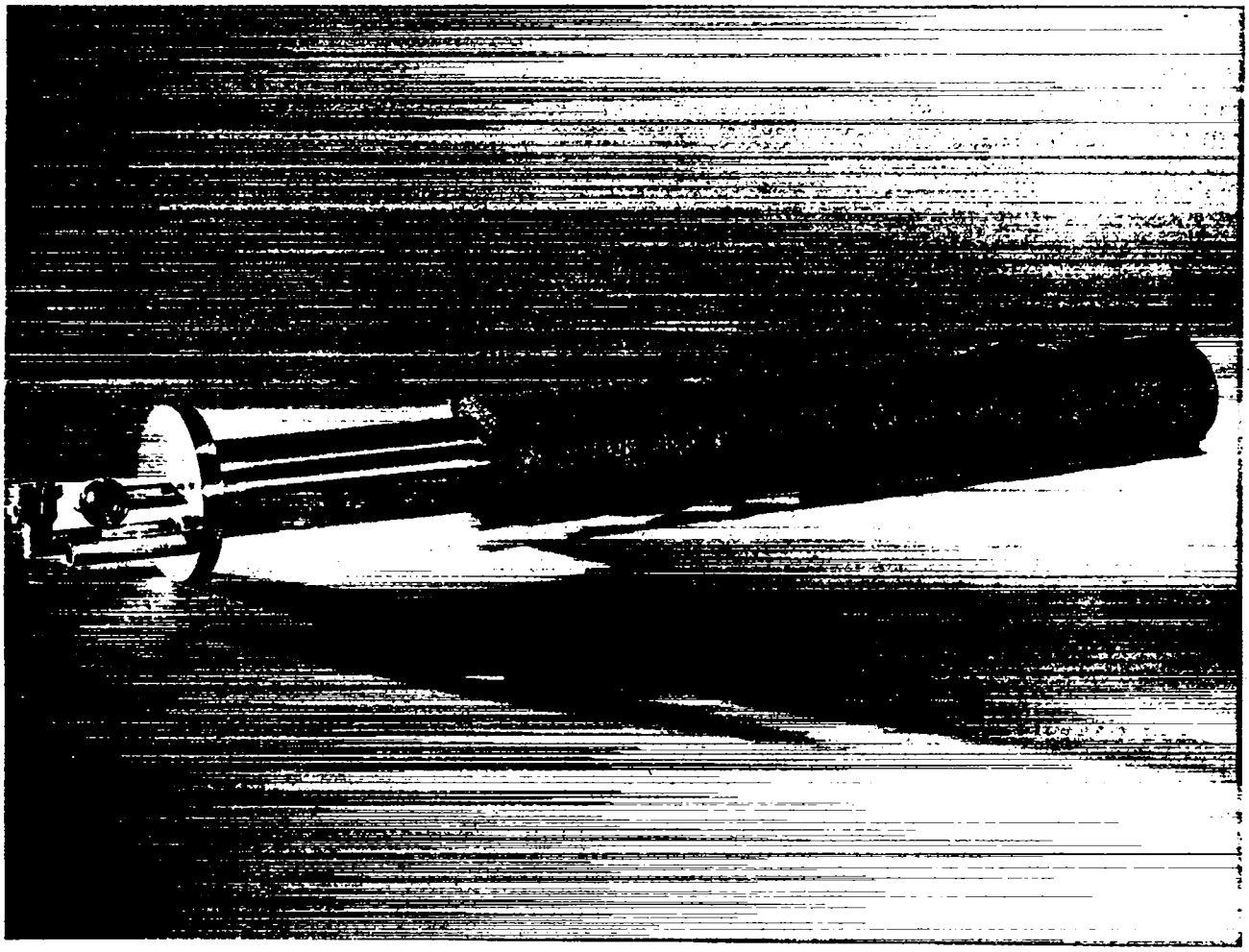

Fig. 462-6. Cold Trap No. 3 Insert.

method of adding pure oxygen to the sodium without introducing other impurities in order to perform unambiguous measurements of oxygen removal rates. The vacuum distillation sample station, in which an overflowing sodium surface is present, is used for oxygen addition. (This surface is free from impurity deposits that would impede absorption of oxygen into the sodium stream.) A glass viewport and a gas bleed valve adjustable to give leak rates from 10^{-10} to 100 std cc/sec were installed above the sample port. Oxygen was added through the valve at a rate of 0.77 g/h to the gas phase over 350°C sodium until a total of 55 ppm had been added to the system. Only 35 ppm was found to be in solution in the sodium; the oscillation plugging meter saturation temperature and the Rutkauskas semi-log solubility curve[2] were used to make this determination. It is postulated that the stainless steel surfaces adsorbed the remaining 20 ppm. This quantity of oxygen absorbed is equivalent to 1.2×10^{-1} mg/cm^2 on the 350°C stainless steel surface.

This addition method utilizing the calibrated, controlled leak valve was very successful. The oxygen was not immediately absorbed by the flowing sodium, however. A reaction zone existed above the sodium surface where the sodium vapor reacted with the oxygen, and sodium and sodium oxide codeposited on the vessel walls at the reaction zone level. Periodically the sodium level was raised above the reaction zone to dissolve the Na-Na_2O deposit. This periodic dissolution of the deposit required a 5 to 10-min interruption of the addition procedure.

B. Study of Soluble Getters for Removal of Impurities from Sodium
(G. E. Meadows, D. N. Rodgers, O. E. Thomas)

1. General

For large sodium-cooled reactor systems, it may be desirable to use soluble getters for control of oxygen and other dissolved impurities in lieu of or in addition to the more conventional hot and cold trapping techniques. The soluble getters of interest occur in the sodium coolant either naturally, as an impurity (calcium), or are produced during reactor operation (as with magnesium). The techniques for the controlled additions of these getters, maintenance of fixed getter levels, and the selective removal of depleted getter metals and other impurities from dynamic sodium systems must be developed if their usefulness is to be evaluated. The significant chemical reactions occurring in a sodium system containing these soluble getters must be understood and controlled. This mode of purity control has the potential for effectively controlling not only oxygen, but also carbon, hydrogen, nitrogen, and possible metallic impurities.

2. Results in FY 1969

a. Summary and Conclusion

Although Analytical Loop No. 2 was built expressly for the study of soluble getters, it was decided that Analytical Loop No. 1 could be used to some advantage for preliminary calcium addition experiments. Thus, all of the experimental work related to soluble getters in FY 1969 was done in Analytical Loop No. 1. A summary of the operating and physical characteristics of the system are given below and in Reference 2.

Volume: 9.5 gal
Tubing size: 1/2 in.
Flow rate: 1 gpm
Maximum operating temperature: 350°C
Cold trap volume: ~1 gal
Cold residence time: ~1 min
Surface area in cold trap: 15.3 ft^2 on knitted wire mesh + 2.7 ft^2 on pipe and tank surfaces.

The experimental work was originally designed to be of a preliminary nature. Due to the lack of data in the literature, preliminary experiments were thought to be necessary to more closely define problem areas as well as to practice sampling and analytical techniques. Despite the preliminary nature of the experiments, the main findings are believed to be substantially definitive.

The fact that calcium does not remain in solution and apparently builds up on metallic surfaces is the important finding of the present experimental study. This conclusion has been mentioned elsewhere[3] but without detailed experimental evidence. The experimental evidence on which the conclusion is based as follows:

(1) Amounts of calcium were found deposited on the outside of the nickel distillation cup. The amount found decreased steadily from the time of the calcium addition.

(2) Calcium was found on the outside of nickel tubing suspended inside the bulk tank. The same density of deposition over the entire loop would account for ~0.65 g or 61% of the calcium added.

(3) Calcium was found on the inside of the tubing on both the inlet and outlet of the cold trap which was removed after the first two additions.

Additional work is desirable to more fully explain the behavior of calcium in solution. The parameters affecting the adherence of calcium to metal surfaces should be determined, as well as the form of adhesion that takes place (i.e., physical adhesion, intermetallic compounds, oxide deposition). Also, it is important to be able to distinquish among metallic calcium in solution, particulate calcium oxide, and calcium oxide in solution. These distinctions were not possible in the present study.

These and other related questions should be answered before the future of calcium as a soluble getter is finally decided. However, results of the present study indicate that calcium probably is not a practical getter material.

In the following, the sequential experimental results are presented. Three calcium additions were made with the system temperature at 350°C. In the first, the cold trap operated at 125°C, in the second, the cold trap was operated at 225°C, and in the third, the system was operated isothermally at 350°C and then at cold trap temperatures of 125°C and 225°C.

b. Calcium Addition No. 1

In the first soluble getter run, Analytical Loop No. 1 was spiked with 1.2 g of metallic calcium. The calcium was added by the tea bag method

to the bulk sodium tank. Under ideal conditions this weight of calcium would give ~50 ppm calcium in the sodium. At the time of the addition the bulk sodium tank was operating at 350°C, the full-flow cold trap tank temperature was 125°C, the oxygen concentration was 1.4 ± 0.3 ppm as determined by vacuum distillation, and the loop flow rate was ~1 gpm. During the run, vacuum distillation samples for analysis of oxygen (from residual sodium) and calcium were taken from the outlet line of the crystallizer tank. Sampling was begun 2 h after the addition of the metallic calcium and continued until the dissolved oxygen value was again in equilibrium with the crystallizer tank. The crystallizer tank outlet sodium was deficient in dissolved oxygen for ~50 h. The lower values (0.3 ppm oxygen) occurred during the first 6 h. The values for calcium increased somewhat during this period (0.3 ppm calcium) and then fell off to the system's original background (<0.1 ppm calcium) within 24 h. After the run, the tea bag was removed from the bulk tank and was analyzed for remaining calcium. The calcium had all dissolved.

c. Calcium Addition No. 2

On January 6, 1969, 1.15 g of calcium metal were added to Analytical Loop No. 1. The procedure was the same as that used for Addition No. 1. The cold trap temperature was 225°C and the bulk tank temperature was 350°C. If the calcium were evenly distributed throughout the system, its concentration in the sodium should have increased by 45 ppm.

No change in the system behavior was observed after the calcium addition. A vacuum distillation sample taken 1-1/2 h after the addition contained 29.0 ppm oxygen and 0.17 ppm calcium in the residue. A second distillation 4-1/2 h after the addition indicated 29.0 ppm oxygen and 0.14 ppm calcium. Five samples analyzed before the addition had a range of 24-34 ppm oxygen (average 28.6) and 0.10-0.14 ppm calcium (average 0.11). Thus, the calcium addition did not significantly alter the bulk sodium analysis.

The basket used to add the calcium was then pulled from the loop to determine how much calcium had dissolved. Out of 8.845 g of metallic substance recovered from the basket, 0.238 g (21% of the calcium added) of calcium were found. The sodium was removed from the basket by distillation. When the residue in the distillation cup was dissolved in 0.01N HCl as per the normal procedure, an extremely strong odor of phosphine (PH_3) was noticed. Apparently, there was a phosphorus compound in the basket when it was pulled from the loop; the compound was not identified.

d. Installation of New Cold Trap to Analytical Loop No. 1

The cold trap used in Additions 1 & 2 had been used on the loop for a number of years and obviously contained many precipitated impurities. For instance, the phosphorus compound that precipitated on the calcium probably was released from the cold trap when the temperature was raised to 225°C. Therefore, a new cold trap was substituted for the old trap and a bypass was installed to allow isothermal loop operation excluding the cold trap. Most of the loop's precipitable impurities were removed with the old cold trap.

e. Calcium Deposition on Tubing Attached to Old Cold Trap

Tubing was removed from both the inlet and outlet of the old cold trap. For analysis, the tubing was cut into pieces about 1-in. long. Each piece was placed upright in the distillation cup and distilled normally. It was observed that the sodium quickly melted and ran down the tube and into the cup. Therefore, the residue analysis was done separately for the material attached to the tube and material melted into the cup. The tubing showed a higher calcium residue content. This observation is a strong indication that the calcium was present on the walls of the tubing rather than in the bulk sodium. The results are summarized in Table 462-III.

The above sample results indicate that an average of 0.0265 mg Ca/cm^2 was deposited on the tubing near the cold trap. If this same surface deposition existed uniformly over the inside surface area of the loop (8.85 x 10^3 cm^2), a total of 0.235 g of calcium would have been removed from the system. This quantity was 10% of the total calcium added in Additions 1 & 2.

f. Calcium Addition No. 3

To establish a background impurity level, the system was operated at a cold trap temperature of 125°C for 6 days. Two distillation samples taken during that period contained an average of 1.6 ppm

Table 462-III

Calcium Deposition on Inside of Tubing Removed with Old Cold Trap

Position	Sample No.	ppm Calcium*		Ca Concentration on Tubing Surface
		On Tube	In Cup	mg/cm^2
Inlet	1	43.0		0.0281
	2	34.7	1.3	0.0341
	3	27.4	0.5	0.0192
Outlet	1	38.6		0.0239
	2	7.9	10.3	0.0104
	3	27.2		0.0435

*Calcium concentration related to sodium in tube section.

oxygen. The cold trap was then valved off and the system operated on the bypass loop. Samples taken over a period of 7 days did not show an increase in apparent oxygen content, but did establish a background level for oxygen and calcium in the distillation residues. These samples are tabulated below in Table 462-IV.

Table 462-IV

Calcium and Oxygen Concentrations Before Calcium Addition No. 3 - Cold Trap Temperature: 125°C

Sample No.	Cold Trap	ppm O*	ppm Ca	Date
119	125°C	1.58	0.15	2/28
120	125°C	1.62	0.094	3/3
121	Bypass	1.54	0.31	3/4
122	Bypass	1.5	0.36	3/5
123	Bypass	1.77	0.11	3/7
124	Bypass	1.34	0.14	3/10

*Oxygen determined from residual sodium in vacuum distillation residue.

After establishing the oxygen and calcium levels for Loop No. 1, 1.06 g of calcium metal were added to the loop. The addition was made as in the previous two additions. The calcium added was sufficient to make a 40 ppm solution if all metal dissolved and was uniformly distributed in the sodium.

The oxygen level of the system as indicated by residual sodium in the distillation residues showed an immediate decrease, as expected. The first distillation sample taken 1 h after the calcium addition contained 0.21 ppm oxygen, the second one contained 0.10 ppm. Subsequent samples yielded oxygen contents ranging from 0.066 to 0.20 ppm. The average of thirteen samples was 0.125 ppm oxygen. The calcium and oxygen concentrations are shown as a function of time in Fig. 462-7 and in Table 462-V.

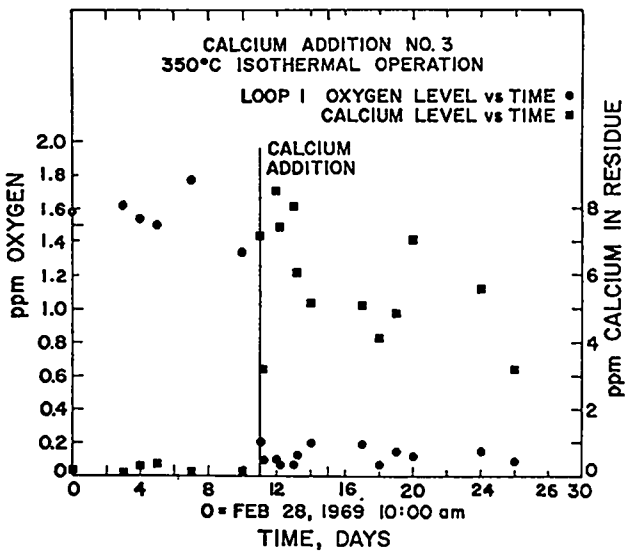

Fig. 462-7. Effect of Calcium Addition on Oxygen and Calcium Concentrations as Determined by Vacuum Distillation after Calcium Addition No. 3.

Table 462-V

Oxygen and Calcium In and On Distillation Cup after Calcium Addition No. 3

Sample No.	Oxygen* ppm	Calcium in Cup ppm	Calcium on Cup Outside mg	Date
125	0.21	7.15	0.216	3/11
126	0.10	3.2	0.045	3/11
127	0.10	8.5	0.035	3/12
128	0.066	7.4	0.024	3/12
129	0.069	8.0	0.046	3/13
130	0.12	6.1	0.024	3/13
131	0.20	5.15	0.047	3/14
132	0.19	5.1	0.035	3/17
134	0.07	4.1	0.056	3/18
135	0.14	4.9	0.038	3/19
136	0.12	7.1	0.050	3/20
138	0.14	5.6	0.053	3/24
140	0.09	3.2	0.039	3/26

*As determined from total residual sodium in distillation residue.

The calcium level in the residue of the sample taken 1 h after the calcium addition was 7.15 ppm. Subsequent samples ranged from 8.5 at 1 day after

addition to 3.2 ppm at 14 days after addition with an average of 5.8 ppm. The techniques used to determine the residue calcium content did not allow a distinction to be made between calcium metal and calcium oxide. No correlation was observed between the calcium level and the oxygen level, and very little calcium (0-0.5 ppm) was detected in the sample distillates.

Calcium was found not only in the distillation residue but also on the outside of the distillation cup. The amount of calcium was determined by washing the outside of the cup with 0.01N HCl and analyzing the resulting solution by atomic absorption. The amounts of calcium found varied from 0.035 to 0.056 mg which would be equivalent to 8.6 to 12.8 ppm in the sodium sample. The cup was exposed to the sodium for varying times up to 2 h, and no increase in calcium adsorption on the outside of the cup was found.

g. Calcium Adsorption on Nickel Tubing

The charger mechanism used to add the calcium includes a 3/4-in. nickel tube which is filled with sodium prior to withdrawal of the calcium basket. Due to a defective mechanism, the tube did not fill. However, the outside of the tube was analyzed for possible calcium deposition.

Three pieces about 12 mm long were cut from the nickel tube while it was inside the inert box. Each piece of tubing was heated under vacuum in the distillation sampler attached to the glove box to drive off the sodium film clinging to the outside. The residue on the tubing was analyzed for calcium and sodium by atomic absorption. The calcium results are presented below in Table 462-VI.

Table 462-VI

Calcium Adsorbed on Nickel Tubing at 350°C

No.	Length mm	Area Outside cm^2	Calcium mg/cm^2
1	12.0	7.30	0.0815
2	11.5	6.96	0.0805
3	15.0	9.07	0.0557
			0.0726 (average)

The average value of 0.073 mg/cm^2 was a factor of 2.7 greater than found on the stainless steel tubing near the cold trap after Calcium Addition No. 2 and 45 times greater than the surface concentration found on the nickel distillation cup after Calcium Addition No. 3.

h. Residue in Calcium Basket after Calcium Addition No. 3

The calcium basket was pulled out of the loop 8 days after it had been put in. The excess sodium was distilled from the basket in preparation for analysis. Inside, was a lump of black, porous-looking material of approximately the same size and irregular shape of the calcium originally added (Fig. 462-8). However, the material weighed 0.1048 g which was only 10% of the original calcium weight. The material was extremely pyrophoric. After dissolving a portion of the lump in water under hexane, very little insoluble black material remained. Thus, the material contained little if any elemental carbon. The neutralized solution was diluted and analyzed for calcium and sodium by atomic absorption. Of the 0.0639 g dissolved, 0.035 g were calcium (55%) and 0.014 g were sodium (22%).

Another piece of the lump was partially hydrolyzed with a small amount of wet helium in a glass reaction chamber. The gas resulting from the hydrolysis was analyzed with a mass spectrometer. The analysis showed the gas to be mostly hydrogen with amounts of helium, water vapor, and air. Traces of methyl acetylene and phosphine were also detected.

A portion of the solid residue was sent to group CMB-1 for spectrophotometric analysis. For comparison, a piece of the calcium metal used for calcium additions was also analyzed. Since the residue weight was about 10% of the weight of the calcium metal added to the loop, any impurity in the metal which remained to talley in the residue would appear concentrated by a factor of 10. Therefore, for comparison, the concentrations reported by CMB-1 for the residue have been divided by 10. The analysis results are summarized in Table 462-VII.

Zirconium was gettered and concentrated in the residue. This behavior is not understood. Magnesium was preferentially leached from the residue by the sodium.

i. Oxygen Addition after Third Calcium Addition

To determine the ability of a calcium-rich sodium system (Table 462-V) to getter oxygen, on March 27, 1969, 0.7256 g of Na_2O were added to the bulk tank (equivalent to 8.0 ppm oxygen). The

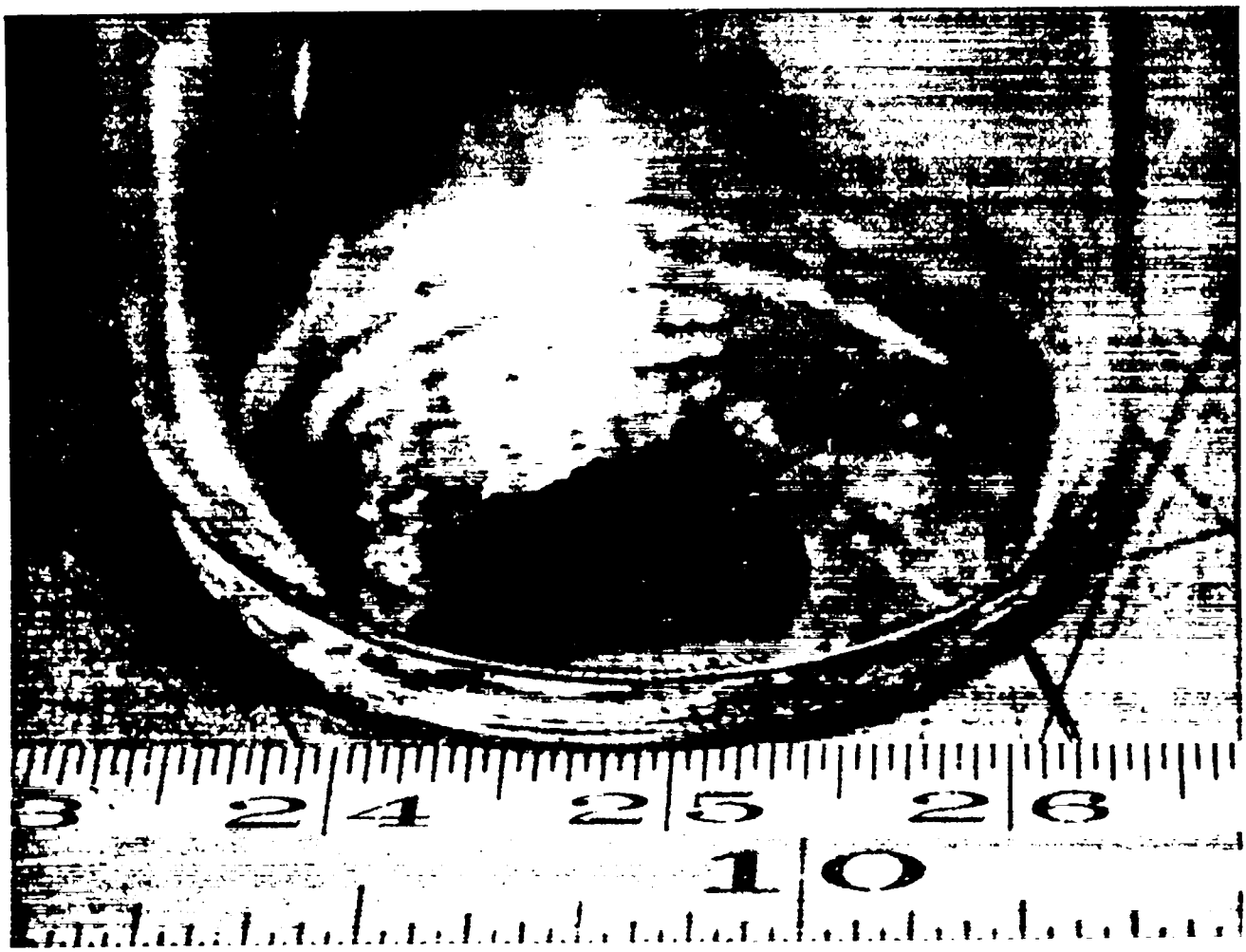

Fig. 462-8. Material Removed from Analytical Loop No. 1 after Calcium Addition No. 3

addition was done in a manner similar to that of the calcium additions. The operating conditions of the system were kept constant (350°C isothermal operation). On April 3, 1969, the cover gas was monitored for hydrogen with a gas chromatograph; the results indicated that little hydrogen was evolved because of the oxide addition. A typical cover gas analysis is given in Table 462-VIII.

After the oxide addition, the oxygen level of the system rose gradually from a steady state level <0.2 ppm to a new level between 4 and 6 ppm. The 8.0 ppm level, representing complete solution of the added oxide, was not reached, however. The results were unfortunately confused by the removal of the valve on the sodium sampler pot. The removal possibly contaminated the sodium in the pot (and hence, in the entire loop) with an unknown amount of impurities. The oxygen and calcium levels are plotted in Fig. 462-9 and tabulated in Table 462-IX. The results in Table 462-IX indicate very little contamination from the valve removal.

j. Cold Trapping at 125°C after Third Calcium Addition

On May 12, 1969, the cold trap (125°C) was valved onto the system (still at 350°C). Within 24 h, the system oxide and calcium levels returned to the values they had before the last calcium addition (1.6 ppm oxygen, 0.21 ppm calcium). The results are tabulated in Table 462-X.

k. Cold Trapping at 225°C after Third Calcium Addition

The cold trap temperature was raised to 225°C on May 20, 1969. An oxygen saturation concentration of 10.6 ppm was found. Since there was a total of 5.5 ppm of oxygen in the loop's cold trap before the third calcium addition and the highest oxygen value reported with the bypass operation is 6.5 ppm,

Table 462-VII

Spectrochemical Analysis of Residue and Calcium Metal

Species Detected	Concentration in Calcium, ppm	Concentration in Residue, ppm
Li	<10	1-10
Mg	10,000-100,000	10-100
Al	not detected	10-100
Si	10-100	10-100
Cr	not detected	1-10
Mn	10-100	1-10
Fe	100-1,000	10-100
Co	<10	not detected
Ni	<10	10-100
Cu	<10	1-10
Sr	100-100	10-100
Zr	10-100	1,000-10,000
Ag	not detected	1-10
Sn	10-100	10-100
Ba	10-100	1-10
Pb	10-100	10-100
Bi	not detected	1-10

Table 462-VIII

Cover Gas Analysis of Loop No. 1 after Sodium Oxide Addition

H_2, Ne	<40 ppm
N_2	47 ppm
O_2, Ar	not detected
CH_4	<5 ppm

Table 462-IX

Calcium and Oxygen (Residual Sodium) Concentration in Sodium after Oxygen Addition - As Determined by Vacuum Distillation

Sample No.	Oxygen ppm	Calcium ppm	Calcium on Cup Outside mg	Date	Comments
141	0.154	2.62	0.033	3/27	
142	0.33	1.20	0.011	3/27	
143	0.51	5.42	0.010	3/28	
144	2.12	5.30	0.009	4/1	
145	2.63	3.08	0.007	4/2	
146	4.18	8.36	0.012	4/7	
147	5.07	5.26	0.008	4/8	
148	4.56	5.25	0.004	4/9	
149	4.75	5.81	0.005	4/10	
150	4.95	2.28	0.011	4/14	Valve removed & replaced on 4/14
151	3.28	3.33	0.006	4/15	
152	5.52	1.4	0.002	4/21	Valve again removed & replaced on 4/18

Table 462-X

Oxygen and Calcium Concentrations after Cold Trapping at 125°C - After Third Calcium Addition

Sample No.	Date	Oxygen ppm	Calcium ppm	Cold Trap
153	5/1	6.5	5.98	Bypass
154	5/5	5.6	1.04	Bypass
155	5/6	5.3	1.68	Bypass
156	5/7	6.2	2.58	Bypass
157	5/8	6.4	1.97	Bypass
158	5/12	2.1	0.17	125°C
159	5/13	1.6	0.17	125°C
160	5/14	1.5	0.25	125°C
161	5/15	1.3	0.12	125°C
162	5/19	1.2	0.29	125°C

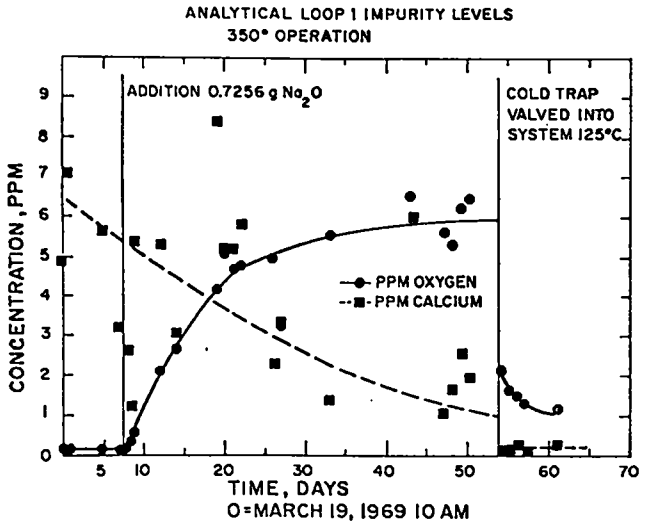

Fig. 462-9. Effect of Oxide Addition on Oxygen and Calcium Levels (as Determined by Vacuum Distillation Analysis) in Analytical Loop No. 1.

the present level represents the total oxygen inventory. Apparently none or very little of the oxygen in the cold trap was gettered by calcium. Table 462-XI summarizes the concentrations during the 225°C cold trapping period.

Table 462-XI

Oxygen and Calcium Concentrations after Cold Trapping at 225°C - After Third Calcium Addition

Sample No.	Date	Oxygen ppm	Calcium ppm	Cold Trap
163	5/20	10.1	0.23	225°C
164	5/21	11.5	0.23	225°C
166	5/23	10.7	0.09	225°C
167	5/27	10.2	0.12	225°C

C. Study of Gas Diffusion Through Metals Into Sodium

(J. P. Brainard)

1. General

Very little quantitative information is available on the diffusion of gases in reactor system containment materials, although the phenomenon has been observed in several high-temperature, liquid-metal-cooled systems. Diffusion of nitrogen through stainless steel in such systems may be misinterpreted as evidence of an air leak in the plumbing. If quantitative information on diffusion were available, the expected rate of nitrogen influx could be estimated, and the existence of small hard-to-find leaks might be substantiated or dismissed by comparing the expected and observed rates of nitrogen accumulation in the system. A program for determining the diffusion rate of nitrogen in stainless steels has therefore been undertaken.

2. Results in FY 1969

This experiment is capable of measuring a wide range of gas permeation rates at temperatures ranging from room temperature to 1000°C. The basic apparatus consists of a diffusion cell housed inside a vacuum furnace. The diffusion cell will contain about 1 atm of nitrogen. A mass spectrometer connected to the vacuum furnace measures the residual gas partial pressure in the vacuum side of the diffusion cell. The partial pressure of nitrogen in the vacuum furnace is correlated with the gas permeating through the diffusion cell by injecting periodically standard nitrogen flows into the vacuum furnace and noting the change in nitrogen pressure. At constant pumping speed, pressure and flow are linearly related. The vacuum furnace is surrounded by a continuously pumped region which prevents nitrogen in the air from permeating back through the furnace.

Since inert gases do not diffuse through metal at significant rates, a small addition of helium to the nitrogen will allow continuous monitoring of any leakage through the diffusion cell. A leak will be indicated when helium is found with the mass spectrometer on the low pressure side of the membrane. Figures 462-2 and 462-3 in the Third Quarterly of FY 1969 show the apparatus.[4]

After the installation of the diffusion cell, the measurement of nitrogen permeation and diffusion rates through 4-mil wall Type 304 stainless steel tubing can begin. The diffusion cell consists of a coil of 4-mil wall tubing 40-in. long with weld adaptors at the ends. The diffusion cell radiographing is now complete. The 4-mil wall thickness was measured with 10% accuracy with this method. Nondestructive tests with more accuracy would cause a serious delay in the program and therefore will not be performed. Additional destructive tests to refine the measurements of the wall thickness will be made after permeation rates are measured. An initial pump-down and bakeout will be accomplished without the diffusion cell in place to prevent damage to the cell due to the possible initial heavy outgassing and leaks in the system.

The research program will determine the permeation rates of nitrogen through the diffusion cell as a function of temperature. The type of temperature dependence will indicate whether the diffusion is bulk metal or surface controlled.

IV. FISSION PRODUCTS IN SODIUM SYSTEMS

A. Study of Fission Product Distribution in Loop Experiments
(J. C. Clifford, J. Fellers)

1. General

The behavior of radioactivity released to sodium from failed or vented fuel elements may limit access to portions of the primary coolant system and may effect the consequences of a loss-of-coolant incident. Depending on the fission-product release fraction anticipated in either circumstance, it may be desirable to scavenge these species (as well as uranium and plutonium) from the coolant.

The immediate goals of this investigation are: (1) to identify sodium-soluble fission-product species and (2) to examine the effects of primary-coolant-system construction materials, design features, and operating conditions on these species.

2. Results in FY 1969

Studies of the distribution of long-lived fission products have been continued with major emphasis on ^{137}Cs.

a. ^{137}Cs Adsorption Loop

The deposition of ^{137}Cs from flowing sodium onto several metal surfaces was studied using the forced-convection loop shown in Fig. 462-1 of Reference 5. Sodium containing 0.1 to 2 μCi ^{137}Cs/g Na flowed upward through a 2-in. diam test column containing coils of metal foil fastened on a stringer. After leaving the test section, sodium passed through an expansion tank, a pump, a flowmeter, and a resistance heater. A cold trap on a bypass line provided oxygen control for the loop. The loop contained approximately 5 lb of sodium flowing at a maximum rate of ~800 lb/h.

The metal specimens used in this study were made by winding a corrugated and a flat strip of 3-mil thick foil together on a nickel spindle and slipping a cylindrical sleeve over the bundle to prevent it from uncoiling. The finished bundle was 2-in. high, 1-1/8 in. in diam and contained ~85 $in.^2$ of surface (see Fig. 462-2 of Reference 5). Four metals were tested: C-1010 steel, Type 316 stainless steel, zirconium, and nickel. The foils were used in a cold worked state. The only surface preparation consisted in removing grease and dirt ultrasonically. A stringer containing a bundle of each material was assembled by pinning the spindles together and by adding upper and lower end pieces, which allow insertion of the stringer into the loop.

The distribution of ^{137}Cs in the bundles and in the cold trap was determined by scanning the test section and trap with a collimated NaI(Tl) crystal and by fixed position counting of specific sections within the test column and cold trap. The scanner is described on Page 19 and Fig. 462-3 of Reference 5.

Experiments were prepared by adding $^{137}CsCl$ to the sodium at 500°C and allowing 3 days for dissolution. The temperatures in the loop and cold trap then were adjusted to the values for the experiment and another period of time, dependent on operating temperature, was allowed for the system to approach equilibrium. At the start of an experiment, the test section was scanned to determine the activity level in the flowing sodium and on the walls, after which the foil bundles were lowered in place and the counting of specific bundle sections was begun. After the foil bundles had been equilibrated, they were removed from the loop, the stringer was disassembled, and the foils were analyzed for total ^{137}Cs by leaching each bundle and β-counting an aliquot of the solution. To establish initial and final ^{137}Cs concentrations in the flowing sodium, a 5-g sodium sample was taken from the loop prior to insertion and immediately after removal of the foil bundles. The activity level and distribution in the cold trap was determined before and after each test and several times during each test.

This experimental procedure was decided upon after extended observation had been made of ^{137}Cs behavior in small cold trapped systems. In general, half of the ^{137}Cs added to a cold trapped system was found in the flowing sodium approximately a tenth deposited on the walls, and the remainder concentrated in the cold trap. (Partition of activity to the loop metal surfaces was a relatively rapid step requiring 200-500 h.) No differences in behavior were detected between ^{137}Cs extracted from irradiated metal fuel and that added as $^{137}CsCl$. Since metals appeared to be weak collectors of ^{137}Cs, it

seemed that a loop containing several pounds of sodium could be equilibrated with ^{137}Cs and that metal specimens could be inserted and equilibrated without changing the cesium concentration in the flowing sodium by more than a few percent. As a first approximation, concentration changes on this order could be ignored.

Three experiments were completed using bundles of C-1010 steel, Type 316 stainless steel, zirconium, and nickel. In each case, the sodium temperature was 200°C and the flow velocity in the empty test section was 0.1 ft/sec, corresponding to a sodium Reynold's number of 2600. The oxygen level in the system was set by continuous operation of the bypass cold trap in the 110-120°C range. The initial ^{137}Cs concentration was in the range 0.5-1.5 μCi/g Na. Although the experiments did not yield quantitative results that were consistent, a qualitative pattern emerged. Figure 462-4 in Reference 5 shows the axial distribution of ^{137}Cs in all four foil bundles after 25, 338, and 840 h of operation during the latest experiment. The principal features were an activity maximum along the upstream edge of each bundle, a minimum near the center, and an increase near the downstream edge. As contact time increased, the upstream edge of each bundle gave up activity while the middle portion and trailing edge gained. The activity distributions also indicated that for some time after start the leading and trailing edges of each bundle acquired activity at a more rapid rate than sections in the middle of a bundle. This effect may be associated in part with flow disturbances at the ends of a bundle and in part with the fact that the bundle edges are the sheared, unannealed edges of the sheet stock.

Although no two regions in any bundle acquired activity at the same rate, the deposition process in all sections examined could be described by an equation of the form $A = kt^x$, where A is ^{137}Cs activity, k and x are constants, and t is time. Although it varied with the materials and region, the time period over which this equation appears applicable is approximately 1 to 200 h. An example of the time dependent behavior of the four metals at 200°C is shown in Fig. 462-5 of Reference 5. The value of x for the curves varied from 0.20 to 0.28 in the time period 2 to 200 h.

The fact that some redistribution of activity was occurring during test, indicated that the assumption of constant cesium concentration during a test was invalid. This condition was confirmed by radiochemical analyses of bulk sodium before and after each test, showing that the ^{137}Cs concentration in solution decreased 20-50% over a 500-800 h period. The inactive cesium level also was changing, but at levels which could not be detected by the analytical method used at present. Therefore, the activity deposition rate data, which do not take the varying concentration of cesium in solution into account, are suspect.

In the coming fiscal year the adsorption of ^{137}Cs on the above materials will be continued. The adsorption temperatures will be increased to 600°C and the flow rates will be increased by at least a factor of two.

b. Trace Irradiated Fuel Loop

Another small, forced-convection sodium loop, whose principal sections can be scanned for gamma-emitting isotopes, has been operating satisfactorily for 8000 h. The loop was to be used to study the release and distribution of fission products ($\tau \geq$ 8 d) from trace-irradiated plutonium-containing fuels. However, mechanical, electronic, and vacuum difficulties were encountered with the gamma scanning equipment. These have been resolved, but there has been a delay in the use of the loop for its original purpose. During part of this delay, the loop has been used for a limited experiment to examine the attrition of unirradiated $(U,Pu)O_2$ particles in flowing sodium.

Approximately 2 g of partially sintered $(U_{0.8}Pu_{0.2})O_2$ powder, with an O/M of 2.015 ± 0.010, were added to the loop with the hot leg operating at 600°C and the cold leg operating at 325°C. The 600°C section contained a removable zirconium hot trap and a stainless steel specimen. A stainless steel specimen also was located in the 300°C section. After 2880 h of operation, the stainless steel specimens, the zirconium hot trap, and a stainless-steel-mesh-packed section were removed for chemical analyses. Samples of bulk sodium were withdrawn from the loop after 4, 29, 55, and 120 days of operation and samples filtered through 10μ screens were withdrawn after 29, 55, and 120 days. The 4-day bulk sample which contained ~20 ppm uranium and ~5

ppm plutonium indicated that a portion of the powder was circulating even at the low sodium velocities (~1 fps, max) of this loop. The remainder of the samples contained 6 ppm uranium and <0.1 ppm plutonium and thus indicated (1) that if any suspended material was present, it was $\leq$ 10μ in size, and (2) that the original mixed oxide had undergone some chemical change, as reflected by the change in U/Pu between the 4- and 29-day samples. Analysis of the traps and specimens have not been completed.

As originally planned, trace irradiated Pu-Co-Ce liquid fuel was to be used to supply relatively short-lived fission products to the loop, and their distributions were to be followed by gamma scanning as a function of time. However, because of funding reductions, this study in this loop will not be continued in FY 1970.

B. Study of Fission Product Gettering in Capsule Experiments
(H. A. O'Brien, C. R. Cushing)

1. General

Capsule experiments have been designed to determine the distribution of gamma-active isotopes in the sodium/stainless steel/helium/adsorber system as a function of time and temperature. Gamma ray scanning permits a study of transport rates, adsorption and desorption phenomena, and the equilibrium distribution between phases to be made.

In the present series of experiments, ^{137}Cs gettering and adsorption capacities of carbon and various oxides have been determined. In each test capsule a basket containing one of the materials being studied was introduced into the sodium after the cesium and sodium had come into equilibrium. The capsule was then scanned with a collimated NaI (Tl) crystal in order to determine the ^{137}Cs distribution and the amount of pickup by the getter.

2. Results in FY 1969

a. Gettering Behavior of Various Refractory Oxides

Various refractory oxides, including Al_2O_3, Cr_2O_3, Fe_2O_3, MgO, and ZrO, were examined as possible gettering agents for cesium in sodium. It was observed that all these oxides behaved in a similar manner and that none of these would be practical as gettering agents.

Perhaps because of scatter in the data, no noticeable differences were observed in the effects of these oxides on the rate of cesium movement from the sodium into the vapor region. In general, it was observed that, after a slight adsorption of cesium on these oxides (which were maintained at 500°C) during the first 24 h after the oxide samples were lowered into the sodium, the cesium began to accumulate in the vapor region in appreciable quantities. Although there had been a noticeable accumulation of ^{137}Cs in the vapor region during the preliminary equilibration period, an acceleration of cesium distillation was observed after the introduction of the oxides into the sodium. The percentage increase of the rate of cesium movement into the vapor region was found to range from 38 to 50% for the various oxides. This observation suggested two possible explanations: (1) the oxides were, to a similar extent, acting as reducing agents for cesium ions; or (2) the increased surface area of the wire-mesh basket was the cause for the accelerated distillation.

An additional experiment was conducted in which only an empty basket was lowered into the sodium. An increased cesium movement into the vapor region did indeed occur after the basket was lowered into the sodium. The percentage increase in the rate of cesium movement was found to be within the narrow range observed for the oxides, and the final rate constant for cesium movement into the vapor region was similar to those observed for the oxides. From these observations it was concluded that the increase in surface area resulting from the introduction of the basket into the sodium was the major cause for the accelerated distillation of cesium from sodium. Apparently the presence of the various oxides had little, if any, effect.

b. Behavior of Cesium Metal vs Cesium Chloride

During the course of these experiments, a question arose concerning the effect of the cesium valence state on its behavior in these systems. In an attempt to resolve this question, 10-mg samples of cesium metal and CsCl were irradiated in the OWR reactor. Following the irradiation, the reactor targets were placed in separate capsules, which, in addition, contained only sodium.

The distribution of ^{134}Cs, both throughout the sodium and in the vapor region above the sodium, was observed by scanning the capsule with a NaI(Tl) crystal. The scanning was initiated while the capsule was at room temperature. The capsule was then

heated to 500°C and maintained at that temperature for about 400 h.

By plotting the natural logarithm of the fraction of cesium remaining in the sodium vs time, it was observed that the resultant curves were similar to a two-component radioactive decay curve. Both components of the curve could be expressed by a first-order kinetic equation of the type

$$A - A_o e^{-\lambda t}, \quad (2)$$

where A_o and A are the fractions of Cs in the sodium at times t_o and t, respectively. The term λ represents the first-order rate constant in units of sec^{-1}, while t is time, expressed in seconds, after the experiment was initiated.

During the first 24 h of the experiment, both Cs metal and CsCl left the sodium and entered the vapor region at a relatively rapid rate. The calculated rate constant for Cs metal during this period was 4.3×10^{-5} sec^{-1}, while that for CsCl was 2.0×10^{-5} sec^{-1}. Thus, the rate for Cs metal was a factor of two greater than that for CsCl. However, at the end of the first 24 h of the experiment, the concnetrations of Cs from both the metal and the chloride in the vapor region were approximately equal, i.e., about 25%. From this point until the termination of the experiments, the rates of cesium movement from both the metal and chloride solutions were approximately equal. The calculated rate constants during this period were 2.2×10^{-7} sec^{-1} for the metal and 1.8×10^{-7} sec^{-1} for the chloride.

Based on the fact that both the metal and the chloride capsules reached essentially the same cesium concentrations in the vapor region after the first 24 h, and, from that point to the end of the experiments, that the rate constants for both capsules were about equal, it was concluded that the initial valence state of the cesium has little effect on its behavior in these sodium systems.

c. Activated Charcoal vs Graphite

Of the materials tested in this program, graphite and activated charcoal appeared to be useful gettering materials for cesium in sodium. Tests at 500°C showed that activated charcoal adsorbed greater than 99% of the cesium within 100 h. Under the same conditions, graphite was capable of adsorbing only about 50% of the cesium.

Adsorption studies carried out at 400°C demonstrated that graphite and activated charcoal exhibited a similar cesium adsorption behavior, although the adsorption rate during the earlier part of the experiment was slower than that observed for charcoal at 500°C. After about 100 h, both materials had adsorbed about 95% of the cesium in the sodium.

Additional tests of these materials at 300 and 200°C showed the adsorption behavior of both species was similar, but, as expected, the approach to equilibrium was slower as the temperature was decreased. At 200°C, the time required to attain equilibrium had increased to 400 h, while the total cesium adsorption had decreased to about 85%.

From the results obtained in this study, it appears that either charcoal or graphite may be effectively utilized to remove radioactive cesium from sodium. For optimum results the trap should be operated between 400 and 500°C for activated charcoal and at 400°C for graphite.

This project has been terminated and a final report is being prepared.

V. ON-LINE MONITORING METHODS

A. Plugging Meter Studies
(C. C. McPheeters, J. C. Biery)

1. General

Sodium plugging indicators have been utilized for many years to give indications of impurity concentrations in sodium systems. Recently, work at the Los Alamos Scientific Laboratory has shown that plugging indicators can be used to give information about impurity saturation temperatures, impurity nucleation characteristics, and impurity mass transfer phenomena.[6] This work has given indications that more than one impurity could be detected and saturation temperatures determined when impurities exist simultaneously in a given sodium system. Also, it may be possible to determine the types of impurities and their concentrations by the kinetic behavior of the growing precipitate on the plugging indicator orifice. In the following, the methods of calculating mass transfer coefficients will be presented, and their utility in determining species, concentrations and nucleation characteristics will be discussed.

2. Results in FY 1969

a. Description of Plugging Meters and Modes of Operation

The plugging meter orifice assembly used in the Los Alamos studies is a regenerative type in which the sodium flows down the center tube and loses heat to the sodium flowing up the outside annulus. The plugging meter is cooled by blowing air around the outside annulus and heated by electrical units on the outside of the meter. Four orifices 0.052 in. diam are situated at the bottom of the inner tube. Sodium velocity through the orifice can be varied from 50 to 500 cm/sec.

During the year meters at four other research organizations were also studied. The meters were of two basic types: (1) either the regenerative type with orifice plate or (2) a valve with slotted seat or a perforated disc with an air cooler upstream. The characterisitics of the various meters are summarized below.

General Electric, San Jose, California: Regenerative type, flow down outside, up center, 4 holes in orifice plate. Hole diameter: 0.036 in.

MSA Research Corporation, Evans City, Pennsylvania: 1/2-in. Hoke valve, 8 half circle slots cut in valve disc. Hole diameter: 1/16 in.

EBR-II, Meter on Secondary: 1/2-in. Hoke valve, 10 square slots cut in valve disc. Slot width: 0.040 in.

Liquid Metal Engineering Center, Canoga Park, California, SCTI Loop, Primary: 1-in. valve, 10 square slots in valve disc. Slot width: 0.040 in.

(1) Operational Mode 1: Initial Bare Orifice, Constant Cooling Rate

This mode is the normal one usually followed. The cooling blower is turned on, and the sodium is allowed to cool until a decrease in sodium flow is noted. The temperature at this "break" is called the "plugging temperature." In a multiple impurity system a second or third change in flow trace slope can be detected as the second and third impurities start to nucleate and grow on the orifice plug.

(2) Operational Mode 2: Initial Bare Orifice, Constant Temperature

In this case, the blower is turned on and the sodium cooled to some desired temperature below the saturation temperature. The temperature is then held constant by properly adjusting the blower louver or by turning the blower on and off at some desired frequency. After some period of time the impurity nucleates, and the plug grows at some rate dependent upon the temperature difference between the saturation temperature and the sodium-orifice temperature.

(3) Operational Mode 3: Partially Plugged Orifice, Oscillating Flow

Once the plug has begun to grow, the partially plugged mode starts. In this case, a partial plug of the impurity is maintained on the orifice, and the temperature of the sodium is adjusted either manually or automatically to add to or subtract from the plug volume by dissolution or precipitation of the impurity involved.

b. Summary of Previously Reported Nucleation and Rate Phenomena

As a background for understanding rate processes in multiple impurity systems, the data and phenomena previously reported will be reviewed.[6] In this previous work, the nucleation characteristics of Na_2O on a bare orifice were studied. The general result was that temperature depressions below the saturation temperatures were observed in all cases where Na_2O was nucleated on a bare orifice. (The temperature depression is the difference between the saturation temperature and the "plugging temperature" at which the first attenuation of flow is noted.) The amount of depression decreased with increasing flow rate and increased with increased cooling rate. When constant temperature runs were made, the time to nucleation increased with decreasing velocity and decreasing concentration driving force. For Na_2O precipitation on a bare smooth stainless steel orifice, a minimum concentration of Na_2O or saturation temperature was found below which no Na_2O nucleation would occur. This temperature was 135°C or 0.45 ppm from the semi-log linear Rutkauskas curve.[2] Because of the temperature depression effect and the influence of operating variables on the effect, a plugging meter must be calibrated when the bare orifice mode is used, and the conditions used must be standardized.

The temperature depression can be eliminated if the meter is operated in the partially plugged mode. In this case, a precipitate exists on the orifice, and the precipitate increases or decreases in size as the temperature of the sodium drops below or goes above the saturation temperature. No nucleation

concentration driving force is required to produce changes in flow. The "oscillating" plugging meter operation was developed to exploit this condition. An on-off switch was installed on the flow recorder to turn on the cooling blower when the flow increased above a set point value and to turn the blower off when the flow decreased below the set point. An oscillating flow and temperature pattern developed with this type of on-off control. The saturation temperature was indicated as the average of the temperatures associated with each maximum and minimum in the flow. Successful operation of this mode of indication was achieved over the Na_2O saturation temperature range from 220 to 108°C.

c. Calculation of Mass Transfer Coefficients from Plugging Indicator Data

Mass transfer coefficients can be calculated from the flow and temperature traces obtained from plugging indicator runs. These coefficients may be dependent upon the flow patterns in the orifice or upon the impurity precipitation characteristics. Even in the case where the coefficient is determined by the liquid flow patterns in the orifice, the actual calculation depends upon a solubility curve for the precipitating impurity and is, as a result, dependent upon the impurity. Therefore, by investigating the variations of mass transfer coefficients with flow, impurity, and orifice characteristics, a method may be developed whereby the type of impurity and its concentration can be determined from its plugging meter traces.

Large quantities of data from the plugging meter traces must be analyzed to determine these functional variations. To help expedite this job, a computer program has been written to process data from the temperature and flow traces. The mathematics and processing characteristics of the program are summarized below.

Program Characteristics

General Input:

Bare orifice flow with throttle valve open, gpm.

Initial plug fraction, i.e., fraction of orifice hole volume filled with precipitate.

Diameter of bare orifice, in.

Saturation temperature of impurity, °C.

Density of impurity in precipitate, gm/cm^3.

Number of holes in orifice plate.

Temperature-Flow Input for Mass Transfer Coefficient Calculations:

The temperature-flow readings from the plugging meter chart are divided up into time segments which allow easy computations. The natural endpoints to the segments occur at changes in slope of the temperature trace and intersections of the temperature trace and the saturation temperature. For each time segment, the following data are required:

Flow rate at beginning and end of time segment.

Length of time segment.

Temperature at beginning and end of time segment.

Number of increments within the time segment that will be used by the program in the numerical integration of the time-concentration integral.

The calculational procedure contains two major steps. First, the plug fraction must be calculated from the change in measured flow. Second, from the plug fraction and the sodium time-temperature plot, the mass transfer coefficients can be calculated. The double orifice effect produced by upstream throttling has been previously described[7] and can be represented mathematically by Eq. 2 presented in Reference 4, Page 24.

Once the plug fraction has been calculated, the rate constant can be determined from Eq. 3 from Reference 4, for any segment of the plugging run. To calculate the mass transfer coefficient, a solubility curve must be selected for determination of both C and C_e in the integral of Eq. 3, Reference 4. For all of the calculations reported here for oxygen, the semi-log linear curve presented by Rutkauskas[2] has been utilized.

The mass transfer coefficient calculated with the above procedure is based upon a model that postulates the precipitate to grow in a smooth cylindrical layer on the inside surface of the orifice. This model is obviously over-simplified. Nucleation of discrete crystals on the orifice surface probably occurs as the plug forms initially. Also, as the plug size approaches 100% of the orifice volume, crystals may bridge across the cylindrical hole. These effects change the area available for precipitation and are not easily included in a mathematical formulation. However, deviations from the expected variation of the mass transfer coefficient with changes in velocity may give some indication of the actual crystal growth patterns in the orifice.

d. Variation of Mass Transfer Coefficient with Velocity

A series of plugging runs made on the LASL cold trap system plugging indicator was analyzed to determine the dependence of the mass transfer coefficient on the velocity of sodium through the orifice. Three types of runs were analyzed. In each run the orifice temperature was held constant at 209°C while the saturation temperature was 218°C. The impurity was assumed to be oxygen, and these temperatures give a driving force of 3.3 ppm. In the three runs the sodium throttling was incrementally increased, left unchanged, and incrementally decreased to give a range of velocities through the orifice.

Because of possible deviations of the mass transfer coefficient in the low and high percentage plug portions of the above ranging velocity runs, only the coefficients in the 23 to 80% plug range were selected for correlation with velocity. If discrete crystals had nucleated, they probably would have grown together in this plug range to form a cylindrical surface similar to that postulated in the simplified mathematical model. At higher percentage plugs, bridging might occur. The selected portions of the three runs are shown in Fig. 462-10. The data appear to indicate a velocity dependence which on a log-log plot has a slope of 0.8. In turbulent liquid phase, eddy diffusion controlled, mass transfer processes, the mass transfer coefficient has been found generally to vary in proportion to the mass flow rate raised to the 0.8 power.[8]*

e. Deviations in Mass Transfer Coefficient Resulting from Crystal Nucleation

The basic simplified model proposed for the growth of the precipitate in the orifice assumes the precipitate to form as a smooth cylindrical layer and to grow uniformly inward. If discrete crystals form, the area for precipitation can be greater than or less than the cylindrical surface area (at equivalent plug fractions) with the variation in area depending on the number of crystals nucleated.

A simple discrete crystal model has been proposed to serve as an example of this surface area effect. In this case, a finite number (n) of square cylindrical block crystals were assumed to nucleate simultaneously on the orifice surface. The calculations with the model give the relative surface area of the blocks as compared to the smooth cylindrical surface as a function of plug fraction and number of crystals nucleated. The calculational development is outlined in Reference 5, Page 23. The results of the calculations are shown in Fig. 462-11.

Since all of the mass transfer coefficient calculations are made with the assumption of the smooth cylindrical layer of precipitate, any variation in area caused by discrete crystal precipitation will show up in the mass transfer coefficient. The actual coefficient being calculated is a product (ka) of the basic coefficient (k) and the area ratio (a), where (a) equals the area ratio of the actual precipitate as compared to the smooth cylindrical precipitate. If the discrete precipitate model proposed above applies, (a) equals A_r/A_c of Fig. 462-11. Since the calculated coefficient includes the area ratio term, the variation of (ka) with velocity can possibly give indications of the number of nuclei precipitating on the orifice.

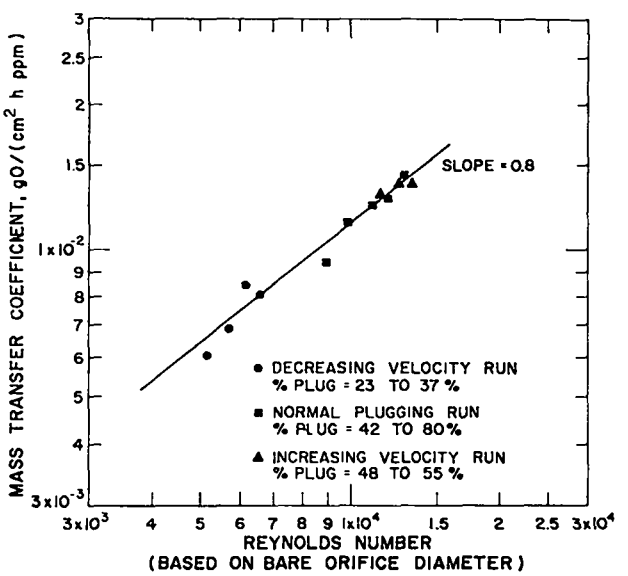

Fig. 462-10. Variation of Mass Transfer Coefficient with Velocity. Data Taken on LASL Meter.

*The more accurate linear dependency of the mass transfer coefficient is on the function $v^{0.8}/D^{0.2}$ where v is velocity through the orifice and D is the diameter of the actual flow channel in the orifice. The $D^{0.2}$ term has not been included in the above relationship because its effect is minor. As the plug grows from 30 to 60%, the diameter decreases 25%, and $D^{0.2}$ decreases 5.5%. The change of $D^{0.2}$ from 0 to 60% plug is 8.8%.

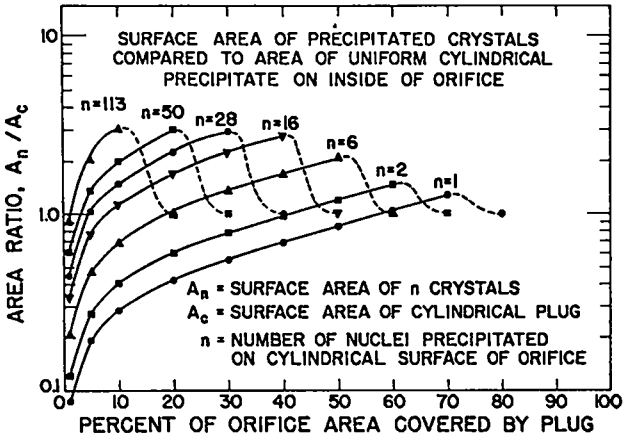

Fig. 462-11. Precipitate Surface Area Ratio as a Function of Plug Fraction and Number of Crystals Nucleated.

f. Nucleation Characteristics in LASL Varying Velocity Runs

The total data from the two increasing velocity runs seem to indicate that from 6 to 16 nuclei were nucleated per orifice. In the two cases the mass transfer coefficient started a factor of 2.5 to 4.0 below the 0.8 slope line and increased up to it and formed a maximum near 0.48 to 0.52 plug fraction. From Fig. 462-11, this performance appears to correlate fairly well with the calculated data for n between 6 and 16. The driving force for the initial nucleation was 3.3 ppm of oxygen.

The decreasing velocity run had a maximum at 0.27 plug fraction after increasing by a factor of 2.5 between plug factors 0.10 and 0.27. This behavior seems to indicate that 28 nuclei were formed per hole initially.

g. Plugging Meter on General Electric Loop 8 (San Jose, California) Mass Transfer Coefficients and Nucleation Characteristics

Data from the General Electric plugging indicator runs were processed as described above. The data from Loop 8 were divided into two runs. In both runs a plug was precipitated on a bare orifice; was partially dissolved off; and then repeatedly precipitated on and partially dissolved off in the oscillating mode. This type of run allowed changes in mass transfer coefficient to be determined as a function of Reynold's number and time. The results from both runs indicated that time had an effect on the mass transfer coefficient in that the plug appeared to approach the cylindrical shape of the postulated model with repeated precipitations and dissolutions. Also, the velocity dependence observed at LASL seemed to be evident in the middle portions of the precipitation run. The time and Reynold's number plots of the coefficients are presented in Reference 4, Page 25.

The two runs may be examples of two types of cases, i.e., few and many initial nuclei. In Run 1, the coefficient started a factor of 2 below the 0.8 slope line and came up to it at a plug fraction of 0.4. The previous analysis suggests that the number of nuclei initially precipitated was 3-5 per hole. In Run 2 the initial coefficients started above the 0.8 slope line by a factor of 1.3 and approached the line at a plug fraction of 0.35 to 0.45. In this case 20-25 nuclei per hole are indicated.

If the nucleation characteristics were in fact different, then the initial precipitation ΔC driving force should have been greater in Run 2 than in Run 1. This condition appears to have existed. In Run 2 the ΔC driving force at the first noticeable flow change was 1.1 ppm while in Run 1 the driving force was 0.6 ppm.

h. Detection of Multiple Species on a Plugging Meter

By operating plugging meters in the partially plugged "oscillating" mode, more than one species can possibly be detected. In nonoscillating plugging runs, the multi-impurity detection has been described as multiple "breaks" or changes in slope in the flow curve. When operated in the "oscillating" mode, as many as three impurities have been detected. This may be done either by preferentially nucleating a lower saturation temperature impurity and then allowing the high temperature impurity slowly to precipitate on the plug with the attendant shift to higher saturation temperatures; or it may be accomplished by successively precipitating lower temperature impurities upon a high temperature plug. These two types of behavior have been demonstrated on meters at Los Alamos and at MSA Research at Evans City, Pennsylvania.

(1) Multiple Impurities in LASL Cold Trap Loop

The cold trap loop and its cold trap were run at higher than normal temperatures and some interesting phenomena were recorded with the use of the plugging indicator. Previously, operation of the meter in the oscillating mode indicated that two

impurity species were in the system. This condition was shown when the meter indicated an equilibrium saturation temperature near 220°C initially but after an hour of operation slowly shifted to an equilibrium temperature of 240°C (which was approximately the cold trap temperature). The frequency of oscillation and the rates of mass transfer for the upper temperature impurity were much slower than for the lower temperature impurity. The lower temperature curve could be repeated by dissolving off the plug and then reprecipitating the lowered temperature precipitate. This precipitate formed preferentially because the concentration of the higher temperature species was not large enough to produce nucleation of crystals in the period allowed. Thus, the more soluble species precipitated first when the temperature was sufficiently reduced.

This same type of phenomenon was not observed as the cold trap temperature was increased. With the cold trap at 280°C, the double saturation temperature was not observed. The nucleation of the upper temperature specie occurred before the temperature could be lowered to the level where the low temperature specie could nucleate and precipitate. In this case the saturation temperature of the upper temperature species was 280°C. At this cold trap temperature there was a sufficient quantity of the specie to saturate the sodium. However, there was an insufficient supply of the lower temperature species to saturate at the high cold trap temperature, and its saturation temperature remained at 220°C.

A further increase of cold trap temperature was made to 350°C and the plugging indicator showed that a third specie may be present. In this case a lower temperature specie precipitated first and the meter oscillated about a temperature in the 290-300°C range. After about 30 min, the temperature slowly changed toward a saturation temperature in the 320-330°C range. After a day this temperature increased to 350°C. The lower temperature species had a kinetic behavior similar to that of the high temperature specie of the previous lower temperature pair. The kinetics of precipitation of the high temperature specie of the high temperature pair were very slow and very little oscillation of the flow curve resulted.

A detailed possible explanation of this behavior was presented in Reference 9, Page 23.

(2) Multiple Impurities Detected on MSA Research Corporation Loop No. 1 (High Carbon) Plugging Meter

Operation of the plugging indicator on Loop No. 1 at MSA Research Corporation, Evans City, Pennsylvania, indicated that three impurities existed with saturation temperatures of 715-765°F, 545-555°F, and 320-328°F. The impurities were not identified; however, they possibly were in order of decreasing saturation temperature, carbon containing, hydrogen containing (NaOH or NaH), and oxygen (Na_2O). The high temperature impurity exhibited a decreasing saturation temperature during the day-long test and the carbon flux in a United Nuclear Corporation carbon meter on the loop also decreased commensurately. Thus, this upper specie was suspected to be a carbon containing compound. The other two species exhibited plugging curves with kinetics that appeared similar to those produced on the LASL meters when these impurities were suspected of being present.

The concentrations of the upper temperature impurities were sufficient to promote nucleation before the lower temperatures could be reached in the cooling run. However, the rate of plug buildup was slow in each case, and the lower temperature impurities could be precipitated and dissolved off almost as though the upper temperature impurity were not there. Thus, an "oscillating" run was made on each of the three impurities and saturation temperatures were thereby obtained. The best estimation of the saturation temperature in each oscillation cycle appeared to be obtained at the minimum of the oscillation. The reason for this effect probably was that at the start of the dissolution cycle only the one impurity was present on the surface of the plug. However, on the precipitation cycle, a portion of the higher temperature precipitate was probably exposed during the previous dissolution and the high temperature impurity would start to precipitate before the saturation temperature of the lower temperature impurity was reached. The flow traces also indicated that when a lower temperature impurity started to precipitate, the precipitation of the higher temperature impurity appeared to be suppressed or possibly completely stopped.

i. Use of Mass Transfer Coefficient Calculations for Specie Identification

The mass transfer calculations seem to indicate that the process of deposition and dissolution is liquid phase controlled. If this condition is the case, then the mass transfer coefficients for various species might be expected to be similar in size under similar flow conditions in the orifice. Therefore, if a specie is suspected of precipitation on the orifice, the correctness of the supposition can be tested by calculating the mass transfer coefficients from the observed kinetic behavior and from the density and solubility curves for the specie. Thus far, very little data has been obtained to verify the above proposition. However, the following data from the LASL cold trap system tend to support the idea.

(1) Mass Transfer Calculations with Unknown Impurity in LASL Cold Trap Loop

Two unknown impurities have been detected in the Cold Trap Loop after a recent startup with a new "removable core" cold trap. The oscillating plugging indicator tended to operate initially around the impurity with a saturation temperature near 195°C but at later time indicated a saturation temperature in the 260-270°C range for the second impurity. Dissolution and precipitation runs for the 195°C impurity were analyzed kinetically by calculating mass transfer coefficients. The impurity was assumed to be NaH, and the Addison[10] solubility curve was used. The oxygen level in the loop appeared to be low with a saturation temperature below 150°C.

The mass transfer coefficients on the precipitation cycle were in the range of 1.1×10^{-2} to $1.5\ 10^{-2}$ g H/[ppm(H) cm^2 h]. These numbers are almost identical with similar coefficients calculated for Na_2O precipitation on the same meter at earlier times. The inference from the agreement is that the assumed species is NaH and that the solubility curve is correct. The quantity of data does not prove the inference. However, this process of guessing at an impurity and its solubility curve to produce a reasonable mass transfer coefficient may be valuable in identifying impurities and estimating their solubility curves.

j. Plugging Meter on FFTF - Small Sodium Chemistry Loop. Mass Transfer Coefficients and Nucleation Characteristics

On April 14, 1969, the plugging meter on FFTF, the small sodium chemistry loop at Richland, Washington, was tested by LASL personnel to determine mass transfer and nucleation characteristics. The meter had the following features:

1/2-in. Hoke valve - No. 4334

Four 1/32-in. square slots cut into valve disc.

Valve positioned 10 in. downstream from end of air cooler.

The loop operating conditions were as follows:

Cold trap: 230-240°F (on less than 1 day before test).

Main loop temperature: 640°F

Main loop flow: ~0.5 gpm with PI open.

Flow split between bypass and PI loop:
~0.2 gpm through PI when closed and clean.
~0.4 gpm total main loop flow with PI closed.

During the short (1 h) test, a plug was formed and five maxima and minima in the flow curve were produced by oscillating the temperature of the sodium. The precipitate nucleated easily with a temperature depression of only 12°F and a nucleation time of 2.7 min. The cooling rate at nucleation was 4.4°F/min. The five maxima and minima indicated that the saturation temperature was 347°F. The range of the estimates of saturation temperature in these determinations was 340-360°F. The 347°F temperature was equivalent to an oxygen concentration of 2.8 ppm as determined from the Rutkauskas semi-log linear solubility curve.[2]

The flow and temperature data were analyzed to generate mass transfer coefficient as a function of time. The results are summarized in Fig. 462-12.

The data are very interesting because they give changes of mass transfer coefficient with changes in plug fraction at constant velocity through the orifice. The velocity was 425 cm/sec and the bare orifice Reynold's number was $6.4 \times 10^{+3}$. As indicated above, the mass transfer coefficient is expected to increase with plug fraction until the individual crystals grow together to form a cylindrical hole. The data in Fig. 462-12 show an inflection point near the 20% plug growth point and then another at 55% plug. The implications of this shape of curve are that the initial nucleation deposited between 50 and 100 nuclei per hole and that

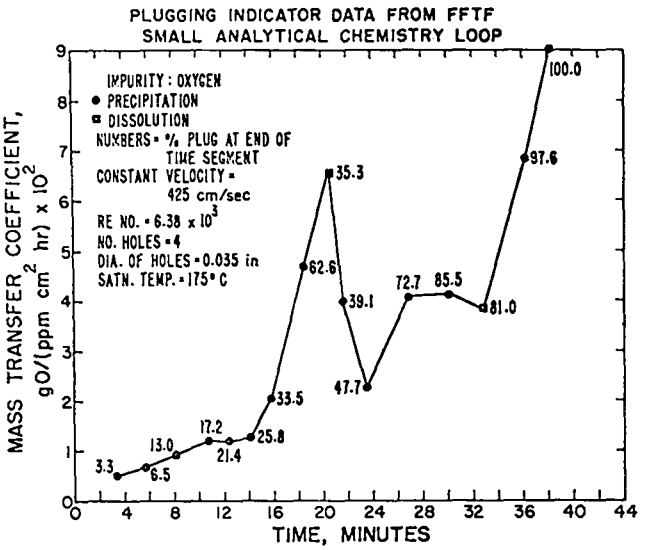

Fig. 462-12. Mass Transfer Coefficients as a Function of Time for the Plugging Meter on the FFTF Small Sodium Chemistry Loop.

a second nucleation of crystals occurred after 14 min of operation with the mass rate increased because of the increased precipitation area. The number of additional nuclei in the second precipitation is estimated to be between 25 and 35 from the data in Fig. 462-11. The ΔC driving force for the first nucleation was 1.1 ppm of oxygen. At the second nucleation, the driving force was 2.0 ppm.

The size of the mass transfer coefficients was between 5 and 12 x 10^{-3} g O/(cm^2 h-ppm) from the first part of the run. These numbers are consistent with 11 x 10^{-3} coefficient obtained at similar Reynold's numbers from the data obtained on the General Electric loops at San Jose and 8 to 10 x 10^{-3} obtained on the LASL meter in the Cold Trap Loop No. 1.

k. Plugging Meter on EBR-II Secondary Saturation Temperature and Nucleation Characteristics

LASL personnel visited the EBR-II facility on June 10 and 11, 1969, to obtain cold trap data and to determine operating characteristics of their plugging indicators. The plugging indicator on the secondary loop was a 1/2-in. Hoke valve with ten 0.040-in. square slots in its disc. The valve was located approximately 12 in. downstream from a regenerative heat exchanger. Heat was removed by a manually controlled fan directed on the valve and nearby piping. The plugging indicator circuit was not throttled. The pressure drop across a throttle valve in parallel with the plugging valve forced sodium through the plugging circuit.

An attempt was made to operate the plugging indicator during the afternoon of June 10, 1969. The plugging indicator temperature was lowered to 225°F and maintained at that temperature for approximately 1 h. No detectable decrease in flow occurred during that time.

On June 11, 1969, a second attempt was made to form an impurity plug on the orifice. The temperature was lowered to approximately 220°F and maintained at that temperature for 3 h and 15 min. No detectable decrease in flow occurred for the first hour and 20 min. After that time, the flow decreased slowly to approximately one third of its original value in 1 h and 55 min. The temperature was then raised and lowered several times to determine the impurity saturation temperature. The saturation temperature was approximately 310°F; however, the kinetic behavior of the impurity was not typical of the behavior of oxygen in sodium. The very slow precipitation and dissolution rates indicated a low impurity concentration.

Constant temperature runs were made both above and below the saturation temperature to obtain data suitable for calculating mass transfer coefficients. These calculations will be done at a later time.

1. Plugging Indicator Test Facility - Future Plugging Indicator Program

The experimental program for Analytical Loop No. 2 has been redirected totally toward testing plugging indicators. The loop at present contains a plugging indicator of the LASL regenerative design which has been tested extensively on Cold Trap Loop No. 1. Initially this meter will be tested with controlled amounts of oxygen added to the loop. Particularly, the kinetics of precipitation and dissolution will be further studied as a function of velocity and oxygen concentration. Other impurities will be added and systematically studied. A removable orifice plugging indicator has been designed and will be installed on one of the side loops to investigate the type of the impurity precipitated and to compare the form of the plug to that postulated mathematically.

The loop was filled with approximately 45 gal of reactor grade sodium on June 18, 1969. The system was operated at 160°F for several days. However, at this low temperature excessive pump power was

required; also, some difficulty was observed in starting flow in the smaller side loops. The temperature was then raised to 225°C with improved wetting and reduced pump power resulting.

The saturation temperature of the system is 175-180°C. The relatively rapid kinetics, as observed on the plugging indicator, indicate that the species observed is probably Na_2O.

In order to observe any other impurity in the system which might have a saturation temperature greater than 180°C, the bare orifice was held at 200°C for over 2 h. No sign of precipitation was observed. Normally, if a higher temperature impurity is present, some evidence of precipitation will be noticed with this operation procedure.

m. Summary and Conclusions

The data collected to date from the Los Alamos Scientific Laboratory (LASL), Mine Safety Appliance Research (MSAR), General Electric, San Jose (GE), FFTF, EBR-II, and LMEC indicate that the plugging indicator can detect up to three impurities in a sodium system and can determine the saturation temperatures for these impurities. Also, the rates of flow change, along with the corresponding temperature data can be used to calculate mass transfer coefficients and to study the general mass transfer and nucleation phenomena that occur on the plugging meter orifice. These observations may help one to understand and design better plugging indicators and cold traps since the phenomena occurring in these two devices are similar.

The mass transfer calculations may also help in the identification of the type of impurity precipitating from a multi-impurity system. The mass transfer appears to be liquid phase controlled. Therefore, the correct selection of the specie and its solubility curve can be checked by the mass transfer coefficient calculation. This procedure has been used on curves obtained from species thought to be Na_2O and NaH with each producing coefficients of the same size under similar flow conditions. With further development work, the plugging meter may be capable of identifying a spectrum of impurities from their kinetic behavior and indicating their concentrations from the saturation temperatures produced during the partially plugged mode of operation.

VI. SAMPLING AND ANALYSIS - Laboratory Methods

A. Vacuum Distillation Studies
(G. E. Meadows, D. N. Rodgers)

1. General

The vacuum distillation technique has been shown to be a valuable method for analyses of oxygen in sodium.[2] As a result, the method is routinely used on many of the experimental loops at LASL. The determination of oxygen using this technique is an indirect method. The assumption is made that the sodium in the residue is Na_2O and the O concentration is computed from the residual sodium concentration. The presence of other compounds of sodium and materials capable of reducing Na_2O can influence oxygen values obtained by this technique. Distillation studies are directed toward understanding these interactions.

2. Results in FY 1969

a. Effects of Calcium on Distillation Results

Using the vacuum distillation sampler which has been installed on the sodium chemistry inert glove box, some of the effects of metallic calcium on sodium residues have been studied. A supply of solid sodium was used as the source of sodium; the concentration of oxygen in it was determined by vacuum distillation to be 18 ± 8 ppm oxygen. Known amounts of calcium metal were added to the individual sodium samples, and the distillations were carried out in the usual manner with an initial distillation temperature of ~300°C, end of cycle temperature of 400°C. It was found that the oxygen concentrations as determined from sodium in the residues were lowered to <2 ppm oxygen when the calcium was present at a level 5-30 times the amount needed for stoichiometric reduction of the Na_2O. The following reaction perhaps explains the reduction of Na_2O in the residues:

$$Na_2O + Ca = 2Na\uparrow + CaO.$$

It was also found that 17-30 wt% of the calcium added to the sodium samples was carried over with the distillate. Ninety-five percent material balances for calcium were obtained when the calcium in the distillate and in the residues were recovered. Calcium metal, when heated alone in a similar manner, was not found to distill nor to exhibit a detectable weight change during the distillation cycle.

b. Off-Gas from Distillation

Observations conducted on sodium samples used in vacuum distillation analysis for dissolved oxygen have indicated that there is a small quantity (10^{-5}-10^{-6} liters) of gas evolved from the 5 g sodium metal sample during the final stages of distillation. The evolution occurs while the sample is being distilled at constant temperature (~360°C) and is associated with the removal of the final portion of the metallic sodium from the nonvolatile residue. Gas chromatographic analysis has shown the evolved gas to be composed primarily of hydrogen with traces of methane. The quantity of the gas released has been observed to be a function of the cold trap temperature in the loop from which the sodium sample was drawn; the lower the cold trap temperature, the smaller the gas release.

Based on these observations it was postulated that the gas evolved might be a decomposition product of sodium hydride. Therefore, hydrogen was added from the gas phase to the liquid sodium sample before distillation to determine whether the amount of gas evolved would increase.

A residual gas analyzer was connected to the vacuum system to continuously analyze the distillation off-gas. The analyzer can be set to monitor a single component of the off-gas.

Preliminary results indicated that the hydrogen addition did increase the amount of gas evolved. However, analysis showed that these results were due to sample contamination. More careful work eliminated the contamination and showed that, in fact, the amount of gas evolved at the end of the distillation did not increase with the addition of hydrogen.

The pressure peak previously observed at the end of the distillation did not change noticeably in tests performed after the new cold trap was installed in Analytical Loop No. 1. However, the shape of the peak has been observed to vary with the total vacuum system pressure. With the cold trap at 125°C and a system pressure of ~1 μ (measured at the distillation chamber), the peak duration is one minute and the height is 2.5 μ. At a system pressure of ~0.5 μ, the peak duration is 30 sec and the height is 1.5 μ. The narrower peak seems more reproducible. In order to run future distillations at the lower pressure, a diffusion pump was connected to the vacuum system.

It was observed that with a high calcium level (5 ppm) the pressure peak was diminished in size and was not as reproducible. Therefore, further analysis was postponed until the calcium additions were terminated and the calcium level returned to its former low level (<0.5 ppm).

c. Determination of Oxygen in Sodium by Vacuum Distillation Followed by Inert-Gas-Fusion
(M. E. Smith, W. B. Hutchinson)

Measurement of O_2 in sodium by inert-gas-fusion methods required quantitative separation of the volatile metal prior to reaction of the oxide with carbon at 1800 to 2000°C to form carbon monoxide. An inert-gas-fusion apparatus was modified by insertion of a nickel conduit into the carbon crucible to permit distillation of the sodium at 400°C. The sodium vapor, under partial pressure, was swept by argon into a trap cooled with liquid N_2. Upon completion of the distillation, the conduit and trap were removed from the apparatus without stopping the flow of argon, and the distillation residue was heated to 1800°C in the carbon crucible. The carbon monoxide evolved was oxidized and measured manometrically as CO_2. Successful distillation of the sodium was demonstrated, and an investigation was started to determine optimum conditions for measuring the O_2 in the distillation residues.

B. Study of Gamma Ray Activation Analysis for Carbon and Oxygen
(D. M. Holm, D. N. Rodgers, G. E. Meadows, B. K. Barnes, J. L. Parker)

1. General

Many analytical techniques for the analysis of oxygen, such as vacuum distillation and amalgamation methods, are not specific for a given compound and give oxygen concentrations by assuming the form of the final residue being extracted or analyzed by flame photometry. Thus, analytical techniques are required which can give concentrations of oxygen and other impurities such as carbon directly without making assumptions about the chemical form of the impurity.

Photon activation of oxygen and carbon may be used to determine total impurity concentration regardless of its chemical nature. The sodium sample is irradiated by high energy photons (~20 MeV); the sodium is extruded from its container and then is transported pneumatically to the counter, where

positron annihilation radiation is detected in a very large segmented NaI crystal. The resulting count rate vs time curve is decomposed by computer analysis into oxygen, carbon, sodium, and potassium decay curves. Thus, oxygen and carbon can be determined from one sample if the potassium and sodium interferences are kept at low levels.

2. Results in FY 1969

a. Radiation Detection Equipment and Techniques

A new, large NaI crystal assembly was tested and found to perform as expected. Figure 462-13 shows the type of data obtained with this assembly when counting positron emitting sources with a gamma ray in coincidence. Because it is a large and highly efficient detector, most of the counts are recorded in the total energy peak and only a few percent in the 1.02 MeV peak. This is particularly useful in photon activations of sodium samples where one is determining the amount of oxygen and carbon impurities. The oxygen and carbon are both pure positron emitters and their signals appear in a peak at 1.02 MeV, whereas ^{22}Na and ^{38}K are interference reaction products and their dominant signals appear at 2.3 MeV and 3.2 MeV, respectively. With smaller detectors, operated in the same manner, most of the counts from the impurities being measured and the interference reactions appear in the same peak at 1.02 MeV, so discrimination between them is much more difficult.

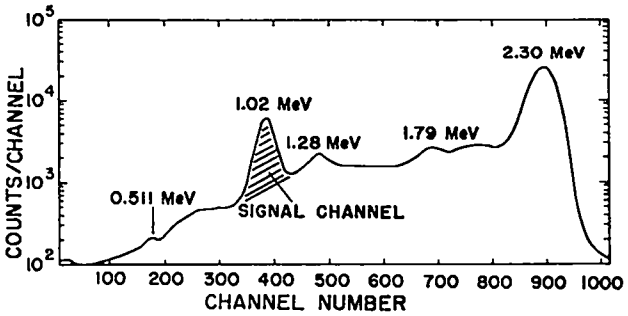

Fig. 462-13. Spectrum with More Than One Gamma Ray in Coincidence.

b. Sodium Irradiations

A sodium sample was irradiated in the Los Alamos Electron Prototype Accelerator (EPA) in an attempt to detect carbon by photon activation. The sample was irradiated at about 18 MeV for about 5 min (1 mA average current). After a 30-min decay, the sample was counted in the gated 4π mode. Some 20.4-min activity (from ^{11}C) was observed along with substantially more ^{22}Na and a large amount of ^{24}Na. The ^{24}Na is from neutron capture in ^{23}Na. The absolute amount of ^{12}C in the sample could not be determined because of the variable energy of the electron beam during the radiation. Also, the source of the neutrons which produced the ^{24}Na was not known at that time, but was subsequently discovered and removed.

A second sodium sample drawn from a barrel of reactor grade sodium was irradiated at the EPA and analyzed for carbon content. The results indicated that there was not sufficient photon energy to activate carbon.

In order to be sure that there would be sufficient photon energy (requiring 18-20 MeV of electron beam energy) for subsequent samples, work was done to determine the electron beam energy of the accelerator as a function of the normal operating parameters. There is no provision at the present time for monitoring electron energy during operation of the accelerator; however, a bending magnet is being designed for this purpose.

The beam energy can be determined to ~5% by using simple techniques and readily available instruments. From data published by a French physicist,[11] a curve was constructed relating the ratio of oxygen to carbon $^{15}O/^{11}C$ activation in Lucite (polymethyl methacrylate) to the electron beam energy for a 300-sec irradiation time. (The procedure is described in Reference 3, Page 29.)

The Lucite irradiations showed that the beam energy was considerably lower than expected. When operating at full power, the actual energy was about 17.1 MeV as compared to an expected 24-25 MeV.

c. Sodium Handling Equipment

The sodium handling equipment (shear, extruder, and rabbit) which is used in the evaluation of the gamma ray activation analytical technique for the determination of oxygen and carbon in sodium has been completed and has undergone operational checkout. Modifications to improve its performance were subsequently made. A thief-tube sampler system for removing characterized sodium samples needed to evaluate this technique has been installed on Analytical Loop No. 1.

d. Future Plans

Because of funding restrictions, the gamma ray activation program will be very limited in scope. One or two more samples probably will be processed early in FY 1970, and the work will then be discontinued.

C. Absorption Spectrophotometry Development for Metal Impurity Analyses
(G. E. Meadows, R. D. Gardner, R. L. Carpenter)

1. General

Soluble getter and corrosion studies require that various metal impurity concentrations be known as a function of operating conditions. One technique for determining these concentrations is absorption spectrophotometry. Refinement of this technique is being made to detect low level concentration (~1 ppm) both in vacuum distillation residues and in bulk sodium samples. The impurities to be studied are calcium, magnesium, potassium, iron, nickel, and chromium.

2. Results in FY 1969

a. Calcium in Sodium

Procedures have been developed for the determination of calcium in vacuum distillation residues and also bulk sodium samples. Precision for calcium in the residue samples is ± 0.05 ppm in the 0.1 to 10 ppm range, and for bulk sodium samples ± 0.5 ppm in the 1 to 10 ppm range. Some data obtained indicates that part of the calcium in sodium can be carried over with the sodium in the distillate.

b. Cesium in Sodium

A procedure has been developed for the determination of cesium in sodium metal in the 20-200 ppm range using atomic absorption spectrophotometry. The sample is dissolved in ethanol and diluted with water. The maximum sensitivity is achieved at a pH of 5 in HNO_3 solution. Nitric acid was chosen for the neutralization after testing the effects of chloride, nitrate, acetate, sulfate, and phosphate on the absorbance of cesium. The light source is an Osram lamp, and the absorbance of cesium is measured at 8521 Å with a red-sensitive photomultiplier tube. At a sample concentration of 1 g/25 ml the sodium has no absorbance, but it does reduce the sensitivity for the cesium. The absorbance-concentration curve for 0-200 ppm cesium in the presence of sodium was found to be a straight line. The procedure, applied to prepared samples containing 24, 50, 100, and 180 ppm of cesium, gave recoveries of 25 ± 1, 52 ± 1, 104 ± 1, and 184 ± 2 ppm, respectively.

D. Total Carbon Analysis Development
(K. S. Bergstresser)

1. General

The low temperature combustion technique for total carbon analysis is being refined. By using a high sensitivity gas chromatograph for quantitative measurement of the CO_2 produced, it is hoped that carbon concentrations in the 1 ppm range can be determined.

2. Results in FY 1969

Operating parameters for quantitative measurements of carbon at the 1 ppm level in sodium were investigated. These carbon measurements were based on the Kallmann and Liu[12] principle of low-temperature sodium ignition and its subsequent wet-method operations to avoid the problems of high-temperature (1100°C) ignition. The developmental work included (a) redesign of a nickel vessel, heated to 300-500°C, for oxidation of sodium and contained carbon traces, (b) preparation and handling of CO_2-free aqueous reagents, (c) quantitative release of carbon dioxide from acid solutions, (d) reduction of moisture level to below 50 ppm in the carrier gas used in transferring trace amounts of carbon dioxide to the detection instrument, and (e) gas chromatographic detection of carbon dioxide at the 10^{-2} microgram level for small aliquots of dissolved 5-g sodium samples. Numerous variations of equipment and operating conditions were tentatively proposed and tested. This method for carbon traces appears to be feasible, but at present the level for blank determinations is disproportionately high. Major improvements also were made in the circulating supply of liquid sodium and the attached inert-atmosphere drybox system, both of which were used during investigation of the proposed low-temperature ignition method for carbon.

E. Development of Remotely Operated Distillation Sampler
(W. R. Wykoff, D. N. Dunning, E. O. Swickard, H. M. Ruess, J. R. Phillips, J. E. Swansen)

1. General

The original objective of the project was to produce three remotely-operated distillation samplers: one as a prototype, one for installation on

the EBR-II primary loop, and one for installation on the EBR-II secondary. Because of program funding reductions, the objective has been curtailed to the production of the prototype unit only.

The sampler is an engineering loop version of a laboratory model in use on Sodium Analytical Loop No. 1 and Cold Trap Loop No. 1 at LASL. Samples are taken from a continuously flowing bypass stream. The sampler is fabricated from Type 304 stainless steel, and energy for sodium evaporation is supplied by induction heating. Figure 462-14 is a schematic of the system. An empty sample cup is loaded at S-1, moved by the transfer mechanism to S-4 for vacuum outgassing, to S-5 where a sodium sample is picked up, to S-4 for sodium evaporation, then back to S-1 for removal from the system. Residue analysis is performed at another location.

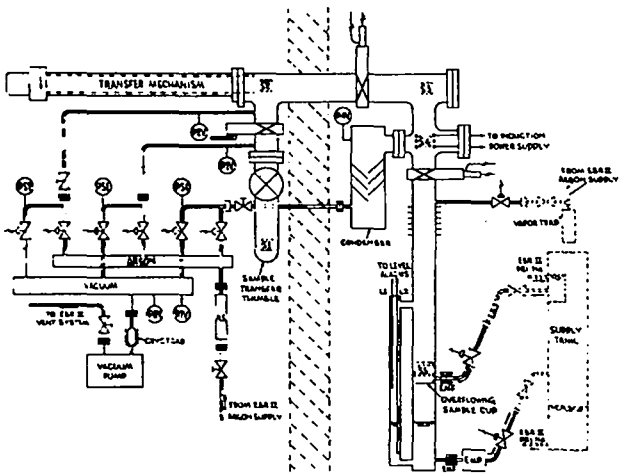

Fig. 462-14. Schematic of Remotely Operated Distillation Sampler.

2. Results in FY 1969

a. Transfer Mechanism

The transfer mechanism for the prototype was built and given an initial test which indicated that the Model 50 Slo-Syn motors were marginal in torque output. The Model 50's were replaced by Model 250's and the unit again placed in test. It appears that the mechanism will meet the requirement of 1000 cycles in a vacuum.

Design of the solid state circuitry for control of both horizontal and vertical motor drives has been completed. Fabrication of the circuits has started.

b. Vacuum-Inert Gas System

Three vacuum-inert gas systems were completed before the program reduction. Each system includes a vacuum pump and cold trap, vacuum and gas manifold, and associated gauges, valves, and pressure switches.

c. Control and Instrumentation

There are three control modes for the sampler: (1) a circuit-enforced sequence of operations that requires the operator to perform the steps in a defined sequence, (2) a less restrictive mode in which any step may be performed, in or out of sequence, provided all interlocks are satisfied, and (3) any step may be performed at any time regardless of interlocks. Figure 462-15 is a photograph of the sequence circuit and the graphic panels.

Design of sequence and graphic panel circuits is complete and fabrication is 90% complete.

d. Stainless Steel Envelope

Design and fabrication of the stainless steel envelope has been completed with the exception of the sample transfer thimble and the region around the weir from which the sodium sample is taken.

e. Induction Heating

Three induction heating power supplies have been received, tested, and accepted (after considerable modification by the vendor to bring them up to specifications). The power supplies are rated at 2.5 kW at 450 KHz. They have an integral coil cooling system employing silicone heat transfer coolant.

Plans have been formulated for a test of sodium evaporation in a mockup of Station S-4 which will employ the internal induction coil.

VII. COVER GAS AND MAINTENANCE ATMOSPHERES

A. Development of a High Temperature Quadrupole Mass Spectrometer for Cover Gas Analysis

(J. P. Brainard, D. C. Kirkpatrick, C. R. Winkelman)

1. General

The purpose of this research is to develop a method for continuous on-line analysis of high temperature (up to 650°C) cover gas in an LMFBR. The analyzer must be capable of detecting impurities such as N, O, H, CO_2, CH_4, and fission products in the cover gas with a sensitivity varying from the part-per-million range to the percent range. A response time of about 1 min is necessary if the analytical data are to serve as an error signal for activating devices for continuous control of cover gas composition.

A quadrupole mass spectrometer was obtained in order to meet the above requirements. It is believed that reasonable representative sampling can be accomplished by transporting the sample gas in sodium loop containment materials and at sodium loop temperatures until it has passed through the spectrometer for analysis.

2. Results in FY 1969

Many problems can be eliminated or minimized by collimating the high temperature gas into a molecular beam and introducing this beam in a one pass sweep through the ionization region of the mass spectrometer. This development will enable the mass spectrometer to be operated at normal operating temperatures and will minimize elution. Two additional supporting vacuum systems are required; one is used to collimate the gas beam before the introduction, and the other is used to absorb the beam after it is analyzed. The cover gas sample will be brought to the analyzer by means of a capillary tube made out of the sodium loop containment material and heated to the temperature of the cover gas.

Before the analyzer could be completely designed, study of molecular beams had to be made to determine appropriate means of efficiently forming the beam in the analyzer. The system used to measure gas source distributions is shown in Fig. 462-16. The gas is led to the source by a 7-mil i.d. capillary on the right. It fixes the total flow through the source to 0.19 Torr-ℓ/sec when one atm of helium is applied at the high pressure end. A

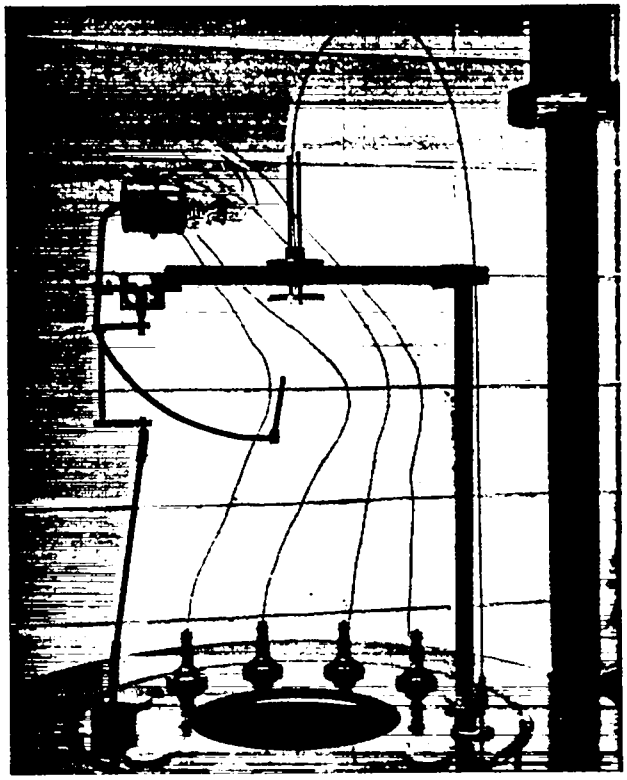

Fig. 462-16. The apparatus used to measure the gas beam flux distribution.

¼-in. o.d. tube is connected to the ionization gauge. The open end of the tube directly under the gas source is the point of measurement. The pressure builds up in the gauge until the flux leaving the tube equals the flux entering the tube. There are two advantages to this method; (1) the signal is amplified six times since the flux in all directions in the gauge must equal that of the impinging gas current and (2) the bulky gauge is removed from the beam. The open end of the tube moves in a plane through the beam axis and on a circle having the gas source as the center. The motion is accomplished by the rotable feed-through at the left (Fig. 462-14). The gas source is aimed down the throat of the diffusion pump in order to increase the pumping speed. Problems of beam reflection from the bell jar envelope are minimized by rotating the point of measurement rather than the gas source. Data on the gas sources used are found in Table 462-XII.

The results are shown in Fig. 462-17 for helium gas. A paper was presented at the American Vacuum Symposium, New Mexico Section, in April, 1969, on these gas beam studies.

Table 462-XII

Data On Gas Sources

Type	Manufacturer	Tube or Hole Diameter	Length	Number of Tubes
Glass (375 mil o.d.) Tube Bundle	ORTEC	5.4 mil i.d. 7.2 mil o.d.	150 mil	2500
Stainless Steel (250 mil o.d.) C. H. S.*	Brunswick Corp.	2.3 mil	120 mil	5500
Stainless Steel (80 mil o.d.) C. H. S.*	Brunswick Corp.	0.65 mil	70 mil	5500
Stainless Stoel (7 mil i.d.) Tube	Superior Tube Co.	40 in.	7 mil	1

*Collimated hole structure.

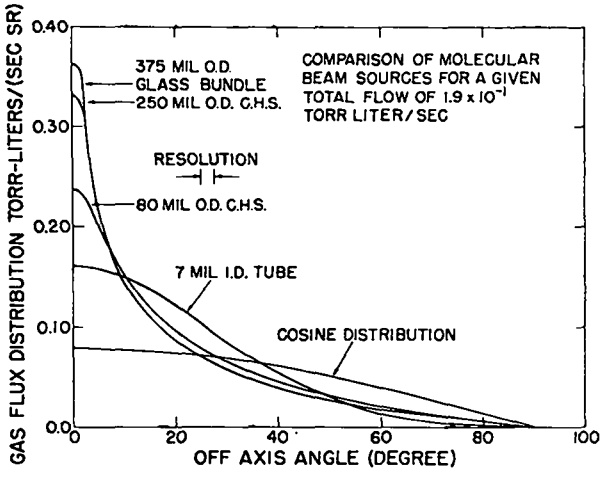

Fig. 462-17. The results of the gas beam flux distributions.

The desired beam is extracted from the gas source by using an aperture. The gas that strikes the aperture plate is pumped away and the gas that goes through the aperture forms the beam.

The 7-mil i.d. long tube with a 32-mil aperture about 0.2 in. away has been chosen for the initial gas beam source for the gas analyzer. The target for the molecular beam is a small opening in the ionization chamber of the mass spectrometer. The closer the gas source is to this opening, the greater the beam divergence that can be accepted and hence, the less total gas flow that would be needed for a fixed beam flux. The aperture must be far enough away from the gas source to make it appear a point source (~15 times the diameter of the source). This means the large diameter of the multi-hole structures must be much farther away from the ionization chamber than does the 7-mil i.d. tube. For this reason the 7-mil tube can place a given molecular beam in the ion source with less than half the total gas flow of the multi-hole structure source even though the multi-hole structures have more resolved flux distribution. Another consideration is the diameter of the aperture. The aperture must be at least the diameter of the gas source for efficient gas beam formation. Too large an aperture will allow effusion of random gas from the collimation region of the gas analyzer system into the ionization chamber. (The small aperture of the 7-mil tube will relieve this problem.) A gas beam flux distribution was obtained from the 7-mil i.d. tube and 7-mil aperture to give an 8° divergence from the beam axis. This divergence is approximately the amount necessary for the gas analyzer beam. The 7-mil i.d. tube beam intensity was found to vary directly with total flow. In other words the shape of the gas flux changed slightly with temperature and pressure drop across the tube. The peak intensity varied as the square of the pressure drop, and varied with temperature as,

$$I(0) = \left[\frac{56.3}{T} - 0.023\right] \text{ Torr-}\ell\text{/sec-Steridian}$$

with the pressure drop of one atmosphere across the tube. The diffusion pumps and the high-quality stainless steel for the high temperature gas analyzer have been received. Cold traps are being adapted to the diffusion pumps. The fabrication drawings of the gas analyzer are nearly completed. Some design modifications were added to help the critical alignment of gas beam with the ion source of the mass spectrometer.

REFERENCES

1. "Quarterly Status Report on the Advanced Plutonium Fuels Program," October 1 - December 31, 1967, Report LA-3880-MS, Los Alamos Scientific Laboratory.

2. V. J. Rutkauskas, "Determination of the Solubility of Oxygen in Sodium Using the Vacuum Distillation Analytical Technique," Report LA-3879, Los Alamos Scientific Laboratory, 1968.

3. Bruggeman, W. H., "Purity Control in Sodium - Cooled Reactor Systems," A.I.Ch.E.J. Vol. 2, pp 153-156, June 1956.

4. "Quarterly Status Report on the Advanced Plutonium Fuels Program," January 1 - March 31, 1969, Report LA-4193-MS, Los Alamos Scientific Laboratory.

REFERENCES - (continued)

5. "Quarterly Status Report on the Advanced Plutonium Fuels Program, October 1 - December 31, 1968, Report LA-4114-MS, Los Alamos Scientific Laboratory.

6. C. C. McPheeters and J. C. Biery, "The Dynamic Characteristics of a Na_2O Plugging Indicator," Nuclear Applications, 6, pp 573-81, June, 1969

7. "Quarterly Status Report on the Advanced Plutonium Fuels Program," April 1 - June 30, 1968, Report LA-3993-MS, Los Alamos Scientific Laboratory

8. G. G. Brown and Associates, Unit Operations, John Wiley and Sons, Inc., New York, New York, 1950, p. 518.

9. "Quarterly Status Report on the Advanced Plutonium Fuels Program," July 1 - September 30, 1968, Report LA-4073-MS, Los Alamos Scientific Laboratory.

10. C. C. Addison, et al. "Solutions of Hydrogen in Liquid Sodium," J. Am. Chem. Soc. (London) pp 116-121, January, 1965.

11. C. Englemann, "Emploi de Particules Autres que les Neutrons en Analyse par Activation," CEA-R-2559, Centre D'Etudes Nucleaires de Saclay, 1964.

12. S. Kallmann and R. Liu, "The Determination of Total Carbon and Sodium Carbonate in Sodium Metal," Anal. Chem. 36, p 590 (1964).

PROJECT 463

CERAMIC PLUTONIUM FUEL MATERIALS

Person in Charge: R.D. Baker

Principal Investigator: J.A. Leary

I. INTRODUCTION

The principal goals of this project are to prepare pure, well characterized plutonium fuel materials, and to determine their high temperature properties. Properties of interest are (1) thermal stability, (2) thermal expansion, (3) thermal conductivity, (4) phase relationships by differential thermal analysis, (5) structure and phase relationships by x-ray diffraction, high temperature x-ray diffraction, neutron diffraction and high-temperature neutron diffraction, (6) density, (7) hardness and its temperature dependence, (8) compatibility, including electron microprobe analysis, (9) compressive creep (deformation).

In addition to phase equilibria and general properties, specific thermodynamic properties such as free energy of formation by vaporization equilibria in the 1000-2000°C temperature range with mass spectrometer identification of vapor species, free energy of formation by electromotive force measurement in the 450-1200°C temperature range, and heat capacity and heat of transition are being determined.

II. SYNTHESIS AND FABRICATION

(R. Honnell, M.W. Shupe, G. Moore, R. Walker, S. McClanahan)

1. Carbides

Cursory evaluation of carbowax 400, napthalene, and paraffin as binder additions to (U, Pu)C indicated that paraffin had less effect on the microstructure than the other 2 materials. Carbowax 400 was the most detrimental with additions of 0.5 w/o resulting in the formation of sesquicarbide as a second phase. Pellets in which paraffin was added as a binder were single phase and exhibited the fewest microcracks. As shown in Figure 463-1, no lessening of microcracking was found with increasing paraffin concentration. However, there was a definite increase in porosity with increasing paraffin concentration. As indicated in the next paragraph, binders do not appear to be necessary for good pellet integrity.

The effects of changes in particle size and pressing pressure were evaluated in a qualitative way by investigating the effect of pressing pressure on the characteristics of sintered pellets prepared from two similar monocarbide powders which differed in particle size. The pellets prepared from the powder ground to a size range of $\leq 64\mu$ in an oscillating mill were free of microcracks when pressed at pressures up to 20 tsi. Pellets prepared from the finer powder (ball milled an additional 16 hr, lot 7-87-1) were found to be free of microcracks up to pressing pressures of 10 tsi. These effects are shown in Figures 463-2 and 463-3, respectively. It is concluded that a pressing pressure of 10 tsi is satisfactory for preparing pellets of good integrity from powder ground to a particle size of $< 64\mu$ in an oscillating mill.

The effect of pressing pressure on densification and

EFFECT OF PARAFFIN ADDITION ON MICROSTRUCTURE $U_{0.8}Pu_{0.2}C$

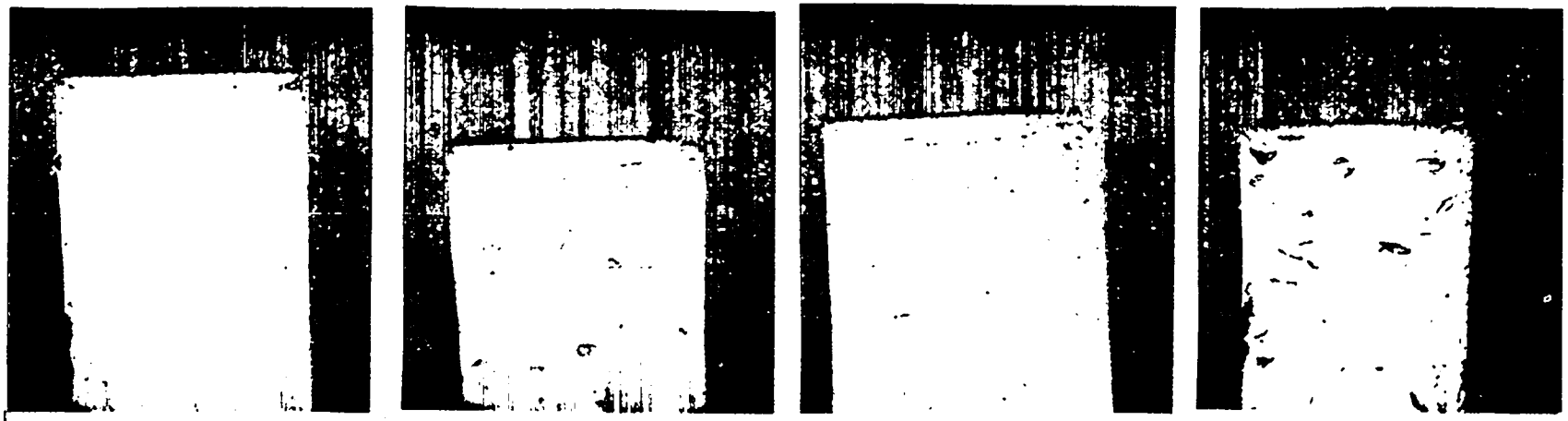

NO PARAFFIN | 0.5 w/o PARAFFIN | 1.0 w/o PARAFFIN | 1.5 w/o PARAFFIN

PHOTOMACROGRAPHS 14X

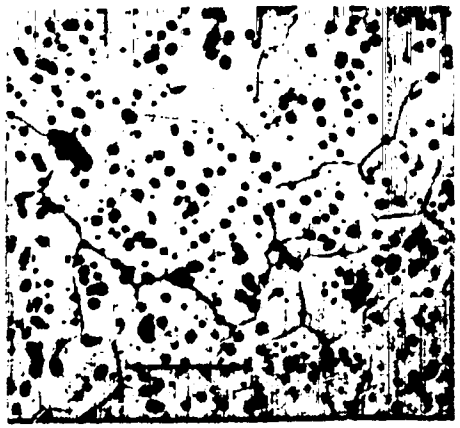

PHOTOMICROGRAPH
380X 1:1:1
ELECTROLYTIC ETCH

Figure 463-1

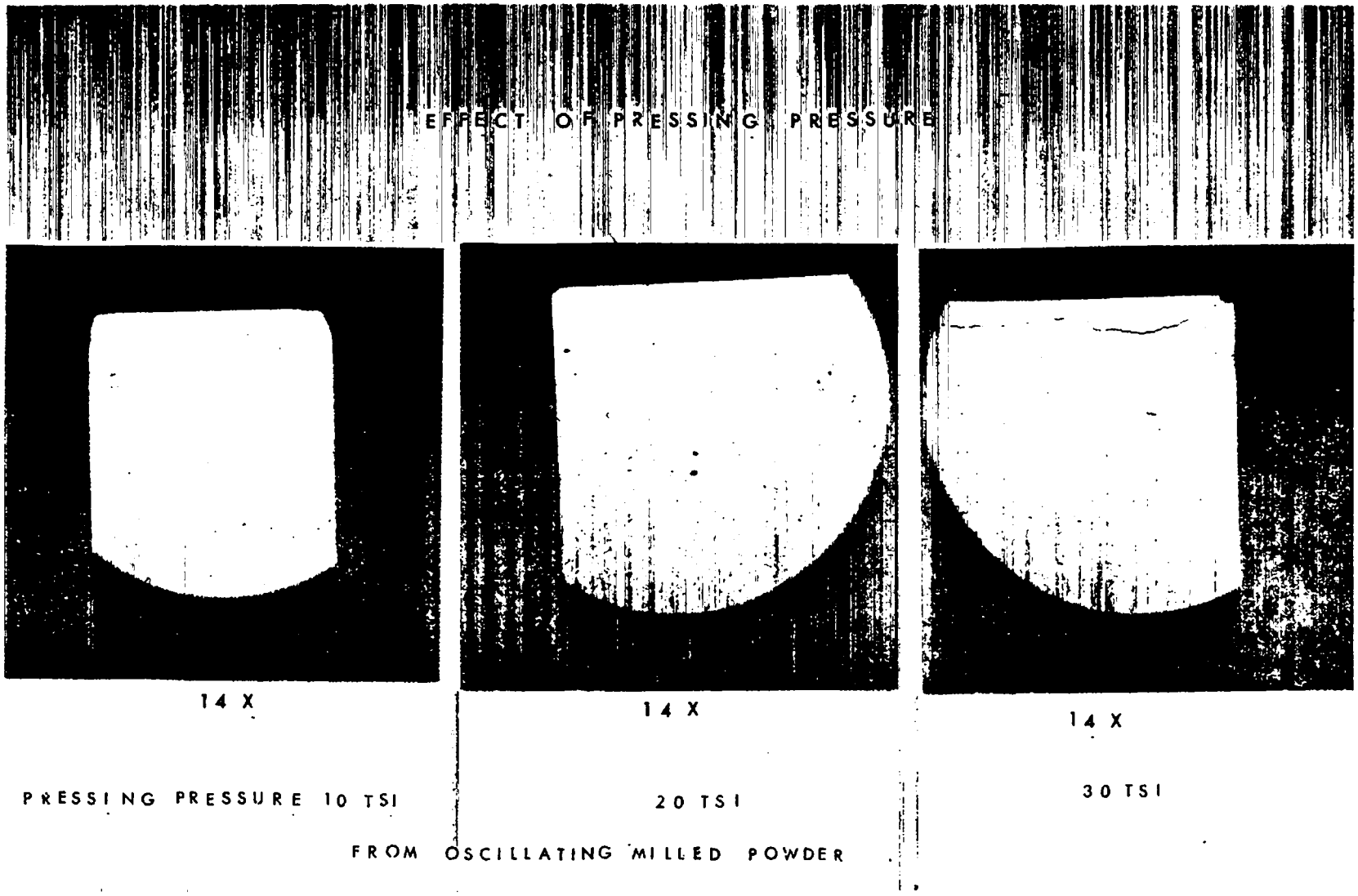

Figure 463-2. The Effect of Pressing Pressure on Microcrack Formation in (U, Pu) C Pellets Prepared from Oscillating Milled Powder

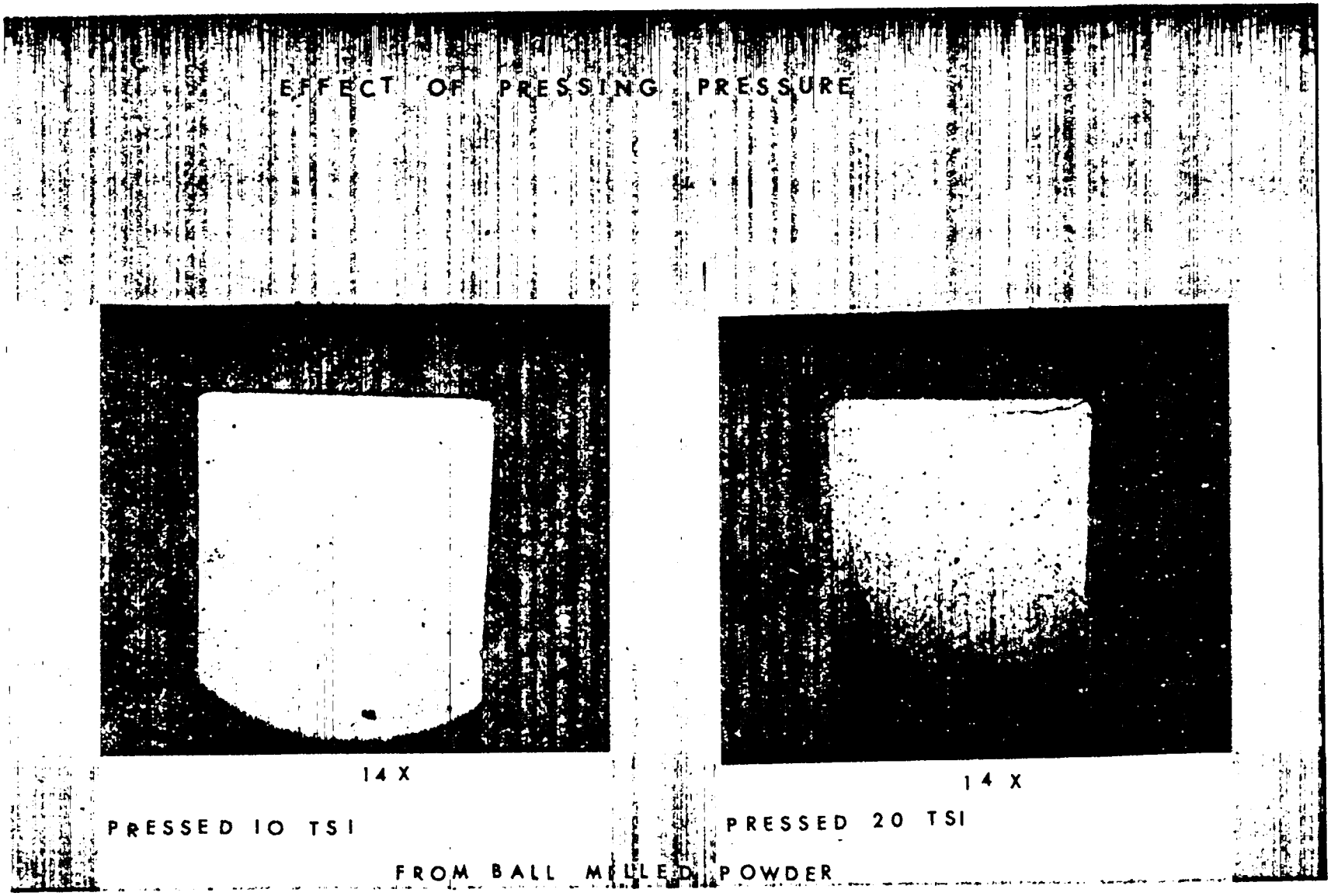

Figure 463-3. The Effect of Pressing Pressure on Microcrack Formation in (U, Pu) C Pellets Prepared from Ball Milled Powder

diametral control was also determined for the powders described above. The experimental results are shown in Figures 463-4 and 463-5. It can be seen that the sintered density has very little dependence on pressing pressure. Pellet densities of 93 and 94 percent of theoretical are attainable at a pressing pressure of 10 tsi with both the coarse and the fine powder, respectively. Densification to 95% of theoretical can be obtained by pressing the ball milled powder at 20 tsi.

Compatibility experiments at other laboratories have indicated that the compatibility of UC_{1+x} with stainless steel may depend on the form of the higher carbide present, i.e., U_2C_3 or UC_2. In order to evaluate this for $(U, Pu)C_{1+x}$, efforts were directed towards determining the conditions necessary to completely convert the platelet-like phase observed in $(U_{0.8}Pu_{0.2})C_{1+x}$ into M_2C_3. If it is assumed that the platelet-like phase is a compound stable only at high temperature (MC_2), a reasonable approach to its elimination would be a heat treatment below the decomposition temperature. The decomposition reaction, $2\,MC_2 \rightarrow M_2C_3 + C$, occurs at 1650°C. Pellets having the compositions $(U_{0.8}Pu_{0.2})C_{1.2}$ and $(U_{0.8}Pu_{0.2})C_{1.1}$ contained some platelets after sintering at 1800°C for 4 hours and soaking at 1400°C for 2 hours, as shown in Figures 463-6 and 463-7. The surface layer of M_2C_3-like material shown in the photomicrograph in the upper left of Figure 463-6 is

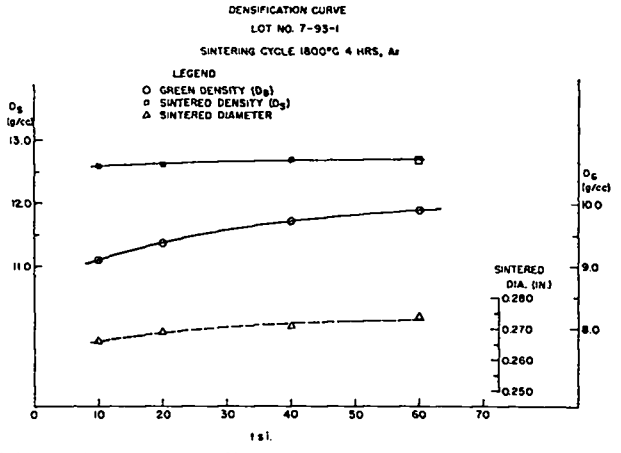

Figure 463-4. The Effect of Pressing Pressure on the Densification of (U, Pu)C Pellets Prepared from Oscillating Milled Powder

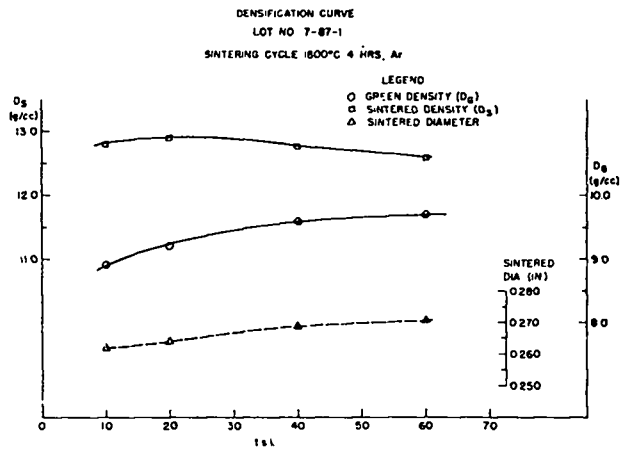

Figure 463-5. The Effect of Pressing Pressure on the Densification of (U, Pu)C Pellets Prepared from Ball Milled Powder

typical of pellets of this composition after sintering. Annealing at 1600°C for 24 hours or 1400°C for 24 hours does not significantly change the amount of the platelet-like phase indicated by Figure 463-6. The same is true for pellets at 1250°C for 36 hours (Figure 463-8). If the platelet-like phase is indeed MC_2, it must be concluded that the kinetics of the transformation are extremely slow. Hyperstoichiometric MC has been prepared essentially free of platelets by sintering pressed pellets below the transformation temperature, e.g., 1525°C, as shown in Figure 463-9. Densification to approximately 93 percent of theoretical was obtained by sintering at 1500°C for 24 hours. A slight trace of the platelet-like phase was detected in the pellet even after an additional soak at 1400°C for 36 hours. Pellets are now being fabricated for evaluation by sintering blended powders of MC and M_2C_3 below the transformation temperature.

A typical single phase $(U_{0.8}Pu_{0.2})C_{1.0}$ carbide pellet was examined for homogeneity using three techniques -- alpha autoradiography, metallography and electron microprobe analysis. Alpha radiographys showed complete homogeneity to the limit of detection. Metallographic examination indicated single phase homogeneous monocarbide. Electron microprobe traces of a typical region showed a variation of only a few percent in the U and Pu X-ray intensities as shown in Figure 463-10. It is concluded that although alpha

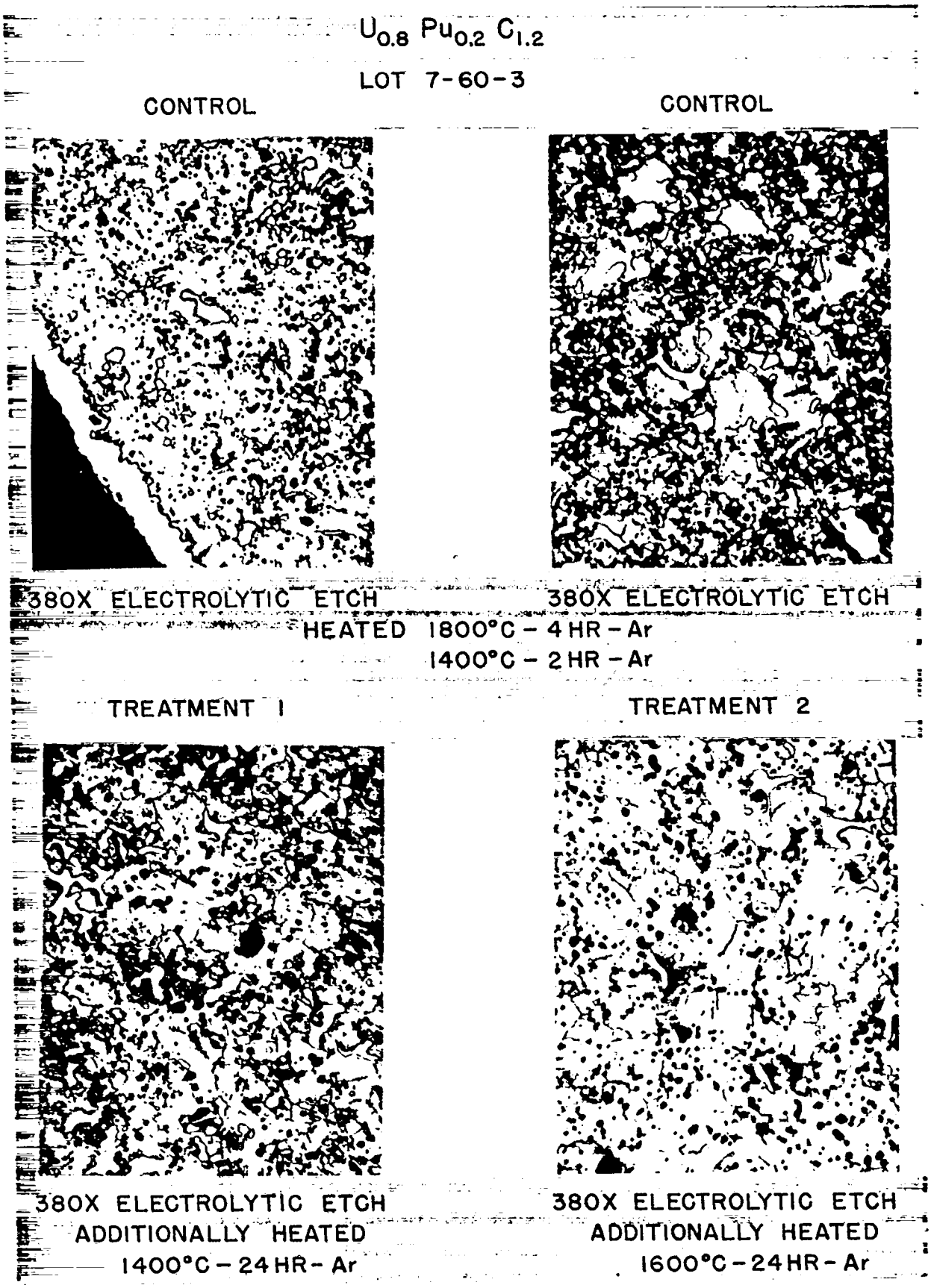

Figure 463-6. The Effect of Sintering Conditions on Platelet Formation in $U_{0.80}Pu_{0.20}C_{1+x}$

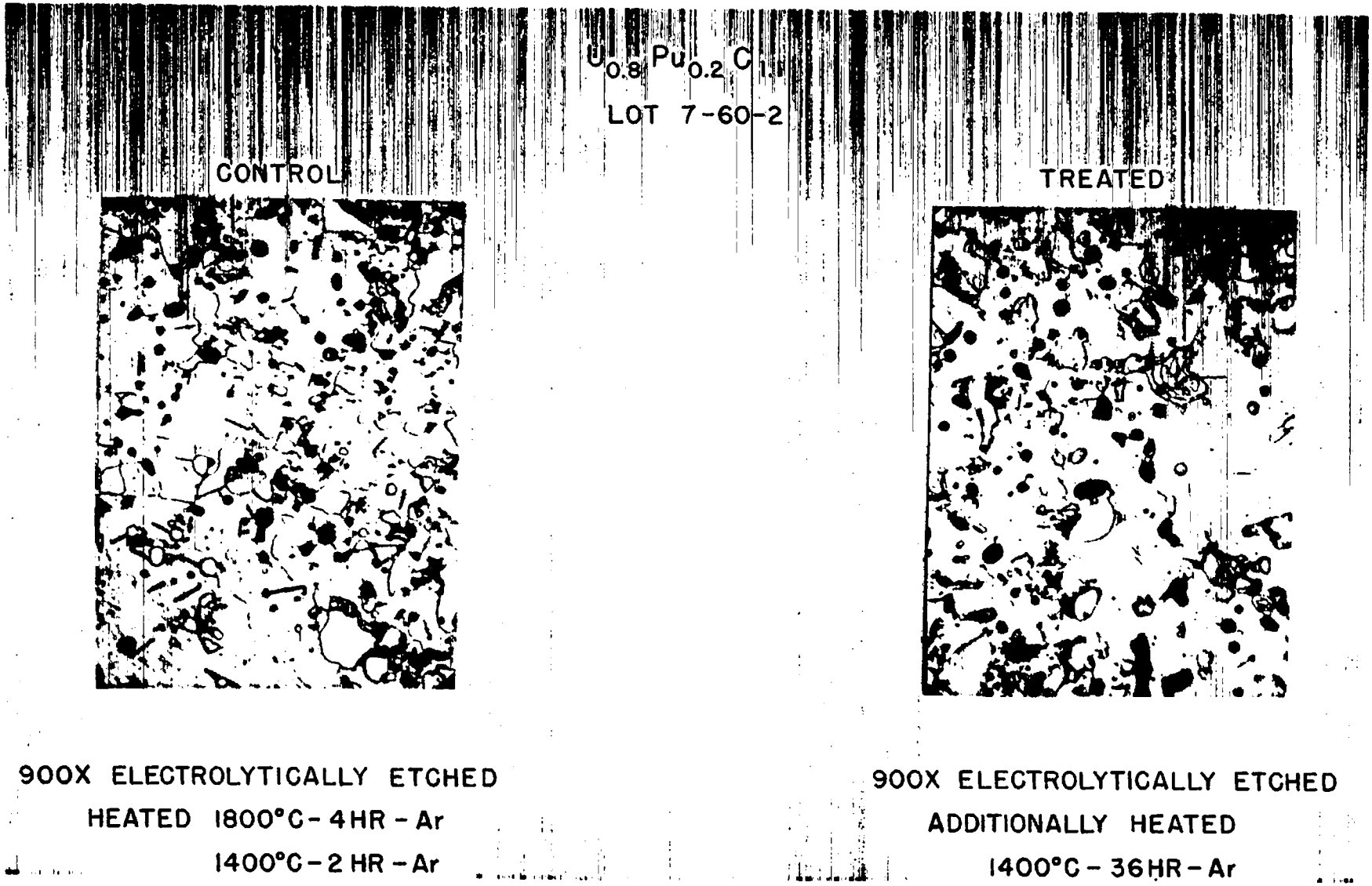

Figure 463-7. The Effect of Sintering Conditions on Platelet Formation in $U_{0.80}Pu_{0.20}C_{1+x}$

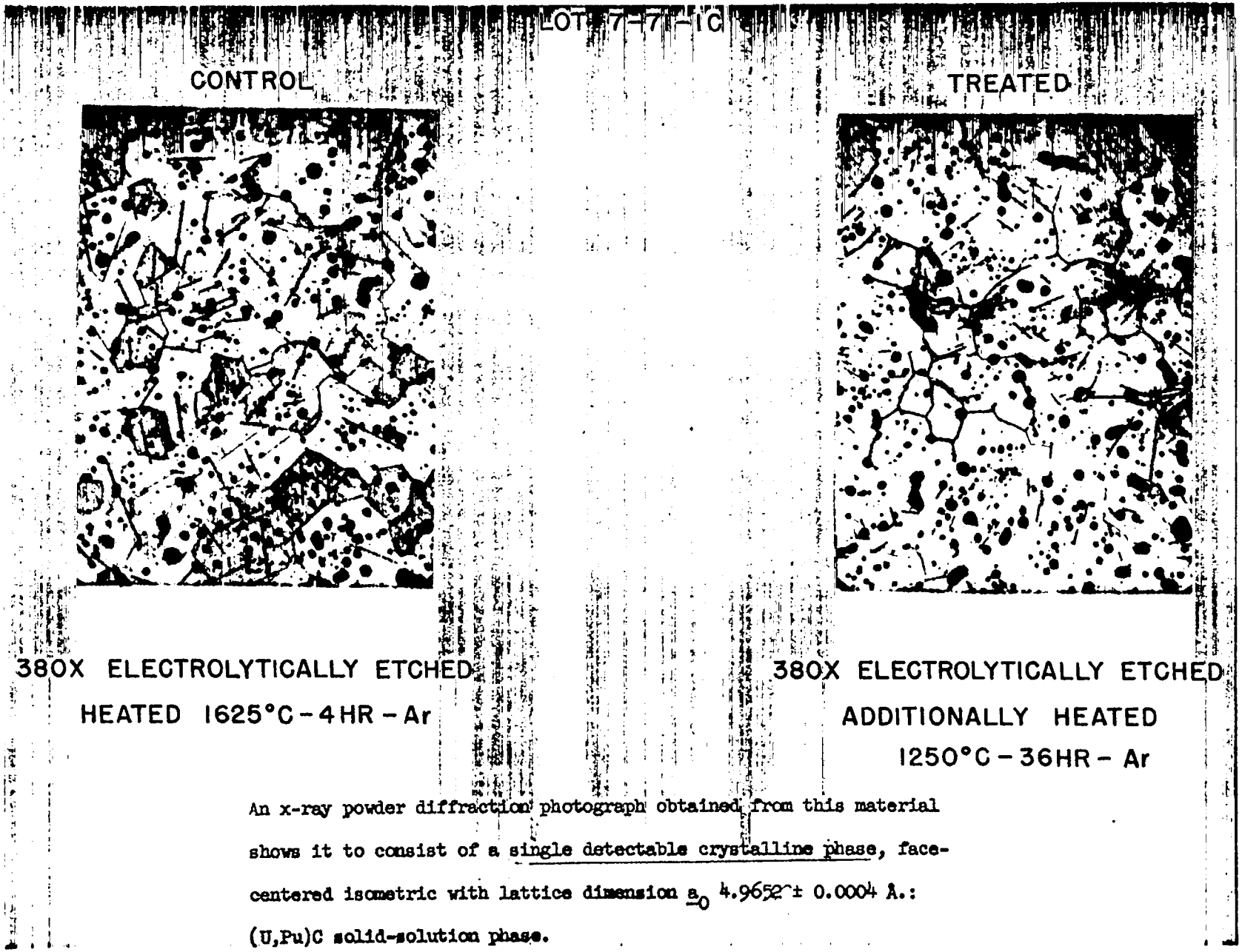

An x-ray powder diffraction photograph obtained from this material shows it to consist of a single detectable crystalline phase, face-centered isometric with lattice dimension a_0 4.9652 ± 0.0004 Å.: (U,Pu)C solid-solution phase.

Figure 463-8. The Effect of Sintering Conditions on Platelet Formation in $U_{0.80}Pu_{0.20}C_{1+x}$

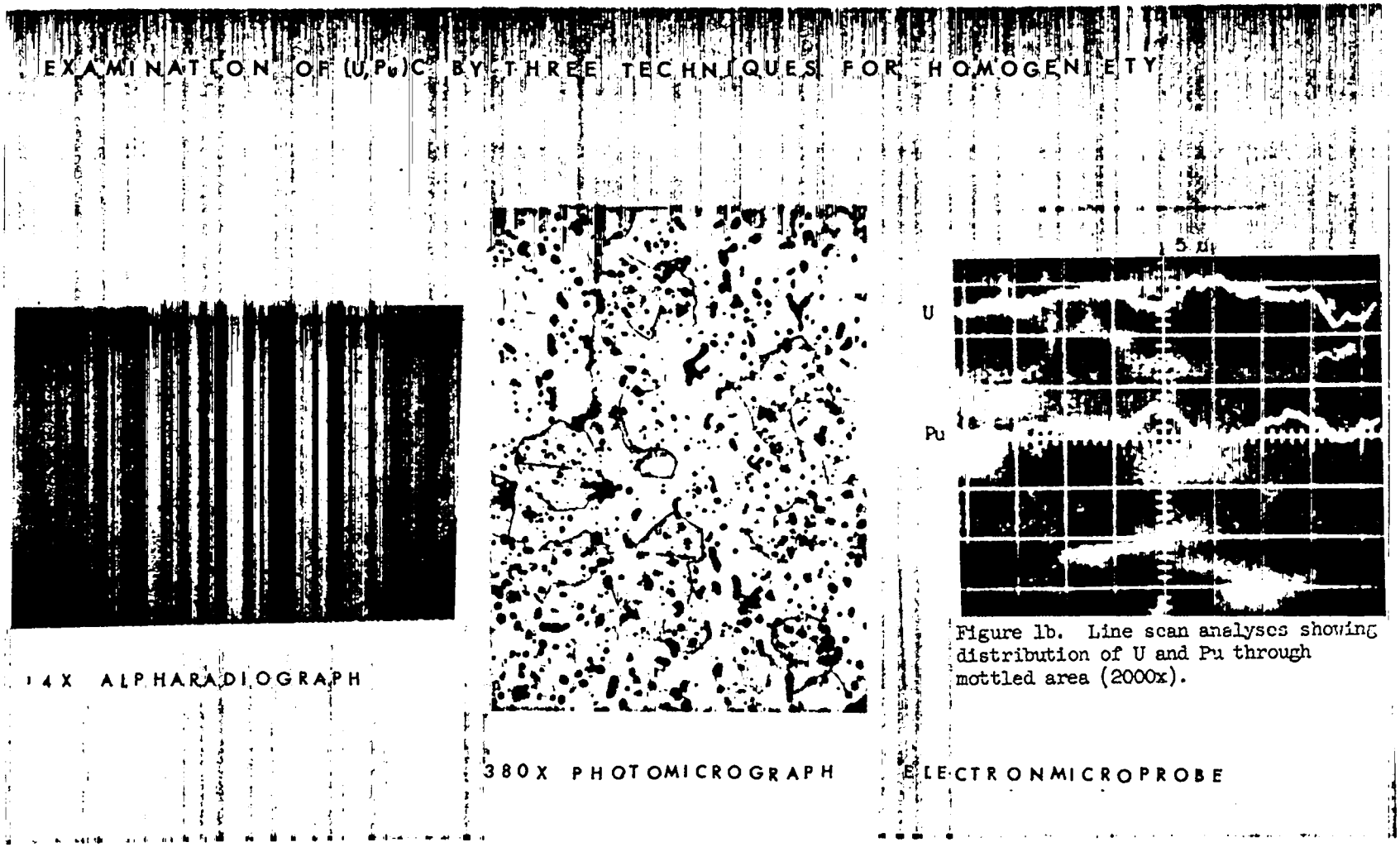

Figure 1b. Line scan analyses showing distribution of U and Pu through mottled area (2000x).

Figure 463-10. Pellet Homogeneity Examinations Using Alpha Autoradiography, Metallography, and Electron Microprobe Analysis

autoradiography is not a particularly sensitive method, it probably is adequate for verifying homogeneity of pellets prior to irradiation testing.

It can be shown theoretically that in an equilibrium mixture of uranium-plutonium monocarbide and sesquicarbide, the sesquicarbide phase will be preferentially enriched in plutonium at the expense of the monocarbide. Experimentally, this was evaluated by an electron microprobe analysis of a high purity pellet of $(U_{0.802}Pu_{0.198})C_{1.13}$ composition and comparing the chemistry of the 2 phases present after subjecting the pellet to a 1500°C diffusion anneal for 24 hours. Point count analysis of the annealed pellet indicated the presence of 28 v/o of M_2C_3. A monocarbide standard having the composition $U_{0.80}Pu_{0.20}C_{0.99}$ was used as the standard for the microprobe analysis. The relative X-ray intensities were as follows:

(a) In the M_2C_3 phase the plutonium intensity was 42 percent greater than that in the standard.

(b) In the M_2C_3 phase the uranium intensity was 16 percent less than in the standard.

(c) In the MC phase the plutonium intensity was 27 percent less than in the standard.

(d) In the MC phase the uranium intensity was 10 percent greater than in the standard.

Photomicrographs of the two phase and of the standard pellets are shown in Figure 463-11, Mount No. 68-0369 and 68-0225, respectively. From the above results, the compositions of the two phases may be calculated to be $(U_{0.70}Pu_{0.30})_2C_3$ and $(U_{0.85}Pu_{0.15})C$. Parallel calculations based on thermodynamic arguments indicated that the compositions of the phases in equilibrium at 1500°C are approximately $(U_{0.66}Pu_{0.34})_2C_3$ and $(U_{0.85}Pu_{0.15})C$. In view of estimates of some of the thermodynamic properties used in the calcuation, these results are in good agreement. Similar results were obtained on mixed carbide pellets produced by carbothermic reduction of oxides; these samples contained approximately 0.3 w/o oxygen.

A variety of carbide samples having various U, Pu, and C compositions were also prepared for use in the determination of high temperature physical and chemical properties.

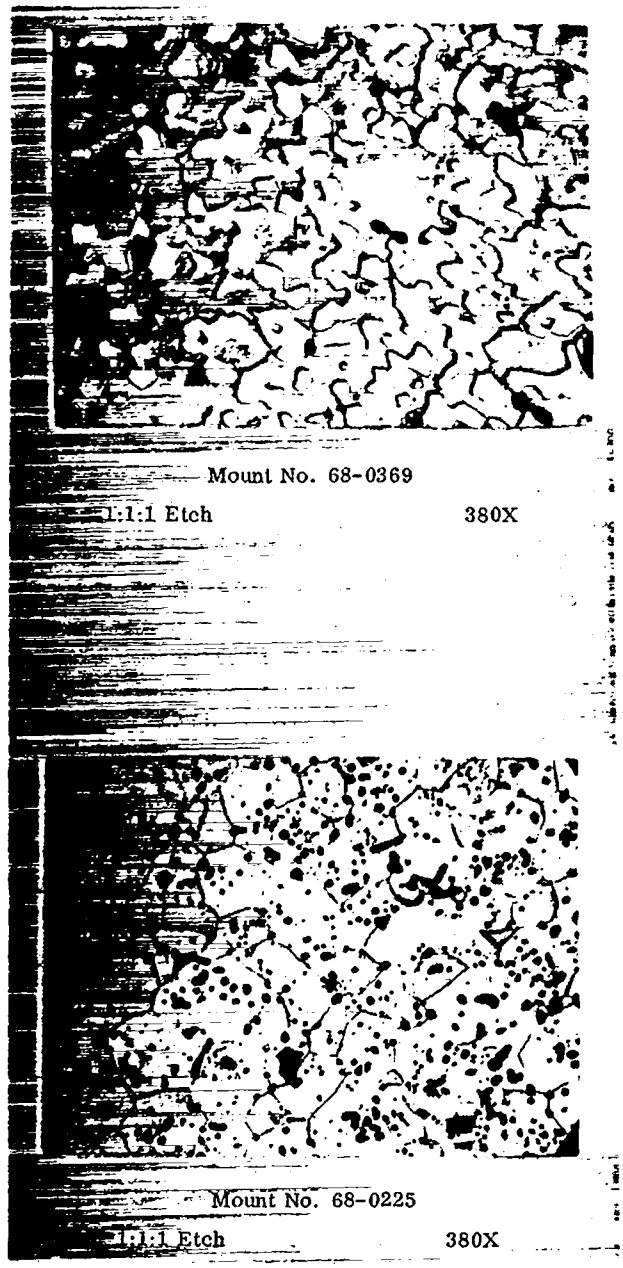

Figure 463-11. Photomicrographs of Samples Used in Demonstrating Partition in $U_{0.80}Pu_{0.20}C_{1+x}$ (M_2C_3 + MC top; Single Phase MC Bottom)

2. Oxides

A. Mixed Dioxides

(M. W. Shupe, C. Gilley, J. Dunn)

Reference pellets of $(U, Pu)O_2$ are needed for an exchange with the UK. The development of satisfactory sintering conditions to synthesize single phase oxide, as determined by X-ray powder diffraction analysis, has

been completed. Pure UO_2 and PuO_2 powders were ball milled for 24 hrs and classified by sieving; the -325 mesh ($\leq 44\mu$) fractions were then combined and blended for an additional 24 hrs. This powder mixture was pressed and then sintered in an alumina tube furnace at 1600°C for various combinations of sintering time and furnace atmosphere compositions. The effect of gas composition on solid solution formation is shown in Table 463-I. Single phase $(U_{0.75}Pu_{0.25})O_2$ was prepared in lots 1, 2, 3, and 6, which were all sintered in an oxidizing atmosphere. Single phase MO_2 was decomposed by heating for 8 hr in a reducing atmosphere. Using the dioxide blend, sintering under a cover gas of 6% H_2-Ar or Ar followed with H_2-Ar will not produce single phase dioxide. Moreover, wet Ar-H_2 mixtures did not produce single phase oxides.

B. Preparation of PuO_2 for FFTF Quality Assurance Standards
(R.L. Nance and D.W. Kelley)

Direct air oxidation of electrorefined Pu yields PuO_2 of good purity. It has been demonstrated that air saturated with H_2O at room temperature can controllably and completely oxidize several hundred grams of Pu to PuO_2 in a conveniently short time. The large particles in this product apparently have a low surface energy which leads to lowered sintered densities of compacted shapes, compared to those obtained from some other sources such as the oxalate or the peroxide.

The goal of further development work will be the large scale preparation of PuO_2 by air oxidation to produce sinterable, pure powder.

Analytical results for PuO_2 lot P-20-23, produced by the first large scale experiment, are as follows:

Li	0.07	Fe	2	Cs	< 2
Be	< 0.001	Co	< 0.5	Ba	< 0.1
B	< 0.3	Ni	2	La	< 0.5
Na	5	Cu	2	Hf	< 0.5
Mg	10	Zn	15	Ta	< 25
Al	3	Rb	< 0.5	W	50
Si	4	Sr	< 0.1	Re	< 0.5
K	< 0.5	Y	< 0.1	Pt	< 100
Ca	10	Zr	2	Pb	< 0.5
Ti	0.2	Nb	<50	Bi	0.5
V	< 0.5	Mo	< 0.5	U	22
Cr	2	Cd	< 0.5	Pu	88.07%
Mn	< 0.1	Sn	< 0.5	Am	38

(All results expressed as ppm by wt. in respect to Pu except for percent Pu)

3. Nitrides
(M.W. Shupe, R.L. Nance, D. Kelley)

Specimens of PuN have been prepared from powder lot PuN-16 for low temperature calorimetry at AERE Harwell and for high temperature calorimetry at this Laboratory. The properties of the PuN pellets are shown in Table 463-II. The Harwell specimens were 0.37 in. dia x 0.33 in. tall with a 0.13 in. dia axial hole. The density was 12.2 g/cc after sintering at 1900°C for 2 hr in N_2. The high temperature calorimetry

Table 463-I

Effect of Sintering Conditions on $U_{0.75}Pu_{0.25}O_2$ Solid Solution Formation

Lot No.	First Sintering Conditions	X-ray Diffraction Analysis	Resintering Conditions	X-ray Diffraction Results
1	a. 1600°C - 12 hr 6% H_2-Ar-0.4mmH_2O	Multiphase	a. 1600°C - 4 hr - CO_2 b. 4 hr - 6% H_2-Ar	Single Phase a = 5.4529 ± 0.0004Å
2	a. 1600°C - 15 hr 6% H_2-Ar	Multiphase	a. 1600°C - 4 hr - CO_2 b. 4 hr - 6% H_2-Ar	Single Phase a = 5.4544 ± 0.0002Å
3	a. 1600°C - 4 hr - CO_2 b. 4 hr - 6% H_2-Ar	Single Phase a = 5.4531 ± 0.0004Å	None	...
4	a. 1650°C - 4 hr - CO_2 b. 4 hr - 6% H_2-Ar	Single Phase	a. 1650°C - 8 hr 6% H_2-Ar (dried)	Multiphase
5	a. 1625°C - 3.5 hr-Ar b. 4.5 hr - 6% H_2-Ar -0.4 mm H_2O	Multiphase	a. 1625°C - 8 hr 6% H_2-Ar (dried)	Multiphase
6	a. 1625°C - 4 hr - CO_2 b. 4 hr - 6% H_2-Ar	Single Phase a = 5.4562 ± 0.0004Å	None	

pellets were 5/8 in. dia x 0.4 in. tall after sintering in the same manner.

Table 463-II

X-ray powder diffraction analysis:

Single phase PuN, a = 4.9046 ± 0.0004Å

Density:

12.2 g/cc

Chemical composition:

Pu (Theor = 94.5 w/o)	94.5
N (Theor = 5.55 w/o)	5.49
O, ppm by wt.	330
U, ppm by wt.	26
Th, ppm by wt.	< 75

Spectrochemical Analysis:

Element	ppm by wt.	Element	ppm by wt.
B	< 0.5	Zr	< 300
Si	10	Nb	< 300
Ti	< 50	Mo	< 30
Cr	< 2	Cd	< 3
Mn	< 0.5	Sn	< 1
Fe	< 5	Ta	< 1000
Ni	< 5	W	< 30
Cu	1	Pb	1
Zn	< 5	Bi	< 0.5

III. PROPERTIES

1. Differential Thermal Analysis

(J. G. Reavis, L. Reese)

Differential thermal analysis observations of the (U, Pu)C_2 system have been completed. Samples have been quenched from the various phase fields and analyzed by X-ray powder diffraction methods to obtain information about the crystallographic species present.

Observations were made to determine the melting behavior of single phase $U_{0.80}Pu_{0.2}C$. The results were in good agreement with previous observations of melting of samples which contained traces of metal or traces of M_2C_3.

Observations of the melting behavior of various Pu-C compositions having C/Pu atomic ratios from 0.86 to 1.6 have produced results which disagree with the currently accepted Pu-C phase diagram.

The (U, Pu)C_2 System: DTA observations of a high purity sample of PuC_2 (containing a slight excess of carbon) have led to establishment of the transformation temperature for the reaction $Pu_2C_3 + C \rightarrow PuC_2$ as 1660 ± 10°C. The temperature of liquid phase formation was 2232 ± 10°C. The sesquicarbide-dicarbide transformation temperature was found to be independent of the C/Pu atomic ratio over the range 1.6 to 8.

Observations of transformation temperatures in the (U, Pu)C_2 system (excess C) have now been made over the entire range from UC_2 to PuC_2. The results are plotted on Figure 463-12. Although unequivocal identification of structures present in the various phase fields is impossible using quenching techniques, tentative identification has been made from X-ray powder diffraction analysis of samples quenched from the various phase fields. Descriptions of these samples are given in Table 463-III. Tetragonal MC_2 is observed in samples quenched from the "MC_2 (+ C)" region of Figure 463-12, although quenched samples containing a high concentration of PuC_2 always contained some bcc M_2C_3. High temperature X-ray diffraction measurements have shown that UC_2 is cubic above 1765°C[1] (or 1785°C, depending on composition) and that PuC_2 is cubic above 1700°C.[2] UC_2 was observed to transform from cubic to tetragonal at 1765°C and to decompose extremely slowly to U_2C_3 + C at 1515°C.[2]

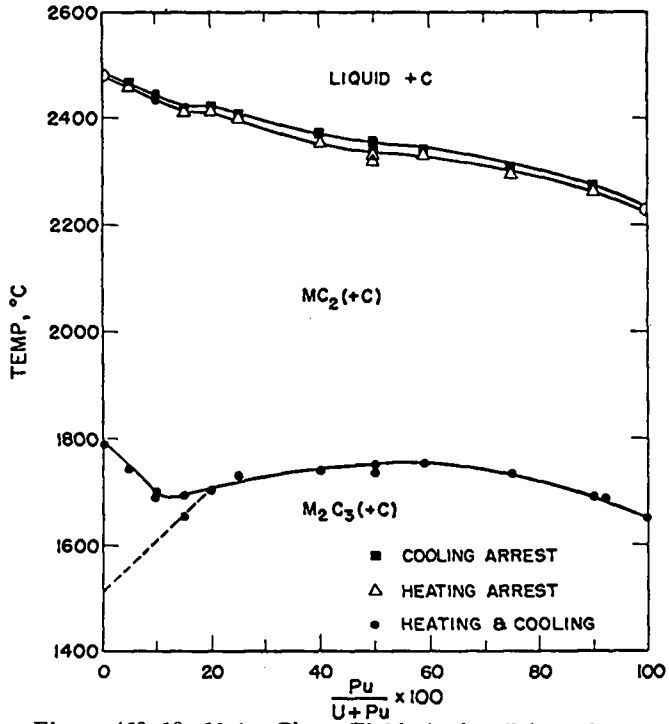

Figure 463-12. Major Phase Fields in the High Carbon Region of the U-Pu-C System by DTA

Table 463-III

Identity of Phases in (U, Pu) C_2 Samples Quenched from Selected Temperatures

Composition	Annealing or Quench Temp., °C	Annealing Time at Quench Temp.	Phases Found[a]
UC_2	1900	< 1 min.	tet. UC_2
UC_2	1460	63 hr.	tet. UC_2
$U_{0.95}Pu_{0.05}C_2$	1800	< 1 min.	tet. MC_2
$U_{0.95}Pu_{0.05}C_2$	1690	< 1 min.	tet. MC_2
$U_{0.95}Pu_{0.05}C_2$	1460	16 hr.	major bcc M_2C_3, minor tet. MC_2
$U_{0.90}Pu_{0.10}C_2$	1730	~ 1 min.	tet. MC_2
$U_{0.90}Pu_{0.10}C_2$	1650	10 min.	major tet. MC_2, trace bcc M_2C_3
$U_{0.90}Pu_{0.10}C_2$	1550	1 hr.	major tet. MC_2, minor bcc M_2C_3
$U_{0.87}Pu_{0.13}C_2$	1725	20 min.	tet. MC_2
$U_{0.87}Pu_{0.13}C_2$	1675	1 hr.	tet. MC_2
$U_{0.87}Pu_{0.13}C_2$	1550	1 hr.	equal tet. MC_2 and bcc M_2C_3
$U_{0.50}Pu_{0.50}C_2$	1800	3 min.	major tet. MC_2, trace bcc M_2C_3
$U_{0.50}Pu_{0.50}C_2$	1675	4 min.	bcc M_2C_3
$U_{0.1}Pu_{0.9}C_2$	1710	~ 1 min.	equal tet. MC_2 and bcc M_2C_3
$U_{0.1}Pu_{0.9}C_2$	1625	~ 2 min.	bcc M_2C_3
PuC_2	1700	~ 3 min.	equal tet. PuC_2 and bcc Pu_2C_3
PuC_2	1625	~ 1 min.	bcc Pu_2C_3

(a) Graphite reflections were also observed in the diffraction patterns.

Tetragonal PuC_2 appears to be metastable.[3] It appears, therefore, that the "MC_2 (+ C)" field is cubic MC_2 and that at high PuC_2 concentrations there is no stable tetragonal MC_2 region. Over the PuC_2 concentration range of 0-13 m/o, the data of Table 463-III indicate a range in which tetragonal MC_2 is stable. The rate of decomposition of tetragonal MC_2 to M_2C_3 + C is extremely slow in the case of pure UC_2 but is accelerated by the addition of PuC_2. It appears that the decomposition temperatures of this phase are reasonably well defined by the dashed line of Figure 463-12. The triangular area above this dashed line is probably the only region in which tetragonal MC_2 is stable.

Melting Behavior of Single Phase $U_{0.8}Pu_{0.2}C$: It was previously reported from observations of samples containing traces of metal or of M_2C_3 that solidus and liquidus temperatures of $U_{0.8}Pu_{0.2}C$ were 2285 ± 20°C and 2485 ± 20°C, respectively. Another series of experiments has been run, using single phase $U_{0.8}Pu_{0.2}C$. Melting behavior was determined by use of DTA techniques and by metallographic examination of samples quenched from temperatures near the solidus temperature. Results of the experiments indicate no change from the previously reported values.

Transition Temperatures in the Pu-C System: The currently accepted Pu-C phase diagram indicates no liquid phase formation below 1650°C in the C/Pu atomic ratio range of 0.86 to 1.5. No transformations of any

sort are indicated below 1650°C in this range except for a shift in the monocarbide-sesquicarbide equilibrium.

Recent observations have indicated slow transformations involving liquid phase formation beginning at 1600 ± 10°C in samples of $PuC_{0.86}$ and $PuC_{0.99}$. Liquidus temperatures for these samples were found to be above 1650°C. Other compositions in the range $PuC_{1.0}$ to $PuC_{1.6}$ exhibited non-reproducible thermal arrests in the 1550-1650°C region. It appears that the phase diagram in this area is more complicated than has been assumed in the past, but additional measurements are needed to define adequately the phase boundaries.

2. Room Temperature X-ray Diffraction

A. Lattice Parameters of Plutonium Carbides
(M.W. Shupe, C.W. Bjorklund, R.M.Douglass)

A series of compositions in the plutonium-carbon system were prepared (mainly by powder metallurgy methods), heat treated, and analyzed by conventional X-ray powder techniques. The results, which are summarized in Table 463-IV, clearly indicate that both PuC and Pu_2C_3 have a range of composition. In addition, the lattice dimension of Pu_2C_3 in the presence of PuC is constant at an average value of 8.1287 Å from a C/Pu ratio of 0.992 to 1.343. The lattice dimension increased significantly at $PuC_{1.485}$ which indicates that this composition is in the single phase "Pu_2C_3" region. The upper limit of the "Pu_2C_3" region apparently lies between $PuC_{1.58}$ and $PuC_{1.68}$.

B. Self-irradiation Damage
(C.W. Bjorklund, R.M. Douglass)

X-ray powder diffraction techniques have been applied to two general areas: characterization of plutonium ceramics, the results of which are incorporated in other sections of this report, and studies of self-irradiation damage in plutonium compounds. The latter studies have reached the stage where X-ray exposures need only be made at approximately six-month intervals since the lattice dimensions of all but the compounds of normal isotopic composition have expanded to their saturation values.

The lattice expansion at ~ 25°C of compounds of normal isotopic composition can be expressed by the following equations:

$$PuO_2: \frac{\Delta a}{a} = 3.04(\pm 0.004)\times 10^{-3}\left[1-e^{-1.36(\pm 0.06)\times 10^{-3}t}\right] \quad (1)$$

$$PuN: \frac{\Delta a}{a} = 2.23(\pm 0.05)\times 10^{-3}\left[1-e^{-1.77(\pm 0.01)\times 10^{-3}t}\right] \quad (2)$$

$$Pu_2C_3: \frac{\Delta a}{a} = 1.54(\pm 0.1)\times 10^{-3}\left[1-e^{-1.27(\pm 0.2)\times 10^{-3}t}\right] \quad (3)$$

Table 463-IV

Effect of Changes in Composition on Lattice Dimensions of Plutonium Carbides

Specimen	Composition	Heat Treatment	Phase	Lattice Dimension Å
7-37-1	$PuC_{0.381}O_{0.001}N_{0.000}$	as melted	α Pu	minor
			PuC	4.9501 ± 0.0007
7-37-2	$PuC_{0.705}O_{0.000}N_{0.000}$	as melted	α Pu	minor
			PuC	4.953 ± 0.002
6-123-1	$PuC_{0.847}O_{0.003}N_{0.004}$	1300°C - 2 hr - Ar	PuC	4.953 ± 0.002
6-123-2	$PuC_{0.992}O_{0.003}N_{0.004}$	1300°C - 2 hr - Ar	PuC	4.9776 ± 0.0005
			Pu_2C_3	8.1283 ± 0.0003
6-123-3	$PuC_{1.228}O_{0.004}N_{0.004}$	1300°C - 2 hr - Ar	PuC	4.9785 ± 0.0004
			Pu_2C_3	8.1289 ± 0.0003
6-123-4	$PuC_{1.343}O_{0.003}N_{0.003}$	1300°C - 2 hr - Ar	PuC	4.9804 ± 0.0009
			Pu_2C_3	8.1280 ± 0.0002
7-5-1	$PuC_{1.485}O_{0.001}N_{0.002}$	1600°C - 6 hr + 1400°C - 2 hr - Ar	Pu_2C_3	8.1306 ± 0.0006
7-19-2	$PuC_{1.500}O_{0.001}N_{0.002}$	1700°C - 3 hr + 1600°C - 2 hr	Pu_2C_3	8.1313 ± 0.0002
7-19-1	$PuC_{1.58}O_{0.001}N_{0.000}$	1700°C - 3 hr + 1600°C - 2 hr	Pu_2C_3	8.1317 ± 0.0003
7-21-1	$PuC_{2.12}O_{0.001}N_{0.001}$	1700°C - 3 hr + 1600°C - 2 hr	Pu_2C_3	8.1324 ± 0.0002
7-11-1	$PuC_{1.678}O_{0.001}N_{0.002}$	1700°C - 3 hr + 1600°C - 2 hr	Pu_2C_3	8.1324 ± 0.0004

where t is time in days and "a" is the lattice dimension in A. At the time of the most recent measurements, the samples of PuO_2, PuN, and Pu_2C_3 were 5.7, 5.3, and 3.6 years old, respectively, and the lattice dimensions were within 94%, 97%, and 81%, respectively, of the saturation values predicted by the above equations.

The lattice expansion of PuO_2 enriched with 3.75 at.% ^{238}Pu at temperatures up to 400°C may be expressed by the following least squares equations:

At 198°C:
$$\frac{\Delta a}{a_o} = 3.14 (\pm 0.03) \times 10^{-3}\left[1-e^{-1.29 (\pm 0.04) \times 10^{-2} t}\right] \quad (4)$$

25°C:
$$\frac{\Delta a}{a_o} = 3.06 (\pm 0.03) \times 10^{-3}\left[1-e^{-1.30 (\pm 0.03) \times 10^{-2} t}\right] \quad (5)$$

100°C:
$$\frac{\Delta a}{a_o} = 2.88 (\pm 0.04) \times 10^{-3}\left[1-e^{-1.23 (\pm 0.05) \times 10^{-2} t}\right] \quad (6)$$

200°C:
$$\frac{\Delta a}{a_o} = 2.38 (\pm 0.04) \times 10^{-3}\left[1-e^{-1.45 (\pm 0.06) \times 10^{-2} t}\right] \quad (7)$$

400°C:
$$\frac{\Delta a}{a_o} = 1.77 (\pm 0.03) \times 10^{-3}\left[1-e^{-1.70 (\pm 0.09) \times 10^{-2} t}\right] \quad (8)$$

The derivation of an equation to express the lattice dimension as a function of both time and temperature was described in a previous report.[4] In a modified form, this equation may be written

$$\frac{\Delta a}{a_o} = \frac{P_1 P_2}{P_2 + P_3 e^{-P_4/T}}\left[1 - e^{-(P_2 + P_3 e^{-P_4/T}) t}\right] \quad (9)$$

where Δa is the lattice expansion $(a_t - a_o)$ at time t and temperature T in °K. A non-linear least squares computer program was used to fit the data to the equation by calculating values for the parameters P_1, P_2, P_3 and P_4, as well as a_o (the lattice dimension at t = 0). For PuO_2 enriched with 3.75 at.% ^{238}Pu, Eq. 9 becomes:

$$\frac{\Delta a}{a_o} = \frac{3.65 (\pm 0.08) \times 10^{-5}}{1.13 (\pm 0.02) \times 10^{-2} + 6.34 (\pm 0.6) \times 10^{-2} e^{\frac{-1341 (\pm 50)}{T}}}\left[1-e^{-(1.13 \times 10^{-2} + 6.34 \times 10^{-2} e^{\frac{-1341}{T}}) t}\right] \quad (10)$$

The uncertainties listed are ± 1 σ.

Although the lattice expansion of PuO_2 of normal isotopic composition was measured only at room temperature, it was possible to calculate the parameters in Eq. 9 for this material also. These calculations were based on the experimental observation that the lattice expansion of PuO_2 at saturation is independent of the dose rate. The parameters P_2 and P_3 can be shown to contain the average disintegration constant, λ, of the Pu in the sample as a factor, whereas P_1 and P_4 do not. Therefore, it was only necessary to calculate new values of P_2 and P_3 for normal PuO_2 from the values obtained for the enriched material. The resultant equation is given by equation (11).

$$\frac{\Delta a}{a_o} = \left[\frac{3.69 \times 10^{-6}}{1.15 \times 10^{-3} + 6.41 \times 10^{-3} e^{\frac{-1341}{T}}}\right] \times \left[1-e^{-(1.15 \times 10^{-3} + 6.41 \times 10^{-3} e^{\frac{-1341}{T}}) t}\right] \quad (11)$$

The calculated curve obtained from this equation for a temperature of 25°C fell just below the corresponding experimental data points in what was considered to be quite reasonable agreement.

As the time, t, approaches infinity, the lattice expansion approaches saturation and, in the limit, Eq. 9 reduces to equation (12).

$$\frac{\Delta a_{sat'n}}{a_o} = \frac{P_1 P_2}{P_2 + P_3 e^{-P_4/T}} \quad . \quad (12)$$

Values of $\Delta a_{sat'n}/a_o$ as a function of temperature for PuO_2 were calculated by means of Eq. 12 and compared with annealing data in the literature.[5] (It should be noted that the same value of $\frac{\Delta a_{sat'n}}{a_o}$ is obtained, within

experimental error, from either Eq. 10 for enriched PuO_2 of Eq. 11 for normal PuO_2.) Satisfactory agreement was obtained over the range -198° to ~ 500°C, but the calculated curve leveled off too soon at higher temperatures. Unsuccessful attempts were made to extend the temperature using the additional experimental fact that lattice expansion due to self-irradiation damage is eliminated at 1000°C. The constant P_4 in Eq. 12 is proportional to an average annealing activation energy, and apparently can not be adjusted to cover a higher temperature range. Annealing probably occurs by several processes with different activation energies as the temperature increases, possibly requiring more than one activation energy term in Eq. 12 to fit experimental data above 500°C.

The samples of enriched Pu carbides (single phase $PuC_{0.86}$ and two-phase $PuC-Pu_2C_3$) are now over 3 years old. No further deterioration in the quality of the X-ray patterns has been observed. The lattice dimensions are still somewhat erratic although they now seem to be constant within rather large limits of experimental error.

3. High Temperature X-ray Diffraction
(J. L. Green)

During the initial stages of testing of the X-ray diffractometer furnace, considerable difficulty was experienced in maintaining an inert atmosphere of sufficient purity to avoid sample oxidation at high temperatures. Extensive revisions were made in the cooling system in the furnace to eliminate the diffusion of water vapor through the flexible cooling water lines in the sample chamber. In addition, a uranium chip furnace was installed in the He cover gas system. These changes appear to have eliminated the oxidation problem. Experiments using NbC samples have demonstrated that no observable oxidation occurs on the sample surface at temperatures up to 1800°C. As a test of the overall system, a thermal expansion coefficient determination was made on a sample of high purity NbC for the temperature interval from 800°C to 1800°C. The results of this experiment are in close agreement with the expansion data published for NbC.[6] A comparison of these data is shown in Fig. 463-13. The maximum deviation from Houska's data is 2% and the average deviation is 1%. This variation is within the estimated limits of experimental error. This is considered to be an adequate demonstration of the overall accuracy of the techniques used for lattice parameter determinations at high temperatures and also for temperature measurement.

The investigation of the carbon rich U-Pu-C system was begun with a material having a composition of $PuC_{2.2}$. Initial difficulty was experienced in the preparation of heater strip samples of this material. The results of a large number of trial sample preparations indicated that Pu_2C_3 has a relatively large thermal expansion coefficient. The samples tended to shatter during the sintering operation and did not adhere properly to the heater strip. These difficulties have been eliminated by using somewhat smaller samples and by supporting the sample with small, undercut, graphite tabs along the edges of the strip. These tabs mechanically retain the sample on the heater strip even though considerable shrinkage occurs on cooling.

Using samples of $PuC_{2.2}$, thermal expansion data for carbon-rich Pu_2C_3 have been obtained in the temperature interval from 800°C to 1600°C. A least squares fit of this set of data yields

$$\frac{\Delta a}{a_o} = 1.2 \times 10^{-5}\, T + 2 \times 10^{-9}\, T^2$$

where T is the temperature in °C. This corresponds to

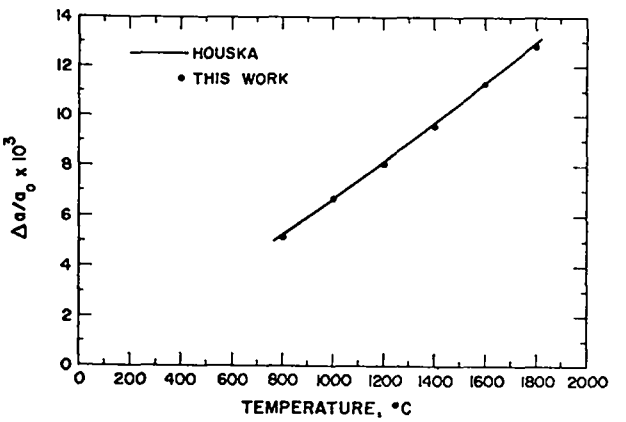

Figure 463-13. Thermal Expansion Data for NbC

a thermal expansion coefficient that is relatively large, e.g., $\bar{\alpha}_{0-1600^{\circ}C} = 15.6 \times 10^{-6}\ ^{\circ}C^{-1}$. High temperature data for carbon rich Pu_2C_3 has recently been reported by Dalton, et al.[7] Only a very limited amount of high temperature lattice parameter information was reported for Pu_2C_3 in that work; however, the mean thermal expansion coefficient implied by the data was estimated to be $\bar{\alpha}_{0-1600^{\circ}C} = \sim 14.5 \times 10^{-6}\ ^{\circ}C^{-1}$. Two determinations have been reported for carbon deficient Pu_2C_3 for lower temperature ranges. Rand and Street[8] reported an average expansion coefficient of $16.22 \times 10^{-6}\ ^{\circ}C^{-1}$ (20°-$935^{\circ}C$) and Pallmer[9] reported a value of $14.8 \times 10^{-6}\ ^{\circ}C^{-1}$ (20°-$780^{\circ}C$). The average low temperature expansion coefficient computed for this temperature range for data from the present study is $14 \times 10^{-6}\ ^{\circ}C^{-1}$ (0°-$800^{\circ}C$), which is somewhat smaller than those reported in the earlier works.

Attempts to determine an independent value for the temperature at which the reaction

$$PuC_{1.5} + 0.5\ C \rightarrow PuC_2$$

occurs have been unsuccessful to date. The kinetics of this reaction appear to be very slow. For instance, at $1750^{\circ}C$ the transformation takes place at an observable rate; however, intensity changes in the diffraction pattern occur slowly. Reaction rates below the reported transformation temperature have not been investigated to date.

The only structure observed above the temperature at which the reaction occurs is the cubic modification of PuC_2. This is in agreement with results reported in the UK.[7] No indication of the tetragonal modification has been observed at or near the transformation temperature. However, it is possible that a region of stability for this structure exists and is being obscured by kinetically sluggish transformations. Further work will be necessary to clarify this point.

Obtaining accurate lattice parameter data for PuC_2 (cubic) is somewhat difficult. To date, all reflections observed for this structure have been limited to the front reflection region. This problem is probably due to intensity and resolution losses arising from thermal effects. Preliminary thermal expansion data have been obtained for PuC_2 (cubic); however, only an estimate of the expansion coefficient may be calculated, due to the small number of observations and to scatter in the data. The average expansion coefficient estimated for the temperature range $1750^{\circ}C$ to $2000^{\circ}C$ is $21 \times 10^{-6}\ ^{\circ}C^{-1}$. No comparable data on PuC_2 are available, but Bowman[10] has reported $25.2 \times 10^{-6}\ ^{\circ}C^{-1}$ (1765°-$2300^{\circ}C$) for UC_2 (cubic).

Two metastable phases have been observed in quenched samples of PuC_2. The first of these is the tetragonal modification of PuC_2[11,12] and the second is a material of unknown composition and structure.[13] PuC_2 (tet.) typically results from rapid quenching rates ($\sim 10^3\ ^{\circ}C$/min). Although the furnace being used in the present study is capable of very rapid quenching, only relatively slow cooling ($\sim$ 500-$600^{\circ}C$/min) has been carried out to date. Under these circumstances, samples containing the unknown phase are easily prepared. The reported diffraction patterns of samples containing PuC_2 (tet.) virtually always contain extra lines which correspond to this unknown phase. It would seem reasonable to postulate that the unknown species is a kinetically trapped metastable intermediate involved in the mechanism of the decomposition of PuC_2 to Pu_2C_3. This investigation is being continued using various carbon rich (U, Pu)C_2 compositions.

4. Thermodynamic Properties of Pu Compounds by High Temperature Electrochemistry
(G. M. Campbell)

Microelectrode techniques are being developed for the determination of thermodynamic properties of Pu alloys in equilibrium with high temperature fused salts. It has been found that alloys containing Pu at a partial molar free energy more negative than about -10 kcal/mole equilibrate with the electrolyte by the reaction

$$3\ Pu(IV) + Pu(alloy) = 4\ Pu(III) \qquad (1)$$

If pure Pu metal is present, this reaction results in steady enrichment of the alloy in Pu. A microelectrode technique has been developed[14] which permits measurement of the equilibrium potential of such an alloy without other Pu species being present. An electrode consisting of Pu_2C_3 + excess C equilibrated with

LiCl-KCl containing 0.00279 mole percent $PuCl_3$ and measured against the Pu/Pu(III) couple resulted in a potential of

$$E = 0.53493 - 0.000196\ T, {}^{o}K\ (volts) \qquad (2)$$

in the temperature range of 917.3 to 1015.7°K. This cell can be represented schematically as

$$Pu\ (l)\ |\ PuCl_3(x_1)\ PuCl_4(x_2),\ LiCl\text{-}KCl\ |\ Pu_2C_3 + C(s) \qquad (3)$$

the cell reaction is

$$1.5\ C + 2\ Pu + 3\ PuCl_4 \rightarrow 4\ PuCl_3 + PuC_{1.5} \qquad (4)$$

the Gibbs free energy for this reaction is

$$-\Delta G = 6\ FE = 74.01 - 0.0244\ T,\ kcal\ . \qquad (5)$$

The cell

$$Pu(l)\ |\ PuCl_3(x_1), PuCl_4(x_2),\ LiCl\text{-}KCl\ |\ W\ (s) \qquad (6)$$

incorporating microelectrode technique is being used to measure the free energy of the reaction

$$3\ PuCl_4(x_1) + Pu(l) \rightarrow 4\ PuCl_3\ (x_2)\ . \qquad (7)$$

The free energy change for this reaction subtracted from (5) will result in the free energy of formation of $PuC_{1.5}$. No final data for this reaction are yet available.

Preliminary work done on the $(U, Pu)_2C_3$ solid solution system indicates that the thermodynamic properties of these compounds may be measured using microelectrode techniques.

5. Mass Spectrometric Studies of the Vaporization of Pu Compounds
(R.A. Kent)

The mass spectrometer-Knudsen cell assembly shown in Figure 463-14 and described previously[15] has been employed to study the vaporization behavior of Pu metal and of various plutonium containing compounds.

Pu: Plutonium metal was effused from both W Knudsen cells and ThO_2 cups contained in W Knudsen cells over the range 1426-1658°K. The data indicate that Pu(ℓ) vaporizes to the monomer with the Pu pressure given by

$$\log_{10} P_{Pu}(atm) = (4.924 \pm 0.120) - (17420 \pm 184)/T, {}^{o}K. \qquad (1)$$

The Pu vapor pressure data are presented in Figure 463-15. The results of this investigation are in excellent agreement with those of previous studies.[16,17] When the data from all the vaporization studies are

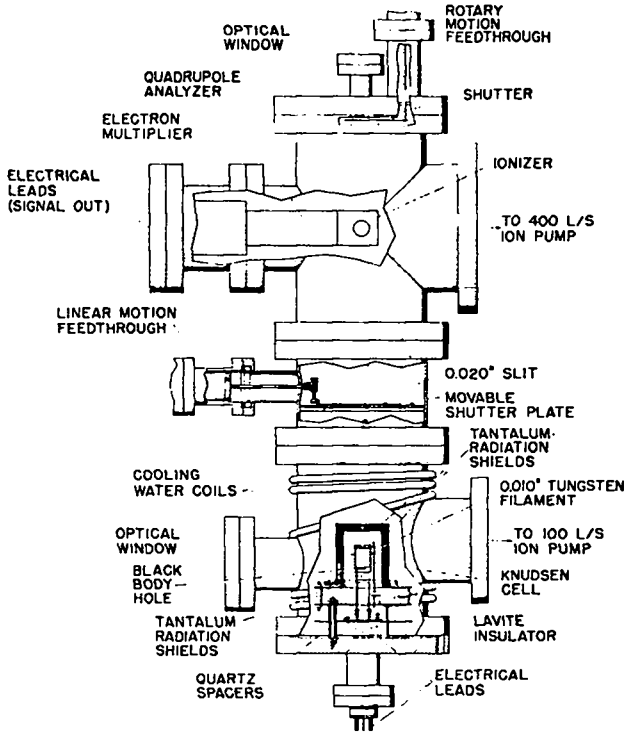

Figure 463-14. Mass Spectrometer-Knudsen Cell Assembly

combined, the heat and entropy of vaporization are calculated to be $\Delta H^{o}_{V\,298} = 83.0 \pm 0.5$ kcal/mole and $\Delta S^{o}_{V\,298} = 29.1 \pm 0.5$ eu. The boiling point is calculated to be 3466°K.

PuN: A mass spectrometric study in which PuN(s) was heated in W Knudsen cells over the range 1658-1976°K, has shown that plutonium mononitride vaporizes congruently to the elements according to the reaction

$$PuN_{0.98}\ (s) = Pu\ (g) + 0.49\ N_2\ (g) \qquad (2)$$

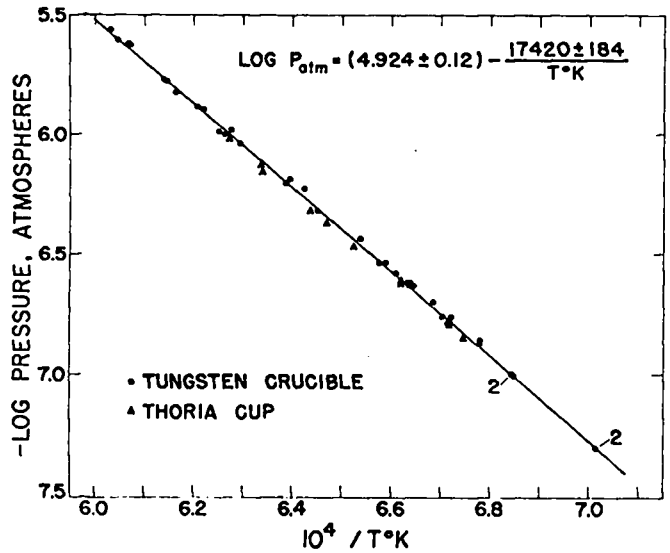

Figure 463-15. Vapor Pressure Data for Plutonium

with the Pu partial pressure given by the equation

$$\log_{10} P_{Pu}(atm) = (6.445 \pm 0.005) - (21958 \pm 98)/T, {}^{o}K \quad (3)$$

The Pu partial pressure data are presented in Figure 463-16.

As no high temperature thermodynamic data exist for PuN(s) C_p values were estimated from known values for UN(s),[18,19] U(s),[20] and Pu(s).[21] These estimated C_p values were then employed to calculate thermodynamic functions for PuN(s). These functions, when combined with vapor pressure date, yield for PuN(s) the values ΔH^{o}_{f298} = 71.2 ± 2.5 kcal/mole and ΔS^{o}_{f298} = -19.9 ± 2.0 eu. These results are in accord with those of Hubbard, et al.,[22] who employed an oxygen-bomb calorimeter to determine for PuN(s), the value ΔH^{o}_{f298} = -71.5 ± 0.6 kcal/mole.

Pu-C System: As a first step in the study of the Pu-U-C ternary system, the vaporization behavior in the Pu-C binary system is being investigated as a function of composition. To date, a series of experiments have been performed with samples ranging in composition from Pu to PuC_2 + C. In addition to the vapor pressure data, some information pertaining to the Pu-C phase diagram has been obtained.

Plutonium monocarbide vaporizes to yield gaseous Pu and Pu_2C_3(s). A series of samples with initial

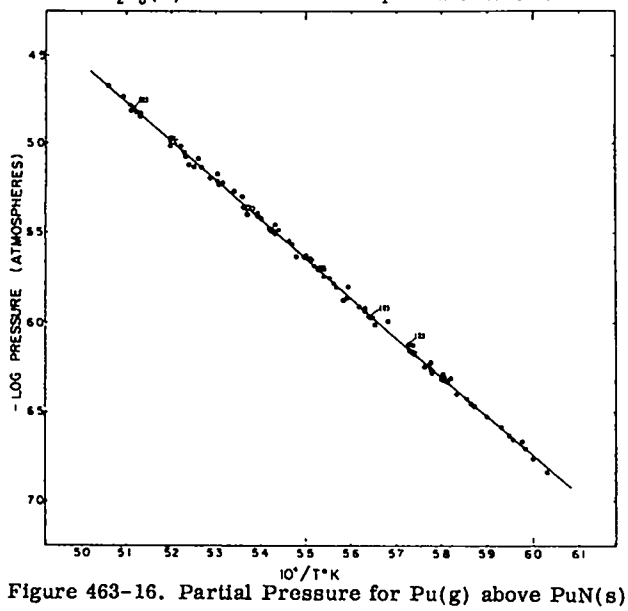

Figure 463-16. Partial Pressure for Pu(g) above PuN(s)

stoichiometries ranging from $PuC_{0.85}$ to $PuC_{1.34}$ were heated in W Knudsen cells over the range 1533-1799°K. The results indicate that the vaporization process is invarient, i.e., the Pu pressure is independent of composition, so long as the condensate consists of both the mono- and sesquicarbides. The low carbon sesquicarbide phase boundary in the Pu-C phase diagram curves toward the monocarbide composition at high temperatures, passing through the stoichiometry $PuC_{1.41}$ at about 1550°C.

A series of experiments, over the range 1745-1928°K, with samples having initial stoichiometries ranging from $PuC_{1.50}$ to $PuC_{2.07}$ indicates that the sesquicarbide vaporizes invariently to Pu(g) and graphite. At 1662 ± 10°C, the sesquicarbide transforms to the dicarbide. Studies in which samples consisting of the dicarbide plus graphite were heated in both W and graphite Knudsen cells over the range 1934-2140°K indicate that the vapor consists predominately of Pu(g) with a small amount of PuC_2(g). Values for the pressure of Pu(g) above various carbide compositions are listed in Table 463-V.

Table 463-V

Plutonium Pressures Above Various Pu-C Compositions

Condensed Phases	Pu Pressure (atm)
PuC + Pu_2C_3	1.0×10^{-6} at 1700°K
Pu_2C_3 + C	2.4×10^{-8} at 1700°K
PuC_2 + C	1.4×10^{-6} at 2000°K

When the Pu(g) pressure data above PuC + Pu_2C_3 and above Pu_2C_3 + C are combined with thermodynamic functions published for PuC(s)[23] and those estimated for Pu_2C_3(s) we obtain for $PuC_{0.87}$(s) the values ΔH^{o}_{f298} = -10.3 kcal/mole and ΔS^{o}_{f298} = + 2.8 eu. For Pu_2C_3(s) the values obtained are ΔH^{o}_{f298} = -25.4 kcal/mole and ΔS^{o}_{f298} = + 9.8 eu.

Miscellaneous: The new Hitachi RMG-K mass spectrometer-Knudsen cell assembly has been received and is being installed. The mass spectrometer employs an 8 in., 90° magnetic sector and has a theoretical resolution of (M/M + ΔM) = 6000 with a 50% valley between peaks. In tests conducted to date, the unit has proved capable of resolving to baseline the mass 29 peak

consisting of $^{14}N\,^{15}N^+$ and $C_2H_5^+$. The Knudsen cell has been heated to 2100°C using less than half of the available power from the heater supply. It is anticipated that the installation will be completed and the unit boxed for studies of plutonium compounds by the end of this calendar year.

6. High Temperature Calorimetry
(A. E. Ogard, D. G. Clifton, and G. Melton)

In a continuing effort to determine the high temperature physical and chemical properties of plutonium-containing materials the high temperature heat content of these materials is being determined. Three calorimeters are in use: (1) a high temperature drop calorimeter, (2) an intermediate temperature drop calorimeter, and (3) an adiabatic calorimeter.

A. High Temperature Drop Calorimeter: During this reporting period, several features of aneroid calorimeters have been investigated that greatly affect the experimental accuracy obtainable. These features should not be peculiar to this particular calorimeter but should apply to all copper block calorimeters used for high temperature drop calorimetry (temperatres greater than 1400°C).

The high temperature calorimeter was described at the 1967 Vienna Thermodynamics Meeting.[24] The important features are a 6" dia gold plated copper block weighing ~ 28 kg, a constant temperature (25.0°C) surface at 2.5 cm from all surfaces of the copper block and an aluminum radiation and convection shield positioned ~ 1 cm from all surfaces of the copper block. The cylindrical surface of the copper block is grooved for placement of a resistance thermometer. If the resistance thermometer is wound on the copper block without any adhesive the calibration constant of the calorimeter was found to be dependent on the gas surrounding the copper block. The difference in calibration constant can be as large as 1-2% between calibrations in argon and vacuum although the precision for calibration in a particular atmosphere is better than ± 1%. This difference in calibration constant is also dependent on the total amount of heat supplied to the calorimeter during calibration. The calibration constant can be made reproducible but not entirely independent of the atmosphere surrounding the copper block by permanently attaching the resistance thermometer to the copper block. This was done by spraying 3 coats of a clear acrylic coating on the thermometer wire and copper block after installation of the thermometer. Although it has not been tested, this problem could equally exist with the use of thermocouples as with the resistance thermometer. A permanent bond between calorimeter block and temperature sensing device is needed.

The high temperature calorimeter must be operated in vacuum if an accuracy of better than ± 1% is desired. The calibration constant of the calorimeter is independent of the difference in temperature (ΔT) between the copper block and constant temperature surface only if vacuum separates them. In the ΔT range of 1 to 10°C the calibration constant increases at the rate of ~ 0.1% per °C of ΔT if the calorimeter is surrounded by Ar. In vacuum, the calibration constant is independent of this ΔT.

The large ΔT capability is needed in high temperature drop calorimetry since only a single sample is normally used over a large range of drop temperatures. The crucibles are difficult and expensive to fabricate so a minimum of samples is used. Ideally, a separate sample should be used at each drop temperature. This sample should be of a size that would give the same amount of heat to the calorimeter at each drop temperature.

The calibration constant of the calorimeter has been redetermined with vacuum surrounding the calorimeter. A ΔT covering the range 1 to 9.2°C and a heating rate over a factor of 2 have been studied. The calibration factor of 2582.6 cal/min ± 0.3% was obtained. The least accurate part of the calibration presently is the recording system and chart paper. An all electronic integrating system with an accuracy of better than 0.1% is being built to replace the recording system.

The apparent heat content of four tungsten crucibles has been determined as a function of temperature from 1500 to 2835°C. The results are listed in Table 463-VI

Table 463-VI

Apparent Heat Content of Tungsten
Vacuum Drop Calorimeter

Temp., °C	ΔH, cal/g	Crucible	Temp., °C	ΔH, cal/g	Crucible
1510	51.6	A	2250	81.0	C
1510	51.3	A	2280	81.9	B
1532	51.1	B	2285	82.2	A
1557	53.2	D	2345	84.9	A
1627	54.7	C	2345	86.3	C
1632	54.2	B	2358	86.4	B
1742	61.0	D	2447	89.3	B
1840	64.6	B	2453	90.4	A
1840	65.0	A	2462	92.6	C
1843	64.7	B	2480	91.4	B
1943	69.2	D	2545	94.2	A
2160	77.5	B	2545	95.7	B
2163	76.6	C	2555	96.6	D
2163	78.0	A	2650	100.4	D
2210	78.5	D	2835	108.1	D

A = 103 g, ~17.1 cm^2 surface area
B = 54.5 g, ~17.1 cm^2 surface area
C = 96.0 g, ~36.1 cm^2 surface area
D = 93.6 g, ~36.1 cm^2 surface area

and are not corrected for any heat loss during drop.

In this set of results there is no apparent systematic relationship of heat content with sample size or weight. These results when plotted on a graph show an experimental precision of ~± 1% at all temperatures. Included as causes of this error are the ± 0.3% calibration accuracy and ± 0.5% calibration of the optical pyrometer used for temperature measurements.

Pellets of PuO_2 weighing 56 g have been loaded into a crack free tungsten crucible. The crucible was then welded shut under a partial atmosphere of argon. The heat content of PuO_2 will be determined up to ~2650°C. The heat of fusion will also be measured. The enthalpy increment between 25° and 1460°C has been determined. A value of 28.2 kcal/mole was obtained. Prior to calculation of the PuO_2 results the data curve obtained from the drop was corrected for the self-heating of the plutonium. The self-heating of the plutonium was determined by direct measurement in the calorimeter. A value of 2.09×10^{-3} watts/g (± 4%) of plutonium was calculated.

B. Medium Temperature Drop Calorimeter: A drop calorimeter covering the temperature range of 300 to 1100°C is being assembled. The design is similar to the high temperature drop calorimeter but with a smaller copper calorimeter block. This will permit the use of the same sample in both calorimeters.

In this temperature range accurate thermocouples can be used for determination of the temperature of the crucible before dropping. The accuracy of these heat content measurements should be ~0.1%. It has been demonstrated in other laboratories that accuracies of ± 0.1% can be obtained.

The calorimeter has been assembled and tested, including the constant temperature surrounding bath, vacuum system, and furnace assembly. The dropping mechanism is now being fabricated.

C. Adiabatic Calorimetry: An evacuable adiabatic calorimeter similar to the one described by Dench[25] is being tested.

The calorimeter should be operative up to about 1400°C and will permit energy measurements upon cylindrical samples of condensed phases that are about 1.6 cm high and 1.2 cm O.D. The system will allow the measurements of heat capacities and heats of reaction and transformations for processes which progress at a reasonable rate in this temperature range.

The calorimeter and its associated vacuum system, as well as a system to provide a cold gas flush of He which has been purified in an uranium-chip furnace, are installed on a temporary work bench in the Laboratory. The glove-box in which the system will be installed has arrived. However, installation is being deferred until further tests of the calorimeter are completed.

Several series of experiments and tests have been conducted in order to fully characterize the calorimeter and its instrumentation.

Calibration of the integrating circuitry, which is used to give a digital read-out of the integral of the current through the sample heater times time, has been accomplished. The power ranges covered were from 0.03 watts to 5.6 watts; the calibration showed the integrator to be accurate to about 0.07%, which is adequate. This integrator in conjunction with a constant voltage power supply allows the measurement of the energy supplied to the sample.

The power settings of the main heater power supply necessary to attain various steady state operating temperatures of the calorimeter (with a representative sample in place) have been determined. Simultaneously

a study was made of the corresponding Δ T gradients across the "adiabatic" shields at various steady state conditions. From these studies two facts became evident. (1) With the present main heater power supply the maximum temperature of the calorimeter and sample is about 1150°C. (2) With the original design 3 radiation shields in the "adiabatic" shield assembly, the ΔT gradients were intolerably large and the response time of the heater and sensing systems was too long. The latter two difficulties have been overcome by modification of the "adiabatic" shield assembly to a single shield. A second power supply in series with the main heater power supply should extend the high temperature limit to about 1400°C.

It has also been found that the response time of the ΔT and sample temperature sensing element to adjustments in the main heater power supply is in an acceptable range only when the temperature of the calorimeter is high enough (600°C) for the predominant mode of energy transfer to be radiative.

A series of calibration experiments, consisting of the following procedures, has been done. The calorimeter was loaded with a sample of single crystal synthetic sapphire and brought to "equilibrium" at an elevated temperature. The temperature-time and dT/dt history was then recorded while the adiabatic shield temperature gradient, ΔT, was recorded and balanced out with a potentiometer system using a mirror and light galvanometer as a null indicator. A pre-programmed amount of energy was then added to the sample heater. Manual control of the main heater power supply was then used to maintain the null balance of the ΔT signal while the energy was being supplied to the sample, and for a reasonable rating period after the energy addition. During the above manipulations the temperature, T, of the sample was recorded as a function of time. (Since ΔT is only weakly dependent upon T, the above procedure is justified.)

From this data a total "heat capacity" representative of the sample, sample crucible and associated supports, plus steady state heat leak can be obtained. Tests of this nature have been done from about 470°C to 700°C. At the upper end of this temperature span, reproducibilities of about ± 4% are found. Furthermore, calculated estimates of the total "heat capacities" agree favorably with the experimental value. Subtraction of the known heat capacity of the Al_2O_3 sample will then provide a calibration constant for the calorimeter without the sample. Further experiments of this nature are underway.

IV. ANALYTICAL CHEMISTRY

1. Electron Microprobe Examinations
(E.A. Hakkila, H.L. Barker)

Electron microprobe examinations of (U, Pu) C samples from various preparatory experiments were made to identify phases and to determine distributions of U and Pu.

Two samples of (U, Pu) C prepared to contain 0.1 percent Ni were examined for Ni distribution, and the characteristic X-ray intensities of U, Pu, and C were compared to intensities measured for a reference (U, Pu) C.

2. Determination of O_2 in Refractory Oxides
(D.E. Vance and M.E. Smith)

A gas chromatographic method was developed to measure O_2 following liberation as CO and CO_2 by inert-gas-fusion from a pellet prepared from 1 g of the refractory oxide and 0.2 g of C. These gases were trapped on SiO_2 gel, desorbed and mixed with an internal standard such as Ne, and then measured chromatographically. Electronic integration of the chromatogram peak areas improved the precision of the measurements. Repeated analyses of special lots of ThO_2, U_3O_8, and (U, Pu) O_2, prepared to contain known quantities of O_2, showed that the method was not biased. The relative standard deviation (1σ) of the method for a single determination was 0.58 percent. The method was applied successfully to analysis of several oxide samples, and now serves as a back-up for a more-precise determination that uses inert-gas-fusion and a gravimetric finish.

V. PUBLICATIONS

1. "Thermodynamic Properties of Plutonium Nitride by Galvanostatic Potential Determination," G.M. Campbell, J. Phys. Chem. 73, 350 (1969).

2. "Mass Spectrometric Studies of Plutonium Compounds at High Temperatures. III. The Vapor Pressure of Plutonium," R.A. Kent, J. High Temp. Science 1, 169 (1969).

3. "Mass Spectrometric Studies of Plutonium Compounds at High Temperatures. IV. The Vaporization of PuN," R.A. Kent and J.A. Leary, J. High Temp. Science 1, 176 (1969).

4. "Characterizing the High-Temperature Thermophysical and Thermochemical Properties of Irradiated Fuels -- Present Status and Future Needs," A.E. Ogard, J.G. Reavis, and J.A. Leary, Proceedings of the 16th Conference on Remote Systems Technology, American Nuclear Society (1969).

5. "Combustion-Manometric Determination of C in Plutonium Sulphide," C.S. MacDougall, M.E. Smith, and G.R. Waterbury, Los Alamos Scientific Laboratory Report LAMS-4047 (1968). This method was also described at the Twelfth Conference on Analytical Chemistry in Nuclear Technology, Gatlinburg, Tennessee, October 8-10, 1968.

6. "Present Status of the Uranium-Plutonium-Carbon Phase Diagram," J.A. Leary, International Symposium on Ceramic Nuclear Fuels, Amer. Ceram. Soc. May (1969), in press.

7. "Metallography of Uranium-Plutonium-Carbon Sintered Pellets," K.A. Johnson, 21st AEC Metallographic Mtg., San Diego, Calif. (1969).

8. "Crystallography and Magnetic Ordering in Plutonium Carbides by Neutron Diffraction," J.L. Green, G.P. Arnold, J.A. Leary, and N.G. Nereson, J. of Nuc. Mater., in press (1969).

9. "Thermodynamic Properties of PuN by Galvanostatic Potential Determination," G.M. Campbell, Los Alamos Scientific Laboratory Report No. LA-3945 (1968).

10. "A Computer Program for Calculation of Particle Size Distribution from Sedimentation Data," J.D. Olson and G.M. Campbell, Los Alamos Scientific Laboratory Report No. LA-4001 (1968).

VI REFERENCES

1. A.L. Bowman, et al., Acta Cryst., 21, 670 (1966).

2. J.M. Leitnaker and W.G. Witteman, J. Chem. Phys. 36, 1445 (1962).

3. Quarterly Status Report on the Advanced Plutonium Fuels Program, Oct. 1 to Dec. 31, 1968, Report LA-4114-MS, p. 43.

4. Annual Status Report on the Advanced Plutonium Fuels Program, July 1, 1967 to June 30, 1968, Los Alamos Scientific Laboratory Report No. LA-3993-MS, p. 40.

5. C.S. Griffin, et al., "Self-Irradiation Damage in Transuranic Elements and Compounds," paper no. 10 in Kay and Waldron, "Plutonium 1965 (1967).

6. C.R. Houska, Union Carbide Research Institute, Report UCRI-TR-18 (1963).

7. J.T. Dalton, E.A. Harper, H.J. Hedger, and R.W. Stannard, AERE-R 5948 (1969).

8. M.H. Rand and R.S. Street, AERE-M 973 (1962).

9. P.G. Pallmer, HW-72245 (1962).

10. A.L. Bowman, J. Inorg. Nucl. Chem., 19, 111 (1966).

11. D.M. Chackraburtty and N.C. Jayadevan, Acta. Cryst., 18, 811 (1965).

12. J.G. Reavis, M.W. Shupe, C.W. Bjorklund, and J.A. Leary, Transactions of the American Nuclear Society 1967 Annual Meeting, 111 (1967).

13. R.N.R. Mulford, F.H. Ellinger, G.S. Hendrix, and E.D. Albrecht, Plutonium 1960, pp 301. London: Cleaver-Hume Press Limited (1960).

14. "Thermodynamic Properties of PuN by Galvanostatic Potential Determination," G.M. Campbell, J. Phys. Chem., 73, 350 (1969).

15. R.A. Kent and J.A. Leary, Los Alamos Scientific Laboratory Report No. LA-3902 (1968).

16. T.E. Phillips, G.W. Sears, R.L. Seifert, and O.C. Simpson, U.N. Int. Conf. PUAE 7, 382 (1956).

17. R.N.R. Mulford, Thermodynamics, Vol. 1, IAEA, Vienna, p 231 (1965).

18. E.F. Westrum, Jr., Nuclear Metallurgy, Vol. X, IMD Special Report Ser. No. 13, The Metallurgical Society, J. AIME, 1964, p. 255.

19. T.G. Godfrey, J.A. Wooley, and J.M. Leitnaker, Oak Ridge National Laboratory Report No. ORNL-1596 (1966).

20. R. Hultgren, R.L. Orr, P.D. Anderson, and K.K. Kelley, Selected Values of Thermodynamic Properties of Metals and Alloys, J. Wiley and Sons, Inc., New York, N.Y. (1963).

21. M.H. Rand, Thermochemical Properties, in Atomic Energy Review, Vol. 4, Special Issue

No. 1, IAEA, Vienna (1966).

22. G.K. Johnson, E.H. Van Deventer, O.L. Kruger, and W.N. Hubbard, J. Chem. Thermodynamics, 1, 89 (1969).

23. M.H. Rand, A Thermochemical Assessment of the Plutonium-Carbon System, presented to the IAEA, Vienna, Sept. (1968).

24. A.E. Ogard and J.A. Leary, "High Temperature Heat Content and Heat Capacity of Uranium Dioxide and Uranium Dioxide-Plutonium Dioxide Solid Solutions," Thermodynamics of Nuclear Materials with Emphasis on Solution Systems, IAEA, Vienna (1967).

PROJECT 464

STUDIES OF Na-BONDED (U,Pu)C AND (U,Pu)N LMFBR FUELS

Person in Charge: D. B. Hall
Principal Investigators: R. H. Perkins
G. H. Best

I. INTRODUCTION

(U,Pu)C and (U,Pu)N are regarded as attractive alternates to mixed oxides as fuels for commercial LMFBR application. The high heavy-atom densities and thermal conductivities of the mixed carbide and nitride make it possible for these fuels to outperform mixed oxides. Full exploitation of carbides and nitrides dictates the use of a gap between fuel and clad to accommodate fuel swelling (with minimal fuel-cladding mechanical interactions) and a high thermal conductivity path across the gap to limit fuel temperature. The conditions can be met by filling an annulus between fuel and clad with sodium.

Before a satisfactory sodium-bonded fuel element can be developed, however, information is required that will identify the number and severity of problems associated with sodium bonding and will suggest solutions to these problems. Problem areas that are being studied in this experimental program are:

1. The mechanisms and kinetics of carbon transfer to claddings through the sodium bond.
2. The significant fuel and sodium variables that affect compatibility.
3. The consequences of exposing fuel to coolant sodium.
4. The behavior of sodium-bonded fuel elements under irradiation.
5. The performance limitations of the sodium bond under high-heat-flux conditions.

Efforts are now concentrated on the mixed carbide fuel. Type 316 stainless steel is the base cladding material being studied, though vanadium alloys are also being tested.

As prerequisites for this compatibility program, a number of developmental efforts have been undertaken. These include establishment of (1) techniques for the production of single-phase monocarbide pellets of known composition and dimensions, (2) techniques and equipment for fuel pin loading, bonding, and inspection, and (3) techniques and equipment for determining the distribution of fission products in irradiated fuel pins.

II. SYNTHESIS AND FABRICATION OF (U,Pu)C PELLETS (M. W. Shupe, S. McClanaham, G. Moore, R. W. Walker, R. Honnell)

A. General

Standardized procedures for producing single-phase monocarbide pellets of known composition and dimensions have been developed. These pellets will be utilized in EBR-II irradiation experiments and compatibility testing. Basic process steps are:

1. Multiple arc melting of a 60-g mixture of ^{235}U, Pu, and C using a graphite electrode.
2. Solution treatment of the arc melted ingot for 24 h at 1600°C.
3. Crushing and grinding of the ingot in a WC vibratory mill, followed by screening of the resulting powder to a particle size range of $\leq$ 62 μ.
4. Elimination of higher carbides by reaction with H_2 at 850°C.
5. Cold compaction at 20 tsi into pellets without the use of binders or sintering aids.
6. Sintering the pellets in Ar at 1800°C for

4 h followed by heat treatment for 2 h at 1400°C.

7. Characterization of the pellets by linear dimensioning, weighing, metallography, x-ray diffraction analysis, chemical analysis for U, Pu, C, N, O, and trace impurities, radiography for determination of possible internal cracks, and isotopic analysis of uranium and plutonium.

B. Results During FY 1969

A total of 464 (U,Pu)C pellets were prepared during this period using the above process. Characterization results were for the most part identical to those reported previously for the 1012 pellets previously prepared.[1] A typical pellet microstructure is shown in Fig. 464-1.

For irradiation studies in EBR-II, 330 single-phase pellets of (U,Pu)C were transferred to the fuel pin loading facility. Averaged characteristics of samples taken from this group of pellets are as follows:

1. All pellets were found to be free of detectable cracks and chips.
2. The average chemical composition is $(U_{0.797}Pu_{0.203})(C_{0.97}O_{0.006}N_{0.005}H_{0.001})$. The average density obtained using an immersion technique was 90.0 ± 1.6% of theoretical (13.52 g/cm^3).
3. The average x-ray lattice dimension was found to be 4.956 ± 0.001 Å.
4. The average concentrations of impurities is shown in Table 464-I. Only single-phase monocarbide microstructures were found; essentially no free metal or higher carbide phases were present. Some specimens were found to contain a few inclusions of 3 μ or less and in total amounts less than 0.5 v/o. Examination of pellets with an electron microprobe analyzer showed the plutonium and uranium to be homogeneously distributed.
5. The distribution of the pellet diameters is shown in Fig. 464-2.

Approximately 900 single-phase pellets with a nominal composition of $(^{235}U_{0.8}{}^{239}Pu_{0.2})C$ and a sintered density of 95% of theoretical also are required for a series of compatibility and irradiation tests. To date 200 of these pellets have been prepared. Further information on these pellets will be reported on completion of all the characterization analyses. Of the 200 pellets prepared, immersion densities were > 12.7 g/cm^3 or ≥ 94.4% of theoretical. Procedures used in the preparation of this denser material are similar to those given previously. However, the powder was ball-milled for an additional 12 h, and sintering time at 1800°C was increased by 4 h. Metallographic evaluation of both electrolytically etched and stained pellets have indicated single-phase structures with intergranular porosity. A typical photomicrograph of an electrolytically etched pellet is shown in Fig. 464-3.

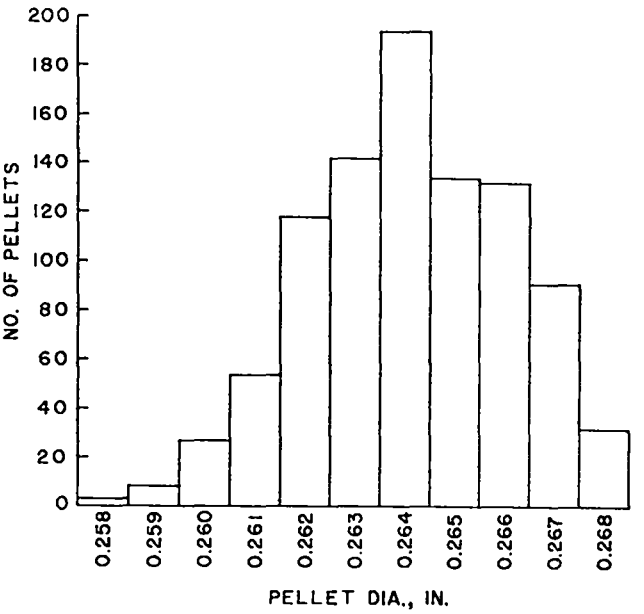

Fig. 464-2. Histogram of $(U_{0.8}Pu_{0.2})C$ pellet diameters (fully enriched uranium-plutonium carbides for EBR-II irradiation fabrication campaign No. 1).

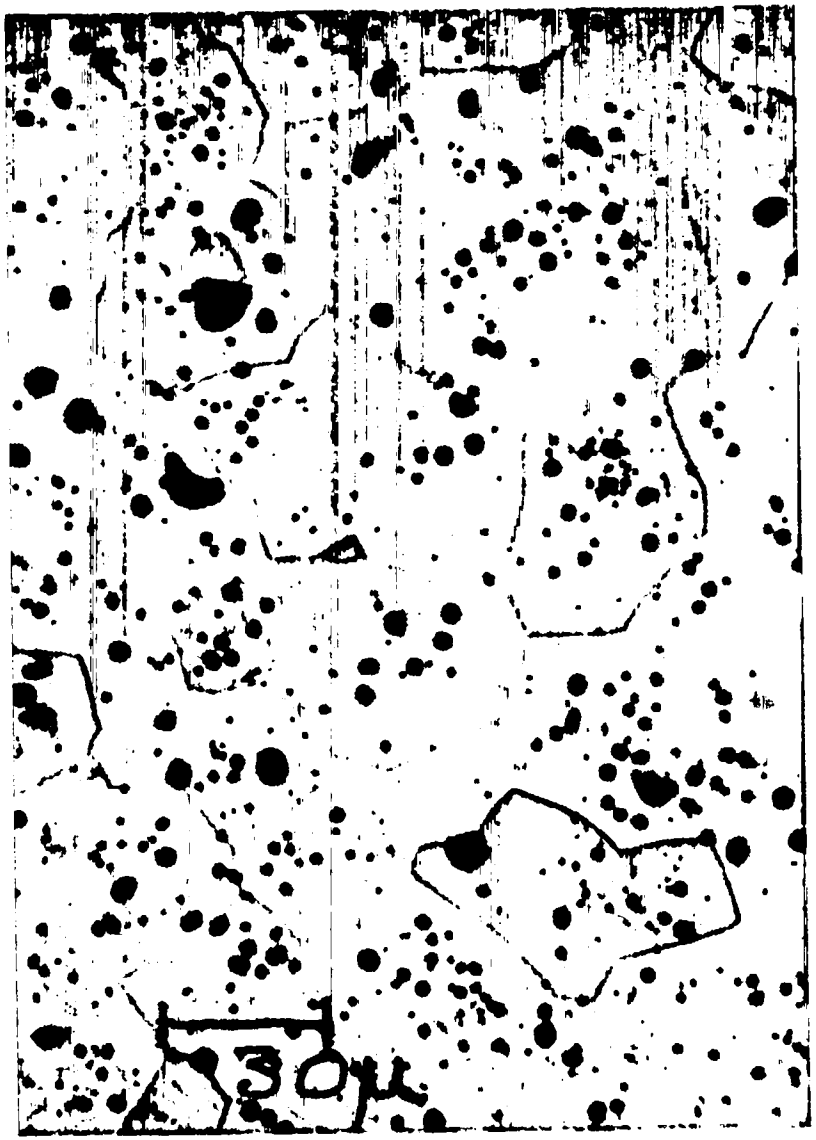

Fig. 464-1 Typical single-phase (U,Pu)C (electrolytic etch).

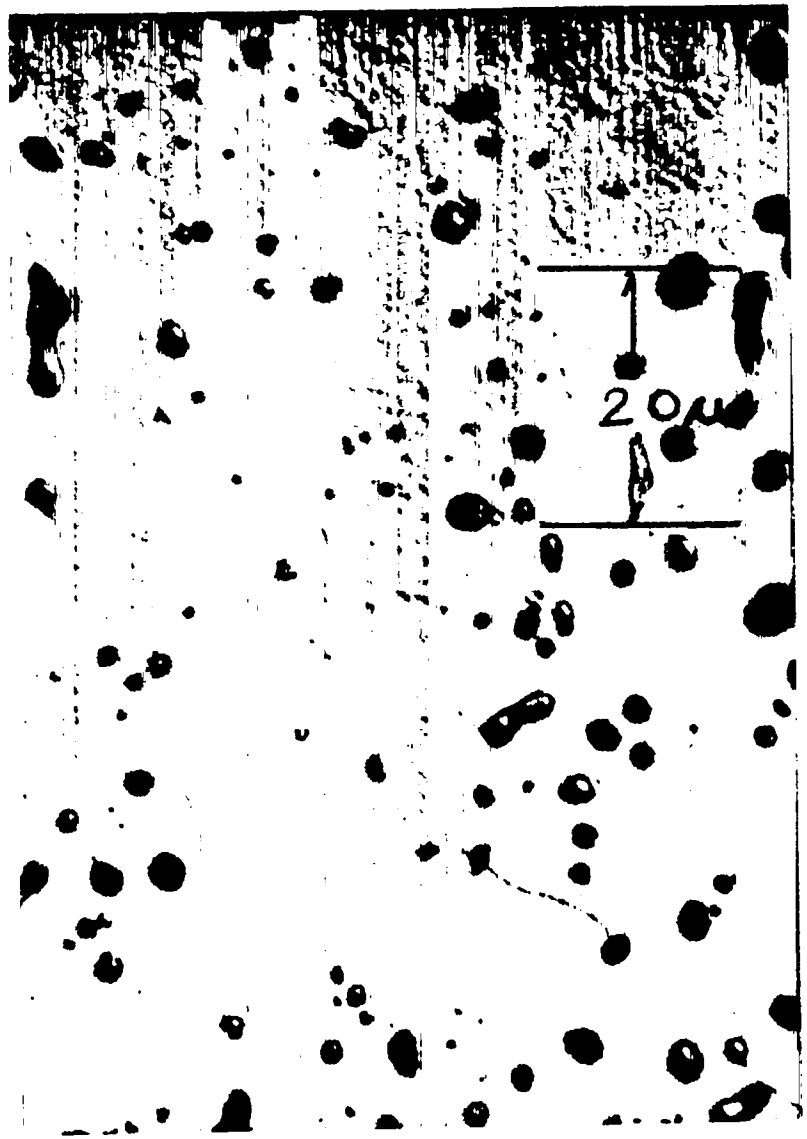

Fig. 464-3. Single-phase ($U_{0.8}Pu_{0.2}$) having density of 94.4% of theoretical (electrolytically etched with a 1:1:1 acetic:lactic: nitric acid mixture at a current density of 90 ma/cm^2).

Table 464-I

Average Spectrochemical Analysis of $(U_{0.8}Pu_{0.2})C$ Pellets

Element	Concentration (ppm by wt)	Element	Concentration (ppm by wt)
Li	< 1	Ni	20
Be	< 1	Cu	40
B	< 1	Zn	< 10
Na	< 2	Sr	< 5
Mg	< 5	Zr	< 100
Al	< 10	Nb	< 50
Si	100	Mo	< 10
P	< 50	Cd	< 10
Ca	< 5	Sn	< 2
Ti	< 50	Ba	< 10
V	< 5	Ta	<1000
Cr	< 10	W	20
Mn	< 2	Pb	< 2
Fe	< 60	Bi	< 2
Co	< 5		

III. LOADING FACILITY FOR TEST CAPSULES
(D. N. Dunning, J. O. Barner, J. A. Bridge)

A. General

A prerequisite to a compatibility program involving (U,Pu)C and sodium is a satisfactory capsule loading and bonding facility. There is little point to obtaining well-characterized materials for testing if these materials are contaminated before they are placed in test. Sodium and (U,Pu)C are sufficiently reactive that all operations must be performed either in vacuum or in a high quality inert atmosphere. The loading facility for handling these materials has been constructed and has been operational most of the past fiscal year. The facility consists of inert-atmosphere gloveboxes equipped with inert-gas cleanup systems to provide an environment for handling fuel pellets and bonding sodium with a minimum of contamination.

B. Results During FY 1969

A two-section fuel loading box has been installed, tested, and put into routine operation. The box consists of an alpha-contaminated section used for fuel pellet storage and inspection and a noncontaminated section for capsule loadings. The pellets are passed through the wall into the capsules using disposable aluminum funnels. In this manner, the alpha contamination is contained in one section of the fuel box and the sodium and welding boxes are maintained in a noncontaminated condition.

The quality of the helium gas during normal loading operations is monitored by periodic mass spectrometer analyses of gas samples. Typical results are shown in Table 464-II. This gas is sufficiently pure that very little contamination of fuel and bonding sodium occurs during the loading and welding operations.

Table 464-II

Analyses of Gas from Loading Facility Gloveboxes

Impurity	Fuel Glovebox (ppm)	Sodium and Welding Gloveboxes (ppm)
H_2O	Not detectable	Not detectable to 2
H_2	3-6	Not detectable
N_2	1-3	6-7
O_2	1	Not detectable

Results of analyses of the sodium used for the thermal bond between fuel and clad, after extrusion and exposure to the box atmosphere, are shown in Table 464-III.

Table 464-III

Impurities in Bonding Sodium

Element	Impurity Concentration (ppm)	Element	Impurity Concentration (ppm)
O_2	< 7-16	Cr	< 3
N_2	< 1	Mn	1
C	< 10	Fe	1
Li	< 3	Co	< 3
Be	< 0.8	Ni	< 3
B	< 15	Zn	<300
Mg	1	Sr	< 0.8
Al	< 3	Ag	< 0.8
Si	12	Cd	< 30
K	300	Sn	< 3
Ca	12	Ba	< 0.8
Ti	< 5	Pb	< 5
V	< 0.8	Bi	< 5

A device for measuring the dimensions of fuel pellets has been designed and built (Fig. 464-4). This machine measures and records the outside profile of the pellet and determines if the ends are perpendicular to the axis of the pellet. The

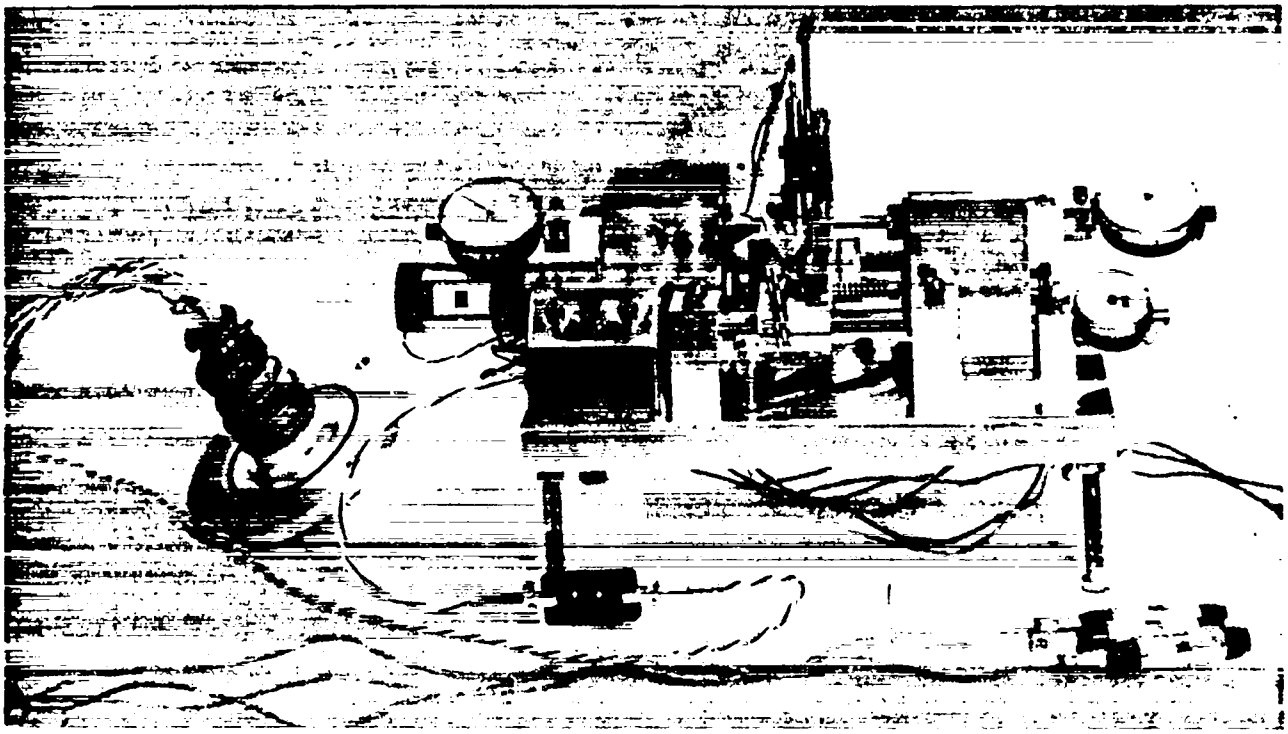

Fig. 464-4. Apparatus for measuring dimensions of (U,Pu)C fuel pellets.

dimensions of all pellets that are now being loaded are measured on this machine.

After test capsules are loaded and the closure weld is made, a multi-step process is used to effect the sodium bond between the fuel pellets and the cladding. No difficulties have been encountered during the bonding of short (3-in.-long) capsules. These are heated to 600°C for 1 h to promote wetting, followed by a 300°C treatment with a magnetostrictive device operating against the bottoms of the capsules. These capsules are centrifuged during cooling.

Attempts were made to eliminate the centrifugation step during the bonding of capsules for testing in EBR-II, because no centrifuge was available to handle these long capsules. However, only limited success was achieved; after several heat treatments most capsules still exhibited defects in the bonds. A centrifuge capable of handling EBR-II capsules was designed and constructed. This centrifuge not only eliminates bubbles from the sodium bonds, but also it provides directional cooling to prevent shrinkage voids from forming during freezing of the sodium. Several passes through the bonding operation are now normally required to achieve a bond free of detectable defects; however, it is anticipated that adjustment of the parameters in the bonding operation will ultimately yield a procedure that will produce satisfactory bonds on a routine basis.

Approximately 90 capsules containing (U,Pu)C fuel and sodium were loaded during the past fiscal year. Eight of these were EBR-II test pins. Six of these have been rejected because of bond defects and suspected oxygen contamination. One of the two satisfactory pins has been loaded into its secondary container and is ready for shipment to EBR-II for irradiation testing.

IV. CARBIDE FUEL COMPATIBILITY STUDIES

(F. B. Litton, H. A. O'Brien, Jr., L. A. Geoffrion, J. H. Bender, A. E. Morris)

A. General

The objectives of this program are to study the interactions among single-phase mixed (U,Pu)C, a sodium bond, and potential cladding materials, i.e., to investigate the technology related to sodium-bonded fuel elements. There are two approaches to the experimental work. One approach

is to determine the reactions occurring between $(U_{0.8}Pu_{0.2})C$ and potential cladding materials, using Type 316 stainless steel and a high strength vanadium-base alloy as the first and second choices of cladding material, respectively. A second concurrent set of experiments is designed to study the mechanism of carbon transport through sodium, the effect of impurities such as oxygen, and the carburizing potential of sodium in mutual contact with carbides and the preferred cladding materials.

Fuels of known composition and thoroughly-characterized sodium are used in all tests. Most of the testing is performed on single-phase (U,Pu)C fuel in which the Pu/U ratio is maintained at 0.25, but some experiments are being carried out on material containing a second phase (either metallic or carbon-rich). Other experiments are being carried out on stoichiometric and hyperstoichiometric UC to determine the effect of plutonium addition on the behavior of the carbide fuel.

B. Results During FY 1969

1. Compatibility of Mixed Fuel Carbides with Type 316 Stainless Steel

The compatibility of essentially single-phase $(U_{0.804}Pu_{0.196})(C_{0.95}O_{0.016})$ fuel pellets sodium-bonded to Type 316 stainless steel capsules was determined by testing at 750°C for 4000 h. Three capsules (0.3-in. o.d. x 0.010-in. wall x 3-in. long) containing three fuel pellets and 1 g of sodium were heated in a forced-convection sodium loop. Prior to examination, the bond sodium was removed from the capsules by vacuum distillation.

The metallographic structures of the capsules and pellets were not changed during the compatibility test. The evidence indicates that sodium-bonded, single-phase mixed carbide fuel is compatible with Type 316 stainless steel under these test conditions.

2. Compatibility of Carbide Fuel with V-15Ti-7.5Cr Alloy

Compatibility tests were performed on V-15Ti-7.5Cr alloy capsules containing three sodium-bonded (U,Pu)C pellets. The pellets were selected from two fuel compositions: $(U_{0.799}Pu_{0.201})(C_{0.967}O_{0.005})$ and $(U_{0.814}Pu_{0.186})(C_{0.950}O_{0.008})$. The capsule dimensions were 0.3-in. o.d. x 0.010-in. wall x 3-in. long, and they contained 1 g of bonding sodium. The compatibility tests consisted of heating two capsules at 650°C and three capsules at 750°C in hot-trapped, forced convection sodium loops for 1000-h periods. Metallographic examination of the test capsules showed that a reaction had occurred between the fuel and clad in one of the capsules heated at 750°C. No reaction product was observed at the areas of contact between fuel and clad in any of the other test capsules. A diffusion zone was observed on the outer surfaces of all the capsules in contact with loop sodium.

Post-test chemical analysis of the fuel pellet adjacent to the reaction zone indicated that this fuel pellet was hypostoichiometric. Its free metal content appeared responsible for the observed reaction product. The pellet contained 77.1% U, 18.4% Pu, 4.61% C, 0.08% O, and 180 ppm N, corresponding to an interstitial-to-metal ratio of 0.963. The desired composition for single-phase carbide fuel is an interstitial-to-metal atom ratio of 0.97 with maximum oxygen and nitrogen contents of 250 and 350 ppm, respectively.

Electron microprobe analyses confirmed the presence of uranium and plutonium throughout the attack area and to an appreciable depth (~ 0.007 in.) in the capsule wall. There was more plutonium than uranium in the reaction product and along the grain boundaries. The uniform zone on the outside of the capsule wall was attributed to the pickup of interstitials, particularly carbon, from the sodium in the loop. The depth of carbon diffusion was about 10 μm. Precipitates of titanium carbide were detected in this layer.

Testing of vanadium alloys has shown that V-15Cr-5Ti is preferred to V-15Ti-7.5Cr alloy for fuel cladding application. However, the compatibility tests described above indicate that the latter alloy is compatible with sodium-bonded, single-phase mixed carbide fuel under the subject test conditions.

3. Effect of Oxygen in Bond Sodium on Compatibility of Mixed Carbide Fuel with Type 316 Stainless Steel

In experiments with "defective" capsules containing (U,Pu)C, it was shown that carbon was transferred by the circulating sodium in the test loop from essentially single-phase pellets to the Type 316 stainless steel container. Oxygen in the sodium was suspected as the cause for this. This was

confirmed by additional experiments which were carried out with carefully sealed capsules. It was shown conclusively that oxygen addition to the bond sodium results in carbon transfer. The technique used in these experiments is described below.

Essentially single-phase mixed monocarbide pellets were loaded in Type 316 stainless steel capsules, and ~ 5 g of bond sodium containing ~ 1.25% oxygen was added to each capsule. These capsules, along with controls (no oxygen addition to the bond sodium), were tested for 1000 h at 550, 650, and 750°C. Metallographic examination after test showed that carbon was moved from single-phase mixed monocarbide pellets to the Type 316 stainless steel in capsules containing excess oxygen in the sodium bond. No carbon transfer was observed in the capsules containing low-oxygen sodium (cold-trapped at 130°C). The extent of carburization at 550°C is shown in Fig. 464-5. A Widmanstätten-type precipitate was observed near the surfaces of the fuel pellets that reacted with oxygen. This is shown

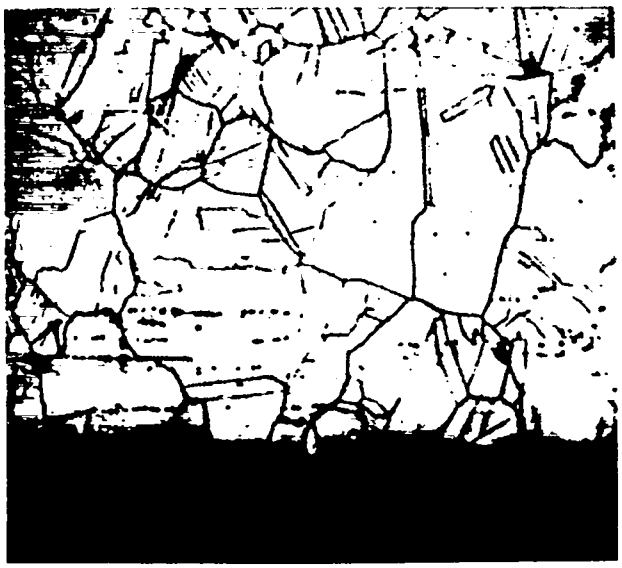

Fig. 464-5. Carburization of Type 316 stainless steel containing oxygen-contaminated sodium and (U,Pu)C pellets. Heated at 550°C for 1000 h. Etched, 300X.

in Fig. 464-6. The surfaces were cracked and the outer portions of the pellets disintegrated. X-ray analyses showed that the products from the disintegration of the pellets (residue remaining in the capsules after distilling off the bond sodium)

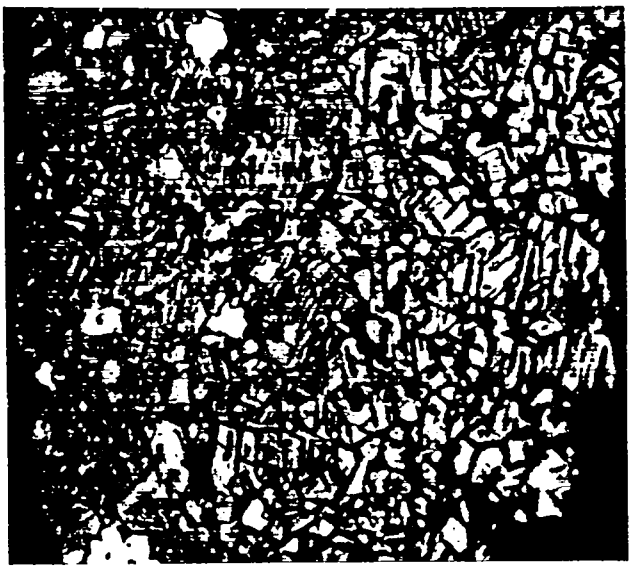

Fig. 464-6. Surface of fuel pellet that reacted with oxygen in the sodium bond. Heated at 750°C for 1000 h. Etched, 300X.

consisted of a mixture of $(U,Pu)O_2$ and (U,Pu)C. The surface material from the fuel pellets consisted largely of dioxide and some monocarbide. In contrast to this, examination of the surface material from a pellet in a control capsule showed only the presence of (U,Pu)C. Chemical analysis of a pellet from a control capsule tested at 650°C for 1000 h showed that it contained 4.60% C, 0.12% O, and 230 ppm N. A pellet heated in oxygen-contaminated sodium contained 4.53% C, 0.68% O, and 270 ppm N.

The carbon transfer may result from precipitation of either free carbon or a higher carbide in the fuel during the reaction of oxygen from the sodium with the fuel. The most probable thermodynamically stable phases are carbon and sesquicarbide, but the data do not indicate the presence of sesquicarbide. Further study is planned to determine the reaction mechanism and the concentration of oxygen in the bond sodium required to produce detectable carbon transfer.

4. Studies of Carbon Transfer in Sodium

Carburization of candidate cladding alloys in sodium is thought to be a diffusion-controlled process in which the difference between the thermodynamic stability of carbides in the carbon source and carbides produced in the clad is the primary driving force. It is apparent that relatively long periods

of time may be required to establish equilibrium in a given system, and that the activities of the carbon and metals in the source and the cladding alloy change during the carburizing process. This, of course, implies that the rate-controlling step also may change, but carbon transfer is primarily dependent on the rate of diffusion of carbon in the carbide source. Carbon is assumed to be soluble in sodium to some small but finite amount. While the transfer mechanism may be contingent on the formation of a particular species in the sodium, the end products of the reaction are independent of the transferring species. Carburization of cladding alloys using carbon sources of different thermodynamic stabilities are being studied in an attempt to determine the rate-limiting step in the reaction. These studies are described below.

Transfer of Carbon from Fe-0.85C Alloy to Type 316L Stainless Steel

Type 316L stainless steel was carburized in zirconium-gettered sodium at 650, 550, and 450°C for periods from 2 to ~ 500 h using eutectoid (0.85 w/o C) iron-carbon alloy as the carbon source. The sodium (~ 200 g) was held in a magnesia crucible under a purified helium atmosphere; four 1/2-in.-square Type 316L stainless steel tabs were suspended in the sodium by nickel wires with the carburizing source at the center of the assembly. The depth of carburization of the tabs and decarburization of the source was measured metallographically. The metallographic measurements were confirmed by microhardness determinations. Chemical analyses of the tabs were made to determine the carbon flux. The carburizing/decarburizing data are recorded in Tables 464-IV, V, and VI. The carbon flux, based on chemical analyses of the stainless steel tabs for carburization at 650 and 550°C, is shown in Table 464-VII. The chemical analyses of the tabs for the 450°C experiments have not been completed.

The initial phase of carbon penetration into Type 316L stainless steel is the formation of a surface film which has been tentatively identified as a solid solution of carbon in stainless steel. This film is shown in Fig. 464-7. No carbide precipitation during this film formation was metallographically detected. The microhardness 0.0005 in. from the surface was 190 VHN (25-g load), which decreased along the concentration gradient to 140 VHN. Surface films persisted up to 24 h at 550°C, and to ~ 500 h at 450°C. No solid solution surface film was observed on the 650°C carburized specimens. After 52 h carburization at 550°C, grain boundary precipitation of carbides preceded general (bulk) precipitation in the grains of the stainless steel. A typical structure of carburized stainless steel is shown in Fig. 464-8.

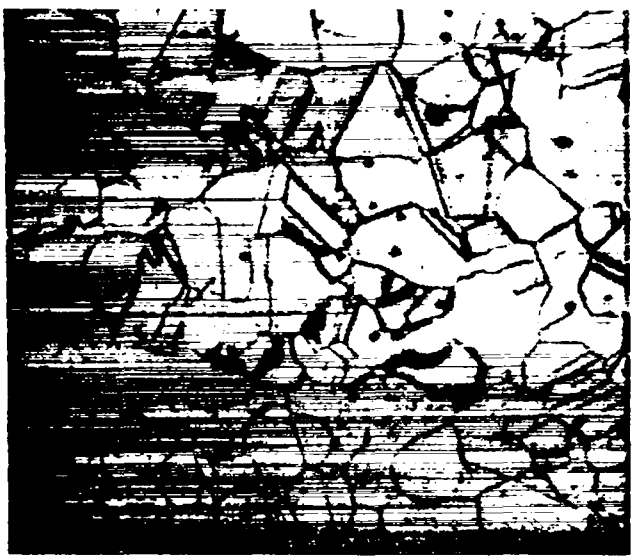

Fig. 464-7. View of the surface of Type 316 stainless steel showing the first stage of carbon diffusion. Specimen carburized in sodium for 24 h at 550°C. Etched, 600X.

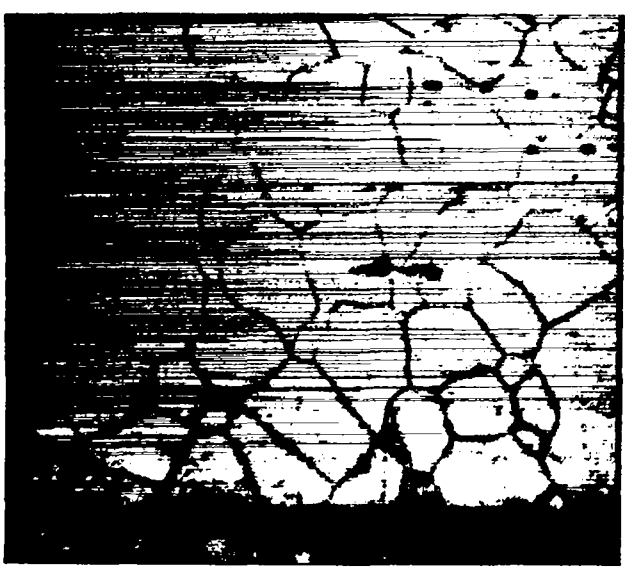

Fig. 464-8. Bulk and grain boundary penetration of carbon at the surface of Type 316L stainless steel after immersion in sodium with iron-carbon alloy source for 52 h at 550°C. Etched, 800X.

Table 464-IV

Diffusion of Carbon from Fe-0.85C Source to Type 316L Stainless Steel in Sodium at 650°C

	$Fe-Fe_3C$ Source			Stainless Steel			
						Depth of Carburization (microns)	
Time (10^3 sec)	Weight Loss (mg)	Area (cm^2)	Depth of Decarburization (microns)	Weight Gain (mg)	Area (cm^2)	Bulk	Total*
7.2	1.90	2.415	70	1.34	14.796	18	40
22.2	3.67	4.031	125	3.19	14.783	25	58
76.2	7.29	3.612	260	7.25	14.782	66	150
163.8	9.36	2.967	500	8.72	14.764	133	216
418.2	18.87	4.979	675	15.93	14.783	150	230

*Bulk plus grain boundary carburization.

Table 464-V

Diffusion of Carbon from Fe-0.85C Source to Type 316L Stainless Steel in Sodium at 550°C

	$Fe-Fe_3C$ Source			Stainless Steel			
						Depth of Carburization (microns)	
Time (10^3 sec)	Weight Loss (mg)	Area (cm^2)	Depth of Decarburization (microns)	Weight Gain (mg)	Area (cm^2)	Bulk	Total*
7.2	0.26	2.212	15.0	0.21	14.815	6.0	6.0
21.6	0.59	2.122	36.2	0.42	14.770	17.0	17.0
86.4	1.59	1.720	72.7	1.43	14.783	39.2	39.2
187.5	3.39	1.862	140.0	3.31	14.783	20.0	48.0
417.6	4.79	1.686	300.0	4.64	14.796	50.0	100.0

*Bulk plus grain boundary carburization; grain boundary diffusion not observed for times less than 86.4 x 10^3 sec.

Table 464-VI

Diffusion of Carbon from Fe-0.85C Source to Type 316L Stainless Steel in Sodium at 450°C

	$Fe-Fe_3C$ Source			Stainless Steel			
						Depth of Carburization (microns)	
Time (10^3 sec)	Weight Loss (mg)	Area (cm^2)	Depth of Decarburization (microns)	Weight Gain (mg)	Area (cm^2)	Bulk	Total*
180.0	0.44	2.407	18.0	0.51	14.783	21.0	21.0
579.9	0.65	2.039	39.0	0.80	14.763	29.0	29.0
1786.5	1.87	2.689	77.0	1.73	14.789	45.0	45.0

*Very slight grain boundary diffusion observed after 1786.5 x 10^3 sec.

Table 464-VII

Carbon Flux to Type 316L Stainless Steel from Fe-0.85C Source in Sodium

Time (10^3 sec)	Temp (°C)	Corrected* Carbon Content (%)	Total Carbon Transferred (mg)	Total Carbon Transferred (mg/cm^2)	Carbon Flux (10^{-9} g/cm^2-sec)
7.2	650	0.0345	1.63	0.11	15.31
22.2	650	0.0725	3.40	0.23	10.36
76.2	650	0.1025	4.80	0.33	4.29
163.8	650	0.1625	7.67	0.52	3.17
418.2	650	0.2825	13.23	0.89	2.14
7.2	550	0.0090	0.43	0.03	3.98
21.6	550	0.0155	0.73	0.05	2.28
86.4	550	0.0395	1.87	0.13	1.46
187.5	550	0.0735	3.47	0.23	1.25
417.6	550	0.1225	5.76	0.39	0.93

*Original carbon content in stainless steel 175 ppm.

A view of the surface of Type 316L stainless steel after more prolonged carburization is shown in Fig. 464-9. A film containing a higher carbon concentration was observed at the surface; this was probably a fine carbide dispersion. Immediately underneath, a carbide network was observed in the grain boundaries. The carbide precipitate was identified as a complex $Cr_{23}C_6$ type, containing molybdenum and iron in addition to chromium and carbon. This area overlaid regions in which bulk and grain boundary diffusion occurred.

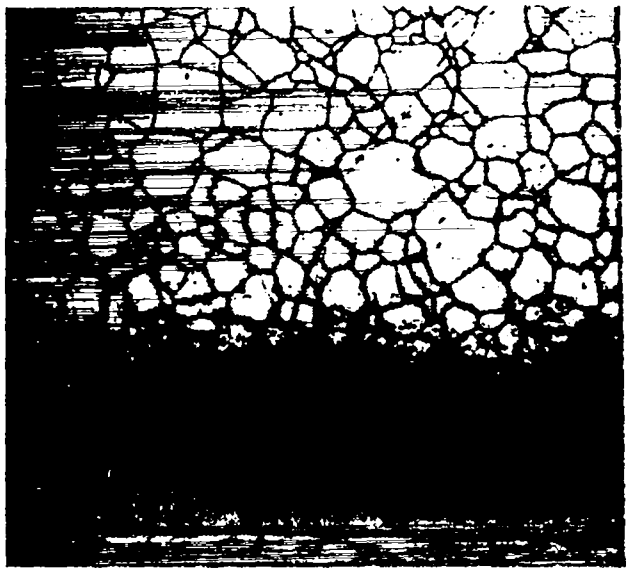

Fig. 464-9. Surface of Type 316L stainless steel carburized in sodium for 116 h at 650°C. Etched, 300X.

The transfer of carbon appears to occur in the following sequence of steps:

1. Diffusion of carbon from the interior of the source to the surface.
2. Transfer of carbon across the iron-sodium interface.
3. Diffusion and convection of carbon through sodium.
4. Transfer of carbon across the sodium-stainless steel interface.
5. Diffusion of carbon from the stainless steel surface to the interior.

Step (1) involves the simultaneous decomposition of cementite and diffusion of carbon in ferrite, and Step (5) involves the formation of a solution of carbon in austenite, followed by the precipitation of one or more carbides along the grain boundaries and in the austenitic matrix. Depending on the experimental conditions, any one of the above steps could be rate-controlling. Since extensive information exists on the rate of diffusion of carbon in ferrite, however, it was decided to examine the data in terms of a mechanism involving Step (1) as the rate-controlling step.

Jost[2] gives a rigorous equation treating the case where diffusion is accompanied by a phase change. Smith[3] used a simplified version of this equation to analyze his experimental data on the

rate of decarburization of iron-carbon alloys, as follows:

$$\frac{(C_i - 2/3C_b)(x^2)}{2(t)} = D(C_b - C_s)$$

where

C_i = the initial concentration of carbon (0.85 w/o) in the steel.

C_b = the solubility limit for carbon in ferrite, saturated with cementite

C_s = the concentration of carbon at the surface of the source.

x = the thickness of the ferrite layer, in cm.

t = the time at temperature, in sec.

D = the coefficient of diffusion, in cm^2/sec.

The results are expressed in Table 464-VIII in terms of x^2/t (which is related to the diffusion coefficient in the above expression) for all the experimental data except those in which graphitization of cementite occurred. The average values from our data are compared in the table to the smoothed data from Ref. 2.

If C_s is assumed to be negligible in comparison to the saturation of carbon in ferrite in quasi-equilibrium with cementite, the activation energy for the carbon transfer process may be calculated from the slope of the plot of $\log(x^2/tC_b)$ against the reciprocal of the absolute temperature. Such a plot is shown in Fig. 464-10, using the most recent set of values[3,4] for C_b and the average values of x^2/t from Table 464-VIII. The C_b values from Ref. 3 in Fig. 464-10 give an activation energy of -23 kcal/mole, while those from Ref. 2 give -19 kcal/mole. These calculated activation energies are close to those calculated with Smith's data[3] for the diffusion of carbon in ferrite, i.e., -22 and -24 kcal/mole for temperatures of 450 and 750°C, respectively. Homan[5] summarized data for the diffusion of carbon in ferrite and concluded that the activation energy of diffusion was temperature dependent. For the temperature range of 400 to 800°C, he calculated an activation energy of -24 kcal/mole.

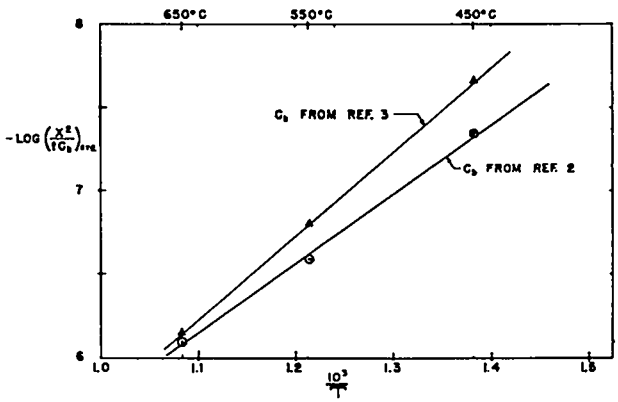

Fig. 464-10. Plot of $-\log(x^2/tC_b)$ against reciprocal of absolute temperature for the transfer of carbon in sodium from Fe-C alloy source to Type 316L stainless steel.

The data obtained in these experiments, expressed either as x^2/t, or as an activation energy, are in good agreement with data from the literature on the diffusion of carbon in ferrite. This strongly indicates that the rate of carburization of Type 316L stainless steel in sodium is controlled by the rate of diffusion of carbon in the source.

Table 464-VIII

Transfer of Carbon in Sodium from Fe-0.85C Alloy to Type 316L Stainless Steel

650°C		550°C		450°C	
Time (sec)	x^2/t (cm^2/sec)	Time (sec)	x^2/t (cm^2/sec)	Time (sec)	x^2/t (cm^2/sec)
7.2×10^3	6.8×10^{-9}	7.2×10^3	3.1×10^{-10}	180×10^3	1.8×10^{-11}
22.2×10^3	7.0×10^{-9}	21.6×10^3	6.0×10^{-10}	580×10^3	2.6×10^{-11}
76.2×10^3	8.8×10^{-9}	86.4×10^3	6.2×10^{-10}	1787×10^3	3.3×10^{-11}
		187.5×10^3	10.5×10^{-10}		
Av cm^2/sec (This work)	$= 7.5 \times 10^{-9}$	Av cm^2/sec (This work)	$= 6.3 \times 10^{-10}$	Av cm^2/sec (This work)	$= 2.6 \times 10^{-11}$
Av cm^2/sec (Ref. 2)	$= 1.0 \times 10^{-8}$	Av cm^2/sec (Ref. 2)	$= 6.3 \times 10^{-10}$	Av cm^2/sec (Ref. 2)	$= 1.6 \times 10^{-11}$

Transfer of Carbon from $UC_{1.04}$ to Type 316L Stainless Steel

Capsule tests were conducted to indicate the mechanism of carbon transfer from $UC_{1.04}$ (heat-treated, and also as-received) to Type 316L stainless steel. Further capsule tests are in process to determine the rate of transfer as a function of temperature. The structure of as-received, cast $UC_{1.04}$ consisted of UC_2 needles distributed in a UC matrix. When this material was heat-treated for ~ 100 h at 1350°C, the metastable UC_2 was partly converted to U_2C_3. The structure of heat-treated $UC_{1.04}$ consisted of U_2C_3 agglomerates in combination with a minor amount of UC_2 distributed in the UC matrix.

Each of the two types of $UC_{1.04}$ samples was crushed to granular form (-10 to +14 mesh) and encapsulated with sodium and a Type 316L stainless steel tab in a Type 316 stainless steel capsule. The capsules were then heated for 1000 h at 750°C. During the test, the as-received granular material (4.4 g) was depleted of the dicarbide phase, resulting in the transfer of 4.4×10^{-5} g/cm^2 of carbon to the stainless steel. This as-received material tended to disintegrate during test due to attack on the dicarbide phase. The metallographic structure is shown in Fig. 464-11. The heat-treated granular material (4.6 g) remained intact during the test and was depleted of the dicarbide phase only at the surfaces of the particles, resulting in the transfer of 1.8×10^{-5} g/cm^2 of carbon to the stainless steel. After test, the structure at the surface consisted of U_2C_3 distributed in the UC matrix. The cores of the particles were not depleted in the UC_2 phase in the heat-treated material. The surface structure is shown in Fig. 464-12.

Fig. 464-11. Structure of as-received $UC_{1.04}$ after heating in sodium for 1000 h at 750°C. Etched, 300X.

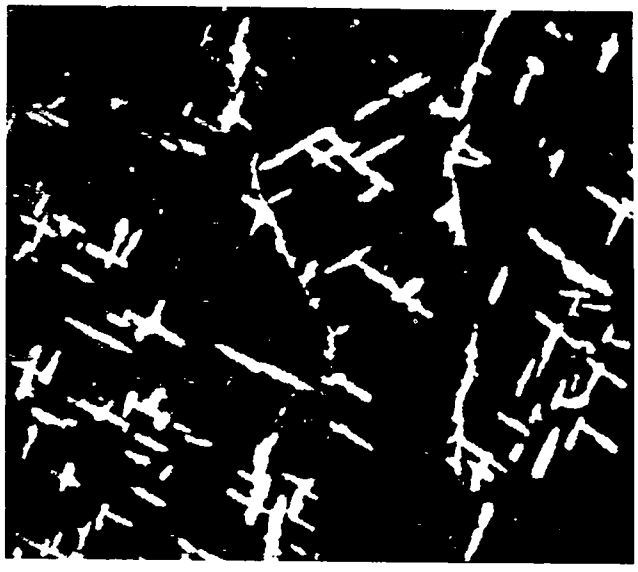

Fig. 464-12. Structure at the surface of heat-treated $UC_{1.04}$ after heating in sodium for 1000 h at 750°C in a Type 316 stainless steel capsule. The $UC_{1.04}$ granules remained intact. The structure consisted of U_2C_3 distributed in the UC matrix, depleted of the UC_2 phase. The UC_2 phase was present in the core of the granule. Etched, 300X.

These data indicate that the carbon transfer from $UC_{1.04}$ is diffusion-controlled and is dependent on the amount of the dicarbide phase and the integrity of the specimen. This experiment did not indicate whether carbon was transferred by sodium from the sesquicarbide phase in the absence of the dicarbide phase.

5. Thermodynamic Considerations

Stabilities of Metal Carbides

A literature search on the stabilities of metal carbides of interest to the carbide compatibility program has been completed. The data on fuel carbides are shown in Table 464-IX. Information from several sources were compared and evaluated,

Table 464-IX

Free Energy of Formation vs Temperature of Fuel Carbides

$-\Delta G_T^\circ$, kcal/mole Carbon

Temp (°C)	$(U_{0.8}Pu_{0.2})_2C_3$ [6]	UC [7]	$PuC_{0.87}$ [8]	U_2C_3 [7]	Pu_2C_3 [8]	$UC_{1.9}$ [7]
450	18.4	24.5	15.5	16.2	13.9	11.8
550	18.0	24.9	15.3	16.5	13.4	12.1
650	17.6	25.1	15.1	16.7	12.9	12.4
750	17.2	25.3	14.9	16.8	12.5	12.6

Table 464-X

Free Energy of Formation vs Temperature for Potential Clad Carbides

$-\Delta G_T^\circ$, kcal/mole Carbon

Temp (°C)	Fe_3C [10]	Ni_3C [9]	$Cr_{23}C_6$ [9]	Mo_2C [11]	Mn_3C [9]	VC [9]	TiC [9]	ZrC [9]	WC [9]
450	-2.1	-6.9	17.5	4.0	3.5	11.3	42.5	36.5	8.4
550	-1.3	-6.7	17.6	7.0	3.5	11.2	41.8	--	--
650	-0.7	-6.5	17.8	10.0	3.6	11.0	41.5	--	--
750	-0.2	-6.4	17.9	11.5	3.6	10.9	41.3	--	--

and it is thought that the cited values are the most accurate available. The standard free energies of formation of possible reaction product carbides from elements present in candidate clad materials are recorded in Table 464-X.

On the basis of the standard free energies of formation for the pure compounds, chromium and molybdenum carbides appear to be the most stable carbides that can be formed by the constituents of Type 316 stainless steel. Though a high strength vanadium alloy for LMFBR application has not been selected, its probable constituents would include iron, chromium, titanium, zirconium, and tungsten. In such an alloy, titanium, zirconium, and chromium carbides should form in preference to vanadium carbide.

Reaction of Fuel Carbides with Sodium Oxide

In conjunction with the program to determine the compatibility of various fuel carbides and cladding materials, calculations were made of the thermodynamic equilibrium constants for the reactions of fuel carbides with sodium oxide, and the subsequent transfer of one mole of carbon from the fuel to chromium in the cladding. The calculations were based on reported standard free-energy equations, which are applicable over the temperature range of interest. The results of the calculations indicate, in all cases, a strong thermodynamic potential for the carbide fuel to react with sodium oxide in solution in sodium, followed by the transfer of carbon to the cladding alloy. However, these calculations give no information about the kinetics of these reactions, or about their dependence on oxygen concentrations in sodium.

6. Behavior of Vanadium Alloys in Hot-Trapped Sodium

Vanadium alloys have been proposed as a backup cladding material for Type 316 stainless steel for the liquid-metal fast breeder reactor. The information being developed in this experimental work, which generally confirms data reported from other laboratories, indicates that care will be necessary in the selection of alloying elements in order to obtain an alloy that is stable for long periods of time while in contact with high purity sodium.

Free energy calculations were made to indicate the most suitable alloying elements for vanadium to form stable cladding alloys in sodium contaminated with oxygen. These calculations are summarized in Fig. 464-13.

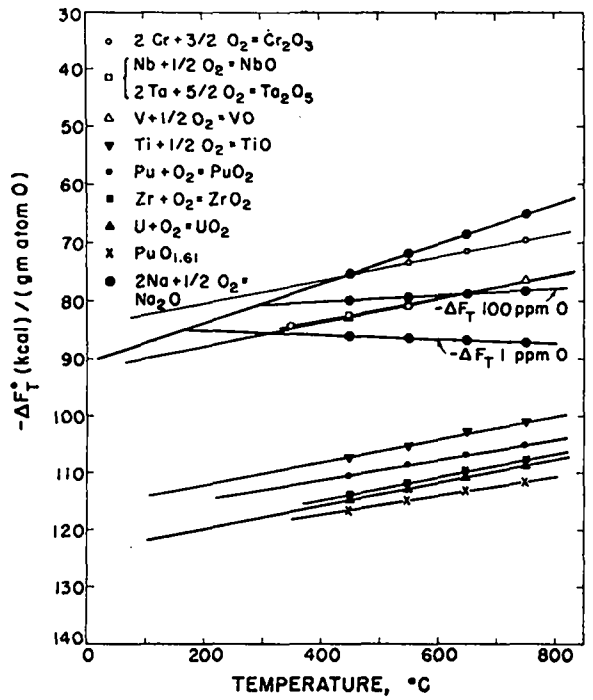

Fig. 464-13. Comparison of free energy of formation of Na, V, Cr, Nb, Ta, Ti, Zr, Pu, and U oxides as functions of temperature.

The oxygen contents of specimens of V, V-20Ti, V-15Ti-7.5Cr, and V-15Cr-5Ti, after corrosion tests in hot-trapped sodium from 500 to 4000 h, are shown in Fig. 464-14. During these tests the oxygen content of vanadium decreased, the oxygen content of

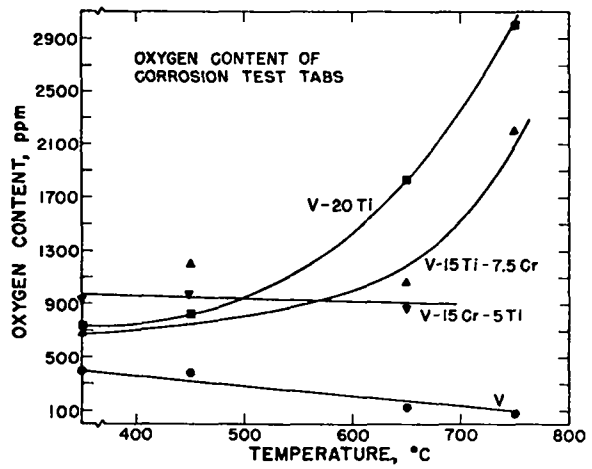

Fig. 464-14. Oxygen content of corrosion test tabs immersed in hot-trapped sodium from 500 to 4000 h.

V-15Cr-5Ti remained relatively constant, and V-20Ti and V-15Ti-7.5Cr picked up substantial amounts of oxygen from hot-trapped sodium. In general, the observations confirm the thermodynamic calculations shown in the preceding figure. As shown in Table 464-XI, all of the materials increased in carbon content during test, indicating that the pickup of carbon from sodium by these alloys may be their primary problem.

Table 464-XI

Carbon Content of Vanadium Alloy Materials Before and After Corrosion Tests at 450 and 550°C

Material	V	V-10Ti	V-20Ti	V-40Ti	V-15Ti-7.5Cr	V-15Cr-5Ti
Original content	420	203	197	171	233	253
Test Temp (°C)						
450	360	370	1800	370	930	850
550	455	365	1700	370	890	825

V. IRRADIATION TESTING IN EBR-II
(J. O. Barner)

A. General

The purpose of the EBR-II irradiations is to evaluate candidate fuel/sodium/clad fuel element systems for the LMFBR program. In the reference design, fuel pellets of single-phase (U,Pu)C are separated by a sodium bond from a cladding of Type 316 stainless steel. Three series of experiments are planned, and approval-in-principle has been received from the AEC.

The capsules (each of which holds a single fuel pin containing the carbide pellets) are to be irradiated under the following conditions:

	Condition	Series 1	Series 2	Series 3
1.	Lineal power, kW/ft	~ 30	~ 42	~ 30
2.	Fuel composition	$(U_{0.8}Pu_{0.2})C$, single-phase, sintered		
3.	Fuel uranium	^{235}U	^{233}U	^{235}U
4.	Fuel density	90%	95%	95%
5.	Smear density	80%	80%	80%
6.	Clad size	0.300-in. i.d. x 0.010-in. wall		
7.	Clad type	316 SS	316 SS	316 SS
8.	Max clad temp, °F	1250	1275	1250
9.	Max fuel centerline temp, °F	2130	2550	2100
10.	Burnup	3 a/o to 8 a/o		

During FY 1970, the EBR-II irradiation tests will be be reported under Project 467, "Fuel Ir-Radiation Experiments."

B. Results During FY 1969

A capsule from Series 1, designated LASL-42B, has operated in EBR-II to a maximum burnup of 1.4 a/o. The capsule was then nondestructively tested utilizing visual techniques, neutron and x-ray radiography, and gamma scanning. It was found that:

1. The outer Type 304 stainless steel and the inner Type 316 stainless steel clads appear to be intact.
2. There are no fuel chips present in the inner sodium fuel annulus that would appear to inhibit fuel expansion.
3. Twenty of the fifty-four fuel pellets were intact. Thirty-four were split, probably due to thermal stresses.
4. It could not be determined if there were any fuel chips in the spaces between split pellets that would inhibit fuel expansion.
5. Based upon the average axial linear expansion rate of the fuel and the assumption of isotropic expansion, the fuel would be restrained by the clad at about 18 a/o burnup. Based upon observed axial expansion in the center of the fuel stack of about 2 mils per pellet, the fuel would be restrained at about 10 a/o burnup.

The probable presence of sodium in the space between split pellets will lower the fuel temperatures, and fuel swelling should be reduced to a lower rate during the balance of the scheduled irradiation.

LASL-42B is at EBR-II awaiting reinsertion and irradiation to a total burnup of 4.5 a/o.

Six additional EBR-II fuel pins were loaded with sodium and fuel. These pins are suspected of having an abnormally high oxygen content in the sodium and cover gas due to an air leak into the loading box. They will be retained for possible testing at a later date.

A second capsule for the Series 1 tests, designated LASL-36C, has been loaded and is available for irradiation. Another pin (#21) is currently being bonded. Fuel for three more Series 1 experiments is available; these capsules will be loaded when the bonding procedure has been completely developed.

Fuel for the Series 3 experiments is being manufactured by Group CMB-11. Fuel manufacture for the Series 2 experiments may start during the first quarter of FY 1970.

VI. GAMMA SCANNING AND RELATED STUDIES
(D. M. Holm, W. M. Sanders, B. M. Moore, B. K. Barnes)

A. General

Gamma scanning is a nondestructive technique for obtaining information on the distribution of fission products and activation products in fuel elements. A new advanced semiconductor detector system has been constructed for this purpose. Computer codes are being developed and adapted to extend the utility of gamma scanning.

Information on the gamma-ray spectra of fission products from fast fission of plutonium is limited when compared to the data available on

uranium fission. To extend the basic data, a program for studying fission product gamma-ray spectra following the fast neutron-induced fission of plutonium is underway. An unshielded uranium metal critical assembly (Hydro)[12] serves as a source of neutrons for irradiating the plutonium.

B. Results During FY 1969

1. Semiconductor Detector System

The intrinsic full-energy peak efficiency for the 25-cm^3 Ge(Li) detector was measured, and corrections were applied for gamma-ray leakage through the sides of the lead collimators and for absorption in the rabbit and end station.

The first model of a conical gold collimator was fabricated. This collimator increases the counting rate of the detector 1000 times over that obtained with a cylindrical collimator, without any loss in spatial resolution on the sample.

One of the important problems in the maintenance of Ge(Li) gamma-ray spectrometers is keeping the detector at dry ice temperature or below. Since the vacuum is maintained in the Dewars by cryogenic pumping with a molecular sieve, even slight warming will cause the insulating vacuum to be lost. A loss of this vacuum causes a rapid and generally catastrophic warmup of the detector. Although it is sometimes possible to revive the detector, there is no guarantee that this can be accomplished. Tests were conducted to determine the usefulness of a vapor pressure thermometer as a disaster alarm on the Ge(Li) detector Dewars. In the temperature range of interest (75 to 85°K), the vapor pressure thermometer can be used to measure temperatures to a fraction of a degree without the problems of electromechanical devices.

A vapor pressure thermometer was constructed with liquid oxygen as the vapor source. The rapid change in pressure during vaporization of the oxygen introduces a signal that is easily detected.

2. Development of Techniques

Experiments were performed in support of some flux monitoring measurements to determine the ratio of ^{101}Rh to ^{102}Rh in a low activity sample. The low activity coupled with complex decay schemes of the isotopes presented new problems in counting. Various combinations of detectors and geometries were tested to determine the optimum conditions for counting. A hollow tantalum cylinder placed around the sample formed a collimator that shielded the large (13-1/2-in.-diam by 6-in.-long) NaI anti-coincidence detectors against direct radiation from the sample. This configuration, with a 25-cm^3 Ge(Li) detector, gave the best results.

3. Computer Code Development

Many of the fuel elements being examined have had a large number of spectra for detailed analysis. However, for well-behaved fuel elements, it is not necessary to perform a sophisticated analysis to determine whether gross mass transfer of fission products or activation products has occurred.

In order to minimize the time required for data analysis, a new code was written that simulates multiscaler analysis (from the spectral data recorded on magnetic tape). Energy windows are set by the computer instead of using a single-channel pulse height analyzer. Since isotopic effects are being studied, only the counts in certain peaks are of real interest. Therefore, the operator selects the peaks of interest and specifies the channels occupied by these peaks. A working magnetic tape is written by the IBM 7094 in which only the channels with peaks of interest are listed. The new code enables the operator to integrate the counts in the peaks and to plot their area (including background) as a function of position.

This code is not as accurate as multispectral analysis by unfolding complex spectra, but it is faster, and can therefore be used to determine when more complex analysis is needed.

Codes were developed for plotting gamma-scanning data in two dimensions. Contour plots, isometric maps, and density plots have been obtained. The results are shown in Figs. 464-15, -16 and -17 for ^{106}Rh in a fuel element section from Battelle Northwest Laboratory. The plots made by the computer were slightly modified in these figures. Figures 464-18 and -19 show a photomacrograph, a beta-gamma autoradiograph, and linear gamma scans across the sample for comparison.

The data were taken in the form of 4096-channel gamma-ray spectra at 0.020-in. intervals across the face of the sample. A conical collimator with a 0.030-in.-diam entrance hole was used. A

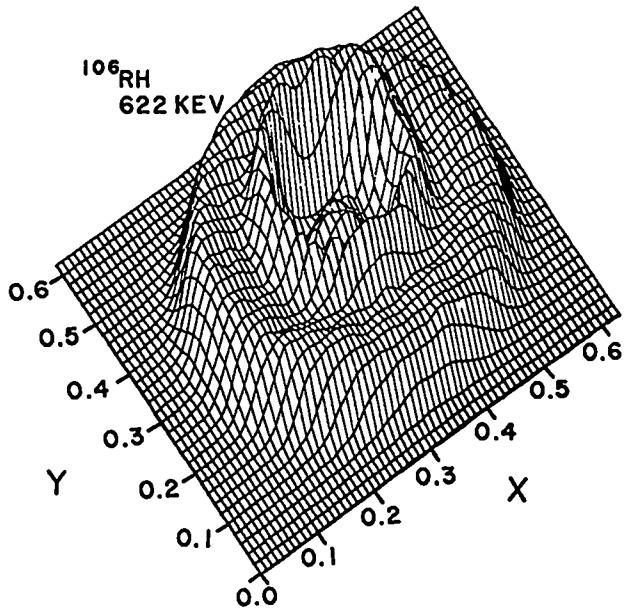

Fig. 464-15. Isometric projection of ^{106}Rh distribution in Battelle fuel element section.

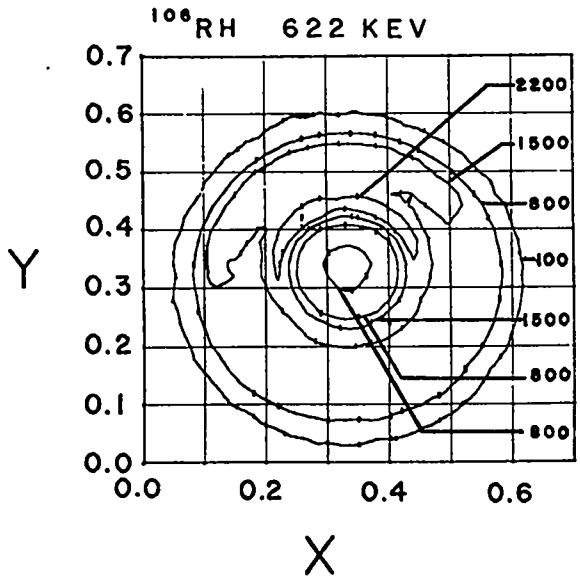

Fig. 464-16. Contour map of ^{106}Rh distribution in Battelle fuel element section.

32 x 32 square matrix (1024 spectra) covered the face of the sample. The spectra were analyzed for the intensity of several isotopes by adding the channels over the gamma-ray peaks to be studied. The intensities were then interpolated with spline functions to obtain smoothed plots.

A technique has been developed for using interpolatory cubic splines and simple smoothing to

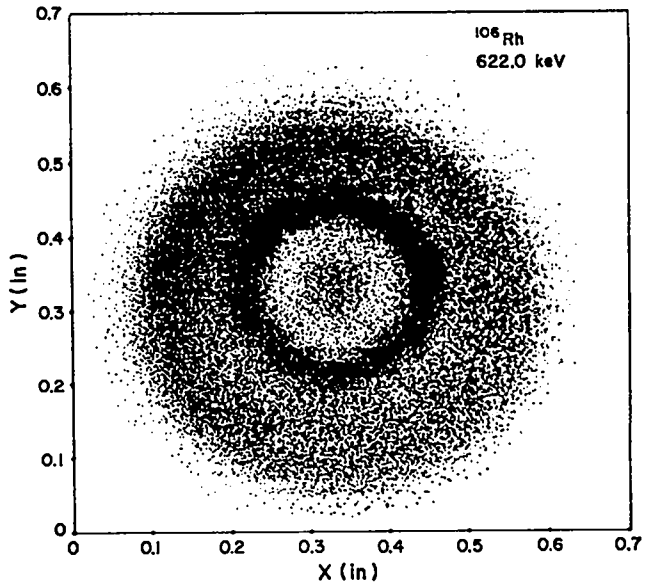

Fig. 464-17. Density plot of ^{106}Rh distribution in Battelle fuel element section.

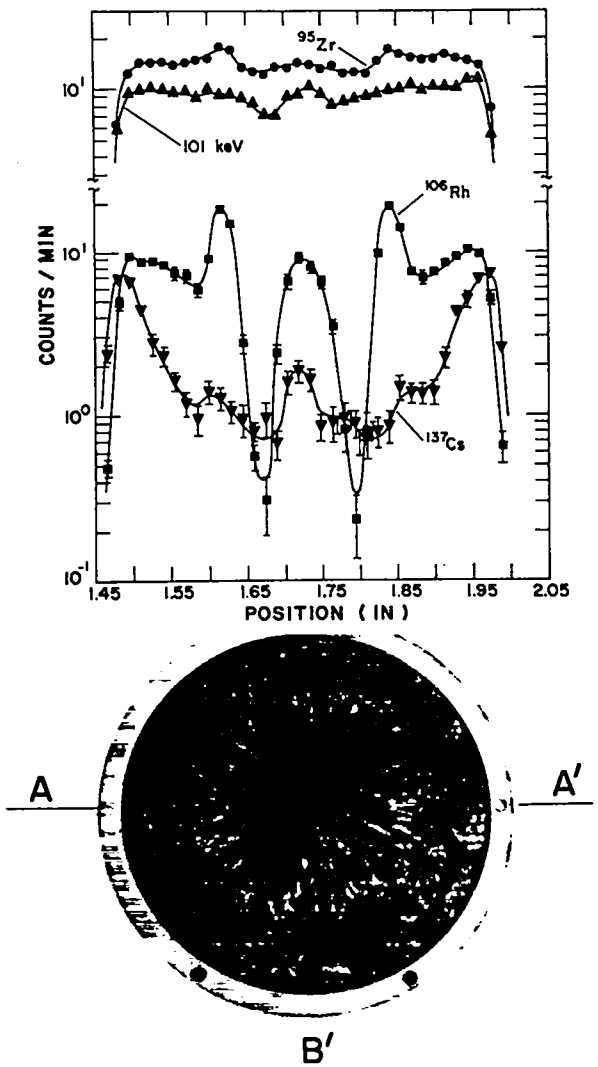

Fig. 464-18. Photomacrograph and linear gamma scan of Battelle fuel element.

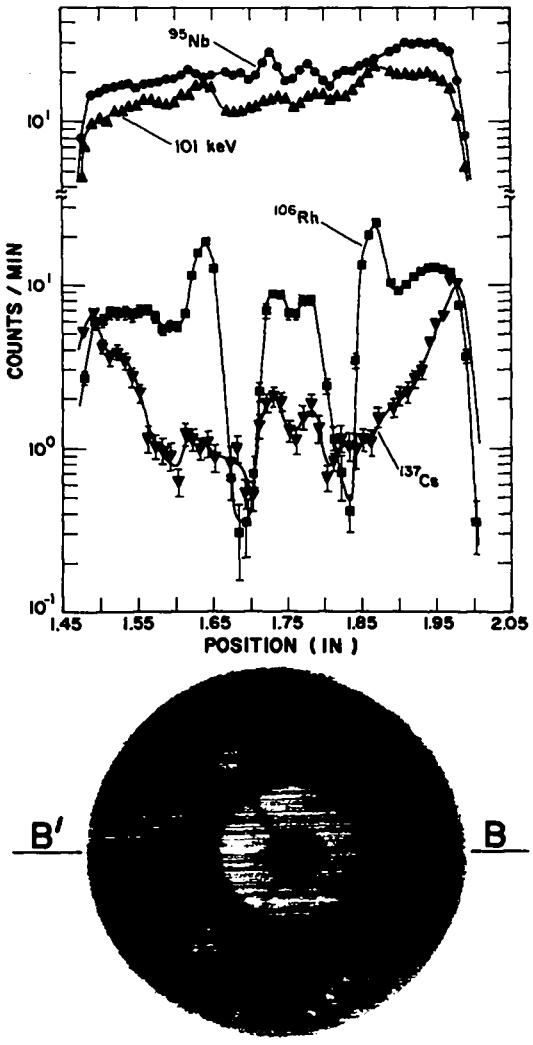

Fig. 464-19. Beta-gamma autoradiograph and linear gamma scan of Battelle fuel element section.

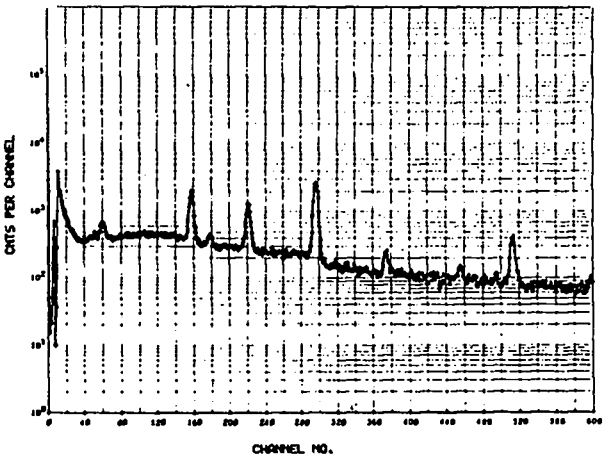

Fig. 464-20. Simple spectrum analyzed in Table 464-XII.

determine analytically the location of full-energy peaks in a complex gamma-ray spectrum. The results of analyzing a simple spectrum (Fig. 464-20) using the code are shown in Table 464-XII. A plot of raw data with its corresponding smoothed curve is shown in Fig. 464-21.

Smoothing the data prior to analysis seems to be the largest problem. Depending on the number of counts in a given channel, the data may or may not be smoothed by simple techniques before smoothing with an interpolatory cubic spline.

Table 464-XII

Analysis of a Simple Spectrum

	Channel (No.)	Energy (keV)	d^2y/dx^2	$d^2y/dx^2/y$	Y
Baby peak	41	68.852	-20.55	-0.042967	385
Baby peak	47	73.074	-21.56	-0.041910	419
Baby peak	60	82.222	-64.10	-0.079919	691
Baby peak	69	88.555	-22.12	-0.043071	421
Baby peak	114	120.222	-35.96	-0.063484	477
Baby peak	145	142.037	-20.13	-0.039647	426
Medium peak	158	151.185	-353.15	-0.166973	2013
Baby peak	167	157.518	-19.37	-0.046286	344
Baby peak	172	161.036	-21.71	-0.051761	345
Baby peak	178	165.259	-24.17	-0.046887	438
Baby peak	195	177.221	-15.17	-0.039081	318
Baby peak	208	186.370	-18.69	-0.051091	298
Medium peak	221	195.518	-228.81	-0.161896	1338
Baby peak	240	208.888	-9.46	-0.029333	259
Medium peak	297	248.999	-529.49	-0.193622	2693
Baby peak	374	303.184	-15.40	-0.056515	221
Baby peak	376	304.591	-15.29	-0.057305	215
Baby peak	456	360.887	-7.52	-0.040246	140
Baby peak	496	389.035	-5.60	-0.038535	100
Medium peak	513	400.998	-59.06	-0.130511	418
Baby peak	598	460.813	-4.81	-0.036070	91

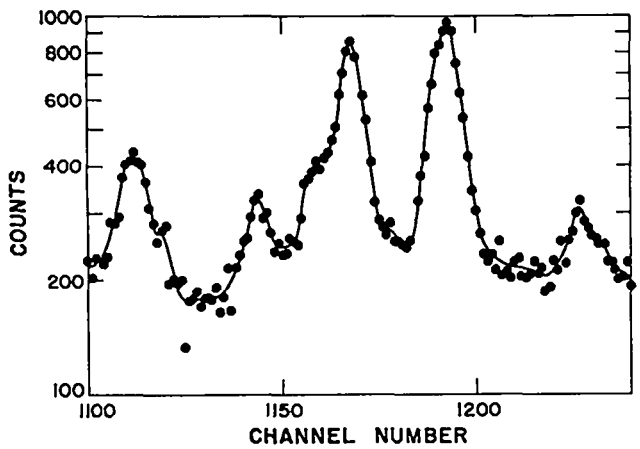

Fig. 464-21. Raw data and corresponding smoothed curve. The points are the raw data; the line is the smoothed curve.

4. Gamma-Ray Spectra of Short-Lived Fission Products from Fast Fission of Plutonium

All equipment was installed and the experimental data have been acquired for determining the short-lived delayed gamma emission from fast fission of plutonium. There remains now to reduce and analyze the data to determine half-lives and energies for the individual photo peaks. ^{235}U was also studied under similar conditions to be compared with plutonium.

VII. SODIUM-BOND HEAT TRANSFER STUDIES
(K. L. Meier, J. O. Barner)

A. General

The purpose of this project is to evaluate methods for determining the effects of fuel-pin defects on heat transfer properties of the sodium bond. Such defects could arise in a number of ways. For example, a void in the sodium bond could: (1) be present before insertion in the reactor, (2) come from dewetting of the pellet due to change in composition as fission products are formed, (3) form from a hot spot on the pellet and consequent local vaporization of the sodium, and/or (4) be produced from desorbed or fission-product gases. Of these, probably the most serious defect would be the presence of fission gas bubbles in the bond region.

There appear to be three methods of obtaining the high heat fluxes necessary for "defect analysis": (1) in-pile experiments, (2) out-of-pile experiments utilizing a central, high heat flux heater, (3) out-of-pile experiments utilizing an induction heat source with the heat flow direction reversed. These three methods are all receiving consideration for use in sodium-bond heat transfer studies.

B. Results During FY 1969

Design, construction, and testing of portions of the apparatus for out-of-pile testing of sodium bonds utilizing a central, high heat flux heater are underway. A graphite rod heater with boron nitride insulation was fabricated. It was placed in an existing sodium loop and tested at a heat flux of 1.5×10^6 Btu/h-ft^2 at the cladding surface. A cylinder of UC (5-in.-long with 0.030-in.-thick walls) which fits over this heater and serves as the fuel mockup was eloxed from a hot-pressed billet. Further testing will be done when the UC cylinder, sodium bond, and cladding tube are placed around the heater. This will be a more stringent test because heater temperatures will increase about 400°C.

An apparatus to inject inert gas bubbles into the sodium bond was designed and fabricated. A mockup was built to test and calibrate the bubble apparatus and to determine how to make the sodium bond. The mockup contained the heater, UC cylinder, bubble injection apparatus, and a glass tube instead of the stainless steel cladding. Tests showed that the sodium bond annulus can be filled with clean sodium at about 120°C if all parts are cleaned, the annulus is evacuated, and atmospheric pressure helium is applied to force the sodium into the voids. Tests on the mockup showed that bubbles of preselected size could be injected into the sodium bond annulus.

Cladding temperatures during test will be measured with 40 thermocouples held in a fixture which can be rotated about the "fuel pin" so temperatures can be measured in 0.100-in. intervals horizontally and vertically on the cladding. This "thermal scanner" has been designed, and all necessary hardware for its fabrication is on hand. The thermal scanner is housed in an outer structure that contains seals to prevent sodium leakage around the thermocouple rotor. This outer structure has been designed and fabrication has begun.

A transition section, which will be mounted at the top of the heater, will be used to contain

the sodium and accommodate thermal expansion. It contains bellows and expansion joints for the heater rod, heat sheath, and the cladding. This transition section has been designed and fabricated.

VIII. ANALYTICAL CHEMISTRY

A. General

Specific analytical techniques have been developed and evaluated to cope with the problems encountered in the investigation of fuel/clad compatibility. The results of many of these special analyses are given in several sections of the report in Project 464. A brief summary of some of the techniques, and the problems to which they were applied, is given below.

B. Results During FY 1969

1. Electron Microprobe Examination (E. A. Hakkila, H. L. Barker)

The electron microprobe was used to examine samples of fuel capsule container materials, (U,Pu)C samples, U-Fe diffusion couples, and UC samples. The fuel capsule container materials included stainless steels, V, V-base alloys, and Nb-10W alloy. The results of these examinations are summarized very briefly below.

Stainless Steels

Along the inner walls of Type 316 stainless steel capsules that had been sodium-bonded to (U,Pu)C, variations in C, Cr, Fe, Ni, and Mo concentrations were found. Diffusion of carbon into the stainless steel occurred at darkened areas of the walls of each sample. Significant variations in Cr, Fe, Ni, and Mo x-ray intensity as a function of proximity to the sample surface were observed in only one of the samples.

The following reaction products were identified in four samples of Type 316 stainless steel that had been exposed to (U,Pu)C and molten sodium: (1) a white phase on the inner surface that contained more Fe, Ni, and C, but less Mo and Cr than the matrix, (2) a brown phase containing less Fe, Cr, Ni, and Mo, but more C than the matrix, and (3) narrow bands containing more Mo and C, but less Fe, Cr, and Ni than the matrix. Diffusion of C to depths as great as 150 microns into the stainless steel had occurred.

A carburized specimen of stainless steel had a higher carbon content at the surface than in the interior. Two phases were identified as: (1) Cr-Mo-C, which appeared as stringers, and (2) a Cr-rich phase that contained less Mo than the surrounding areas.

Diffusion of carbon to a depth of 250 microns was observed in one sample of "as-received" Type 316 stainless steel, but not in another.

V and V-Base Alloys

The surface of a sample of vanadium metal contained chromium and nickel. The nickel had diffused into the vanadium to a depth of approximately 20 microns.

Two reaction layers were identified at the surface of a V-20Ti alloy: (1) a V-Cr-C layer approximately 10 microns thick, and (2) a V-Ti layer approximately 25 microns thick that contained more titanium and less vanadium than the matrix.

Precipitates containing titanium and carbon were observed near the surfaces of two V-40Ti alloys. Significant amounts of chromium from an unknown source had diffused into each alloy.

At the surface of a V-Ti-Cr alloy was a gray layer that contained more V, Cr, and C, but less Ti than the matrix. A white outer layer contained more Ti and C, but less V and Cr than the gray phase.

Nb-W Alloy

A Nb-W alloy contained significant amounts of carbon distributed throughout the matrix. Evidence for reaction of the alloy with its environment was not found.

(U,Pu)C

Impurity phases identified in several (U,Pu)C samples that had been tested in sodium-bonded stainless steel capsules included: (1) precipitates that contained more Pu and less U than the matrix, and were contaminated with Fe, W, and Si, (2) tungsten precipitates, and (3) precipitates containing more uranium and less plutonium than the matrix. The plutonium contents at the surfaces of four of the samples were greater, and the uranium contents less than in the interiors of the samples. Grain boundary precipitates contained predominantly Si, W, and Pu. One (U,Pu)C sample which had been tested in a sodium-bonded V-Ti-Cr capsule contained a V-Ti-Pu

precipitate at the surface. Grain boundary precipitates were essentially free of carbon and contained more plutonium and less uranium than the matrix.

U-Fe Diffusion Couple

Measurements of the variations in uranium and iron concentrations across the diffusion interface of a U-Fe diffusion couple showed that iron had diffused into the uranium to a depth of approximately 550 microns along grain boundaries, but that uranium had not diffused into the iron.

UC

Differences in the x-ray intensities for either uranium or carbon from various grains in the matrix were smaller than the standard deviation for repeated measurements at one location. These data indicate that there was a uniform distribution of uranium and carbon in the matrix.

2. Miscellaneous Analytical Support
(H. M. Burnett, C. B. Collier, D. C. Croley, R. G. Hurley, N. L. Koski, J. A. Mariner, C. J. Martell, J. F. Murphy, W. M. Myers, R. T. Phelps, O. R. Simi, L. E. Thorn, G. R. Waterbury, W. W. Wilson)

The semiquantitative spectrochemical method used to analyze sodium for impurity elements was tested in a hot cell facility. Two portions of a sodium sample were converted to NaCl by remote manipulation. The mechanics of handling the samples in the hot cells were satisfactory, but the NaCl was contaminated with impurities. Higher concentrations of Mg, Al, Si, Ti, Cr, Mn, Fe, Ni, Cu, and Mo were observed in the NaCl prepared in the hot cell (which has been assigned for solution processing) than were found in NaCl prepared outside the cell from the same lot of sodium. This cell is also used to dissolve samples which require prolonged heating with acids. As a result, the apparatus and parts of the cell become corroded, and the efforts made to clean the cell before analyzing the sodium were apparently not adequate. Further analysis awaits the completion of other work being done in the cell.

The limits of detection for impurity elements in sodium determined in the hot cells are listed in Table 464-XIII.

Table 464-XIII

Limits of Detection for Impurity Elements in Sodium

Element	Limit of Detection (ppm)	Element	Limit of Detection (ppm)
Li	0.8	Co	3
Be	0.8	Ni	3
B	30	Cu	0.8
Mg	0.8	Zn	300
Al	3	Sr	3
Si	3	Mo	3
K	3	Ag	0.8
Ca	3	Cd	30
Ti	3	Sn	3
V	0.8	Cs	30
Cr	0.8	Ba	3
Mn	0.8	Pb	3
Fe	3	Bi	8

The following materials were analyzed by quantitative, semiquantitative, and qualitative spectrochemical methods to determine trace impurities: Na, $(U_{0.8}Pu_{0.2})C$, Pu, PuO_2, U, stainless steels, carbon steels, V alloys, Nb-W alloys, and Nb-Zr alloys.

Controlled-potential coulometric and combustion-gravimetric methods were used without difficulties in measuring U, Pu, and C in pre-test (U,Pu)C samples and (U,Pu)C pellets. The coulometric methods for measuring have a relative standard deviation of 0.2 to 0.3 per cent, and the combustion-gravimetric method for determining carbon has a precision of (1 σ) of 0.5 relative per cent.

Spectrophotometric methods were satisfactory in measuring: (1) N in (U,Pu)C pellets, Pu metal, and pre-test (U,Pu)C samples; (2) Ta in pre-test (U,Pu)C samples and Pu metal; and (3) W in Pu metal and (U,Pu)C. The standard deviations are 2 to 3 relative per cent in measuring N and W in the ppm concentration range, and 5 relative per cent for determining the low ppm concentrations of Ta found.

An inert-gas-fusion/manometric method, having a precision (1 σ) of 10 relative per cent, was applied without difficulty in measuring O in specimens of Zr metal, V-base alloys, Nb-base alloys, (U,Pu)C, UC, U metal, Th metal, Pu metal, and stainless steels.

A combustion-manometric method was used to determine carbon in plutonium metal. The relative

standard deviation of the method in measuring low concentrations of carbon is 10 per cent.

Two sodium samples that had contacted $(U,Pu)O_2$ powder were analyzed spectrophotometrically for uranium. The precision (1 σ) of the method is 3 relative per cent.

A potentiometric titration method, having a precision (1 σ) of 0.05 per cent, was used to assay a plutonium metal to be used in the preparation of mixed carbides.

X-ray fluorescence spectrometry was very satisfactory in rapidly identifying a suspect alloy as V-Ti.

IX. REFERENCES

1. "Quarterly Status Report on the Advanced Plutonium Fuels Program, April 1 to June 30, 1968 and Second Annual Report, FY 1968," LA-3993-MS, Los Alamos Scientific Laboratory (1968).

2. W. Jost, "Diffusion in Solids, Liquid, Gases," Academic Press, p. 71 (1960).

3. R. P. Smith, "The Diffusivity and Solubility of Carbon in Alpha-Iron," Trans. Met. Soc. AIME, Vol. 224, p. 105 (1962).

4. J. C. Swartz, "The Solubility of Graphite and Cementite in (Alpha, Delta) Iron," Trans. Met. Soc. AIME, Vol. 245, p. 1083 (1969).

5. G. G. Homan, "Diffusion of Carbon in Alpha-Iron," Acta Met., Vol. 12, p. 1079 (1964).

6. G. M. Campbell, private communication.

7. E. K. Storms, "Uranium-Carbon Systems," Report to the IAEA Panel on Thermodynamics of Uranium and Plutonium Carbides, Vienna, Sept. 1968.

8. G. M. Campbell, L. J. Mullins, and J. A. Leary, "Thermodynamics of Plutonium Compounds by EMF Techniques" in Thermodynamics of Nuclear Materials, 1967, IAEA, Vienna, 1968.

9. F. D. Richardson, "The Thermodynamics of Metallurgical Carbides and of Carbon in Iron," J. Iron and Steel Inst., Sept. 1953.

10. R. A. Robie and D. R. Waldbaum, "Thermodynamic Properties of Minerals and Related Substances," U. S. Geological Survey Bull. 1259 (1968).

11. E. K. Storms, The Refractory Carbides, Academic Press, New York and London, 1967.

12. W. Bernard, "Hydro - A Small, Water-Cooled, and Water-Reflected Neutron Source," Report LA-3374, Los Alamos Scientific Laboratory, March 14, 1966.

PROJECT 465

REACTOR PHYSICS

Person in Charge: D. B. Hall
Principal Investigator: G. H. Best

I. INTRODUCTION

Basic to the evaluation of various fast breeder concepts and proposals are the analytical techniques and physical data used in the analyses. Valid comparisons between different concepts and proposals depend on minimization of differences in results due to the methods of analysis. To this end, the Los Alamos Scientific Laboratory is cooperating with other AEC laboratories and contractors in the development of evaluated cross section data and associated processing codes. In addition, the Laboratory is working on the development and maintenance of digital computer programs pertinent to the nuclear analysis of fast breeder concepts. Finally, the Laboratory is evaluating the performance characteristics of various fast breeder reactor concepts.

II. CROSS-SECTION PROCUREMENT, EVALUATION, AND TESTING (M. E. Battat, R. J. LaBauve, A. C. Niethammer, R. E. Seamon)

A. General

Accurate predictions of reactor design parameters, such as critical mass, sodium worth, and spectral response, require the development and maintenance of up-to-date basic microscopic nuclear data files. To meet this need, a national cooperative program is in progress to prepare an evaluated nuclear data file (ENDF/B). The large amount of experimental data which is becoming available, together with the theoretical data, makes the maintenance of ENDF/B a continuing task. In addition, a large effort is needed in evaluating and testing the microscopic data prior to use in reactor calculations.

B. Data Testing

In June 1968, the Data Testing Subcommittee of the Cross Section Evaluation Working Group (CSEWG) proposed two fast reactor benchmark problems (ZPR-3 Assemblies 48 and 11) for calculation by members of the subcommittee. At LASL, multigroup constants for these problems were generated by the ETOE and MC^2 codes using the ENDF/B data tapes received in July 1968 from BNL. Calculations to determine k_{eff} and neutron fluxes (real and adjoint) were performed with both the MACH1 (diffusion)[1] and DTF-IV (transport)[2] codes. Central reactivity worths and perturbation cross sections were also computed. Results were transmitted to the Data Testing Subcommittee for comparison with results from other installations.

In view of some current uncertainties about the present ENDF/B evaluations for ^{235}U, ^{239}Pu, and ^{238}U, the Data Testing Subcommittee of the CSEWG recently specified eight additional benchmark problems to test these data over a broader range of neutron energies.[3] For these problems, the use of a consistent P_1 fundamental mode calculation (IOPT = 3 in MC^2) was recommended; heretofore, only the P_1 fundamental mode option (IOPT = 1) had been used in the version of MC^2 employed at LASL; therefore, this part of the code was debugged and made operational. Furthermore, because various laboratories use slightly different versions of the MC^2 code, it was decided to investigate results obtained using three versions of this code which were available to us. These investigations are summarized in Sec. II.C.1 of this report. Data testing for the new benchmark problems will be initiated after an evaluation of the different versions of the MC^2 code is made.

Transport calculations, using ENDF/B data, for three unreflected fast critical assemblies were made and compared with similar calculations performed at LRL using Monte Carlo methods and their evaluated library.[4] The systems calculated were the plutonium (JEZEBEL), oralloy (GODIVA), and ^{233}U assemblies. These calculations differ from those reported previously in that the isotopic contents of oralloy and plutonium were carefully reconstructed by LRL. Because the ENDF/B library did not contain gallium data (required for JEZEBEL), calculations using LRL data[5] were made to obtain the effect of gallium addition on criticality. Also, the theta value for the ^{233}U fission spectrum quoted in ENDF/B was changed from 1.965 MeV--a value which is definitely high--to 1.306 MeV.[6] The k_{eff} values obtained by LRL for the JEZEBEL, GODIVA, and ^{233}U assemblies were 1.003, 1.005, and 1.002, respectively; the corresponding values using the ENDF/B data were 1.0072, 1.0128, and 1.0051.

The preparation of gallium for the ENDF/B file is in progress. The main source of data for this material has been the Howerton evaluation.[5]

The ETOE code has been used to prepare a new MC^2 data tape from ENDF/B. Altogether, 63 materials are now on the MC^2 tape.

An error in the zirconium ENDF/B data was discovered in file 2. Very large elastic scattering cross sections, on the order of 10^7 b, were being computed. The error was in the value of C, a quantity used in calculating the penetration factor in the resolved resonance region. The value of C received from the ENDF/B data was <u>one</u>, but a calculation using the formula

$$Kr_c = \frac{r_c}{\hbar}\sqrt{2M}\sqrt{E} = C\sqrt{E} \qquad (465\text{-}1)$$

where

$$C = \frac{r_c}{\hbar}\sqrt{2M}$$

K = neutron wave number in CM system

M = 1.6474×10^{-24} g,

r_c = 7.136×10^{-13} cm (the neutron channel radius), and

h = 1.05444×10^{-27} erg-sec

gives a value of C for zirconium equal to 1.57×10^{-3} $(eV)^{\frac{1}{2}}$. Another calculation using the equations in ETOE gives a value of 1.5506×10^{-3} $(eV)^{\frac{1}{2}}$ for C. The ENDF/B data have been corrected, and the cross-section values recomputed.

C. Processing Codes

1. MC^2. The Multigroup Constants Code[7] is an important link in the process which translates ENDF/B microscopic data into multigroup cross-section sets. At present, there exist at LASL three versions of this code:

a. BNLMC2--a version obtained from BNL. This version bears the closest resemblance to the original formulation of the code as described in Ref. 7.

b. WAPMC2--a version obtained from R. Dannels, of Westinghouse, which contains several modifications to the original code.

c. BAWMC2--a version obtained from A. Livolsi of Babcock and Wilcox. This version contains extensive changes (which were made at Rensselaer Polytechnic Institute) to optimize the running time; specifically, the changes are concerned with reducing the peripheral processor time for a problem.

At LASL, we have used the WAPMC2 code for the ENDF/B benchmark problems and reactor design studies. Results obtained appear reasonable and compare favorably with reference calculations at other laboratories using the ENDF/B data. However, in order to understand the differences between the three versions of MC^2, a comparison of calculations made with these versions has been undertaken. For the initial comparisons, a system containing ^{239}Pu and ^{12}C was chosen, and P_1 fundamental mode calculations (IOPT = 1) were made for both the all-fine- and ultrafine-group options. In the comparison between WAPMC2 and BNLMC2, the BNL version, as received, did not yield correct cross sections because of coding and systems difficulties; these have been corrected and agreement between the two versions has been achieved. At the same time, a minor discrepancy was discovered in WAPMC2 and corrected. Several changes were also required in BAWMC2 to remove coding and systems problems. Hence, for the test problem specified, and for the P_1 fundamental mode calculation (IOPT = 1), the three versions of MC^2 yield cross-section sets which agree and appear to be correct. Work is in progress to check out the other options--consistent P_1 and B_1 for both isotropic and anisotropic neutronics--in the different versions. Preliminary

tests indicate that much debugging will be necessary before these options can be used with confidence.

To compare running times, a test problem (35 broad groups, 2 materials, ultrafine-group option, IOPT = 1) was run with both the WAPMC2 and BAWMC2 codes. For WAPMC2, the central processor and peripheral processor execution times were 180 and 1800 sec, respectively; the corresponding figures for BAWMC2 were 160 and 600 sec, which represents a significant reduction in peripheral processor time.

2. SINTAB. A code has been written for generating multigroup cross sections from the ENDF/B thermal data. In the first version of this code, SINTAB, only single table cross sections are generated, using a transport correction for an anisotropic approximation. SINTAB consists mainly of the codes FLANGE2, used for the generation of the inelastic kernel, and THERM2, used for collapsing the thermal cross sections to a broad-group structure, in an overlay arrangement. Cross sections for nonscattering isotopes needed for input to THERM2 are obtained from MC^2, as are all nonthermal cross sections for all materials. A schematic representation of SINTAB is shown in Fig. 465-1.

3. FLANGE2. ENDF/B thermal inelastic data (file 7) for graphite as processed by the FLANGE2 code was compared with that from the TOR[8] and SUMMIT[9] codes at temperatures of 296 and 500°K.

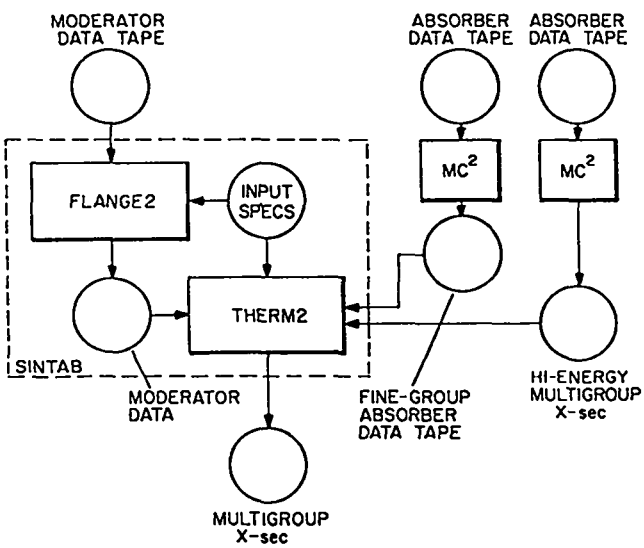

Fig. 465-1. Schematic representation of SINTAB.

Thermal spectra were generated for each case. At 296°K, the curve for the ENDF/B-FLANGE2 spectrum lies between the curves for the TOR and SUMMIT spectra, the maximum difference between the spectra amounting to 1.3% at 0.04 eV. At 500°K, the SUMMIT curve lies below the other two by less than 1.0% at 0.05 eV. These values indicate that insofar as the graphite data is concerned, there is little difference in the results obtained with the three codes.

4. GLEN. The GLEN code,[10] originally written as a thermal-group collapsing code, has been modified to accept the output of FLANGE2, a thermal code used for processing ENDF/B moderator data. Also, MC^2 has been modified to supply the absorber data needed by GLEN. Thus, in principle, codes are now linked so that multigroup cross sections can be obtained from ENDF/B data for energies from thermal (about 0.001 eV) to 10 MeV. Thermal data in the ENDF/B format are presently available for H_2O, D_2O, beryllium, graphite, polyethylene, and ZrH.

D. Shielding

1. Translation Codes. The translations of Drake's evaluations of sodium and calcium data[11] from the UK to ENDF/B format using the codes LUTE and LATEX have been revised to account for photon production at neutron energies above those for which level de-excitation schemes are well known. The data which account for this additional photon production are entered in the ENDF/B file with reaction type number MT = 110. A unit cross section has been placed in file 3 (MF = 3) and photon production cross sections, instead of photon yields, have been placed in file 15. This arrangement, with the exception of using MT = 110, fits within the present ENDF/B system without compromising any of the data.

2. Los Alamos Photon Production Code (LAPH). In order to allow for the storage and convenient subsequent retrieval of data needed for shielding calculations, the ENDF/B format was extended to include photon production and photon interaction data. A format to store such data was devised[12] and approved for incorporation into the ENDF/B system. For the photon production data, files were

provided for photon angular distributions, photon production multiplicities, and photon energy-angle distributions. Photon multiplicities are given either as (1) normalized photon energy distributions and associated total photon yields for those photons not identifiable with a level structure, or (2) transition probabilities and associated photon yields for those photons from de-excitation of known levels.

To retrieve the photon production data, a multigroup photon production code, LAPH, has been written.[13] The LAPH code retrieves photon production data from the ENDF/B data file and calculates a G x N photon production matrix for N specified neutron energy groups and G photon energy groups. In addition to the ENDF/B data, neutron fine-group weighting fluxes, as well as fine-group capture and fission cross sections, must be supplied as input to the LAPH code. At LASL, these quantities are obtained from the Multigroup Constants Code, MC^2.

As presently written, the LAPH code will not use transition probability data for incident neutron energies above the highest energy level in such an array. Photon production at these higher energies is treated as a special reaction type (MT = 110).

The LAPH code has been developed to the point that gamma-ray production matrices can be calculated using all three types of data either separately or combined. For the integrals which are carried out over arbitrary neutron and photon energy groups, different weighting options are available. The code requires 150000_8 locations of core storage; central processing times required are usually less than 1 min. In the next phase of development, the photon energy production matrices will be combined with flux vectors from a neutronics code to give photon source vectors for use with photon transport codes.

For each material, the LAPH code uses files 3 and 15 on the ENDF/B tape. These files contain only about 1% of the total data stored for each material, and large amounts of peripheral processor time were being spent in reading past the other data. A code, ETOL (ENDF/B to LAPH), was written to prepare a library tape containing only files 3 and 15 for each material. The peripheral processor time required by LAPH using the abbreviated library tape was reduced by more than a factor of 10.

3. Biological Dose Studies. Studies of the fast neutron biological dose attenuation by metal shields succeeded by thin hydrogenous shields were completed. After the work reported[14] at the ANS 1968 Annual Meeting, a study was made of the effect of finite polyethylene shields. That is, the backscatter contribution in an effectively infinite thickness of polyethylene, as used in previous calculations, was removed. As would intuitively be expected, the backscatter contribution is significant (up to 16%), but its fractional contribution to the biological dose is essentially the same for all lead thicknesses. Thus, the effect on the removal cross section of the lead is minimal; a maximum change of 0.3% was found in the removal cross sections of lead followed by 9 cm of polyethylene.

E. ^{239}Pu Alpha in the 100 eV to 10 keV Range

Recent experiments have indicated that the alpha (σ_c/σ_f) values for ^{239}Pu in the 100 eV to 10 keV range are, in general, higher than those used in many cross-section libraries, including ENDF/B. In order to define the problem, the ETOE-MC^2 processing codes were used to generate multigroup capture and fission cross sections for ^{239}Pu using the current ENDF/B data; the computed alpha values over the range of interest are shown in Fig. 465-2. The calculations were made using fine-group lethargy widths of 0.25 and infinite dilution. A flux weighting of 1/E within a fine group was used, except for the resolved resonance region (up to 300 eV for ^{239}Pu), where MC^2 uses a flux weighting proportional to the reciprocal of the total macroscopic cross section for the medium. Calculations were also performed to generate broad-group cross sections with lethargy widths equal to 0.50. Although the evaluation of the experiments which have yielded the high alpha values is still continuing, the ENDF/B alpha values are low compared to, for example, the values recommended by Barre et al.[15] A plot of the alpha values recommended by Barre is also shown in Fig. 465-2.

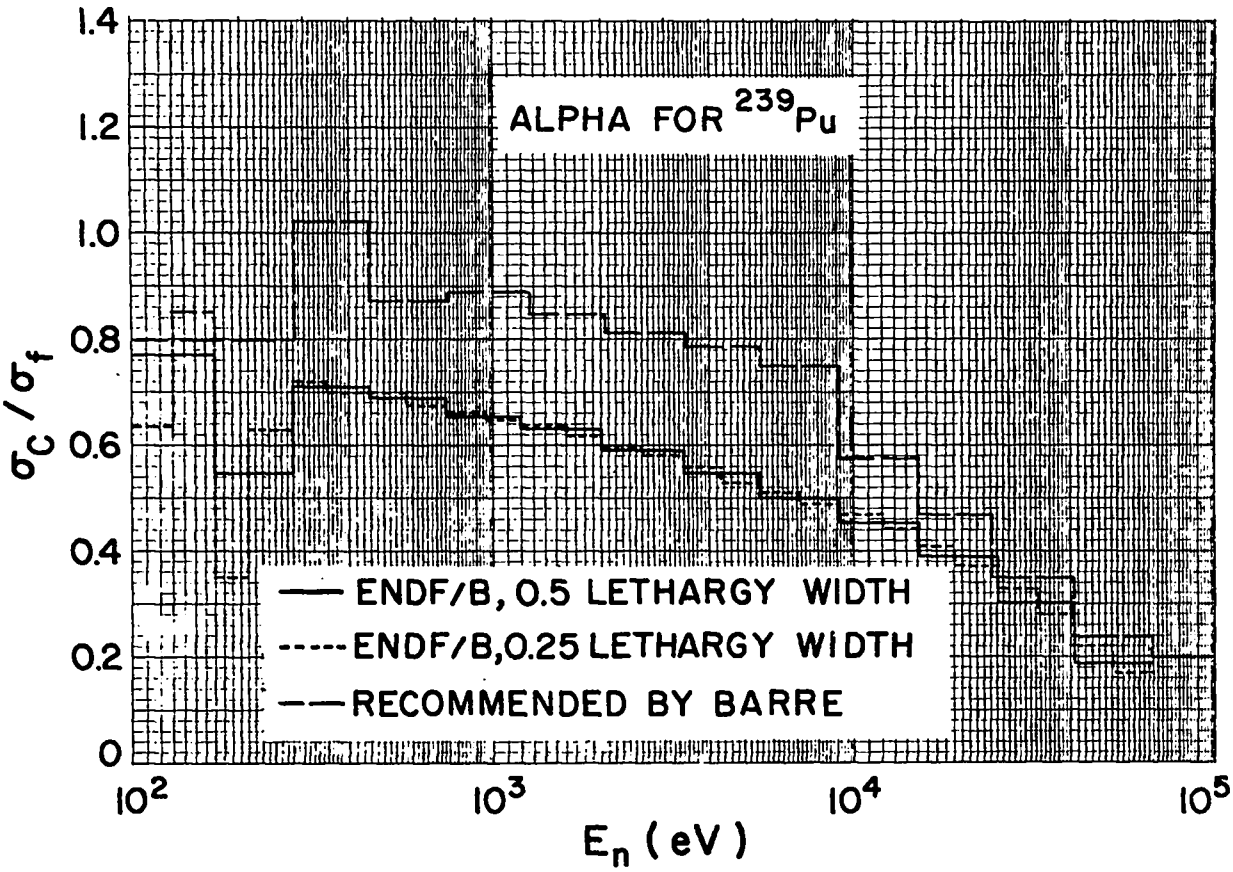

Fig. 465-2. Alpha for ^{239}Pu.

III. REACTOR ANALYSIS METHODS AND CONCEPT EVALUATIONS

A. General

A continuing task in fast reactor analysis and evaluation is the improvement of computer programs and the development of new computational methods. In addition to new methods, advances are constantly being made in computer technology which make possible the extension of existing calculational techniques.

B. Variational Principles Applied to Transport Problems (R. E. Alcouffe)

When one-dimensional transport calculations are performed on two-dimensional systems, the leakage must be estimated in the spatial direction transverse to the calculation. In DTF-IV, this is done by using a buckling type of correction to the total cross section.[2] Since this estimate is unsatisfactory when the medium in the transverse direction is large, it is desirable to have a more precise estimate. For this more precise estimate, it would be desirable to preserve the simplicity of the buckling type of correction.

In order to formulate such a method, the neutron transport process is written as a variational problem. To obtain one-dimensional equations, the functional is reduced by using trial functions for the dependent variable and its adjoint, which are separable in the independent variables. An analogous equation is also developed for the radial direction.

These two one-dimensional equations in each of the transverse directions can be used in a cyclic manner to generate one-dimensional transport solutions starting from some initial estimate of either the radial or axial leakage. The process will be considered successful if the eigenvalues resulting from the transverse calculations are essentially

TABLE 465-I

DESCRIPTION OF EXAMPLE SYSTEMS
AND RESULTS FROM DIFFERENT ESTIMATES OF TRANSVERSE LEAKAGE

	Case 1	Case 2	Case 3	Case 4
Geometry	Cylinder	Cylinder	Cube	Cylinder
Core				
diameter (cm)	5.7	15.2	10.16	12.1
height (cm)	50.0	3.9	10.16	12.4
% ^{240}Pu	5	6		
% ^{235}U		93.2	94	93.8
Reflector				
radial thickness (cm)	7.6	7.6	22.9	5.08
axial thickness (cm)	0	7.6	22.9	5.08
% ^{235}U	0.3	0.7	0.7	0.7
k(2DF)	1.0093 (618)[a]	1.0424 (1208)	1.0262 (1838)	1.0035 (1005)
k_z	1.0401	1.0832	1.0644	1.0391
k_r	1.0023 (262)	1.0621 (272)	1.0644 (198)	1.0352 (199)
k_c	0.9932 (74)	0.8434 (54)	0.8659 (42)	0.9102 (41)
k_R	-	1.1968 (54)	1.1950 (42)	1.0762 (41)

[a]Numbers in parentheses are central processor time in sec.

the same. Presumably, this eigenvalue will be a better approximation to the two-dimensional eigenvalue than that resulting from a single one-dimensional buckled calculation.

Since the trial functions come from DTF-IV S_n calculations, the information may be in either a P_n moments form or the discrete angle S_n form. If the leakage is large, it is necessary to retain a large number of terms in the moments expansion in order to represent the flux adequately at the boundary, and thus give a good estimate of the leakage. The additional terms significantly complicate the evaluation of the parameter, especially in a cylindrical geometry. Therefore, to conserve simplicity and accuracy, the trial functions are taken to be in the discrete angle form.

A scheme based upon this functional has been programmed for the CDC 6600 and was tested on a variety of realistic problems. The method is most effectively demonstrated on small fast systems in which leakage effects are large. Four such example calculations and the effects on the eigenvalue are given in Table 465-I. In this table,

k(2DF) is the eigenvalue computed from 2DF,

k_z is the eigenvalue resulting from an axial calculation using the transverse leakage correction,

k_r is the eigenvalue resulting from a radial calculation using the transverse leakage correction,

k_c is the eigenvalue resulting from a standard DTF-IV radial calculation using the core height as the buckling height, and

k_R is the eigenvalue resulting from a standard DTF-IV calculation using the total core plus reflector height as the buckling height.

This method leads to a significant improvement in the eigenvalue over other one-dimensional methods. However, a 2 to 4% error in the eigenvalue remains because of an underestimate of the two-dimensional leakage.

C. Collapsing of Cross-Section Sets (J. S. Philbin, B. M. Carmichael)

Tests were performed to verify the accuracy obtainable when using regular-flux-weighted cross sections in reactor calculations. These cross sections were generated by the REGFLX code.

The preservation of k_{eff} when using spectrum collapsed cross sections for two reactors, UHTREX and a large fast reactor, is summarized in Figs. 465-3 and 465-4.

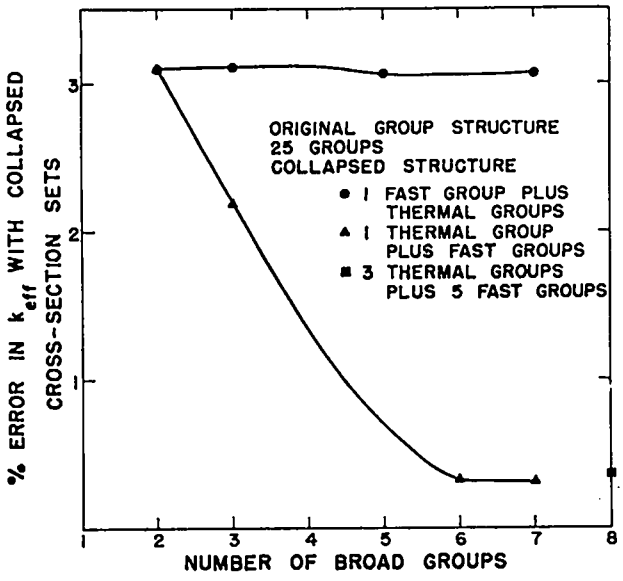

Fig. 465-3. Preservation of k_{eff} for UHTREX reactor.

The preservation of k_{eff} under group collapse on the large fast reactor was slightly better than on UHTREX. The error remains below 2% even with only two broad groups.

REGFLX is now available for use on the DTF-IV codes. A dummy subroutine, EXFINP, can be equipped to call REGFLX and perform any collapsing routine specified by the user.

D. Development of a Space-Energy Collapsing Scheme Applicable to Fast Reactor Burnup and Fuel-Cycle Analysis (R. E. Alcouffe, T. J. Hirons, R. D. O'Dell)

1. Theory. In sodium-cooled fast-breeder reactors, there is a marked difference between the neutron spectra for the core and blanket regions. In order to calculate the reaction rates accurately, it is necessary to account for the spectral differences between core, blanket, and other types of regions. For example, when such a problem is analyzed by group-diffusion theory, either the space-dependent spectrum can be used to derive appropriate diffusion equation parameters, or some approximate averaging spectrum can be used and the number of energy groups increased to compute the required shift in spectrum as a function of space. The former approach requires extensive data not normally available until the criticality calculation has been performed, whereas the latter method

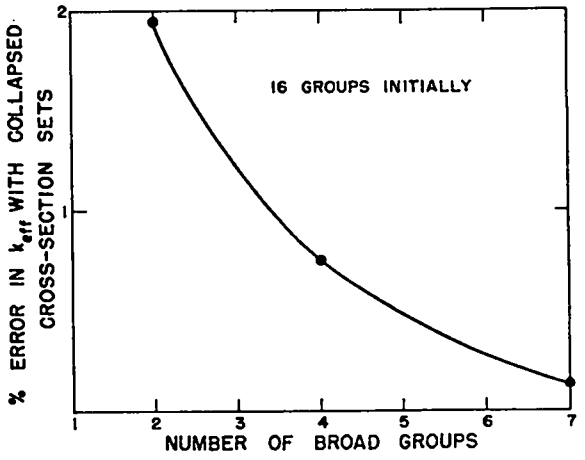

Fig. 465-4. Preservation of k_{eff} for a large fast reactor.

merely requires sufficient computer time and storage, with the averaging spectrum coming from an infinite-medium calculation.

However, for burnup and fuel-cycle studies, the number of space and energy mesh points must be kept to a minimum. Therefore, if the second approach mentioned above is used for the analysis, undetected errors may occur because of the restriction on mesh points. On the other hand, the two approaches can be combined in order to do the fuel-cycle problem consistent with a higher-order static problem.

The combining can be done by performing a fine energy-space mesh calculation at some representative state of the system (i.e., beginning of life or shortly thereafter). This fine-group space-dependent spectrum is then used to derive broad-group diffusion equation parameters. Furthermore, if the problem is recast in terms of a functional, it can be shown that the collapsing can be done so that the eigenvalue, average fluxes, reaction rates, and leakages of the fine-group problem are preserved in the broad-group calculation. That is, if the broad-group problem is done on the same system, the same result is obtained as with the fine-group and mesh problem.

With data derived in this way, the energy and spatial regions can be intelligently partitioned by determining how much and in what regions the problem changes from the averaging data used. Therefore, if the system changes little in time or if

large changes are confined to small regions, the number of mesh points needed for an accurate solution to the time-dependent problem can be drastically reduced.

2. Preliminary Results. Several static calculations to determine the effect of energy-group collapsing on the initial eigenvalue have been performed for the 1000-MWe mixed-oxide pancake LMFBR.[16] In the collapsing procedure,

a. A fine-group reference criticality run is performed with cross sections generated directly from MC^2;

b. The reference calculation is used to generate a separate set of microscopic cross sections for each region, and, in some cases, a special treatment is given to the calculation of the diffusion coefficients and leakage constants. These values are then collapsed according to the desired broad-group energy structure; and

c. A broad-group criticality run is performed.

The two-dimensional diffusion theory code 2DB[17,18] was used for both the fine- and broad-group criticality runs, although modification of the code was required for the broad-group runs to accommodate a separate set of microscopic cross sections for each region.

The collapsing technique used in Step b was designed to preserve the energy-averaged flux and reaction rates in each broad group. Three different methods were used for calculating the leakage in the broad-group problem:

a. No special treatment, i.e., diffusion coefficients in the broad-group problem were calculated as $1/3\Sigma_{tr}$, where Σ_{tr} is the collapsed total cross section;

b. A group-averaged value of $1/3\Sigma_{tr}$ is calculated for each region using flux weighting; these collapsed diffusion coefficients were then read directly into the broad-group version of 2DB; or

c. A group-averaged value of the leakage coefficient at each mesh point leakage interface (total of four times the number of groups per mesh point) is calculated using detailed flux weighting; these collapsed leakage coefficients were then read directly into the broad-group version of 2DB.

In Table 465-II, some results of collapse from a 16-group reference calculation are shown. For all runs, the spatial mesh and region detail used were identical for both the fine- and broad-group problems. The collapses to eight and four groups, using flux weighting only with no special treatment of the leakage, gave errors in the eigenvalue of 0.07% and 0.66%, respectively. When the special calculation of the diffusion coefficient was added to the four-group collapse, the error was reduced from 0.66% to 0.22%, indicating the importance of the leakage effect on the collapsing procedure. Finally, use of the collapsed mesh point leakage constants further reduced the error to 0.05%, and this method is the most accurate for calculation of the leakage in the broad-group problem. The result of the eight-group fine-structure problem is included in the table to demonstrate the significant improvement obtained when the eight-group collapsed set of cross sections, based on the 2DB space-dependent spectrum, is used instead of the eight-group set calculated directly from the MC^2 infinite-medium spectrum.

TABLE 465-II

EIGENVALUES OBTAINED WITH 16 FINE GROUPS AS THE REFERENCE CALCULATION

Groups	Eigenvalue
16 (reference calculation)	1.0003
8 (no special treatment of leakage)	1.0010
4 (" " ")	1.0069
4 (leakage calculated using region-wise collapsed diffusion coefficients as described in method b)	1.0025
4 (leakage calculated using collapsed mesh point leakage coefficient as described in method c)	0.9998
8 (fine-group problem, direct from MC^2)	1.0060

In Table 465-III, initial results of collapse from a 49-group reference calculation for the same reactor are shown. These results were obtained using the collapsed mesh point leakage constants, and the errors in the eigenvalues for both the

TABLE 465-III

EIGENVALUES OBTAINED WITH 49 FINE GROUPS AS THE REFERENCE CALCULATION

Groups	Eigenvalue
49 (reference calculation)	1.0025
8 (leakage calculated using collapsed	1.0028
4 mesh point leakage coefficient as described in method c)	1.0023

eight- and four-group problems were 0.02 to 0.03%. These results indicate that this overall collapsing scheme is accurate in preserving both eigenvalue and leakage from the fine-group problem. The collapsed flux distributions are in error by at most ±0.5% in the core regions, but may vary as much as ±6% in the outer regions and in the lower groups. A tightening of the flux convergence criterion should alleviate this problem.

Application of the energy-collapsing technique described above to fuel-cycle analysis has begun, and the effect on burnup and important fuel-cycle parameters of using a collapsed group structure will be investigated.

E. Preparation and Maintenance of Reactor Code Packages

1. Multiple User Experiment (MUX) (B. M. Carmichael). A system of remote terminals for the CDC 6600 called the Multiple User Experiment (MUX) is being developed by the Computing Division of LASL. The basic remote terminal device is the Teletype Corporation Model 35 Teletype.

With proper procedures, the debugging phase on problems can be performed much more efficiently through MUX than otherwise. The system is well adapted to output sampling of problems for checking results. By such sampling, one can verify results before releasing the output to the high-speed printers for full printing.

Large production codes can be called off tape using MUX. For problems requiring extensive input, the input for a reference problem is read off cards in the usual way and stored on tape. Then MUX can be used for modifying such input to perform parameter studies.

2. ANCON (J. C. Vigil). An additional feedback option was incorporated into the ANCON kinetics code. This additional option gives the reactivity feedback when the temperature coefficient is of the form

$$\frac{d\rho}{dT} = \frac{a}{T^b}, \qquad (465\text{-}2)$$

where ρ is the reactivity, T is the temperature (°K), and a and b are arbitrary constants. Equation 465-2 is the form commonly used for Doppler coefficients.

The reactivity feedback F(T) due to a change in temperature from T_0 to T is given by the integral of Eq. 465-2. Results are

$$F(T) = a \ln(T/T_0) \qquad \text{for } b = 1$$

$$F(T) = \frac{a}{1-b}\left(T^{1-b} - T_0^{1-b}\right) \qquad \text{for } b \neq 1 \qquad (465\text{-}3)$$

A feedback term of the type shown in Eq. 465-3 is available for each lump in the heat-balance equations. Different values of the constants a and b may be specified for each lump.

3. DAC (J. C. Vigil, J. L. Meem). The DAC output processing code was modified to reduce data handling. This new version, called DAC2, reads reactor specifications, unperturbed cross sections, and both regular and adjoint fluxes and currents directly from the 2DF output tapes. For the old version of DAC, tapes containing fluxes and currents had to be prepared from cards punched by 2DF. Also, reactor specifications and cross sections were input on cards in the old version.

4. Coupled Neutronic-Hydrodynamic Codes (M. E. Battat, J. C. Vigil). Two different computer programs that solve the coupled neutronic-hydrodynamic equations were compiled on the CDC-6600 computer, and test problems were run successfully with modifications of these programs.

The RAC code[20] was originally programmed at LASL to describe the coupled neutronic-hydrodynamic behavior of a graphite-uranium reactor core in space and time. This code was modified to describe excursions in a reactor composed of a UO_2 core and a BeO reflector.

The AX-1 code,[21] as obtained from the Argonne Code Center, was coded for a step input of reactivity. It was modified to include a ramp input of reactivity.

Briefly, the major differences between the RAC and AX-1 codes are:

a. AX-1 computes reactivity feedback and fission distributions from S_4 neutronic calculations as the reactor expands during the transient. RAC uses a fixed relative fission distribution specified in the input, and feedback is proportional to the fractional change in density. Proportionality factors are specified as input and can be obtained from perturbation calculations of the original configuration.

b. RAC takes into account changes of state while AX-1 does not.

Considering the differences between RAC and AX-1, results obtained with the two codes for various test problems agree reasonably well.

5. Burnup Code (R. D. O'Dell, T. J. Hirons).

A version of the burnup-refueling code PHENIX is now complete and running. The code has the capability of performing multiple burnup steps with search options on the control poison available both before and after each burnup step. The refueling option accounts for the flux shift over the reactor lifetime and gives a nearly exact treatment of the fuel discharge at any time for the different refueling fractions. A complete description of the code is now being prepared as an LA report.

6. Linked Codes (B. M. Carmichael, F. McGirt).

Considerable progress was made in refining existing neutronics codes DPC, DTF-IV, 2DF, DAC1, and DAC2 to a consistent code format and input style. This involved mainly the conversion of DPC, DAC1, and DAC2 into variable dimensioning form of FORTRAN-IV, and the conversion of all input into the DTF format.

The problems of linking these free-standing codes were also investigated. The overlay technique could be used for the linking, but this entailed some code modifications. The UPDATE facilities available on the CDC 6600 may provide a better approach to code linking, since by use of UPDATE no modification of the free-standing codes is required.

DAC1 was linked directly to DTF-IV by the overlay technique. With the new system, the regular and adjoint DTF-IV problems and the DAC1 perturbation calculation can all be performed in one run on the computer, or the sequence can be interrupted at any intermediate stage, whereupon the interim results are dumped on tape for future resumption of the sequence.

The DPC code was linked to the two-dimensional neutron transport theory code 2DF to form an independent computational package. Several test problems have been executed with the criticality search option of 2DF. Additional programming in DPC, which will allow automatic preparation of 2DF input for the zone thickness and nuclide concentration search options, is in progress.

7. Modular Programming Systems (F. McGirt).

The traditional method of attacking reactor problems with a number of self-contained and often unrelated codes is rapidly becoming obsolete. Not only is this approach cumbersome because of required human intervention between computer runs, but the problem of documentation so that programs can be shared with other users is also formidable. A modular program system provides a possible solution to these problems.

A modular computer program system allows a series of functional program units (modules) to be linked to perform a specific task. As a result, several modules can be used on a single job rather than a number of independent, free-standing codes, and no user intervention between jobs is necessary.

Two existing modular programming systems are presently being investigated here. The ARC (Argonne Reactor Computation) System,[22] now in production use at Argonne, has been designed so that an ARC job is compatible with other types of input jobs. However, this feature has led to large numbers of job control commands which, at present, must be supplied by the user.

The KAPL DATATRAN System[23] makes some stringent demands on the computer operating system, but provides simple job control and module manipulation.

Practical experience gained from the use of both systems should permit a valid comparison of modular systems to linked-code systems for guiding future code developments.

F. Fast Reactor Design Analysis (T. J. Hirons, R. D. O'Dell)

Analytical methods are being developed for evaluating the performance potentials of carbide- and metal-fueled fast breeder reactors. A 1000-MWe mixed-oxide fast breeder reactor[16] is being utilized as a model during the technique development. It is intended that parametric nuclear design analyses be made on such a reactor for use as a reference in evaluating the comparative performance potential of the other fuels. These studies will take cognizance of and be coordinated with the fuels and materials studies being conducted by this Laboratory.

Work during this fiscal year has been directed toward the formulation of consistent calculational models to be used for the fuel-cycle analysis of large fast breeders. The variation of fuel-cycle parameters, such as breeding ratio and fuel discharge rate with several burnup-model characteristics, was studied.

These characteristics were the amount of region detail used in describing the reactor, the initial fissile content of the reactor, the maintenance of criticality during the burnup step, the distribution of the control poison during the burnup step, and the flux or power shift over the reactor lifetime. Each model characteristic was studied in detail for its effect on the burnup history of the reactor. The mass balances obtained from several of the burnup studies were input to a reactor economics code to determine the economic effects of changes in the model characteristics. The greatest effect on the fuel-cycle analysis was produced by the treatment of the relative flux shift between burnup intervals. The assumption of constant flux produced errors in ^{239}Pu discharge of up to 7% in the axial blankets. When the charge-discharge data were input to the economics code, the assumption of constant flux produced negligible differences in power costs, but resulted in an error of some 5% in the net yield of fissile isotopes per megawatt-year. Complete details of these studies have been prepared as an LA report.[24]

IV. COOPERATIVE ARRANGEMENTS

W. H. Hannum returned from his assignment at the United Kingdom Atomic Energy Research Establishment at Winfrith, England. Reports of his work and his visits to other research centers were distributed.

REFERENCES

1. D. A. Meneley et al., "MACH1, A One-Dimensional Diffusion Theory Package," ANL-7223, Argonne National Laboratory (1966).
2. K. D. Lathrop, "DTF-IV, A FORTRAN-IV Program for Solving the Multigroup Transport Equation with Anisotropic Scattering," LA-3373, Los Alamos Scientific Laboratory (1965).
3. CSEWG Newsletter 18 (March 20, 1969).
4. S. T. Perkins, Lawrence Radiation Laboratory, private communication (October 1, 1968).
5. R. J. Howerton, "Semi-Empericial Neutron Cross Sections. Part II, Vol. I. 0.5-15 MeV," UCRL-5351, University of California (1958).
6. "Reactor Physics Constants," ANL-5800, Argonne National Laboratory (1963).
7. D. J. Toppel et al., "MC^2, A Code to Calculate Multigroup Cross Sections," ANL-7318, Argonne National Laboratory (1967).
8. W. W. Clendenin, "Thermal Neutron Scattering Cross Sections for Crystalline Materials: The TOR Program," LA-3823, Los Alamos Scientific Laboratory (1967).
9. J. Bell, "SUMMIT, An IBM-7090 Program for the Computation of Crystalline Scattering Kernels," GA-2492, General Atomic (1962).
10. W. W. Clendenin, "Calculation of Thermal Neutron Diffusion Length and Group Cross Sections; The GLEN Program," LA-3893, Los Alamos Scientific Laboratory (1968).
11. M. K. Drake et al., "Neutron and Gamma Ray Production Cross Sections for Sodium, Magnesium, Chlorine, Potassium, and Calcium," GA-7829, Vols. I, II, and III, General Atomic (1967).
12. D. J. Dudziak, ed., "ENDF/B Format Requirements for Shielding Applications," LA-3801, Los Alamos Scientific Laboratory (1967).
13. D. J. Dudziak and R. J. LaBauve, "Storage and Retrieval of Photon Production and Interaction Data in the ENDF/B System," in Neutron Cross Sections and Technology, NBS Special Publication 299, Vol. II, p. 1101 (1968).
14. D. J. Dudziak, "Attenuation of Fast-Neutron Biological Dose in Nonhydrogenous Shields Followed by Thin Hydrogenous Shields," Trans. Am. Nucl. Soc. 11 (1), 197 (1968).

15. J. Barre et al., "Examen Critique des Valeurs de $\alpha = \sigma_C/\sigma_F$ pour le ^{239}Pu au-dela de 1 keV et des Experiences Pouvant Ameliorer sa Connaissance," CEA-N-989, Saclay (1968).

16. "Liquid Metal Fast Breeder Reactor Design Study (1000 MWe UO_2-PuO_2 Fueled Plant)," GEAP-4418, General Electric (1963).

17. W. W. Little, Jr. and R. W. Hardie, "2DB, A Two-Dimensional Diffusion-Burnup Code for Fast Reactor Analysis," BNWL-640, Battelle Northwest Laboratory (1968).

18. W. W. Little, Jr. and R. W. Hardie, "2DB User's Manual," BNWL-831, Battelle Northwest Laboratory (1968).

19. J. C. Vigil, Nucl. Sci. Eng. 29, 392 (1967).

20. C. G. Chezem and W. R. Stratton, "RAC, A Computer Program for Reactor Accident Calculations," LAMS-2920, Los Alamos Scientific Laboratory (1963).

21. D. Okrent et al., "AX-1, A Computing Program for Coupled Neutronics-Hydrodynamics Calculations on the IBM-704," ANL-5977, Argonne National Laboratory (1959).

22. B. J. Toppel, "The Argonne Reactor Computation (ARC) System," ANL-7332, Argonne National Laboratory (1967).

23. H. J. Kopp et al., "DATATRAN Modular Programming System for Digital Computers," Knolls Atomic Power Laboratory, Schenectady, New York (1968).

24. T. J. Hirons and R. D. O'Dell, "Calculational Modeling Effects on Fast Breeder Fuel-Cycle Analysis," LA-4187, Los Alamos Scientific Laboratory (in press).

PROJECT 466

FAST REACTOR METALLIC FUEL STUDIES

Persons in Charge: R. D. Baker
D. B. Hall
Principal Investigators: W. J. Maraman
R. H. Perkins

I. INTRODUCTION

The objective of this program is the development of metal fuels for fast reactor application. Much of the primary effort is placed on preparation and fabrication development of U-Pu-Zr alloys, and on the irradiation behavior of these alloys. Supporting effort is directed toward areas of physics and system evaluation, determining of physical and chemical properties of the fuel, and studying fuel-cladding interactions.

II. FUEL PREPARATION AND FABRICATION
(D. R. Harbur, B. N. Robbins, A. K. Murdock, E. L. Grady, K. Johnson)

A. General

The initial goals of this project are to prepare high purity, homogeneous U-15Pu-6Zr to U-15Pu-15Zr alloys, and to fabricate these alloys into fuel pins of the EBR-II size. Work has been concluded on this project with the completion of the above goals.

B. Results During FY 1969

Two methods for preparing and casting U-Pu-Zr alloys have been evaluated during the course of this investigation: inductive melting and stirring on a metallic hearth and inductive melting and mechanical stirring in crucibles. It has been concluded that the cold-crucible technique, whereby the molten alloys is in contact with a water-cooled hearth, while feasible, still requires a great deal of development work. The zirconium segregation due to a zone-refining effect associated with the liquid-to-solid interface within the alloy button can only be eliminated by levitation of the entire charge. Another disadvantage of this technique for a production-oriented program is the size limitation of the charge.

The important factor which led to the adoption of the more conventional alloying and casting technique was the development of two ceramic coatings which could be easily applied to standard bottom-pour graphite crucibles making them virtually inert to the molten U-Pu-Zr alloys. These two coatings are NbC and colloidal Y_2O_3 with a K_2SiO_3 binder. The former coating is the more inert; however, the latter coating has the advantage of not being wet by the molten alloy. The NbC coating is applied to the graphite crucible, stirrer and stopper rod by a special process developed at LASL. The Y_2O_3 suspension is made commercially by the Acheson Colloids Co. and is listed under their No. EC 3327X. It is easily applied to the desired surface using a spray gun.

The conventional alloying and casting technique which has been adapted for this alloy development program consists of co-melting the metals (U, Pu and Zr) in a NbC-coated graphite bottom-pour melt crucible using induction heat. The molten metals are heated to 1400-1500°C and mechanically stirred for 30 min to aid in the dissolution of zirconium into the melt. The stopper rod is then raised and the melt is poured. The minimum diameter to which a 15-in.-long rod can be gravity-cast in a heated mold is approximately 0.3 in. These rods are subject to centerline porosity, piping, and segregation. The segregation and porosity can be reduced by chill casting the metal into aluminum billet molds with a

0.75-in.-diam cavity. The chemical analyses of three typical batches of cast U-Pu-Zr alloys which were made by this casting technique are given in Table 466-I.

Further fabrication of these cast billets was accomplished by standard hot-extrusion methods whereby the die body and billet were heated to between 500 and 570°C, which is still within the alpha-phase temperature region for these alloys. Using a relatively small 50 T press, extrusions were made with extrusion ratios as high as 9 to 1. The extrusion die, die body, punch, and ram were made of M-2 tool steel hardened to R_c 60 to 64. The extrusion die had a 60° included angle and the lubricant was WS_2 (commercially available in a pressurized spray can under the trade name "Tungspray"). Curvature of the rods, as they were extruded from the die was eliminated by flowing the rods into a slightly oversized tube. Some recrystallization occurred in the extruded alloys at extrusion rates below 0.5 in./min; however, the degree of recrystallization was minimal.

The feasibility of fabricating either the cast or extruded material by swaging was also investigated. It was found that neither of these products could be swaged bare even though temperatures well into the gamma-phase temperature region were tried. The extruded material could be swaged in the Fenn 4-die swaging machine if the material was first placed inside a thin-walled stainless steel tube. The first pass through the swaging machine could be made at temperatures as low as 300°C. The material was noticeably toughened by the swaging operation. Area reductions of 30% in the alloy were accomplished

Table 466-I

Chemical Analyses of Cast U-Pu-Zr Alloys*

	JUZ-98071		JUZ-98069		JUZ-98074	
Element	Top	Bottom	Top	Bottom	Top	Bottom
Pu	14.79 w/o	14.89 w/o	15.15 w/o	15.10 w/o	14.60 w/o	14.62 w/o
Zr	6.8 to 7.4 w/o	6.6 to 7.0 w/o	10.1 to 10.4 w/o	9.9 to 10.2 w/o	13.3 to 14.1 w/o	13.4 to 13.6 w/o
U	78.1 w/o	77.9 w/o	75.4 w/o	74.7 w/o	72.3 w/o	72.0 w/o
O	90	90	85	80	80	65
C	130		130	130	40	
H	< 5		10	5	5	
Fe	240		58	39	240	
Ga	< 12		79	59	< 12	
Nb	14		19	18	24	
Th	17		13	11	18	
W	15		16	17	32	
Li	< 1		< 2	< 2	< 1	
Be	< 1		< 1	< 1	< 1	
B	< 1		< 1	< 1	< 1	
Na	2		< 2	< 2	< 2	
Mg	5		< 5	< 5	< 5	
Al	10		25	25	< 10	
Si	30		30	30	40	
P	< 50		< 50	< 50	< 50	
Ca	< 5		< 5	< 5	< 5	
Cr	< 5		< 10	< 10	< 5	
Mn	3		2	2	< 2	
Ni	50		10	10	10	
Cu	5		5	5	< 2	
Zn	20		< 10	< 10	< 10	
Sr	5		< 5	< 5	< 5	
Cd	< 10		< 10	< 10	< 10	
Sn	< 5		< 2	< 2	< 5	
Pb	< 5		< 10	< 10	< 5	
Bi	< 2		< 2	< 2	< 2	

*Expressed as parts per million unless otherwise stated.

when using 0.030-in.-wall stainless steel tubing. When a 0.060-in.-wall stainless steel tubing was used, most of the reduction occurred in the tubing, and only a 7% area reduction was accomplished in the alloy rod.

It appears necessary to completely anneal the alloy between reductions. The minimum time required for this annealing operation was not determined. The annealing operation should be carried out above 700°C in the gamma-phase temperature region where complete homogenization occurs.

The fabrication studies on this alloy system show that the most practical method for making 0.144-in.-diam rods with a large length-to-diameter ratio is the bare extrusion of the chill-cast billets. With a 100 to 150 T press, no difficulties are encountered in extruding 0.75-in.-diam billets down to this final EBR-II size. The alternative to this fabrication method would be to first extrude and then swage to final size. Since the swaging operation can only be performed with the extruded rod encapsulated in a thin-walled tube, this method would involve the removal of this tube after the swaging operation.

The tensile and tensile-creep properties were determined for several of the U-Pu-Zr alloys in both the cast and extruded conditions. These data are summarized in Tables 466-II and III. The zirconium content of the nominal U-15Pu-Zr alloys had only a minor effect upon the physical properties of these alloys. All of the alloys containing between 6 and 15 w/o Zr were extremely brittle at 25°C. The 6 w/o Zr alloy became ductile at 290°C whereas those alloys with more than 10 w/o Zr became ductile above 350°C. About 100°C above these temperatures these alloys became extremely plastic. Hardness values for the as-cast and as-extruded materials were identical; the hardness of the 6 and 10 w/o Zr material was 440 DPH, whereas the 13.5 w/o Zr material had a hardness of 380 DPH. The variation in densities with zirconium content in both the cast and extruded conditions is given in Fig. 466-1.

Powder x-ray diffraction and diffractometer studies by C. Land and F. Ellinger confirmed that these alloys consist of an alpha uranium matrix with small amounts of the UZr_2 and UPu zeta phases present. EMX data showed the presence of zirconium-rich particles in the material containing over 100 ppm O;

Table 466-II

Tensile Properties of U-Pu-Zr Alloys[a]

Alloy Composition (Nominal w/o)			Temp. (°C)	UTS (psi)	Y.S.[b] (psi)	Elongation (%)	Fabrication History	E (psi x 10^6)
U	Pu	Zr						
75	15	10	25	70,000	-	Nil	As-Extruded	2.2
			300	39,000	-	Nil	"	2.1
			350	44,000	44,000	3	"	0.9
			400	14,000	10,000	53	"	0.4
73.3	14	11.7	25	76,000	-	Nil	"	2.3
			100	80,000	-	Nil	"	2.2
72.5	15	12.5	25	95,700	-	Nil	"	2.7
			300	64,800	-	Nil	"	2.6
			350	55,700	55,000	Nil	"	2.5
			450	8,140	6,800	31	"	0.4
			525	5,740	4,100	62.5	"	0.5
71.5	15	13.5	25	84,000	-	Nil	"	1.0
79	15	6	25	97,000	-	Nil	"	2.5
72.8	15	12.2	25	61,000	-	Nil	As-Cast	1.4

(a) Tensile test performed at a strain rate of 0.015 in./in./min.

(b) Yield strength at 0.2% offset.

Table 466-III

Time (in minutes) To Attain 2% Strain in U-Pu-Zr Alloys
In The As-Extruded Condition

Alloy Composition (Nominal w/o)			Stress (psi)	Temperature, °C			
				290	350	400	500
U	Pu	Zr					
75	15	10	2,000	-	-	-	20
			3,000	-	-	-	5
			8,000	-	-	30	ruptured
			10,000	-	-	9	"
			11,000	-	-	3	"
			20,000	-	300	ruptured	"
			30,000	-	20	"	"
			40,000	-	9	"	"
72.5	15	12.5	2,000	-	-	-	8
			3,000	-	-	-	4
			15,000	-	-	15	ruptured
			17,000	-	-	8	"
			19,000	-	-	4	"
79	15	6	1,000	-	-	-	0.3
			5,000	30	ruptured	ruptured	ruptured
			6,000	9	"	"	"

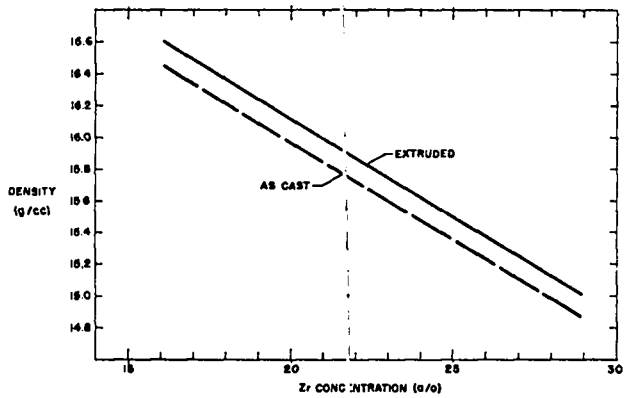

Fig. 466-1. Variation of density with zirconium content of U-15Pu-Zr alloys in the as-cast and extruded condition.

isolated zirconium-rich particles were also found metallographically in material containing less than 80 ppm O. These are the oxygen-stabilized alpha zirconium particles first reported by D. O'Boyle. Microhardness readings on these small alpha zirconium particles showed them to be extremely hard with hardness values as high as 2500 DPH. The presence of such particles would no doubt have a great effect upon the low-temperature tensile properties of these alloys.

A photomicrograph of the U-15Pu-10Zr alloy in the chill-cast condition is shown in Fig. 466-2 along with a typical EMX scan. The same alloy after extrusion at 570°C is shown in Fig. 466-3. As would be expected, the extrusion process completely breaks up the as-cast microstructure of these alloys. The effect of a relatively short-term heat treatment on the extruded material in the gamma temperature region is shown by the photomicrograph and EMX scan in Fig. 466-4. After only 17 days of heat treatment at 750°C, the alloy had become almost completely homogenized. The density of this specimen decreased by 0.07 g/cm^3 during this heat treatment, presumably due to the homogenization and resultant redistribution of phases. The photomicrograph of the beta heat-treated specimen in Fig. 466-5 shows the development of a duplex microstructure. The EMX data shows that the microstructure developed at 650°C consists of alternating grains of alpha zirconium and UZr_2 with plutonium solution in each. The density decreased by 0.09 g/cm^3 during heat treatment due to the resulting redistribution of phases. The complex microstructure and EMX scan shown in Fig. 466-6 was produced by holding the extruded material in the high alpha phase temperature region (500°C) for 19 days. These data indicate the presence of the three phases (alpha uranium, UZr_2, and zeta uranium-plutonium) found in the as-cast microstructure. The more extensive formation of the zeta uranium-plutonium phase is due to the limited solubility of plutonium in the uranium-rich phase. The density decrease caused by this heat treatment was only 0.02 g/cm^3.

900X

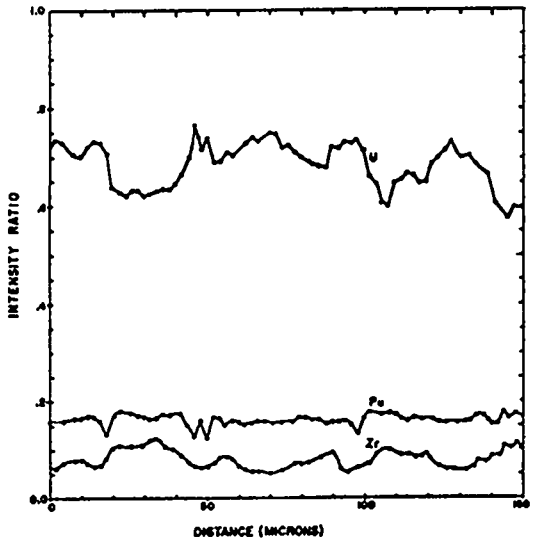

Fig. 466-2. Photomicrograph and EMX scan of as-cast U-15Pu-10Zr alloy.

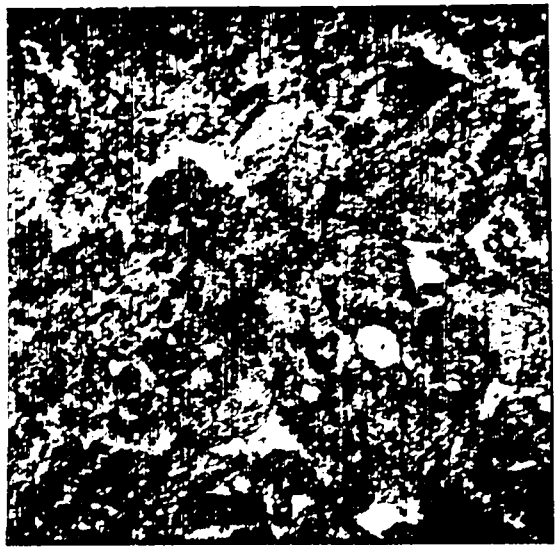

900X

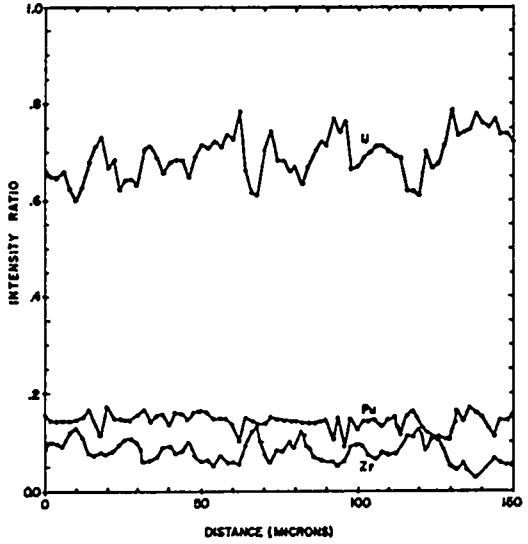

Fig. 466-3. Photomicrograph and EMX scan of extruded U-15Pu-10Zr alloy.

900X

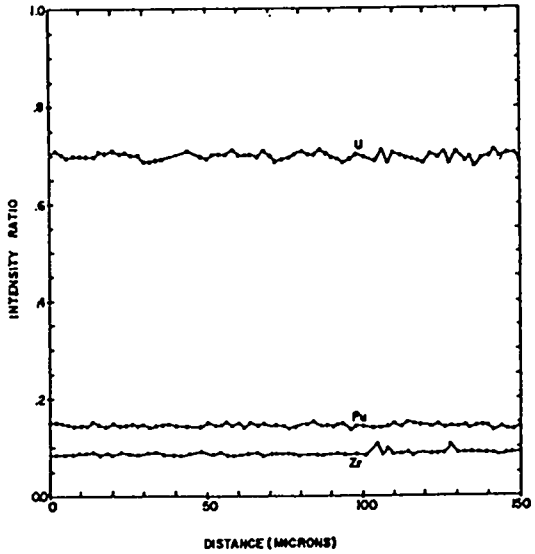

Fig. 466-4. Photomicrograph and EMX scan of extruded U-15Pu-12Zr alloy after a 17 day heat treatment in the gamma-phase at 750°C. Materi- contains 300 ppm O. Note alpha zirconium particles in photomicrograph.

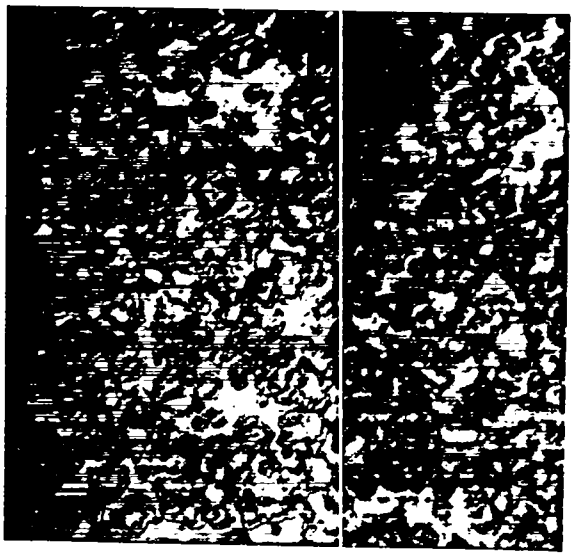

900X

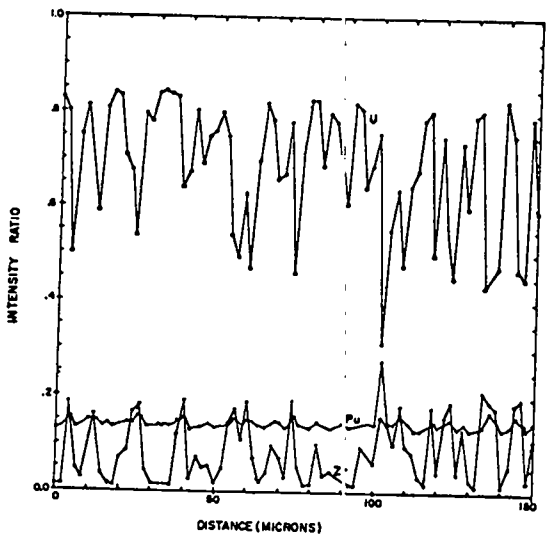

Fig. 466-5. Photomicrograph and EMX scan of extruded U-15Pu-12Zr alloy after an 18 day heat treatment in the beta phase at 650°C.

To delineate the effects of thermal cycling from those due to irradiation, thermal cycling experiments were performed on U-15Pu-12Zr alloy rods in the as-extruded condition. Three separate thermal cycling treatments were investigated: (1) 500° (alpha phase) - 650°C (beta phase); (2) 500° (alpha phase) - 750°C (gamma phase); and (3) 630° (beta phase) - 750°C (gamma phase). The behavior of this material during the various thermal cycles is shown in Fig. 466-7.

Each of the three thermal cycling treatments caused the extruded material to exhibit anisotropic growth patterns up through 200 cycles. Metalographic examination of these specimens after 100 thermal cycles showed that all of the specimens had a recrystallized-equiaxed grain structure. The EMX data for the specimens after 100 cycles showed that a great deal of homogenization had occurred; this was especially evident in the samples that were cycled into the gamma phase temperature region. This

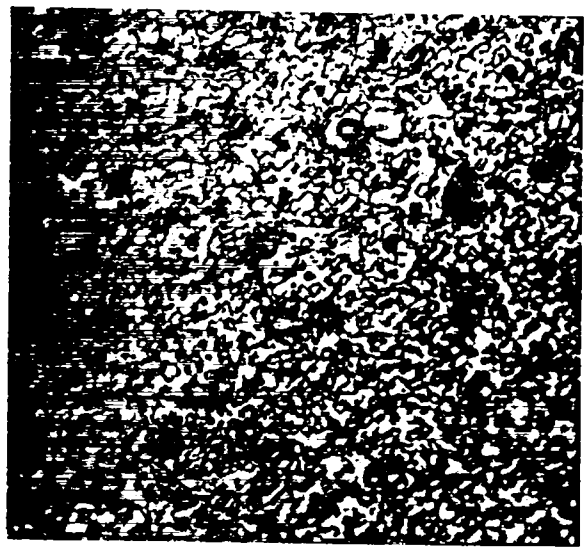

900X

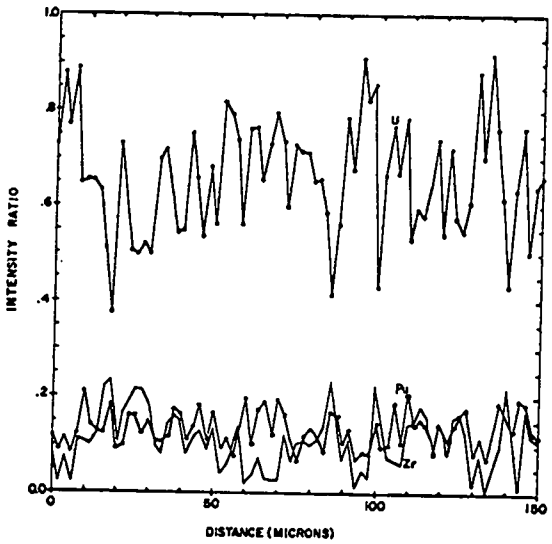

Fig. 466-6. Photomicrograph and EMX scan of extruded U-15Pu-12Zr alloy after a 19 day heat treatment in the high alpha phase temperature region at 500°C

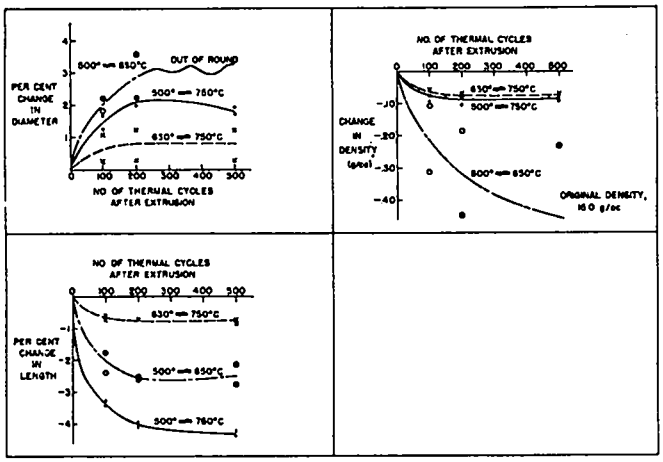

Fig. 466-7. Physical changes in as-extruded U-15Pu-12Zr alloy due to thermal cycling.

initial homogenization occurs due to the randomness of the microstructure resulting from the extrusion process.

The resulting microstructures after 500 thermal cycles, together with typical EMX scans, are shown in Figs. 466-8, -9, and -10 for the three different thermal cycling treatments investigated. The material cycled between the alpha and beta phases continued to homogenize, except for the growth of 20-micron-broad UZr_2 particles widely separated in what appears to be a homogeneous matrix. Metallographic examination of this matrix revealed at least a two-phase, fine-grain (~ 0.5 micron) microstructure. Since the EMX readings were taken at 2 micron intervals, the multiple phase nature of this fine-grained matrix was not detected.

A catastrophic density decrease occurred in the two specimens cycled between the alpha and beta phases. After 500 thermal cycles the density decrease was 0.23 to 0.68 g/cm^3. Both specimens had developed longitudinal surface cracks. A 0.030-in.-diam hole had opened up in the center of the specimen which had the greater density decrease. The center of the other specimen had numerous smaller holes. Prior to the thermal cycling experiments, the extruded rods were shown to be radiographically free of internal voids. It should be noted, however, that there was centerline porosity present in the cast material and that these voids were closed during the extrusion operation.

During both the $\beta \leftrightarrow \gamma$ and $\alpha \leftrightarrow \gamma$ thermal cycles the formation of the zeta uranium-plutonium phases was extensive. The matrix of the alloy formed after these thermal cycles consisted mainly of the alpha uranium and zeta uranium-plutonium phases containing zirconium in solution. The segregation and extensive formation of the zeta uranium-plutonium phase was caused by cycling through the two-phase region between the beta uranium and gamma uranium phases.

Since most of the original irradiation data was determined for this alloy with both radial and longitudinal thermal gradients imposed upon the fuel pin, it was desirable to determine the effects of such a thermal gradient upon an unirradiated rod. One end of a 1-in.-long, 0.178-in.-diam U-15Pu-13.4Zr rod was held for 17 days in the gamma-phase temperature region (750°C) while the other end was maintained in the alpha-phase temperature region (500°C). Subsequent examination of the rod using metallographic and EMX techniques showed an abrupt change between the area held in the gamma-phase temperature region and the adjacent area which was in the beta-phase temperature region (Fig. 466-11). (The homogeneous matrix of the material heat-treated in the gamma phase abruptly changed into the large duplex grain structure of the material held in the beta-phase temperature region.) The large grains characteristic of the high beta-phase temperature region gradually decreased in size toward the low temperature end of the rod. Metallography failed to reveal any line of demarcation between the beta-phase and alpha-phase material. EMX data showed that alpha uranium-UZr_2 matrix characteristic of beta heat-treated material gradually decreased in grain size and finally evolved into a three-phase mixture characteristic of the alpha-phase temperature region. Chemical analysis of approximately 0.15-in.-long sections along this rod gave the composition profile shown in Fig. 466-12. The section of rod designated 2A contained the region which was maintained in the beta-phase temperature region. The transport of zirconium from this region in such a short time is noteworthy.

In summary, the U-Pu-Zr alloys can be prepared by conventional casting techniques with little addition of impurities, provided NbC- or Y_2O_3-coated graphite crucibles are used. The cast product is subject to segregation and centerline porosity which can be minimized by chill-casting into metal molds. The cast material lends itself to hot extrusion

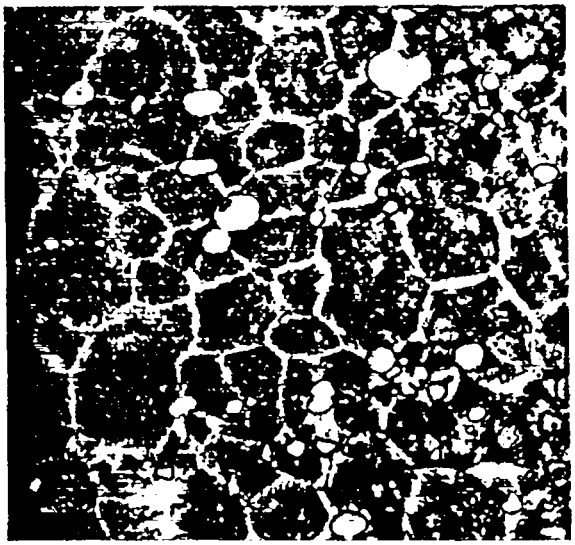

Fig. 466-11. U-15Pu-13.4Zr alloy rod held for 17 days with a thermal gradient along the length of the rod. End to left of photomicrograph at 750°C. Other end at 500°C. Depicts gamma-phase microstructure at left changing into beta-phase microstructure at right. 900X

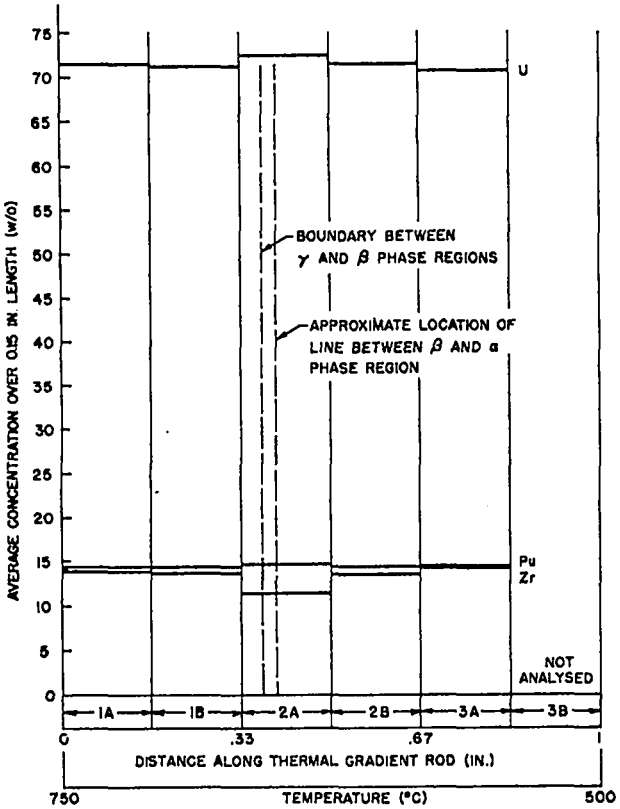

Fig. 466-12. Composition profile along the length of a U-15Pu-13.4Zr rod held in a thermal gradient. Obtained by dissolving and analyzing ~ 0.15-in.-long sections of the rod.

processes, and a final sizing operation by swaging techniques is possible provided the extruded rod is swaged inside a thin-walled tube.

The adverse effects caused by holding these alloys in the high-alpha-phase temperature region or the beta-phase temperature region, together with the transport of zirconium from the regions of a rod held in the beta field into those adjacent areas maintained in either the alpha or gamma field may preclude the use of this alloy as a reactor fuel unless the minimum temperature of the fuel is above the β-γ transformation temperature of 655°C.

III. PHYSICAL PROPERTIES

A. General

The principal goal of this project is the determination of pertinent physical properties of metal fuels. Important physical properties that are being studied include: (1) phase transformations; (2) hot hardness; and (3) thermal conductivity.

B. Results During FY 1969

1. Differential Thermal Analysis (J. G. Reavis, L. W. Reese)

Two samples of U-Pu-Zr alloys have been observed by use of differential thermal analysis techniques. Thermocouples were used for observation of solid transformations below 1000°C, while optical detectors and an optical pyrometer were used to observe the samples above 1000°C. The thermocouple system was calibrated by observation of transitions of pure uranium. Calibration and use of the optical system have been described elsewhere.[1]

For brevity of discussion, the alloys will be designated "Alloy 6" and "Alloy 13." The nominal composition of Alloy 6 was 78.2U-15Pu-6.8Zr, while Alloy 13 was nominally 71.5U-15Pu-13.5Zr. The observed temperatures of solid transformations are listed in Table 466-IV. The temperature ranges of energy absorption or release listed are the ranges covered by sample temperatures between the beginning of the arrest and the time of maximum lag of sample temperature behind reference temperature. It is estimated that not less than 75% (and in many cases more than 90%) of the energy involved in the transition was transferred in this interval.

No attempt was made to identify the crystallographic transformations producing the thermal

Table 466-IV

Thermal Arrests and Ranges of Temperature Over Which a Major Fraction of Energy Release or Absorption Occurs in U-Pu-Zr Alloys

Alloy	Transition	Heating Arrests (°C) Start	Heating Arrests (°C) Range	Cooling Arrests (°C) Start	Cooling Arrests (°C) Range
6	A	588	588-598	594	594-586
6	B	643	643-658	634	634-626
13	A	588	588-593	593	593-588
13	B	638	638-653	626	626-610
100% U	α-β	665	665-669	Supercooled	
100% U	β-γ	775	775-778	Supercooled	

arrests and they are simply labelled "A" and "B" to allow easy comparison of temperature observed for the two different alloys. Arrest temperatures and ranges for pure uranium are included to establish the temperature calibration scale and to show the narrow range of temperature observed for a transition of a pure material in the same geometric configuration as the alloy samples which showed wide ranges.

With only one exception, no arrest temperature was observed below 586°C. The exception was the first heating of Alloy 6. In this case, the ΔT curve indicated probable energy absorption in the range 518 to 588°C. The energy absorbed was < 5% of the total energy involved in transitions A and B. This is near the detectability limit of the apparatus.

The thermal arrests of Alloy 6 could not be separated into additional arrests. Cooling arrest B of Alloy 13 could, however, be separated into two overlapping arrests with a reasonable degree of confidence. The minor transition was in the range 626 to 618°C, while a transition involving about four times as much energy covered the range 618 to 610°C.

In the case of Alloy 13, the energy of transition A was about equal to that of B. In Alloy 6, the energy of transition B was about four times as large as that of transition A.

Solidus and liquidus temperatures of the two alloys are listed in Table 466-V. These temperatures are in fair agreement with those predicted from the solidus and liquidus lines of the isopleth between U-15Pu and pure zirconium, using the assumption of ideal liquid and solid solution behavior.

Table 466-V

Solidus and Liquidus Temperatures Observed for U-Pu-Zr Alloys

Alloy	Solidus (°C)	Liquidus (°C)
6	1105 ± 10	1240 ± 20
13	1195 ± 10	1425 ± 20

2. Hot Hardness
(M. Tokar)

A specimen of U-15Pu-6.8Zr alloy was heated to 880°C for 20 h, and hardness readings were taken as the specimen cooled. The data are given in Table 466-VI.

Table 466-VI

Hot Hardness of U-15Pu-6.8Zr (200-g load)

Temp (°C)	DPHN	Temp (°C)	DPHN
800	3.4	625	18.2
750	4.3	610	20.2
730	5.4	600	39.6
720	5.6	590	46.6
700	7.4	580	59.1
700	6.4	570	60.9
690	8.8	550	83.5
680	8.8	500	148
670	10.0	450	202
650	11.0	400	256

3. Thermal Conductivity
(K. W. R. Johnson)

The thermal conductivity of an extruded specimen of U-15Pu-6.8Zr was measured from 110 to 892°C. The thermal conductivity was significantly greater than that for cast material reported by ANL and increased from 0.305 to 0.757 cal/sec-cm-°C. Above the transition temperatures, the material became sufficiently soft that deformation occurred. Measurements in this temperature range were adjusted to reflect the magnitude of this deformation.

IV. ANALYTICAL CHEMISTRY

A. General

Specific analytical techniques have been developed and applied to the analysis of metal fuel alloys. The results of many of these analyses are included in other sections of Project 466. A brief summary of some of the techniques, and the problems to which they were applied, are given below.

B. Results During FY 1969

1. Determination of Zirconium in U-Pu-Zr Alloys
(R. G. Hurley, E. A. Hakkila)

An x-ray fluorescence spectrometric method was developed for determining plutonium and zirconium in 200-mg samples of U-15Pu-12Zr alloys to supplement the controlled-potential coulometric and spectrophotometric methods now used in the chemical characterization of these alloys. The samples were dissolved in HF and HNO_3, thorium was added as an internal standard, and the intensities of the Kα x-ray for zirconium and the $L\alpha_1$ x-rays for plutonium and thorium were measured. The Zr|Th and Pu|Th x-ray intensity ratios were calculated and compared to ratios for solutions having known uranium, zirconium, and plutonium concentrations to obtain the plutonium and zirconium contents of the samples. An arithmetic correction to eliminate interference caused by overlap of the Kα x-ray for zirconium by an L x-ray for plutonium was included in the Fortran program written for use on the CDC6600 computer in calculating the results. Repeated determinations at three known concentrations in prepared solutions that also contained uranium showed that the precisions (1 σ) were about 1% and 0.6%, respectively, in measuring between 10 and 20% of zirconium and plutonium. Of all other elements that might cause interference by x-ray overlap or absorption, concentrations as large as 3% were tolerated, except for platinum, bismuth, and strontium for which maximum tolerable concentrations ranged between 0.2 and 1%. The method was used successfully in analyzing several U-Pu-Zr alloys.

2. Electron Microprobe Examinations
(E. A. Hakkila, H. L. Barker)

Several U-Pu-Zr alloys, which had been annealed at various temperatures, were examined to determine the distributions of uranium, plutonium, and zirconium. The intensities of the characteristic x-rays of uranium, plutonium, and zirconium, relative to x-ray intensities from the respective pure metals, were measured at 2-micron intervals along selected paths 150-microns-long in each sample. A computer program was written for calculating the intensity ratios and plotting the ratios as a function of position on the scan. Most scans showed uniform distributions of the three elements. A few small white areas crossed in some scans contained more zirconium and less uranium than the major portions of the matrix.

Two minor phases were identified in each of five U-Pu-Zr alloys. In one phase, consisting of irregularly-shaped white precipitates, zirconium was the major constituent. A light-colored, needle-like phase contained more uranium and less plutonium than the matrix.

3. Determination of Oxygen in U-Pu-Zr
(W. B. Hutchinson, M. E. Smith)

The inert-gas-fusion method was modified for the determination of oxygen in U-Pu-Zr alloys by substituting a Pt-20Sn bath at 1800°C for the customary molten plutonium bath at 2000°C. The U-Pu-Zr alloys dissolved more rapidly and completely in the Pt-Sn bath which facilitated the release of oxygen as CO and improved the precision of the method. The evolved CO was oxidized to CO_2 and measured manometrically. Repeated analyses of a U-Pu-Zr alloy using each bath showed that the precision (1 σ) of a single determination of oxygen was 9 relative per cent using the Pt-Sn bath as compared to 15 relative per cent with the platinum bath.

V. METAL FUEL COMPATIBILITY TESTING
(J. C. Clifford, J. A. Horak)

A. General

The purpose of this task is to examine the out-of-pile compatibility of LASL-produced U-Pu-Zr alloys with Type 316 stainless steel and with a vanadium alloy. Of prime interest are the effects of (1) zirconium and oxygen content of the fuel on reactions between fuel and stainless steel, and (2) gross inhomogeneities within the fuel on fuel-stainless steel reactions. The temperature range of interest is 550 to 750°C.

This work scope is a departure from those of earlier reports and reflects a shift of interest away from metal alloys as LMFBR fuels. The compatibility work currently is being reviewed and further alterations may result.

B. Results During FY 1969

Enough specimens of fuel, of Type 316 stainless steel, and of a V-15Cr-5Ti alloys have been prepared to complete the compatibility testing program. Four fuel alloys are being used; three were produced at LASL by chill casting and one at ANL by injection casting. Two LASL lots are nominally U-15Pu-12.5Zr, containing 180 and 820 ppm oxygen, while the third LASL lot is a U-14Pu-6Zr alloy containing 125 ppm oxygen. The ANL material has a composition of U-15.6Pu-10.7Zr and contains 650 ppm oxygen. The LASL materials are being used to study the effects of varying oxygen and zirconium content on compatibility between fuel and clad. A comparison between the ANL material and the LASL high-oxygen, high-zirconium material may show whether fuel inhomogenieties affect fuel-clad interactions.

At present, compatibility specimens consist of sandwiches of Type 316 stainless steel, fuel, and vanadium alloy held together in presses of stainless steel or molybdenum. Specimens of the individual alloys are prepared by grinding the flat surfaces of cylindrical balnks on 600 grit paper. These specimens are transferred to a high purity inert gas glovebox train where final polishing is done immediately before assembly. The compatibility specimens are assembled in the presses, encapsulated and then transferred from the glovebox train to forced-convection sodium loops for testing. The use of loops rather than furnaces is a convenience: the loops have larger constant temperature zones than the available muffle furnaces.

Tests to date have been restricted to an evaluation of the effects of specimen surface condition and contact pressures on the extent and rapidity of interaction. Long time testing at 550, 650, and 750°C will be initiated after specimen surface preparation, press material, and initial loading have been standardized.

Eighteen diffusion couples of U-15Fs-304L stainless steel were incorporated into a thermal flux irradiation experiment in the LASL Omega West Reactor. The experiment was terminated after a few hours because of higher-than-anticipated variations in temperature around the periphery of the fuel pins in the assembly. Because of the short time at temperature, the diffusion couples have not been examined. No additional U-5Fs experiments are planned.

VI. IRRADIATION EFFECTS STUDIES
(J. C. Clifford, J. A. Horak, R. L. Cubitt, D. C. Kirkpatrick)

A. General

As with the metal fuel compatibility studies, the metal fuel irradiation program is being reduced and reoriented because of the diminishing interest in metal alloys as LMFBR fuels. Thermal irradiations are being conducted to evaluate the behavior (intrinsic swelling, migration of fuel constituents, fission gas release, fuel-sodium-clad compatibility) of on-hand, U-Pu-Zr alloys produced by LASL (Part II, Project 466). Irradiations are conducted at the Omega West Reactor in an environmental cell in which temperature changes accompanying reactor power level changes are minimized with electrical heat and with a variable conductivity heat leak. Using this cell, it is possible to prevent thermal cycling of the fuel through phase transformations that otherwise might affect its behavior.

The environmental cell being used is one of two installed in the OWR starting in 1965. The cells and their operation have been described previously[2] in connection with the irradiation of liquid plutonium alloy fuels, the experiments for which they were designed. No significant modifications have been made to the design since that time.

A schematic of the in-core section of the cell, with an experimental insert in place, is shown in Fig. 466-13. The outside diameter of the cell is

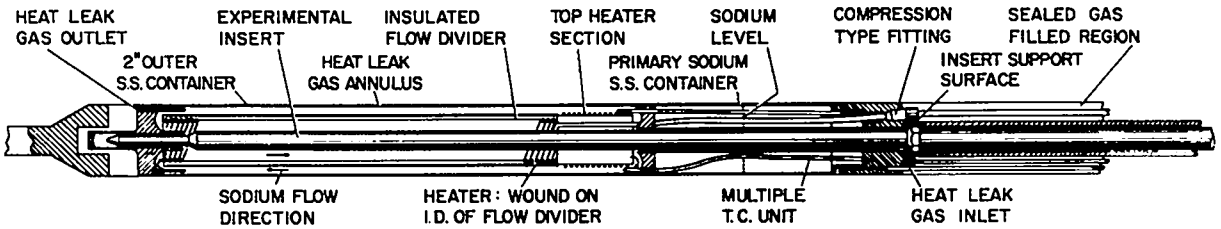

Fig. 466-13. In-Pile Test Assembly

2 in. and its over-all length is 22 ft. At the lower end of the cell is a 13-in.-long, electrically-heated convecting sodium loop and the variable conductivity heat leak. The legs of the sodium loop are separated by an argon-filled stainless steel flow divider on the inside surface of which are wound the main resistance heaters. The heat leak annulus is formed by the primary sodium container and the cell outer tube. The annular gap varies from 12 to 20 mils and contains a continuously flowing gas stream of He and N in any desired proportion. Helium, at several pounds above atmospheric pressure, is used as the cover gas over the sodium in the cell.

The experimental insert, occupying the central portion of the cell, includes the fuel pins and additional thermocouples sodium-bonded to a secondary container. The insert is 28 ft long and is 0.60-in. outside diameter throughout the in-core portion. The entire 28-ft-long insert is installed and removed as a unit. Fuel pins occupy the lower 3 to 10 in. of the insert and, at operating temperature, the height of sodium in the secondary is approximately 2 in. above the top pin. As a check on fuel pin integrity, a helium purge is directed through the volume above the sodium level in the insert. This stream is exhausted from the experiment through a molecular sieve which is monitored continuously for fission gases.

During operation, sodium in the annulus between the fueled insert and the flow divider is heated by fuel in the insert and by the heaters wound on the inside of the flow divider. Sodium rises in this annulus and then descends in the annulus between the flow divider and the heat leak wall, transferring heat through the heat leak gas annulus to the reactor cooling water. The temperature of the fuel surfaces can be maintained in the 600-700°C range both during reactor operation and shutdown.

During FY 1970, the OWR irradiation of metal fuels will be reported under Project 467, "Fuel Irradiation Experiments".

B. Results During FY 1969

Prior to the start of the metal fuel irradiations, both OWR cells were observed to be discolored on the outside surfaces in the core region. The older cell was removed from the reactor and examined destructively. The blue-brown discoloration on the surface of the outer stainless steel tube was extremely thin and could not be identified. The affected area was examined metallographically, and rings taken from this area were subjected to a rather crude compression test to determine whether the material was dectile. The same inspection and ductility tests were performed on tubing from an unaffected portion of the same cell and on stock intended for another cell. All of these materials exhibited the same ductility and microstructure, indicating that the discoloration in the core region of the cell was not the result of overheating. Since no changes in heat transfer characteristics had been noted over the lifetime of the older cell, and since the second cell exhibited the same operating characteristics as the first, the second cell was kept in the reactor for the metal fuel work.

The electrical, gas, and alarm system associated with the remaining cell were refurbished, and satisfactory operation of the cell was demonstrated during an experiment to measure the gamma heating contribution from an unfueled insert. Gamma heating was measured as a function of reactor power. Heat transfer calculations, involving heat leak gas compositions different than those used previously, were confirmed experimentally. The thermal response of

the cell to changes in nuclear and electrical heat input was measured as a function of time, and the transient behavior of the system was determined following a reactor scram.

Following the gamma heating experiment, a fuel experiment composed of stainless-steel-clad, sodium-bonded U-5Fs pins and U-5Fs/stainless steel diffusion specimens was operated for a short period. Three fuel pins were clustered in a triangular array with a pitch to diameter ratio of ~ 1.2. The pins occupied the lower four inches of the insert with the encapsulated diffusion specimens clustered above the fuel pins. Total power production in this assembly agreed well with the predicted values. However, the fuel pin clad surfaces exhibited unacceptably large peripheral temperature variations between the outward and inward facing sections of the cladding. At a reactor power of 6 MW, a 75°C variation was measured. The experiment was terminated after measurements were made of the response of the cell temperature control system to changes in heat leak gas composition and to changes in reactor power level. Because of the short irradiation time, no postirradiation examinations are planned.

To avoid the temperature gradients associated with the three-pin cluster, the next insert was assembled with four fuel pins stacked one on another at the axis of the insert. Two pins contained LASL chill-cast U-15Pu-12Zr and the other two contained LASL chill-cast and extruded fuel of the same nominal composition. The 1-in.-high fuel slugs were sodium-bonded to nickel containers. No diffusion couples were included. A few hours after the experiment reached full power, a 15°C temperature increase was observed in the top fuel pin. No other pin was affected. After two days at this value the temperature of the top pin again began to increase. After a total rise in clad temperature of approximately 45°C, the temperature of the experiment was lowered, returning the top capsule to its original full power temperature and reducing the temperature of the bottom 75°C below its starting value. The experiment was operated for another 1-1/2 days, at which time fission gases were detected in the sweep gas from the experiment insert. The experiment was terminated and the fueled portion of the insert was transferred to the hot cell for destructive examination.

Radiographic examination of the insert shows no abnormalities in three capsules. However, fuel relocation has taken place in the top capsule and no sodium meniscus can be located, although the meniscus is visible in the other three. The erratic temperature history of the top capsule and the redistribution of fuel over the entire fueled length of the capsule suggest that bonding sodium may have been expelled as the result of failure of the bottom weld. (The pressure differential between the fuel capsule plenum and the insert sweep gas space, at operating temperature, was approximately three atmospheres.) The loss of a substantial fraction or all of the sodium bond could have resulted in fuel overheating and slumping. However, visual inspection followed by dissection of the capsule will be required to determine the cause of failure.

REFERENCES

1. J. G. Reavis, J. B. Buchen, and J. A. Leary, Report LA-4103, Los Alamos Scientific Laboratory, 1969.
2. R. L. Cubitt, G. L. Ragan, D. C. Kirkpatrick, "Thermal Irradiation of Liquid Plutonium-Alloy Fuels," Report LA-3832, Los Alamos Scientific Laboratory, June 1968.

PROJECT 471

OTHER ADVANCED SYSTEMS - RESEARCH AND DEVELOPMENT

Person in Charge: D. B. Hall
Principal Investigator: G. H. Best

I. PULSED REACTOR NEUTRONICS (G. C. Hopkins)

In a repetitively pulsed neutron facility excited by some form of accelerator, it is desirable to have the maximum neutron intensity compatible with pulse width requirements for high resolution. Several combinations of parameters were investigated, including the addition of synchronously pulsed reactivity.

The basic reactor system under study is a small fast assembly fueled with either ^{239}Pu or ^{233}U. The relationship of the pulse characteristics is shown graphically in Fig. 471-1, and typical values of reactor and pulse parameters are listed in Table 471-1, where Λ is the neutron generation time, k_1 is the reactivity during the pulse, k_2 is the off-pulse reactivity, t_p is the pulse width, T is the cycle duration, $(S/N)_n$ is the ratio of the maximum to the minimum values of the neutron density, $(S/N)_p$ is the ratio of the average pulse power to the average background power, and peak n is the peak neutron density.

For simplicity, the monenergetic point kinetics equations were used, with six delayed neutron groups, but neglecting feedback. This program produces survey comparisons of responses resulting from various combinations of parameters, in a short amount of computing time.

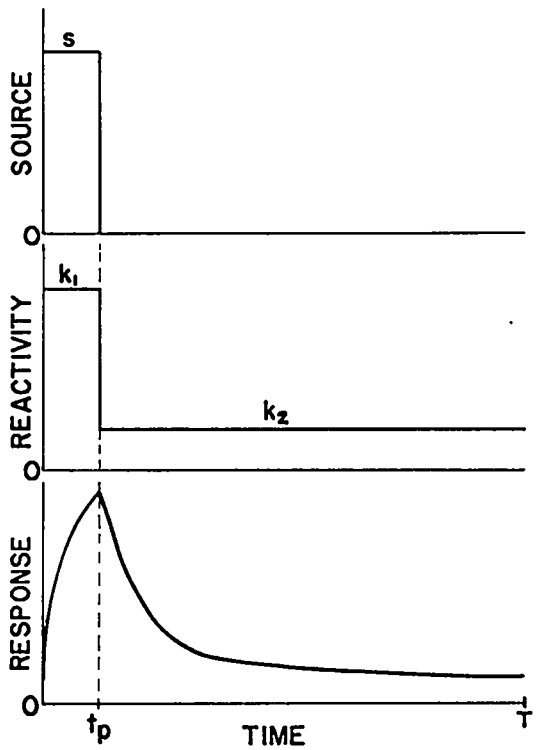

Fig. 471-1. Relation of input source pulse, reactivity pulse, and neutron output.

TABLE 471-I

PARAMETER VARIATION RESULTS

(S = 1 x 10^{17} neutrons/sec)

Fuel	Λ (10^{-9} sec)	k_1	k_2	t_p (10^{-6} sec)	T (sec)	$(S/N)_n$	$(S/N)_p$	Peak n
^{239}Pu	5.0	0.990	0.990	5.0	0.005	5,056	2954	4.1×10^{10}
		0.990	0.980			10,618	7187	4.1×10^{10}
		0.999	0.990			6,305	2920	1.6×10^{11}
			0.980			13,373	7137	1.6×10^{11}
			0.990	1.0		26,248	575	7.5×10^{10}
				1.0	0.001	5,247	406	7.5×10^{10}
	6.0			5.0	0.005	6,410	2694	1.8×10^{11}
	8.0					6,481	2328	2.3×10^{11}
^{233}U	6.0					4,718	2129	1.6×10^{11}

Some of the results obtained, seen by comparing cases in Table 471-I, are:

1. Synchronously adding reactivity in phase with source pulse improves the peak n by a factor of 4, decreases $(S/N)_p$ by about 2%, and increases $(S/N)_n$ by about 25%.
2. Achieving an even lower reactivity during off-pulse considerably improves the S/N ratios.
3. Decreasing t_p results in a substantial increase in $(S/N)_n$, but at the expense of a decreased $(S/N)_p$ and peak n.
4. A shorter generation time slightly increases $(S/N)_p$ and slightly decreases $(S/N)_n$ and peak n.
5. Although shorter generation times are possible with ^{233}U, ^{239}Pu gives better S/N ratios and peak n.

These survey results can aid the experimenter in determining specifications based on his particular design requirements.

II. ^{3}He ACTIVATION (D. M. Holm, W. M. Sanders, B. K. Barnes)

A. General

Carbon and oxygen impurities in high-purity materials are being studied by means of charged-particle activation and spectroscopy. These impurities are of interest because of the effect they have on the properties of the materials. In addition, for crystalline materials, charged-particle channeling gives information about the location of the impurities in the crystal structure.

Before the impurities in the body of the material can be studied, it is necessary to determine their amounts on the surface and how to remove them or distinguish them from impurities in the body. A method of abrading and etching the samples before bombardment has been developed to clean off the surface contaminants. In order to calibrate the results on surface contaminants, surface films of oxygen on tantalum were studied. Anodizing of tantalum provides surface oxygen films of controlled and known thickness. The thickness of the surface layer varies directly with the anodizing voltage.[1]

B. Results During FY 1969

A preliminary problem in measuring the surface oxygen was separating the reaction protons from the Coulomb-scattered ^{3}He particles. These elastically backscattered ^{3}He ions can be degraded in energy below the electronic thresholds by placing absorber foils between the detector and the target. With a suitable absorber, only the less ionizing protons from (^{3}He,p) reactions have sufficient energy after traversing the foils to be recorded by the detector system.

Surface contaminants are removed from germanium crystals by abrading with 600-grit emery cloth and etching with CP-4 acid solution. The acid is washed off with water after each etch, and some of the water remains on the germanium. To remove the water prior to irradiation, the samples are placed in a high-vacuum system for up to one hour following the water wash.

Preliminary charged-particle channeling data has been taken on germanium crystals. The crystal face was mapped to locate the principal planes accessible within the range of the goniometer used (Fig. 471-2). The principal axes ⟨111⟩ and ⟨112⟩ were located, and backscatter and reaction data were taken at both axes. Figure 471-3 shows a typical backscatter dip

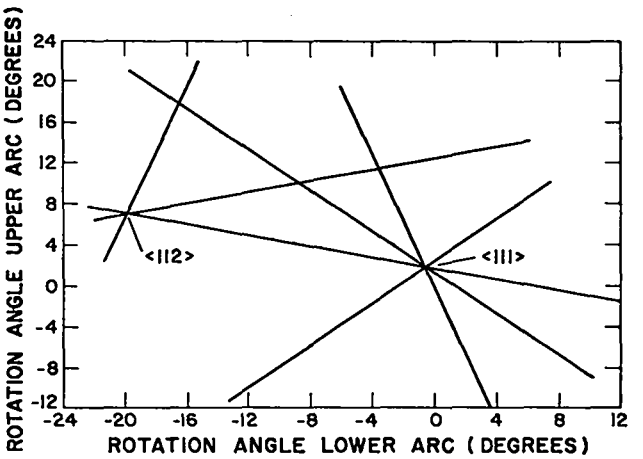

Fig. 471-2. Principal planes within the range of the goniometer.

when passing in angle over the ⟨112⟩ axis. The ratio of the number of high-energy backscatter events for a nonchanneling direction to those for a channeling direction is given in Table 471-II. That table also

TABLE 471-II
EFFECTS OF CHANNELING

Channeling Axis	Backscatter Ratio	^{16}O Proton Ratio
⟨111⟩	6.4	2.0
⟨112⟩	10.6	5.7

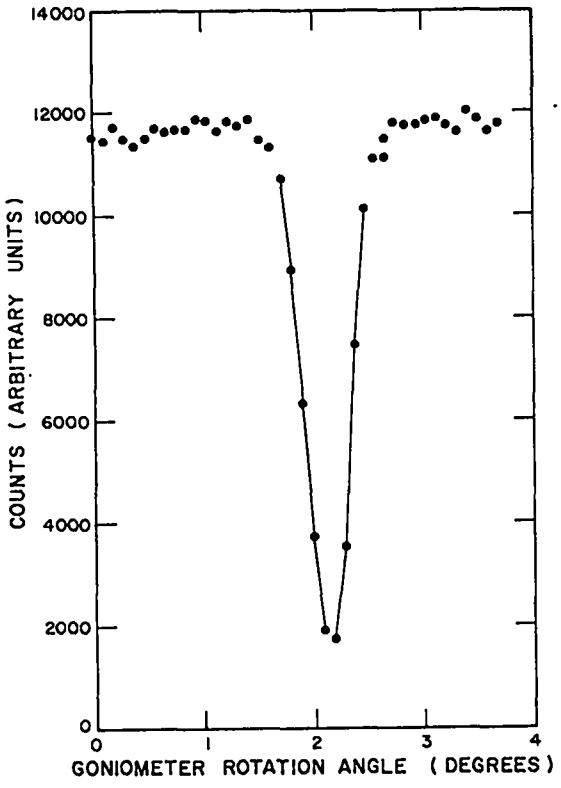

Fig. 471-3. Typical backscatter dip at <112> axis.

gives the ratio of the protons from the $^{16}O(^{3}He,p)^{18}F$ reactions channeling direction to those for a non-channeling direction. This ratio is for the volume-distributed oxygen, which was separated from the surface oxygen concentration by fitting analytic functions to the data. The statistical uncertainty of the proton data shown in Table 471-II indicates that at the present level of surface contamination the number of counts from the volume-distributed oxygen is not well enough known to draw valid conclusions about the position of the oxygen in the lattice structure. Work to improve the surface cleanup is continuing. Activation data taken on the cleaned crystals indicates that the present level of surface contamination is approximately 0.03 μg/cm^2. This much oxygen corresponds to slightly less than one atomic layer, where an atomic layer would be one oxygen atom for each germanium atom on the face of the crystal.

Problems encountered in developing a method for the removal of surface oxygen has interfered with plans to obtain the quantitative data needed for a final evaluation of the channeling technique as an analytical tool. The qualitative channeling data which have been obtained show that the method is feasible. Improvements are being made in the experimental technique and the data analysis to give quantitative results. In a practical test of the technique, ^{3}He activation was used to determine the amount of diamond dust imbedded in the surface of a platinum disc, as a service to another group in the Laboratory. Seven 20 μin. foils of nickel were placed in front of the sample during irradiation to reduce the energy of the ^{3}He particles to the desired value and to prevent surface contamination from oils in the vacuum system. The results showed that the dust had an average concentration of about 1 μg/cm^2. It was distributed in spots and small scratches on the surfaces. Two autoradiographs were made to show the distribution. The absolute accuracy was limited to a factor of 2 (all that was required) by the short time available for preparations.

III. EQUATION OF STATE OF REACTOR FUELS (B. C. Goplen)

All the scheduled experiments to obtain data on the equation of state of reactor fuels have been completed. Uranium dioxide was the only material studied; no further work is planned because of the recent reduction in AEC funds which supported this program.

A final (classified) report has been drafted, and will be published soon.

IV. HIGH TEMPERATURE NEUTRON DETECTOR TEST

During FY 1969, all data from experiments conducted during FY 1968 were reduced and evaluated. The results were reported at IEEE Nuclear Science Symposium.[2] No further work is planned.

REFERENCES

1. F. Kover and M. J. Musselin, Thin Solid Films 2, 211 (1968).

2. E. O. Swickard and J. A. Bacastow, "Test of Six High Temperature Neutron Detectors to 650°C," IEEE Trans on Nuclear Science, 15th Nuclear Science Symposium, Montreal, Canada, pp 177-183 (October 1968).

SPECIAL DISTRIBUTION

Atomic Energy Commission, Washington

Division of Research

D. K. Stevens

Division of Naval Reactors

R. H. Steele

Division of Reactor Development and Technology

L. J. Colby
G. W. Cunningham
D. E. Erb
Nicholas Grossman
W. H. Hannum (2)
K. E. Horton
J. R. Humphreys
R. E. Pahler
J. M. Simmons (2)
E. E. Sinclair
Bernard Singer
C. E. Weber
G. W. Wensch
M. J. Whitman

Division of Space Nuclear Systems

G. K. Dicker
F. C. Schwenk

Safeguards & Materials Management

J. M. Williams

Idaho Operations Office

DeWitt Moss

Ames Laboratory, ISU

O. N. Carlson
W. L. Larsen
M. Smutz

Argonne National Laboratory

F. G. Foote
Sherman Greenberg
J. H. Kittel
W. B. Loewenstein
R. E. Macherey
M. V. Nevitt

Idaho Falls, Idaho

D. W. Cissel
R. C. Robertson

Atomics International

R. W. Dickinson, Director (2)
Liquid Metals Information Center

J. L. Ballif

Babcock & Wilcox Co.

C. Baroch
J. H. MacMillan

Battelle Memorial Institute

D. L. Keller
S. J. Paprocki

Brookhaven National Laboratory

D. H. Gurinsky
C. Klamut

Combustion Engineering, Inc.

S. Christopher

Donald W. Douglas Laboratories

R. W. Andelin

General Electric Co., Cincinnati, Ohio

V. P. Calkins

General Electric Co., Sunnyvale, California

R. E. Skavdahl

Gulf General Atomic, Inc.

E. C. Creutz

Idaho Nuclear Corporation

W. C. Francis

IIT Research Institute

R. Van Tyne

Lawrence Radiation Laboratory

Leo Brewer
J. S. Kane
A. J. Rothman

LMFBR Program Office

Alfred Amorosi
D. K. Butler (Physics)
L. R. Kelman (Fuels & Materials)
J. M. McKee (Sodium Technology)

Mound Laboratory

R. G. Grove

NASA, Lewis Research Center

J. J. Lombardo

Naval Research Laboratory

L. E. Steele

Oak Ridge National Laboratory

G. M. Adamson
J. E. Cunningham
J. H. Frye, Jr.
C. J. McHargue
P. Patriarca
O. Sisman
M. S. Wechsler
J. R. Weir

Pacific Northwest Laboratory

F. W. Albaugh
E. A. Evans
V. J. Rutkauskas
W. R. Wykoff

FFTF Project

E. R. Astley
B. M. Johnson
D. W. Shannon (2)

U. S. Department of Interior

Bureau of Mines, Albany, Oregon

H. Kato

United Nuclear Corporation

A. Strasser

Westinghouse, Advanced Research Division

E. C. Bishop

SPECIAL SPECIAL DISTRIBUTION
(Continued)

Westinghouse, Atomic Power Division

R. A. Markley

Westinghouse, Bettis Atomic Power Laboratory

E. J. Kreigh

Australian Atomic Energy Commission

J. L. Symonds